Flexible Utilization of Transmission Grid Capacity for Wind Power Integration.

Viafora, Nicola

Publication date:
2020

Document Version
Publisher's PDF, also known as Version of record

Center for Electric Power and Energy

Flexible Utilization of Transmission Grid Capacity for Wind Power Integration

Nicola Viafora

PhD Thesis, April 2020, Kongens Lyngby, Denmark

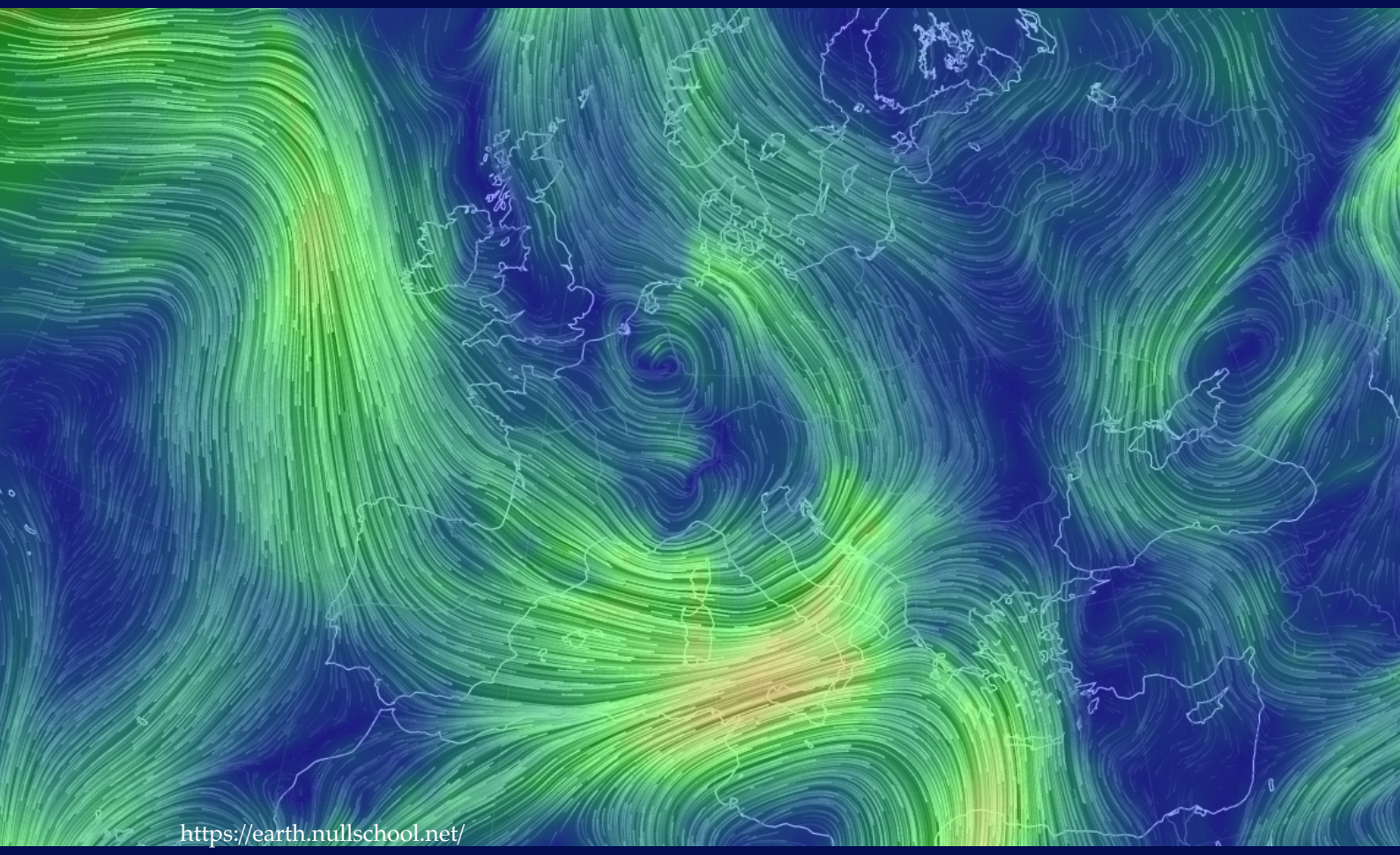

DANMARKS TEKNISKE UNIVERSITET
Center for Electric Power and Energy (CEE)
DTU Electrical Engineering

Flexible Utilization of Transmission Grid Capacity for Wind Power Integration

Dissertation, by Nicola Viafora

Supervisors:
Professor Joachim Holbøll, Technical University of Denmark
Chief Engineer Anders Steen Kristensen, Energinet

DTU - Technical University of Denmark, Kogens Lyngby - April 2020

Flexible Utilization of Transmission Grid Capacity for Wind Power Integration

This thesis was prepared by:
Nicola Viafora

Supervisors:
Professor Joachim Holbøll, Technical University of Denmark
Chief Engineer Anders Steen Kristensen, Energinet

Dissertation Examination Committee:
Associate Professor Spyridon Chatzivasileiadis
Department of Electrical Engineering, Technical University of Denmark, Denmark

Associate Researcher Andrea Michiorri
MINES ParisTech, Ecole des mines de Paris, France

Associate Professor Vijay Venu Vadlamudi
Department of Electric Power Engineering, Norwegian University of Science and Technology, Norway

Center for Electric Power and Energy (CEE)
DTU Electrical Engineering
Elektrovej, Building 325
DK-2800 Kgs. Lyngby
Denmark

Tel: (+45) 4525 3500
Fax: (+45) 4588 6111
E-mail: cee@elektro.dtu.dk

Release date: April 2020

Edition: 1.0

Class: Internal

Field: Electrical Engineering

Remarks: The dissertation is presented to the Department of Electrical Engineering of the Technical University of Denmark in partial fulfillment of the requirements for the degree of Doctor of Philosophy.

ISBN: 000-00-00000-00-0

Ad maiora

Preface

This thesis is prepared at the Department of Electrical Engineering of the Technical University of Denmark in partial fulfillment of the requirements for acquiring the degree of Doctor of Philosophy in Engineering. It collects the work carried out by the author as a Ph.D. student from the 15th of November 2016 to the 13th of April 2020. During this period, the author was employed at the Technical University of Denmark under the OPTIMUM project, a cooperation with the Danish transmission system operator, Energinet, who funded the project together with DTU

The thesis summarizes the research work proposed in five scientific papers, four of which have been published with a peer-review process, while the remaining one is currently under revision. The main body of the thesis serves the purpose to introduce and discuss the proposed contributions from a broader perspective, whereas for in-depth technical details the reader is referred to the papers attached in the appendix.

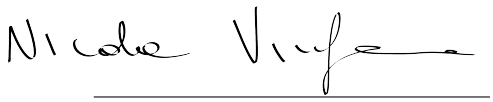

Nicola Viafora
April 2020

Acknowledgements

This thesis would not have been possible without the extensive support from the OPTIMUM project team members at Energinet, Ørsted and DTU. In particular, Anders Steen Kristensen, Rasmus Aabye Olsen, Mie Thomsen, Syed Hamza Hasan Kazmi, Thomas Herskind Olsen, Troels Sørensen, Jakob Glarbo Møller and Joachim Holbøll, even though many more contributed during several meetings and discussions, offering their perspectives, important feedbacks and valuable data that has been crucial for the entire research project. One special remark for my main academic supervisor, Joachim, thanks to whom I believe I experimented the value of flexibility in first person.

For the exceptionally positive working environment from which I benefited from, I have to thank all my colleagues and friends at the Center for Electric Power and Energy (CEE) at the Technical University of Denmark (DTU). Being surrounded by inspiring people gave me the strength I needed to never hold back. A special mention to Pierre Pinson, Vassilios Agelidis, Fabio Moret, Jiawei Wang, Alessandro D'Ambrosio, Stephan Vogel, Anne Due, Georgios Misyris, Andreas Venzke, Andrea Tosatto, Vladimir Dvorkin, Anna Schwele and Marjan Gjelaj. Also, I can't forget Mattia Marinelli and Andrea Hahmann for helping me at the beginning of my project with large amount of weather data.

The Ph.D. project led me to the very best research institutions in the world. I am honoured to have had the opportunity to join the Power System Laboratories (PSL) at the Swiss Federal Institutes of Technology (ETH), which has been made possible by the support of the Otto Mønsted foundation. For making it an unforgettable experience, thank you Stefanos Delikaraoglou, Gabriela Hug, Johanna Vorwerk, Thierry Zufferey, Connor O'Malley, Conleigh Byers, Alex Jovicic, Uros Markovic, Stavros Karagiannopoulos, Yi Wang, Deep Kiran, Jack Chin and everybody else at PSL with whom I shared hard work and steep hills.

A final, heartfelt thanks goes to Alberto Dalla Riva, Damiano Toffanin, Martina Lughi, Christine Rüegg, Peter Joss, Federico Zarelli, Matteo Baù, Roberto Benato, Lorenzo Leandro, Daniele Cadario, Nicola Mazzanti, Maria Olzai, Giovanni Galiano, Alessandro Bellini, Matteo Zampieri, Marco Ulgelmo, Gianmaria Martella, Giorgio Lambriola, Flavio Rendine,

my family and

my gingia.

Nicola

Copenhagen, Denmark, 2020

Table of Contents

Preface i

Acknowledgements iii

Table of Contents v

List of Figures vii

Abstract ix

Acronyms xi

1 Introduction 1
- 1.1 Background . . . 1
- 1.2 Research directions . . . 2
- 1.3 Contributions and list of publications . . . 4
- 1.4 Structure of the thesis . . . 6

2 Potential of dynamic thermal rating 7
- 2.1 Thermal models of components . . . 7
  - 2.1.1 Overhead lines . . . 7
  - 2.1.2 Power transformers . . . 11
- 2.2 Dynamic network rating . . . 12
  - 2.2.1 Literature review . . . 12
  - 2.2.2 Combining DTR of different components . . . 13
  - 2.2.3 Lifetime-based utilization of transformers . . . 15
- 2.3 Remarks . . . 17

3 Operational planning challenges under uncertainty 19
- 3.1 Modelling preliminaries . . . 19
  - 3.1.1 Organization of short-term electricity markets . . . 19
  - 3.1.2 Wind power and line rating uncertainty modelling . . . 21
- 3.2 Risk-averse transmission capacity allocation . . . 24
  - 3.2.1 Literature review . . . 24
  - 3.2.2 Chance-constrained optimal power flow with DTR . . . 25
- 3.3 Network-aware reserve procurement . . . 27
  - 3.3.1 Literature review . . . 27
  - 3.3.2 Zonal pre-emptive methodology . . . 28
- 3.4 Remarks . . . 30

4 Conclusion and future work **33**
4.1 Concluding remarks 33
4.2 Future work 34

Bibliography **37**

Collection of publications **43**
[Pub. A] Historical Data Analysis for Extending Dynamic Line Ratings Across Power Transmission Systems 45
[Pub. B] Day-ahead Dispatch Optimization with Dynamic Thermal Rating of Transformers and Overhead Lines 53
[Pub. C] Load Dispatch Optimization using Dynamic Rating and Optimal Lifetime Utilization of Transformers 69
[Pub. D] Chance-Constrained Optimal Power Flow with Non-Parametric Probability Distributions of Dynamic Line Ratings 77
[Pub. E] Dynamic Reserve and Capacity Allocation in Wind-Dominated Transmission Systems 89

List of Figures

2.1 Steady state vs. transient temperature rise in a "Drake" 26/7 ACSR conductor following a step change in current assuming constant weather variables. 9
2.2 Histogram of hourly DTR on high-voltage transmission lines in the Danish system. Values of DTR estimated with the solution of the proposed thermal rating in (2.3). . . 10
2.3 Steady state vs. transient hot-spot temperature rise following a step change in transformer current assuming constant ambient temperature. 12

3.1 Overview of a simplified sequential market clearing sequence. 20
3.2 Wind power forecast errors with parametric model. (a) Beta distributions and (b) variance estimation based on expected wind power. 21
3.3 Non-parametric probabilistic vs point forecasts for (a) wind power generation and (b) overhead line thermal rating. 22
3.4 Example of joint probabilistic forecast of wind power and line rating. Realizations simulated with a Gaussian copula and fitted GMM. 23
3.5 Analysis of simulated power flow with DTR over a 24h period [Pub. D]. 26
3.6 Schematic representation of the zonal pre-emptive methodology 28
3.7 Partition into 3 zones of the IEEE RTS-96 system with corresponding reserve capacity offers from generators in each zone. Highlighted part is the procured amount. Triangles indicate nodes with wind power injection. 30

Abstract

Power systems around the globe face increasing shares of renewable energy sources, whose variable and stochastic nature calls on grid operators to rethink their approach to system planning and operation. Attaining the best trade-off between security of supply and operational costs under uncertainty is closely tied to a flexible utilization of transmission systems, defined as the ability to withstand unexpected variations of power on different timescales. This thesis investigates novel solutions in this regard and proposes original decision-making support-tools that favour the large-scale integration of wind power.

Grid operators around the world are constantly under pressure, as the rate at which new generation capacity is connected to the system outpaces their ability to upgrade it with traditional grid expansion projects, such as the construction of new overhead lines. To this end, recent advances in the field of wide-area monitoring suggest how additional network capacity can be revealed in the existing systems by assessing the thermal state of critical components in real-time. Known as dynamic thermal rating, this novel approach is listed as a promising solution, although several challenges lay ahead.

While dynamic thermal rating indicates that a significant margin for higher power flows is possible, accessing this potential requires innovative solutions in the operational horizon to limit the impact of the associated weather-dependent uncertainty. Novel analytical tools presented in this thesis let grid operators take advantage of this technical solution, by proposing revisited thermal models of components and accounting for common risk-aversion levels in the allocation of transmission capacity for day-ahead energy markets. Simulation results show that significant savings can be achieved in wind-dominated power systems by allowing higher power flows, without compromising on the high standards of security of supply, which grid operators must adhere to. Additionally, key contributions show that the full potential of this approach can be maximised by applying the core physical methodology of dynamic thermal rating not only to overhead lines, but to other components as well, such as power transformers.

Contributions presented in this thesis further elaborate how a flexible utilization of transmission systems can also be achieved by focusing on operational aspects rather than novel infrastructural functionalities. The need for higher power flows can be anticipated by pre-positioning operating reserves while accounting for network limitations in a way that current sizing practices have not considered so far. An original perspective on the definition of zonal reserve capacity markets is offered in this thesis, which closely approximates ideal solutions while being compatible with fundamental properties of current electricity market structures.

Overall, the results indicate that the successful integration of large-scale wind power generation would greatly benefit from enhanced transmission system flexibility, and that increased awareness of natural phenomena and extensive cross-border cooperation would be needed to achieve it.

Acronyms

DTR Dynamic Thermal Rating

STR Static Thermal Rating

DNR Dynamic Network Rating

TYNDP Ten Year Network Development Plan

ENTSO-E Europen Network of Transmission System Operators for Electricity

SCUC Security Constrained Unit Commitment

SA Security Assessment

HVDC High Voltage Direct Current

PTDF Power Transfer Distribution Matrix

GMM Gaussian Mixture Model

CDF Cumulative Density Function

PDF Probability Density Function

CHAPTER 1

Introduction

1.1 Background

The World Energy Outlook published in 2019 by the International Energy Agency reiterates the global trend that sees electricity demand rising at a steady pace of 2% on an annual basis [1]. While CO_2 emissions from the power sector reached a record high in 2018, the falling cost of renewable energy sources such as solar and wind power generation is paving the way to a significant decarbonisation of the energy sector. The share of renewables in the additional electricity generation up to 2040 is expected to range from 50%, in a conservative scenario, to 100%, in a more sustainable and proactive course of action [1]. Ultimately, the synergy between a carbon-free power sector and the adoption of electrical energy for transportation and heating too is perceived as one of the possible concrete responses to climate change.

Projections to 2040 show that wind power installations triple with respect to the current status, covering significant shares of electricity demand in China, United States and Europe. The Offshore Wind Outlook 2019 [2] indicates that the wind resource in particular will be pivotal in Europe, where the cumulative share of on- and off-shore wind power generation is expected to cover 40% of the demand by 2050.

Growing demand for electricity on one side and newly installed power generation from renewable sources on the other, put transmission systems under an unprecedented stress, as they underpin the transition towards a carbon-free and sustainable power system. The Ten Year Network Development Plan (TYNDP) [3] issued by the Europen Network of Transmission System Operators for Electricity (ENTSO-E) highlights how the ambitious goal of reducing CO_2 emissions down to 1990's levels requires increasing grid capacity across the continent, while at the same time minimizing the societal cost of the power system transformation. Most of the initiatives that strive in this direction are related to grid reinforcements by means of AC overhead lines, which remain the predominant technology so far with 60% of the total projects. Despite the need for additional infrastructures, new overhead lines have traditionally encountered low social acceptance that hindered their deployment, whereas current alternative options such as underground cables entail significantly higher investment costs [4].

A recent report from a group of European TSOs [5] points to a second and more critical aspect of new overhead line projects, that is the ability of grid operators to match the pace at which additional generation capacity is added to the grid. The report finds that the average installation time lasts 5 years longer for grid expansion projects as opposed to the connection of new renewable energy sources. This constantly puts grid operators in the position of finding viable and cost-effective solutions for the security of supply in a shorter amount of time. Given the need for increased grid capacity and the difficulties associated with achieving it, improving utilization of existing transmission assets seems to be a necessary, even though not sufficient, measure to address such challenges.

Besides higher network capacity, the large-scale integration of wind power generation needs to factor in the uncertain nature of this energy source. While conventional thermal units can regulate their output in a highly controlled manner, renewables[1] lack the ability to do so, since they are governed by stochastic processes related to the underlaying natural phenomena. The inability to dispatch power generation from non-controllable sources is problematic in common electricity market structures, where the market clearing process and the schedule for power delivery are determined far prior to the actual realization of the uncertainty, i.e., from 12 to 36 hours in advance. This market structure was congenial in highly controllable and monopolistic power system that had to face only limited uncertainty due the variations in load demand. However, as the share of renewables in liberalized electricity markets increases, so does the frequency and the extent of deviations from scheduled operations. These deviations are remedied by grid operators with expensive out-of-market corrective actions, which worsen the economic efficiency of the system, thus mining the basis for further integration of renewables.

The evolution towards a carbon-free and sustainable power system requires increased levels of *flexibility*, which is regarded as the number one priority in The Status of Power System Transformation 2019 [6]. The term refers to the ability of a system to withstand unexpected variations of power on different timescales, without jeopardizing the security of the supply. Following the definition provided in [7], *flexibility* develops around three interdependent categories: the infrastructure, the operational framework and the role of stakeholders. Increasing network capacity in order to face the rapid diffusion of new wind power installations falls within the first category, whereas counteracting the uncertainty in electricity markets and power system operations points to the second. Clearly, these categories need to be developed in harmony as they all account for necessary aspects of the evolution of power systems, which may not be sufficient if considered independently of one another. The content of this thesis explores these two categories from the point of view of grid operators, considering the challenges they face and the solutions at their disposal.

1.2 Research directions

The research work presented in this thesis explores solutions for a flexible utilization of transmission systems, where the contribution of wind power generation is significant. In particular, the work suggests innovative models and operational practices that grid operators may resort to, considering different aspects, components and timescales of power systems.

The work is articulated in two main research directions: the first considers recent advances in the field of wide-area monitoring and it studies the possibilities of increasing network capacity in existing transmission systems; the second focuses on measures that address uncertainty in power system operation due not only to wind power generation but also novel data-driven approaches. These research directions recall the categories in the definition of flexibility, namely the infrastructural and the operational one. The interdependence between the two is made evident throughout the thesis: on the one hand, the increase in network capacity by means of additional monitoring introduces new uncertain variables, which need to be taken into account during operational planning; on the other hand, current power system and market operation need to adapt to the evolving infrastructure by allowing different sources of flexibility.

[1] Excluding hydro power and biomass

Increasing network capacity with dynamic thermal rating

The first research direction stems from the consideration that, although transmission systems would not be adequate without future reinforcements, the existing asset is considerably oversized. However, accessing the available margin for higher utilization requires a novel approach to system operations.

Maximum power flow on overhead lines is limited by a variety of factors, which can be classified according to the length of the interconnection [8]. Lines longer than 300 km are usually limited by small-signal stability, whereas for those in the range from 100 to 300 km the voltage drop is the constraining factor. For shorter lines, maximum power flow is usually determined by the line thermal rating, which reflects the ability to dissipate heat generated by Joule effect in the conductors. This property is heavily dependent on weather parameters like ambient temperature, wind speed and solar radiation, which influence convection and radiation processes. For this reason, the actual line thermal rating can be interpreted as a random variable, whose evolution is linked to the stochastic nature of weather phenomena.

Traditional overhead line dimensioning practices assume overly conservative values of the above-mentioned weather parameters in order to safeguard the grid operator from the risk of overestimating the line capacity [9]. Excessive heating would cause the line to sag beyond the clearance security limit exposing high-voltage conductors to nearby objects. Given the high risk-aversion to these eventualities, values of line thermal ratings are usually fixed or seasonal, which guarantee that the actual ones would be far greater most of the time.

Recent advances in the field of wide-area monitoring have rendered the continuous and real-time assessment of overhead lines thermal state a practical solution [10]. Therefore, rather than assuming safe values of weather parameters, grid operators can measure them in real-time and set the line thermal rating accordingly. Alternative options to determine the real-time thermal state include measuring the conductor temperature directly or indirectly by means of line tension and sag measurements. Overall, this data-driven approach is known as Dynamic Thermal Rating (DTR) and it allows grid operators to significantly increase the maximum power flow on thermally limited components. While this topic has recently gained particular interest from the research community, early works date back to the late 70s [11].

The latest ENTSO-E report on Technology for Transmission Systems [12] lists DTR as one of the promising solutions that can help improving network utilization in the evolution of the European power system. Several pilot projects have already demonstrated its effectiveness on the field [13–15], confirming it as a viable and mature technology, whose benefits would be particularly relevant for the integration of wind power. Authors of [16–18] showed that the positive correlation between the additional cooling of overhead lines and wind power generation translates into increased network capacity when needed the most. Therefore, the use of DTR would entail significant advantages for grid operators considering timescales in terms of hours, for contingency management, days, for market scheduling, and years, for system planning [19]. However, as pointed out in [12], the system-wide implementation of DTR would also require proper upgrade and adaptation of other power system components.

The contributions presented in this thesis that advance the state-of-the-art in this direction consists in solutions and tools for increasing the applicability and potential of DTR. The focus is not only on overhead lines, but on other critical components too such as power transformers, which may bear the consequences of higher network utilization.

Operational planning challenges under uncertainty

The second research direction aims at providing grid operators with novel support-tools that may compensate the increasing presence of uncertainty in power systems. While there exists a variety of uncertain quantities that may be considered, this thesis focuses on those that are crucial whenever the contribution of wind power is significant. In view of the potential that DTR has to facilitate wind power integration and given its weather-dependent stochastic nature, the uncertain quantities considered in this thesis are not only wind power injections, but thermal line ratings too. Uncertainty in power systems is directly related to common electricity market structures, where energy is traded one day prior to the actual delivery. This setup implies that grid operators face the challenge of making critical decisions based on predicted values that inevitably entail approximations and partial descriptions of the underlying stochastic processes. Therefore, flexibility during real-time operations is necessary to cope with deviations arising from an incomplete representation of the system.

The increase in network capacity offered by DTR certainly favours system operations in this direction by allowing higher power flows. However, the adoption of DTR also suggests that uncertainty is not confined to the generation and consumption assets, but extends also to the transmission one. Therefore, the increased network capacity has to be traded-off against higher levels of uncertainty in order to safeguard the high standard of security. The contributions in this regard focus on analytical methods developed for maximising the benefits of DTR, while controlling the associated risks and considering potential synergies with other uncertain variables

As the share of wind power generation increases, so does the need for sufficient and readily available back-up power, i.e. reserves, that would balance out any short-term deviations during real-time operation [20]. Reserves are generally classified as contingency, which are deployed in case of emergencies, or operating, which are needed to regulate the system under fluctuations around a scheduled operating point [21]. The latter in particular is necessary to integrate intermittent renewable sources in electricity markets, which are cleared well prior to the realization of the underlying stochastic processes. Current reserve sizing practices, however, fail to address important aspects such as limitations of the transmission system that would prevent the accessibility of these resources. Since the cost of procuring reserves falls on grid operators entirely, their optimal allocation is of primal importance to limit the cost of wind power integration. Considering this aspect of flexibility, the contributions listed in this thesis propose original reserve allocation practices that take grid limitations into account, while still being compatible with existing market structures. This latter aspect is deemed to be fundamental, as the evolution of power systems depends not only on the technical feasibility of novel solutions, but also on the appealing that these have on power system and market operators.

1.3 Contributions and list of publications

The main contributions presented in this thesis are the following:

i Reformulation of existing overhead line thermal model in order to account for radial temperature drop in high-voltage conductors.

ii Analysis of possible gradations of DTR for large scale implementation with varying levels of monitored variables.

iii Formulation of a DC-OPF algorithm that includes DTR of both overhead lines and power transformers. The algorithm is formulated as a convex optimization problem with second-order conic constraints.

iv Study of seasonalities in overhead lines and transformers thermal ratings considering weather data from an actual power system.

v Formulation of a lossy DC-OPF algorithm that includes a lifetime-based utilization of power transformers considering different loading strategies.

vi Formulation of a risk-averse energy and reserve co-optimization algorithm based on DC-OPF and chance constraints. The algorithm can be used to set line capacities during operational planning taking into account non-parametric predictive distributions of DTR and wind power generation.

vii Testing Gaussian distributions for modelling DTR probabilistic forecast derived with quantile regression algorithms.

viii Formulation of a decision-making support-tool for redefining the boundaries of zonal reserve capacity markets and setting zonal reserve requirements based on total expected operating costs. The methodology can also serve to allocate available transmission capacity between day-ahead and balancing market stages.

These contributions have been proposed in the following publications:

[**Pub. A**] N. Viafora, J. G. Møller, R. A. Olsen, A. S. Kristensen and J. Holbøll, "Historical Data Analysis for Extending Dynamic Line Ratings Across Power Transmission Systems," *2018 IEEE International Conference on Probabilistic Methods Applied to Power Systems (PMAPS)*, Boise, ID, 2018, pp. 1-6.

[**Pub. B**] N. Viafora, K. Morozovska, S.H.H. Kazmi, T. Laneryd, P. Hilber, J. Holbøll, "Day-ahead dispatch optimization with dynamic thermal rating of transformers and overhead lines", *(2019) Electric Power Systems Research*, 171, pp. 194-208.

[**Pub. C**] N. Viafora, J. Holbøll, S. H. H. Kazmi, T. H. Olesen and T. S. Sørensen, "Load Dispatch optimization using Dynamic Rating and Optimal Lifetime Utilization of Transformers," *2019 IEEE Milan PowerTech*, Milan, Italy, 2019, pp. 1-6.

[**Pub. D**] N. Viafora, S. Delikaraoglou, P. Pinson, J. Holbøll, "Chance-constrained optimal power flow with non-parametric probability distributions of dynamic line ratings", *(2020) International Journal of Electrical Power and Energy Systems*, 114, art. no. 105389.

[**Pub. E**] N. Viafora, S. Delikaraoglou, P. Pinson, G. Hug, J. Holbøll, "Dynamic Reserve and Capacity Allocation in Wind-Dominated Transmission Systems", submitted to *IEEE Transactions on Power Systems*

Other publications have not been included in this thesis being outside the scope of this thesis or still partially completed at the time this thesis is submitted for approval:

[Pub. F] K. Morozovska, W. Naim, N. Viafora, E. Shayesteh, and P. Hilber, "A framework for application of dynamic line rating to aluminum conductor steel reinforced cables based on mechanical strength and durability", *(2020) International Journal of Electrical Power and Energy Systems*, 116, art. no. 105491.

[Pub. G] N. Viafora, S.H.H. Kazmi, T.H. Olsen, T.S. Sørensen, J. Hølboll, "Grid Reinforcement Planning for Wind Power Integration with Dynamic Network Rating", *Working paper*.

1.4 Structure of the thesis

The contributions included in this thesis are organized as shown in Table 1.1. The chosen classification serves the purpose to present the research work considering two main categories of flexibility in power systems: the infrastructural and the operational.

Table 1.1: Classification of the contributions in publications and chapters

	Chapter 2	**Chapter 3**
[Pub. A]	i - ii	-
[Pub. B]	iii - iv	-
[Pub. C]	v	-
[Pub. D]	-	vi - vii
[Pub. E]	-	viii

Chapter 2 This chapter is centered around the infrastructural aspect of flexibility. Given the need for increasing network capacity and the difficulties associated with achieving it, this chapter focuses on the potential that DTR systems have for unveiling hidden capacity as a way to support wind power integration. This potential is assessed with weather data simulated across an actual transmission system in combination with historical load demand and wind generation data. Power systems and day-ahead market operation is considered in a deterministic fashion in order to focus on the synergies between overhead lines and transformers thermal ratings under various weather patterns throughout the year.

Chapter 3 The focus in this chapter is on the operational aspect of flexibility, in particular the operational planning phase of power systems where grid operators face critical decisions for the efficient functioning of system and market operations. The core aspect in this case is how to deal with uncertainty, both in wind power generation and DTR systems. The chapter reviews common electricity market structure and uncertainty modelling before presenting key contributions on the risk-averse allocation of transmission capacity and operating reserves in systems with high share of wind power.

Chapter 4 This chapter draws final conclusions and traces future research directions stemming from the results achieved in this thesis.

CHAPTER 2

Potential of dynamic thermal rating

The current-carrying capability of transmission systems is as vary and diverse as the weather conditions they are exposed to spanning over hundreds of kilometers. Asking these systems to provide more than they were originally designed for is possible under the condition that new information on their real-time state is made available to grid operators and decision-makers. Starting from a discussion on state-of-the-art thermal models in Section 2.1, this chapter lays out the potential that DTR has to unveil additional network capacity in the existing infrastructure. This first step offers the opportunity to introduce a modified version of a popular overhead line thermal model presented in [Pub. A], which considers temperature distributions within conductors and the consequent impact on thermal rating. Once the relation between weather variables and operating temperature of components is assessed, Section 2.2 presents [Pub. B], where the impact of DTR applied to a network of overhead lines and transformers is evaluated considering different seasonal patterns. Effects of higher utilization on power transformers are discussed together with a novel methodology proposed in [Pub. C], that allows to load such components based on cumulative lifetime utilization, rather than standard nameplate ratings. Lastly, Section 2.3 concludes the chapter by collecting the most relevant assumptions and discussing the main findings.

2.1 Thermal models of components

The following sections elaborate on the core physical aspect of DTR, i.e., the ability to load components depending on their temperature, rather than pre-specified quantities that are indirectly related to it. Ratings are commonly expressed in terms of current or power, however, these inputs are only part of the equation when determining the operating temperature. Surrounding environmental conditions and thermal dynamics also play a key role and their real-time knowledge can be used to safely increase power flows.

2.1.1 Overhead lines

Two main models are regarded as the state-of-the-art when considering the thermal dynamics of overhead transmission lines: the IEEE [22] and the Cigrè [9]. Both approaches rely on similar analytical formulations that are centered around the heat balance equation (2.1). This fundamental relationship links the operating temperature of conductors to the current flow and the surrounding environmental conditions. It is expressed as a first order differential equation, i.e.,

$$q_J + q_S - q_C - q_R = C_{\text{th,ohl}} \frac{d\vartheta_{\text{av}}}{dt}, \tag{2.1}$$

where the right-hand-side represents the evolution of temperature ϑ_{av} over time scaled by the thermal capacitance $C_{\text{th,ohl}}$ and the left-hand-side the per-unit-length thermal energy balance of the

conductor. While there may be several more heating and cooling mechanisms q, standard thermal rating guidelines narrow them down to the these four: Joule heating, solar heating, convective cooling and radiative cooling. A detailed analytical description of each term can be found in [9], whereas a synthetic one is presented as follows:

Joule heating (q_J) — The main source of heat generation in the conductors is caused by the flow of current and the corresponding power losses. It is the only term in (2.1) that depends on the current and therefore it represents the link between the electrical and the thermal quantities. An accurate calculation of power losses requires considering temperature-dependent electrical resistivity, skin effect for alternating current as well as the type of conductor.

Solar heating (q_S) — The global solar radiation that reaches the conductor causes an exogenous temperature increase, which may become significant depending on the geographical location, seasonal cycles or particular conditions, such as near-zero wind speed, when other cooling terms are drastically reduced. The main source of uncertainty in this term is given by cloud coverage, whose rapid variations can change the amount of direct radiation reaching the conductors. Specific material properties as the absorptivity of the conductors also affect the contribution of this term.

Convective cooling (q_C) — The principal cooling mechanism on overhead lines is convection driven by the air flow in the proximity of conductors. This depends on the difference between conductor surface and ambient temperature in addition to a variety of meteorological parameters and surface properties of the conductors. Wind speed and wind direction, however, are the most important factors to be considered as well as the most uncertain and hard to predict.

Radiative cooling (q_R) — Part of the heat generated in the conductor is dispersed through thermal radiation emitted from the surface. This process is highly dependent on the difference between conductor surface and ambient temperature together with dimensions and material properties of the conductor.

An accurate estimation of the operating temperature under varying loading patterns and environmental conditions requires a detailed modelling of all the heating and cooling mechanisms that intervene in the heat balance equation (2.1), including the influence of the thermal capacitance $C_{\text{th,ohl}}$. This latter parameter models the thermal inertia of the conductors: the larger the value, the slower the temperature rate of change. Tracking the evolution of conductor temperature over time can be achieved with a discretized version of (2.1), which is solved for the operating temperature ϑ_{av} using a sufficiently small time step, usually in the order of few minutes. Clearly, (2.1) has local validity, as it depends on quantities that may vary greatly within a short space. Therefore, the operating temperature has to be evaluated at several locations in order to identify the hot-spot which eventually limits the entire line capacity.

This approach highlights the margin for higher utilization in real-time, however, it is impractical for operational and long term planning studies, where grid operators need to calculate expected ratings that fit a variety of conditions. To this end, the steady-state version of (2.1) is commonly adopted, where setting the right-hand-side to 0 represents a condition of thermal equilibrium.

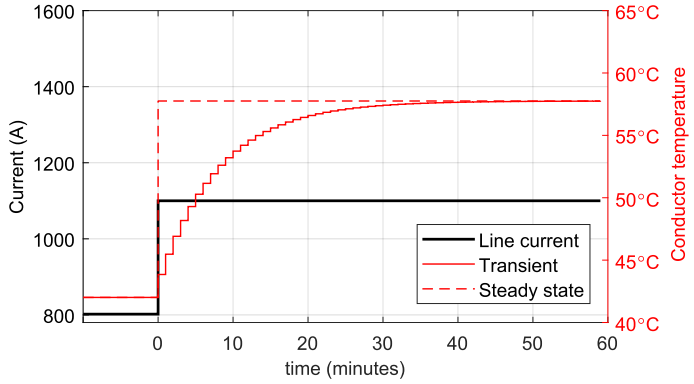

Figure 2.1: Steady state vs. transient temperature rise in a "Drake" 26/7 ACSR conductor following a step change in current assuming constant weather variables.

In this case, a maximum operating temperature is set *a priori* and the following equation is solved for the current appearing in the Joule heating term q_J, i.e.,

$$q_J + q_S - q_C - q_R = 0. \tag{2.2}$$

The result represents the maximum current that can be sustained for a indefinite period of time without violating the temperature criterion, provided that environmental conditions remain the same. Grid operators usually follow this approach to set seasonal thermal ratings, assuming highly conservative values of the surrounding weather condition. The Danish grid operator, Energinet, provided some indications in this regard, which have been discussed in [Pub. A]: seasonal wind speed values fall in the first quantile of the distribution of historical realizations, while wind direction is not considered; ambient temperature values correspond to the top 90-*th* quantile and solar radiation to the 99-*th*. In agreement with [23], the resulting Static Thermal Rating (STR) leaves out a significant potential for higher power flow.

In order to access this hidden potential, a common approach is to consider hourly averaged values of selected weather parameters, typically wind speed, wind direction, ambient temperature and solar radiation in combination with the steady-state thermal model. This is possible due to the small thermal inertia of the conductor, which quickly reaches its steady-state temperature. The illustrative example in Fig. 2.1 shows the comparison between the steady-state and the transient model considering a "Drake" 26/7 ACSR conductor subject to a step change in current. The difference between the two models is negligible at the end of the 60-minutes interval, indicating that this approach is applicable whenever power flows are defined on an hourly basis. For any other application that needs to consider sub-hour time periods, the use of the full differential equation is advised. For a discussion on how the rating estimation varies depending on the time resolution used in the discretization, the reader is referred to [24].

Accounting for radial temperature drop

Building upon the steady-state version of the Cigrè model [9], [Pub. A] presents a modified version which addresses a novel modelling aspect. As mentioned in [25–28], there may be a significant temperature difference between the core and the surface, when operating the conductor at high current densities. Core temperature is particularly critical in ACSR conductors, as the steel core is responsible for bearing the tension of the line. Exceeding the design temperature limit may result in unacceptable thermal dilatation of the conductor with the consequent violation of clearance

security limits. Surface temperature, instead, is a key parameter in the estimation of convective and radiative cooling, thus considering the average temperature in these calculations leads to an overestimated line capacity.

In order to account for these aspects, [Pub. A] introduces two additional variables in the solution of the steady-state heat balance equation: the surface temperature ϑ_s and the average cross-sectional temperature ϑ_{av}, while specifically imposing the maximum operating value to the core ϑ_c. Instead of solving (2.2) for the current, the proposed methodology requires solving the following system of non-linear equations

$$q_J(I_{\text{ohl}}^{\max}, \vartheta_{\text{av}}) + q_S - q_C(\vartheta_s) - q_R(\vartheta_s) = 0, \tag{2.3a}$$

$$\vartheta_c - \vartheta_s = \Delta\vartheta_{\text{cs}}(I_{\text{ohl}}^{\max}, \vartheta_{\text{av}}), \tag{2.3b}$$

$$\vartheta_c + \vartheta_s = 2\vartheta_{\text{av}}, \tag{2.3c}$$

where the variables are: maximum admissible current $I_{\text{ohl}}^{\max}$, surface temperature ϑ_s and average temperature ϑ_{av}. In addition to the steady-state heat balance (2.3a), the system accounts for the difference between core and surface temperature in (2.3b), where $\Delta\vartheta_{\text{cs}}$ is an analytical expression presented in [9] that depends on dimensions and material properties of the conductor other than current and average temperature. Lastly, (2.3c) defines a linear relation between conductor temperatures at different locations on the cross-section.

[Pub. A] and [Pub. B] further elaborate on the modelling details and conclude that, although this approach is not expected to consider the actual temperature distribution within conductors, it provides a simplified way to account for the radial temperature drop by means of readily available expressions that are included in the guidelines for thermal rating calculations. By imposing the temperature limit on the hottest point of the cross-section, i.e., the core, the thermal rating derived from the solution of (2.3) is more conservative than (2.2), especially under high wind and high current conditions, where the difference between core and surface temperature is more prominent. Nevertheless, as shown in Fig. 2.2, the expected value of the distribution of hourly ratings is still more than 50% higher than the seasonal line ratings, based on simulated weather data across the

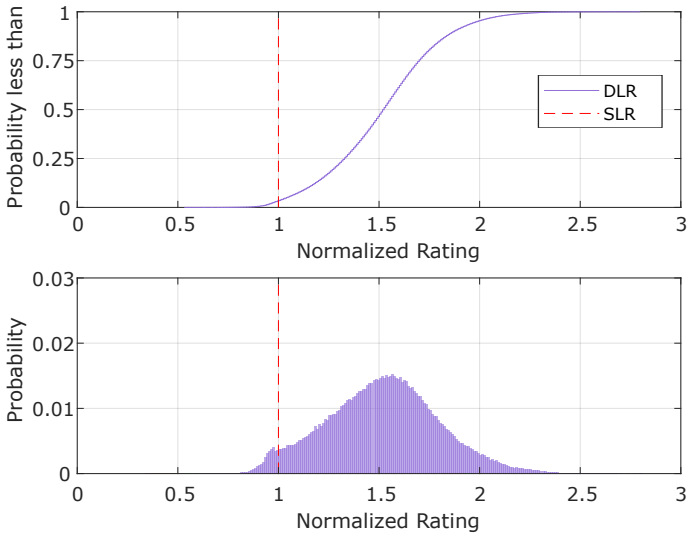

Figure 2.2: Histogram of hourly DTR on high-voltage transmission lines in the Danish system. Values of DTR estimated with the solution of the proposed thermal rating in (2.3).

Danish power system. Furthermore, DTR are greater than static ratings by at least 10% nearly 90% of the time and by at least 30%, 75% of the time, thus indicating a consistent margin for higher utilization.

Gradations and sensitivity analysis

The large amount of variables that affects overhead line thermal rating motivated the work in [Pub. A] to consider simplified versions, where only a subset of them is taken into account. The different nature of weather variables involved implies that some may be more straightforward to measure and predict than other. For example, this is the case of wind direction, which although guidelines in [9] indicate as significantly relevant, its accurate and reliable estimation poses considerable challenges given its high variability. At the other end of the spectrum, ambient temperature is a slow varying and spatially uniform variable, which still affects line thermal ratings, but does not require measurements as distributed and extensive as those for wind speed and direction. Therefore, [Pub. A] studies a series of gradations of DTR, where the thermal model is used in combination with groups of variables. It is concluded that accounting for the full spectrum of inputs guarantees the highest increase in rating, but at the cost of dealing with higher variability. Alternative options that purposely leave out the most aleatory contributions, would still entail significant benefits for grid operators.

2.1.2 Power transformers

While the thermal rating of overhead lines is predominantly dependent on the temperature of conductors, two critical parts of transformers need to be modelled: the top layer of cooling oil in the reservoir tank and the low-voltage winding hot-spot. The previous section discussed how the unexpressed potential for higher ratings on overhead lines is mainly owed to the conservative assumptions on environmental conditions. When considering DTR of transformers, instead, a second determinant factor to take into account is the larger thermal inertia, which allows to cyclically load this component beyond nameplate ratings, without exceeding recommended operating temperatures.

Section 2.2 of [Pub. B] reviews in detail the IEEE Loading Guide [29], which has been adopted for transformer DTR in this thesis. What follows is a discussion on the main modelling assumptions that have been introduced with the purpose of incorporating transformer thermal dynamics in convex optimization problems. Top-oil ϑ_{top} and hot-spot ϑ_{hst} temperatures are modelled in [29] with the following first-order differential equations,

$$-\vartheta_{\text{top}} + \vartheta_{\text{amb}} + \vartheta_{\text{u}} \left(I_{\text{trf}}^{2\nu}\right) = \tau_0 \frac{d\vartheta_{\text{top}}}{dt}, \tag{2.4}$$

$$-\vartheta_{\text{hst}} + \vartheta_{\text{hu}} \left(I_{\text{trf}}^{2\mu}\right) + \vartheta_{\text{top}} = \tau_h \frac{d\vartheta_{\text{hst}}}{dt}, \tag{2.5}$$

where τ are the thermal time constants, ϑ_{amb} the ambient temperature, ϑ_{u} and ϑ_{hu} are the steady-state top-oil temperature rise over ambient temperature and hot-spot rise over top-oil, respectively. These values are a function of the transformer per-unit load I_{trf}, where the empirical factors ν and μ depend on cooling mode of the transformer. Setting them to 1, restricts the validity of the model to a particular class of transformers, however, it allows to handle these expressions with quadratic constraints that do not compromise the sought-after convexity property of optimization problems. With this decision, the contribution in [Pub. B] prioritizes the computational aspect over

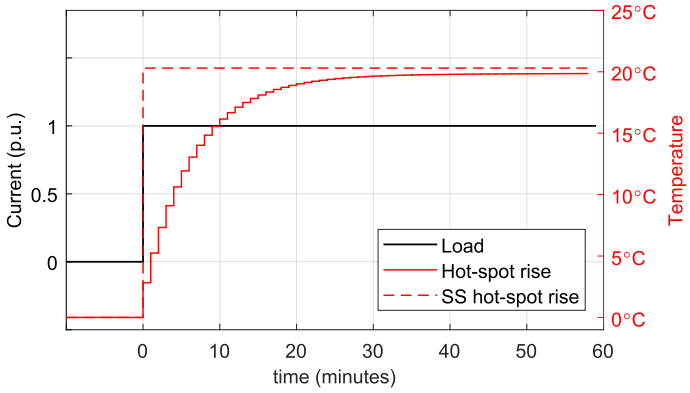

Figure 2.3: Steady state vs. transient hot-spot temperature rise following a step change in transformer current assuming constant ambient temperature.

the accuracy, while still conveying novel insights in the potential of DTR applied to transformers. The final discretized version of (2.4) and (2.5) used in this thesis to express the time-dependent evolution of top-oil and hot-spot temperatures are formulated as

$$\vartheta_{\text{top}}(t) = K_1 I_{\text{trf}}^2(t) + K_2 \vartheta_{\text{amb}}(t) + (1 - K_2)\vartheta_{\text{top}}(t-1) + K_3, \tag{2.6}$$

$$\vartheta_{\text{hst}}(t) = \vartheta_{\text{hr}} I_{\text{trf}}^2(t) + \vartheta_{\text{top}}(t) \tag{2.7}$$

where K_i are constants depending on the transformer type and the time step used in the discretization, i.e., 1 hour. Note that as opposed to top-oil, hot-spot temperature dynamics evolve at a higher rate due to a smaller time constant τ_h and are fully extinguished after 60 minutes. Therefore, since the purpose of [Pub. B] is to incorporate these models in hourly load dispatch optimization problems, the steady-state version of (2.5) is adopted, where temperature rate of change is set to 0. Figure 2.3 illustrates the comparison between the steady-state and the dynamic hot-spot temperature model when considering a step change in current. It stands out as the difference between the two approaches is minimal at the end of the 60-minutes interval.

To summarize, accounting for thermal dynamics in transformers offers increased levels of flexibility, provided that critical top-oil and hot-spot temperature evolution are monitored. As in the case of overhead lines, grid operators usually assume worst-case ambient condition in order to safeguard the utilization of these assets. However, the use of simulated weather conditions and realistic ambient air temperature values shows that a significant margin for higher utilization can be harvested from these components.

2.2 Dynamic network rating

Having introduced the principles of DTR in both overhead lines and transformers, this section presents the methodology proposed in [Pub. B], which, for the first time, considers the joint DTR of these components in a market clearing algorithm. Building upon the same methodology, [Pub. C] proposes a lifetime-based utilization of transformers, where not only temperature but also aging dynamics are accounted for.

2.2.1 Literature review

Operating a power system based on the temperature of components rather than standard power flow limits affects the dispatch of generators and daily market operations, as the available network

capacity varies during the day [30, 31]. Increased network capacity is beneficial under many circumstances such as generator re-dispatch, line outages and grid congestions, although the use of DTR requires modifying current market clearing algorithms.

In this vein, the flexibility of DTR is incorporated into a N-1 Security Assessment (SA) and a Security Constrained Unit Commitment (SCUC) algorithm in [32] and [33], respectively, considering a set of predetermined contingencies where the value of DTR would come into play. The impact of DTR on market operation is also studied in [34], where it is concluded that although higher losses should be expected from a system-wide utilization of this technology, the benefits would still outweigh the costs due to the increased availability of low-cost renewable energy. Given the ability of DTR to significantly increase network capacity, [35, 36] consider this technology as a viable option to postpone grid reinforcements in highly congested networks, while [37] includes it in a transmission expansion planning problem.

Given the significantly higher power flows that DTR allows on overhead lines, the system-wide implementation would also require proper upgrade and adaptation of other power system components. To this extent, [38] considers the potential of dynamically rating power transformers and underground cables too. Indeed, the conservatism used for overhead lines is typically adopted for other components as well. Authors of [39, 40] focus on DTR applied to transformers, whereas in [41] the benefits of Dynamic Network Rating (DNR), i.e., the combined application of DTR on several components, are investigated concluding that the limiting asset in a congested power system is likely to change depending on the season.

While [41] focuses on estimating weather-dependent network rating in distribution systems based on predicted operating conditions, [Pub. B] incorporates thermal models discussed in Section 2.1 into a day-ahead market clearing algorithm. The novelty consists in showing how a coordinated approach can increase network capacity considering the synergies between various components. Furthermore, to the best of our knowledge, no loading criteria has ever considered the temperature-dependent aging of transformers as in [Pub. C]. The following sections elaborate on the proposed methodologies and discuss their main implications.

2.2.2 Combining DTR of different components

The proposed methodology is based on a DC-OPF algorithm in a multi-period formulation, which is required to account for the temporally coupled constraints on the transformer rating. Unlike overhead lines, whose hourly ratings are independent from one another, transformer top-oil thermal dynamics span over several hours, thus they need to be taken into account whenever the loading is temperature-based. The implication is that dynamic transformer ratings cannot be defined *a priori*, since they depend in particular on the loading pattern they have been through, other than the environmental conditions such as ambient temperature. Instead, due to their shorter thermal time constant discussed in Section 2.1, overhead lines do not require this modelling approach, since their rating in one hour would not affect the following. Assuming hourly averaged weather forecasts, DTR for transmission lines are pre-calculated with steady-state thermal model (2.3) and passed on to the optimization problem as time-dependent parameters.

In the formulation that follows, unit commitment constraints are not included. This limitation, however, is not expected to reduce the applicability and generality of the proposed methodology since those constraints that model transformer and overhead lines thermal ratings could be

easily implemented with other assumptions on the modelling of the power system. Furthermore, no uncertainty is considered in the following formulation neither in the weather forecasts nor in wind power generation. This limitation is addressed in Chapter 3, where support-tools for decision-making problems under uncertainty are presented. While the proposed methodology is formulated in detail in [Pub. B], a compact version with properly defined $\boldsymbol{h}$ and $\boldsymbol{q}$ matrices for equality and inequality constraints is formulated as

$$\min_{\boldsymbol{\xi}_t} \quad \sum_t \boldsymbol{c}^\top \boldsymbol{\xi}_t \tag{2.8a}$$

$$\text{s.t.} \quad \boldsymbol{h}_1^\top \boldsymbol{\xi}_t - \boldsymbol{h}_{0,t} = 0 \qquad \forall t \in \mathcal{T}: \qquad \textit{Power balance}, \tag{2.8b}$$

$$\boldsymbol{q}_1^\top \boldsymbol{\xi}_t - \boldsymbol{q}_1'^\top \boldsymbol{\xi}_{t-1} - \boldsymbol{q}_{0,t} \leq 0 \qquad \forall t \in \mathcal{T}: \qquad \textit{Operational limits}, \tag{2.8c}$$

$$\sum\nolimits_{\tau=1}^{t} \boldsymbol{q}_2^\top \boldsymbol{\xi}_\tau^2 - \boldsymbol{q}'_{0,t} \leq 0 \qquad \forall t \in \mathcal{T}: \qquad \textit{Thermal dynamics} \tag{2.8d}$$

where $\boldsymbol{\xi}_t = \{p_g, d_n^{\text{sh}}, w_j\}_t$ collects the DC-OPF decision variables for each time step t, i.e., scheduled power output, nodal load shedding and dispatched wind power. The objective function accounts for the total generation cost over a 24-hours period including a penalty term on the load not supplied in order to guarantee feasibility in any condition. Constraints (2.8b) model power system balance at each time step, whereas (2.8c) collects other operational limits such as power generation upper and lower bounds, generator ramp rates and power flow limits modelled with the Power Transfer Distribution Matrix (PTDF) matrix [42]. Note that the term $\boldsymbol{q}_{0,t}$ is dependent on the time index t as it includes the time-varying pre-calculated DTR for overhead lines and available wind power generation. Lastly, constraints (2.8d) model the transformer top-oil and hot-spot temperature dynamics, whose hourly discretization is provided in Section 2.1.

Besides a linear objective function, affine equality and inequality constraints that are standard in a DC-OPF algorithm, problem (2.8) includes conic quadratic inequality constraints, which model transformer thermal dynamics. These temporally coupled constraints express the effect of high thermal inertia, which can be used to cycle the utilization of these components at higher operating temperatures.

Mutual dependencies

Testing the proposed methodology in a RTS-24 bus system [43] with simulated weather data and additional wind power generation showed that substantial savings can be achieved in the total generation costs, when the full flexibility is in place. The combined DTR of overhead lines and transformers facilitates the dispatch of wind power, as opposed to a reference case with statically rated components. This is particularly evident when simulating highly congested systems, where upgrading either lines or transformers might not be sufficient to deliver higher power flows across the network. In this regard, it is shown that the potential of DTR on overhead lines may not be fully expressed unless transformers are also considered and vice versa.

Seasonal effects

The mutual dependencies are more evident during the winter season due to positively correlated line ratings and wind power generation levels. The available data also showed a significant negative correlation between wind speed and ambient temperature, which strengthens the synergy between thermal ratings of overhead lines and transformers. When high wind speed occurs in conjunction with low ambient temperatures, both overhead lines and transformer ratings increase.

Although the reverse case during the summer period shows a narrower margin for higher capacity, the increase with respect to the reference case is still significant, given the highly conservative assumptions on static ratings. Results are based on weather, load demand and wind generation profiles mapped from the Danish power system.

Cyclic loading

The main advantage of incorporating transformer thermal dynamics into system operation is that higher asset utilization can be synchronized with daily peak load demand. By running the component at low-load during the night, top-oil temperature cools down in preparation for the higher loading patter occurring in the central hours of the day. This loading strategy allows grid operators to face growing wind power generation in the system with minimal infrastructural investments, thus offering the possibility to postpone necessary grid reinforcements.

2.2.3 Lifetime-based utilization of transformers

Unlike overhead lines, transformers undergo significant and quantifiable temperature-dependent degradation over the course of their service. Although this process is influenced by a variety of factors, hot-spot temperature is generally regarded as a good indicator of the aging rate. The aging considered in [Pub. C] is based on the IEEE model [29], i.e.,

$$\Psi(t) = \int_{t_0}^{t} \psi(\tau)\, d\tau, \qquad \text{with} \qquad \psi(t) = e^{\left(\frac{15000}{110+273} - \frac{15000}{\vartheta_{\text{hst}}(t)+273}\right)} \tag{2.9}$$

where $\Psi(t)$ represents the cumulative lifetime utilization of the asset up until time t and $\psi(t)$ the aging rate expressed as an exponential function of the hot-spot temperature ϑ_{hst}, which is modelled with (2.7). Given the cycling patterns at higher operating temperature entailed by DTR, it is reasonable to investigate the consequences of such a loading strategy on the lifetime utilization of transformers. The benefits of increased power flow would need to be traded-off against a shortened lifetime and the anticipated cost of replacement units. While this first consideration may apply to grid operators that manage aging infrastructures, utilities in the wind power sector face the opposite problem. For those applications with a limited asset lifetime, such as offshore wind farm systems, any overdimensioned component with abundant residual lifetime at the end of the designed period translates into extra weight and extra capital costs for newly built offshore platforms. In this case, it is preferred to maximize the utilization of the components so that their designed lifetime fits the planned window of operation.

The novel methodology proposed in [Pub. C] builds upon [Pub. B] and addresses these topic by incorporating both thermal and aging dynamics into a multi-period DC-OPF. Three main aspects differentiate the two studies:

1. [Pub. C] does not include DTR on overhead lines, as it is assumed that the main bottleneck lies on the transformer;
2. [Pub. C] accounts for power losses in the system by means of an iterative approach based on quadratic constraints;
3. [Pub. C] includes piece-wise linearized exponential aging models that are used to infer the temperature-dependent aging during system operations.

The proposed iterative methodology is compactly formulated for iteration η as

$$\min_{\boldsymbol{\xi}_t} \quad \sum_t \boldsymbol{c}^\top \boldsymbol{\xi}_t \tag{2.10a}$$

$$\text{s.t.} \quad \boldsymbol{h}_1^\top \boldsymbol{\xi}_t - \boldsymbol{h}_{0,t} = 0 \qquad \forall t \in \mathcal{T}: \qquad \textit{Power balance}, \tag{2.10b}$$

$$\boldsymbol{q}_1^\top \boldsymbol{\xi}_t - \boldsymbol{q}_1'^\top \boldsymbol{\xi}_{t-1} - \boldsymbol{q}_{0,t} \leq 0 \qquad \forall t \in \mathcal{T}: \qquad \textit{Operational limits}, \tag{2.10c}$$

$$\sum\nolimits_{\tau=1}^{t} \boldsymbol{q}_2^\top \boldsymbol{\xi}_\tau^2 - \boldsymbol{q}'_{0,t} \leq 0 \qquad \forall t \in \mathcal{T}: \qquad \textit{Thermal dynamics}, \tag{2.10d}$$

$$\sum\nolimits_{\tau=1}^{t} \boldsymbol{q}_2'^\top \boldsymbol{\xi}_\tau^2 - \boldsymbol{q}''_{0,t} \leq 0 \qquad \forall t \in \mathcal{T}: \qquad \textit{Aging dynamics}, \tag{2.10e}$$

$$\boldsymbol{q}_2''^\top \boldsymbol{\xi}_t^2 - \boldsymbol{q}_1'' \boldsymbol{\xi}_t^1 - \boldsymbol{q}_0'''^{(\eta)} \leq 0 \qquad \forall t \in \mathcal{T}: \qquad \textit{Power losses} \tag{2.10f}$$

where $\boldsymbol{\xi}_t = \{p_g, d_n^{\text{sh}}, w_j, \gamma_\ell\}_t$ collects the same DC-OPF decision variables as in [Pub. B] adding branch power losses γ_ℓ, whereas $\boldsymbol{h}$ and $\boldsymbol{q}$ are properly defined constant matrices that describe the structure of the problem. For the detailed problem formulation, [Pub. C] offers an exhaustive description.

Accounting for power losses estimation in a DC-OPF algorithm has gathered particular attention in the literature. The method adopted in this study is inspired by [44], where quadratic inequality constraints are used to model branch power losses as additional nodal load demand in the system. However, as discussed in [45] and more recently in [46], this approach might prove wrong under some circumstances, where, due to negative locational marginal prices, the solver introduces additional fictitious losses. To compensate for this effect, [Pub. C] adopts a method which iteratively bounds the losses by restricting the power flow solution. Although accounting for losses in the solution of the DC-OPF, further research is required to assess the generality of the method.

Higher transformer rating

The proposed methodology is tested in the RTS-24 bus system [43], assuming that one transformer in a strategic location is equipped with DTR. Three loading criteria are then considered based on: 1) standard nameplate ratings, 2) operating temperature, 3) cumulative lifetime utilization and a higher temperature limit. Simulation results show that the utilization of the transformer in the third case can safely exceed the other two, while in the first case the operating temperature is far from the maximum limit, even though the component runs at full nameplate power. Provided that the lifetime utilization does not violate the operator requirements and that security limits suggested by international standards are not breached, loading criteria 3 unlocks extra capacity by operating the component at higher temperatures.

Collateral effects

A first direct consequence of higher utilization is that the aging process is accelerated, although the proposed methodology allows the operator to manage this aspect by adjusting the temperature limit based on the health status of the component. A second one is that higher losses should be expected, not only in the thermally rated component, but elsewhere too, given higher power flows across the system. The findings of this study are in agreement with the literature, where it is argued that the benefits still outweigh the costs. However, it should be noted that since power losses are modelled as additional load demand, their cost has been only indirectly accounted for in the total generation costs. Grid operators are responsible for the energy efficiency of their networks,

therefore there might be a direct interests in limiting higher losses with *ad hoc* measures. Further research should evaluate a cost-benefit analysis in the long term.

To conclude, optimizing the expected duration of components by limiting their size and pushing their utilization can be an advantage for limited lifetime assets such as off-shore platforms for wind power, where weight savings are prioritized. Instead, grid operators that need to increase the utilization of their network while controlling the asset health, may rely on this methodology with more restrictive requirements in terms of cumulative lifetime consumption.

2.3 Remarks

The assessment of the potential of DTR begins from the understanding of core physical aspects that govern thermal dynamics of single components and considers their impact on the whole transmission system. The work in [Pub. A] shows how modelling the temperature distribution of conductors can help grid operators prevent extreme conditions on overhead lines, by imposing operating temperature limits on the most vulnerable part of conductors. Although this novel approach may require further testing and verification, it provides a robust model for DTR that enables higher utilization of overhead lines, based on widely known and accepted guidelines in the industry. While it is shown that higher current-carrying capability can be achieved in transmission systems, accessing this potential on a large scale may pose significant challenges for grid operators. In this vein, the gradations of DTR studied in [Pub. A] offer simplified approaches, which ease the adoption and assimilation of this technology in power systems.

The margins for higher power flows are certainly more evident on overhead lines, however, the same principle can be applied to other components as well. The key contribution in [Pub. B] shows that in order to enable higher utilization of transmission systems, it may be necessary to upgrade not only overhead lines, but other strategical components too, while taking advantage of dependencies between them. Long term collateral effects on lifetime utilization of transformers can be managed with the methodology proposed in [Pub. C].

Overall, one of the most appealing arguments in favour of DTR is the ability to quickly upgrade transmission systems, considered that the construction of new traditional overhead lines is increasingly more difficult and time demanding. Unveiling extra capacity in a relatively short amount of time would grant system operators enough flexibility to postpone critical reinforcements in the long term. However, accurately assessing the potential of DTR requires further research in terms of its applicability. Large-scale and geographically diverse power systems pose more challenges to the implementation of DTR, given varying environmental conditions and different correlation patterns with renewable energy sources. Furthermore, the assumptions of thermally limited components should be dropped, thus evaluating the benefits of DTR from a more complete power system perspective.

In conclusion, the main assumptions and key points of each publication presented so far have been listed in Table 2.1. This chapter studied the potential of DTR with a strong assumption of perfectly known weather and wind power forecasts, however, assessing the value of DTR for grid operators cannot overlook the increasing uncertainty introduced in daily system operations. The next chapter addresses this aspect and takes a closer look at operational planning challenges faced by grid operators, where critical decisions for the correct functioning of power systems are made considering the stochastic nature of data-driven technologies and wind power generation.

Table 2.1: List of major assumptions and conclusions for each contribution presented in Chapter 2.

	Assumptions	**Conclusions**
[Pub. A]	• Wind speed, wind direction, ambient temperature and solar radiation are considered on an hourly basis. Other weather variables that may affect the thermal ratings are not considered. • The right-of-way of overhead lines is assumed to be piece-wise linear to facilitate the calculation of the relative angle between wind speed and conductors. • Modified thermal model used for the calculation of DTR does not consider temperature transients. Radial temperature drop estimated according to state-of-the-art guidelines.	• Simulated DTR are greater than static ratings by at least 10% and 30%, nearly 90% and 75% of the time, respectively. • Accounting for radial temperature drop in conductors reduces DTR in high wind conditions with respect to standard guidelines. • Significantly higher ratings can still be obtained with safe assumptions on highly variable inputs of the thermal model, e.g., wind direction.
[Pub. B]	• Overhead line DTR are pre-calculated on a hourly basis and transformer hot-spot dynamics are assumed to be over after 1 hour. • Efficient cooling mode typical of high power and high voltage transformers • Lossless power flows, small voltage angles and negligible voltage drops (DC-OPF assumptions) • Perfectly known wind power injections and thermal ratings • Both overhead lines and transformer constraints are binding in the reference case with statically rated components. Components are thermally limited.	• In highly congested grids, potential of DTR is fully expressed if applied both to overhead lines and transformers. Total generation costs are reduced by 10%. • Clear seasonal behaviour of DTR with higher ratings in winter due to high wind speed and low ambient temperatures. • Higher temperature cycles of transformers can be synchronized with daily peak load demand
[Pub. C]	• Same assumptions of [Pub. B] for transformer modelling. • Only insulation paper aging is considered. No impact from residual moisture and oil. • DC-OPF assumptions as in [Pub. B]. • Congested system with bottleneck on a transformer.	• Higher operating temperature further increases maximum power flow on transformer. • Power losses increase not only on the component equipped DTR, but across the system too. • Methodology can favour limited asset lifetime applications or network reinforcement while managing accelerated aging.

CHAPTER 3

Operational planning challenges under uncertainty

Power systems are increasingly reliant on stochastic processes, whose ever-changing dynamics require innovative solutions for daily system operations. This chapter delves into operational planning challenges faced by grid operators in wind-dominated systems and proposes an original perspective on capacity calculations and the scheduling of operating reserves. Seizing the core aspects of the proposed contributions requires taking a closer look at the electricity market clearing process, which is reviewed in Section 3.1 together with uncertainty modelling techniques adopted in this thesis. The allocation of additional transmission capacity unlocked by DTR into power system operations is studied in Section 3.2, where [Pub. D] is presented. Section 3.3 instead focuses on the contribution proposed in [Pub. E], which elaborates on a novel approach for the network-aware provision of operating reserves. Lastly, Section 3.4 draws final remarks.

3.1 Modelling preliminaries

During the operational planning of power systems, grid operators go through a decision-making process, which is interfaced with the ordinary functioning of electricity markets. It is mostly in this phase that, confronted with the uncertain nature of renewable energy sources, decision-makers seek the best compromise between security of supply and economically efficient ways to operate the system. [Pub. D] and [Pub. E] propose analytical support-tools to optimize this trade-off, based on descriptions of the underlying stochastic processes. With this regard, special attention is dedicated to modelling the uncertainty associated to wind power and DTR of overhead lines, as they form the inputs to the decision-making support-tools.

3.1.1 Organization of short-term electricity markets

The common denominator of existing electricity market structures is a sequence of trading floors where energy is exchanged on different timescales. The contributions listed in this chapter consider short-term markets, i.e., those that take place close to the actual energy delivery up to 24 hours ahead. More importantly, the analysis is carried out from the point of view of grid operators, whose role is to supervise market operations and ensure technical feasibility of all the transactions. While there may be several intra-day markets where participants can adjust their offers, three main trading floors are considered in this treatise: reserve, day-ahead and balancing markets, which are arranged as shown in Fig. 3.1. A more in-depth discussion on the organization and functioning of electricity markets can be found in [47].

Electrical energy is traded in the day-ahead market, whose clearing produces an hourly schedule for conventional and stochastic producers, p_g and w_j, respectively. Grid operators have the

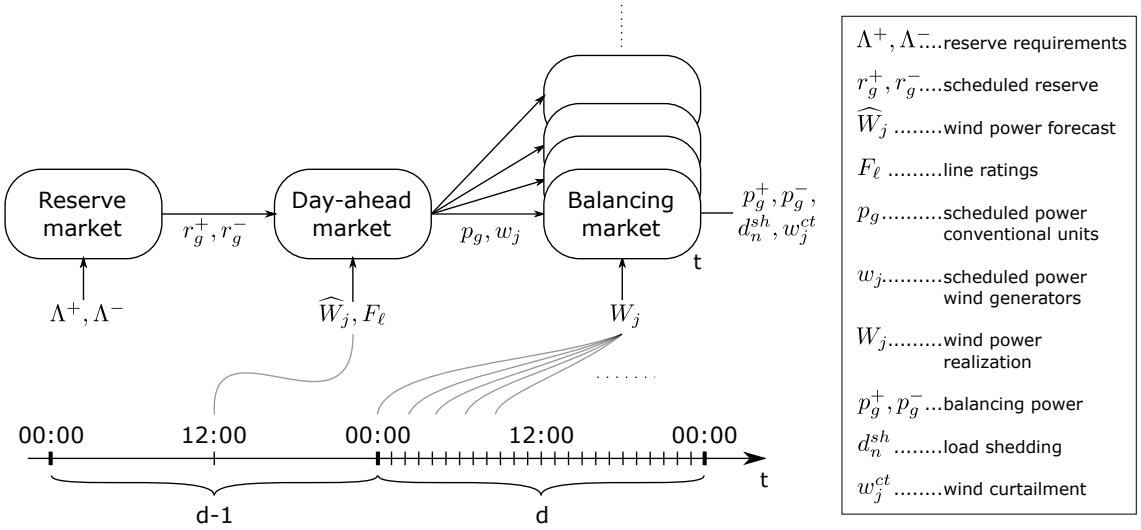

Figure 3.1: Overview of a simplified sequential market clearing sequence.

responsibility to ensure that resulting power exchanges are physically possible by allocating enough transmission capacity F_ℓ to the system. At this stage, however, the trading of renewable energy is based on simplified point forecast values $\widehat{W}_j$, which do not carry any information regarding the associated uncertainty. Therefore, the balance between generation and demand is not guaranteed until the grid operator clears a series of hourly balancing markets, where controllable generators can adjust their output based on more recent information on the uncertainty in the system, i.e., actual wind power generation W_j. Failing to balance out power fluctuations, forces the operator to resort to expensive corrective actions, such as load shedding d_n^{sh} and wind power curtailment w_j^{ct}.

It is therefore crucial to guarantee that enough upward and downward balancing power p_g^+, p_g^- are, in fact, available during real-time operation to compensate power shortages or excesses, respectively. To this end, grid operators clear a reserve market prior to or in combination with the day-ahead market: in the first case energy and reserve are procured independently of one another, whereas in the second they are co-optimized. While [Pub. D] deals exclusively with the second case, [Pub. E] compares the proposed methodology with both. Overall, the reserve market ensures that sufficient power is withdrawn from the energy market and set as a reserve, i.e., ready to be deployed in case of deviations from the scheduled operations.

This simplified description of a sequential market clearing highlights those critical decisions that grid operators are responsible for. Two in particular are the focus of this chapter: setting line ratings F_ℓ, which establish the network capacity available for power exchanges; setting upward and downward reserve requirements, Λ^+ and Λ^-, respectively, which are directly related to the share of wind power in the system. The first decision in particular is where DTR poses a novel challenge. How should the grid operator decide the capacity for energy trading if line ratings themselves are random variables no different than wind power production levels? [Pub. D] addresses this question by proposing a novel methodology whose objective is to maximise the benefits of DTR, while at the same time considering the high-risk aversion of grid operators and the correlation with wind power generation. The second critical decision instead consists in a measure of operational flexibility that is pivotal for the successful large-scale integration of wind power.

[Pub. E] proposes a novel reserve procurement approach that improves the position of flexible resources in the system and challenges common strategies which fail to address key topological aspects.

3.1.2 Wind power and line rating uncertainty modelling

In the market clearing process described above, wind power is commonly dispatched based on single-value forecasts, which easily fit into a deterministic view of power system operations. Single-value or point forecasts typically correspond to the conditional expectation of random variable $\boldsymbol{Y}_t$, which here identifies the underlying stochastic process at time t [48]. The information provided by a point forecast, however, is not sufficient to characterize the uncertainty in the system, thus other methods are required to gain awareness during operational planning as the share of renewable energy increases. To this end, probabilistic forecasts $\widehat{f}_{t+h|t}$ issued at time t for a lead time h aim at predicting the marginal density function f_{t+h} of the stochastic process. The work presented in this thesis assumes that forecasts are issued at noon for each hourly time slot of the following day from 12 up to 36 hours in advance. Although a decay in the quality of the forecasts should be expected as the lead time h increases [49], this aspect is not considered in the thesis.

Two main classes of probabilistic forecasts can be identified: *parametric* and *non-parametric*. While in the first case the forecaster assumes a certain family of the distribution and estimates the set of its defining parameters with available data, in the second case no assumption is made about it. Assuming a predefined distribution certainly eases the modelling approach but it may introduce further approximations that are passed on to the decision-making models and the solutions they provide. Contrarily, a non-parametric approach is more flexible and allows to capture statistically significant properties with higher accuracy, however, it usually implies higher computational burden.

Parametric models

[Pub. E] deals with large-scale systems with several injections of wind power, whose marginal predictive distributions are modelled with a parametric approach. As discussed in [48], a variety of parametric distributions fits wind power forecast errors, provided that their double-bounded nature is accounted for. Figure 3.2(a) shows an example of Beta distributions used in [Pub. E] where the modelling approach in [50] is adopted. Shape parameters α and β are estimated as a function of expected wind power production p and associated variance σ^2, while the analytical

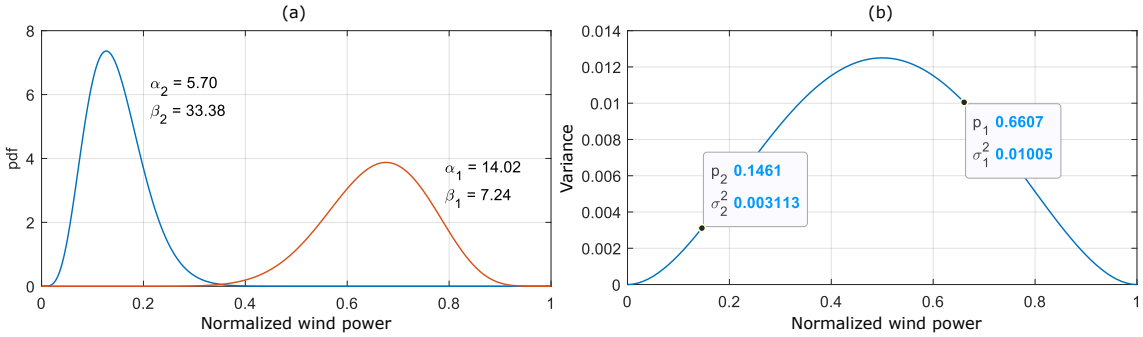

Figure 3.2: Wind power forecast errors with parametric model. (a) Beta distributions and (b) variance estimation based on expected wind power.

relation that links the latter two quantities is shown in Figure 3.2(b). This simplified relationship is used as a variance estimator, assuming that grid operator has knowledge of the expected wind power production p. It shows that a sharper distribution of forecast errors is considered whenever p is close to the lower and upper limits. Although a more complete approach should also consider space-time trajectories and more complex dependencies as in [51], in this case the marginal predictive distributions model wind power forecast errors at a specified time t without any inter-temporal relation. Overall, this approach offers a computationally efficient way to model probabilistic forecasts by simply requiring the expected wind power production level p.

Non-parametric models

In [Pub. D], instead, the focus is on both wind power generation and DTR of overhead lines, whose probabilistic forecasts exhibit highly irregular shapes [52]. Furthermore, authors of [52] show that the nature of the forecast is likely to change depending on which weather variable is predominant for the estimation of the line thermal rating. These considerations motivated the adoption of a non-parametric approach that provides the maximum flexibility for the input of the decision-making tool.

Non-parametric probabilistic forecast are constructed by linearly interpolating a series of m point forecasts obtained with quantile regression [53]. In [Pub. D] a piece-wise polynomial quantile regression has been adopted for wind power generation, whereas a multivariate linear one has been used for DTR, both trained on historical data from the Danish power system. Assuming a linear dependence of line rating with respect to the regressors could be acceptable for ambient temperature and solar radiation, but not quite for wind speed and direction, which exhibit highly non-linear behaviors as shown in [Pub. A]. This approach has been adopted nonetheless owing to its simplicity, while more advanced forecasting tools applied to DTR of overhead lines are discussed in [54]. By taking advantage of the notation in [55], where non-parametric probabilistic forecasts are applied to wind power, the predictive density function can be expressed as

$$\widehat{f}_{t+h|t} = \{\widehat{q}^{(\varepsilon_i)}_{t+h|t}, i = 1, \ldots, m \,|\, 0 \leq \varepsilon_1 \leq \varepsilon_2 \leq \ldots \leq \varepsilon_m \leq 1\} \tag{3.1}$$

where $\widehat{q}^{\varepsilon_i}_{t+h|t}$ is the ε-quantile forecast issued at time t for lead time $t+h$ and ε_i is a monotonic sequence of equally-spaced quantile levels with a sufficiently small granularity, e.g., 1% or 0.1%. The resulting probabilistic forecast for wind power and DTR are shown in Fig.3.3(a) and Fig.3.3(b), respectively. Note that, unlike Beta distributions in Fig.3.2(a), non-parametric forecasts lack a

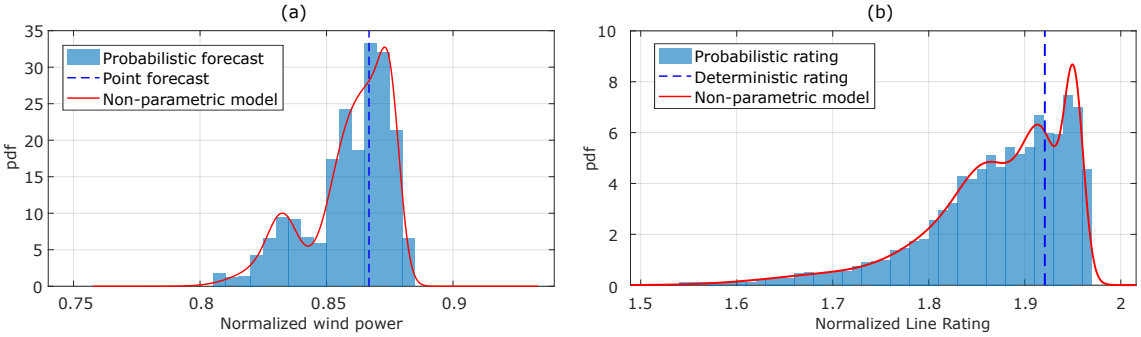

Figure 3.3: Non-parametric probabilistic vs point forecasts for (a) wind power generation and (b) overhead line thermal rating.

close form expression which is necessary to incorporate them into the class of decision-making models proposed in [Pub. D]. Therefore, the last step consists in fitting a Gaussian Mixture Model (GMM), which provides an analytical description of the Probability Density Function (PDF) and the Cumulative Density Function (CDF).

From marginal to joint distribution

Both [Pub. D] and [Pub. E] model multivariate stochastic dependencies in power systems, i.e., spatial correlation between different wind farms in the first case and also between wind power and line ratings in the second. This is achieved by means of the methodology in [56], which may be briefly summarized with the following points:

1. Generate a sufficiently large number of samples $\boldsymbol{x} = (x_1, x_2, \ldots, x_n)$ from a n-dimensional Gaussian distribution, which is assumed to model the interdependence structure between stochastic variables. Each $\boldsymbol{x}$ consists in a realization of the multivariate random variable $\boldsymbol{X} \sim \mathcal{N}(\boldsymbol{0}, \boldsymbol{\Sigma}_r)$, which is centered in 0 with a rank correlation matrix $\boldsymbol{\Sigma}_r$ estimated from historical data. Spearman's rank correlation is preferred to Pearson's as the former is invariant to monotonic transformations and better represents the stochastic dependence between random variables.

2. Each realization $\boldsymbol{x}$ is transformed to the rank domain with the CDF, i.e., $\boldsymbol{u} = \Phi_{\boldsymbol{X}}(\boldsymbol{x})$, where $\Phi_{\boldsymbol{X}}$ is the multivariate Gaussian CDF. Initial samples $\boldsymbol{x}$ are now transformed to $\boldsymbol{u}$ which are uniformly distributed $\boldsymbol{U} \sim \mathcal{U}(0, 1)$, but preserve the rank correlation structure as the CDF transformation is monotonic. This step bridges the initial samples from the Gaussian interdependence to the actual domain of the stochastic random variables.

3. Lastly, samples $\boldsymbol{u}$ are transformed to the actual domain with the inverse CDF of each predictive marginal distribution, i.e., $y_n = F^{-1}_{Y_n}(u_n)$. This step requires the inversion of F_{Y_n} that is the predictive CDF of the n-th random variable in the system. Figure 3.4 shows the realizations $\boldsymbol{y} = (y_1, y_2)$ in the actual domain considering wind power and line rating together with a fitted multivariate GMM which models the joint predictive distribution.

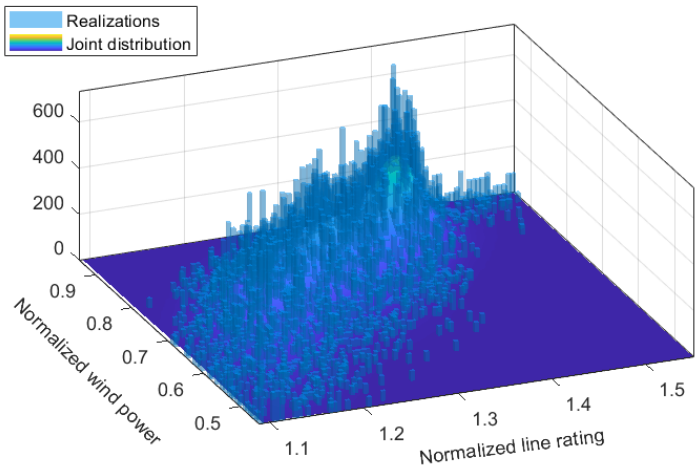

Figure 3.4: Example of joint probabilistic forecast of wind power and line rating. Realizations simulated with a Gaussian copula and fitted GMM.

3.2 Risk-averse transmission capacity allocation

Chapter 2 showed the potential that DTR has to unveil extra capacity in the system, however, the available margin can be successfully utilized only if the uncertainty associated with it is taken into account. This section discusses the contribution proposed in [Pub. D], where a risk-averse methodology is defined for maximising the potential of DTR, while not jeopardising the security of the system. The high positive correlation between DTR and wind power generation is taken into account, thus promoting the integration of this renewable energy source in transmission systems.

3.2.1 Literature review

Several methodological approaches have been proposed in the literature to address the uncertainty of DTR during operational planning. Authors of [57] propose a two-stage stochastic programming framework, where a set of possible line rating realizations and their associated probabilities is considered in day-ahead and balancing markets. The chosen line rating minimizes the total expected operating costs considering potential re-dispatch actions such as load shedding and wind power curtailment. The same principle is also adopted in [58], where a security constrained unit commitment is considered instead together with network topology changes. While accounting for the uncertainty, these studies do not consider the typical risk-aversion of grid operators, as they provide the best solution in terms of expectation.

In order to enforce more conservative solutions that still take advantage of DTR, authors of [59] adopted a chance-constrained optimization framework, which allows grid operators to set a predetermined risk-aversion in the day-ahead capacity calculation. With this approach, the same low violation probability that is commonly accepted for seasonal line ratings can be used for DTR in a more adaptive way. The problem, however, is that this requires a detailed description of the uncertainty. To circumvent this aspect, a robust optimization framework is studied in [60], where both centralized and decentralized corrective actions are taken into account for deviations from the chosen line rating. In the same vein, authors of [61] rely on distributionally robust optimization framework that considers possible valid probabilistic descriptions of the uncertainty.

The methodology proposed in [Pub. D] is aligned with the literature, although two important differences are put forward. Existing studies treat the uncertainty with parametric models and introduce a risk measure by considering either worst-case scenarios in [60] or worst-case distributions that fit the data within a predetermined statistical distance [61]. Rather than using parametric models, which may poorly represent DTR forecasts, and enforce a risk measure *a posteriori*, the proposed approach opts for modelling the input forecasts with higher fidelity using non-parametric distributions and incorporate them directly in the decision-making tool. Ultimately, the effectiveness of this approach should be seen in particular when combined with advanced forecasting tools, such as quantile random forests proposed in [62], which provide a clearer picture of line rating forecasts.

The second key contribution considers the synergies between DTR and wind power generation, again with non-parametric distributions. The proven correlation between the two can be taken into account to further increase the available margin for higher power flows in wind-dominated power systems. Thus, line ratings are determined not only based on the selection of a quantile from their probabilistic forecast, but also considering the stochastic part of power flows. The combination of these two aspects is expected to maximise the benefits of DTR.

3.2.2 Chance-constrained optimal power flow with DTR

The impact of line rating and wind power uncertainty is studied in a reserve and energy co-optimization problem formulated as a DC-OPF, where power flow limits and reserve procurement constraints are enforced in a probabilistic fashion. To this end, line ratings and wind power generation are modelled with spatially correlated non-parametric probabilistic forecasts, as described in Section 3.1.

The objective is to minimize total generation and reserve procurement costs of a given transmission system, including penalty terms for curtailed wind power and shed load. All conventional generators are assumed to respond to imbalances caused by wind power forecast errors according to linear decision rules, so that each response is proportional to the installed capacity of the unit. Such a reserve allocation policy reflects a condition where the grid operator does not consider the location of flexible units during the procurement phase and implies that the relative positioning of reserves in the system cannot be changed. The implications of this assumption are further discussed in Section 3.3, whereas the focus of this section remains on the uncertainty of DTR.

Although simulation results are derived over a 24h period, no inter-temporal constraints are considered since hourly thermal ratings are temporally decoupled, as discussed in Section 2.1. The proposed methodology is compactly formulated with proper $\boldsymbol{c}$, $\boldsymbol{h}$ and $\boldsymbol{q}$ matrices as

$$\min_{\boldsymbol{\xi}} \quad \boldsymbol{c}^\top \boldsymbol{\xi} \tag{3.2a}$$

$$\text{s.t.} \quad \boldsymbol{h}_1^\top \boldsymbol{\xi} - \boldsymbol{h}_0 = 0 \quad : \quad \textit{Power balance}, \tag{3.2b}$$

$$\boldsymbol{q}_1^\top \boldsymbol{\xi} - \boldsymbol{q}_0 \leq 0 \quad : \quad \textit{Operational limits - Deterministic}, \tag{3.2c}$$

$$\mathbb{P}\Big\{ \boldsymbol{q}_{1_i}'^\top \boldsymbol{\xi} - \widetilde{\boldsymbol{q}}_{0_i} \leq 0 \Big\} \geq 1 - \boldsymbol{\varepsilon}_i \quad \forall i \in \mathcal{I} : \quad \textit{Operational limits - Probabilistic} \tag{3.2d}$$

where $\boldsymbol{\xi} = \{p_g, r_g^+, r_g^-, d_n^{\text{sh}}, w_j^{\text{ct}}\}$ is the set of decision variables, i.e., scheduled power generation, up- and downward operating reserves, load shedding and wind curtailment. System power balance at the day-ahead stage is enforced with (3.2b), whereas upper and lower bounds for conventional units and corrective actions are modelled with linear deterministic constraints in (3.2c). Instead, power flow and reserve adequacy constraints are considered in (3.2d), where line ratings and wind power probabilistic forecasts appear as random variables $\widetilde{\boldsymbol{q}}_{0_i}$. The separable structure of each individual chance-constraint i allows the problem to be solved with a deterministic equivalent problem, whose formulation is presented in details in [Pub. D].

The risk level ε is defined as the probability of violating the inner inequality in (3.2d), so it is commonly fixed at low values, in this case 2% for reserve adequacy and 5% for power flows, which are chosen in accordance with standard practices. Enforcing low violation probabilities requires a reliable model for the tails of the distributions and that is where non-parametric models come into play. Clearly, the introduction of probabilistic constraints entails more conservative solutions compared to the fully deterministic version of (3.2), where (3.2d) is replaced by its inner inequality constraint. However, the value of such methodology consists in the ability to safeguard the grid operator against potentially critical situations, which may require expensive corrective actions.

Simulation results are derived from the RTS-24 bus system [43], where additional wind power generation is localized diametrically opposite to the major load centers. These assumptions configure a highly stressed transmission system, where the value of additional network capacity can be easily evaluated. Both wind power and line ratings are simulated based on historical weather data from the Danish power system.

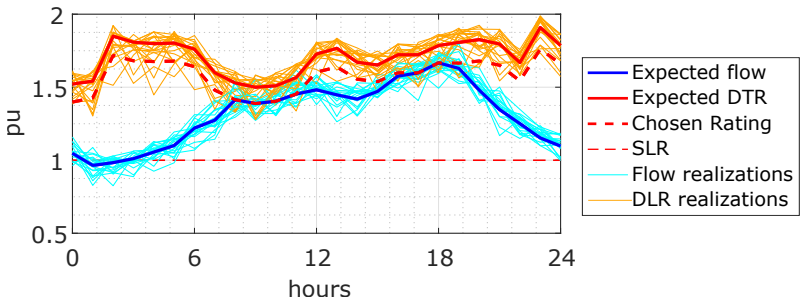

Figure 3.5: Analysis of simulated power flow with DTR over a 24h period [Pub. D].

Power flow analysis

The reformulation of chance-constraints highlights a safety margin that can be used to reduce transmission capacity allocated to the market, so that the sought-after risk-aversion of the grid operator is accounted for. Whenever lines are operated with conventional STR, this margin reflects the uncertainty in power flows caused by wind power generation. However, when also DTR is in place as in Fig. 3.5, the chosen rating considers both sources of uncertainty, while accounting for their correlation. This approach allows the grid operator to push the utilization of the lines even further, as opposed to a case where wind generation and line ratings are considered statistically independent. Overall, considering a day with favourable windy conditions, where the actual thermal rating of the line is 1.7 times the STR, this methodology allows to use approximately 90% of the extra margin, while accepting the same 5% violation probability adopted for the other lines.

Robustness test

To test the validity of this approach against perturbations in wind power and DTR, a sufficiently large number of realizations is simulated from the joint predictive distributions that models their stochastic dependence. These realizations are plugged in the inner inequality of (3.2d) together with the solutions $\boldsymbol{\xi}^*$ obtained by solving (3.2) with varying assumptions on the random variables. It stands out as the commonly used approach of normally distributed line ratings entails an overestimation of the lower tail, which results in higher violation probabilities. This result points to the fact that, if the utilization of the lines needs to be maximised, an accurate representation of the uncertainty is necessary.

Cost analysis

The use of DTR entails significant cost differences as opposed to STR, especially in terms of wind power curtailment, which is nearly halved thanks to the high correlation between DTR and wind generation. Some side effects are also evident on the procurement of reserves, although an in-depth analysis should study different allocation policies. Considering the linear decision rule assumed in this study, upward reserve costs decrease and downward reserve costs increase. In the first case, higher network capacity guarantees that larger and cheaper generators can provide operating reserves, while not reducing their capacity for the market. In the second case, instead, more down-regulating power is needed to dispatch extra wind power generation that can be injected into the system thanks to highly correlated line ratings. Overall, as a result of extra transmission capacity in a windy day, total generation cost is 17% less, in line with results from [Pub. B], although higher savings can be expected for grid operators if reserve procurement is also considered.

3.3 Network-aware reserve procurement

The large-scale integration of wind power requires increased levels of operational flexibility, which is interpreted as the ability to anticipate and quickly adapt to fluctuations of power from stochastic generators. On the one hand, the contributions presented so far aimed at increasing the available transmission capacity, so that such fluctuations can easily flow through the network without violating thermal limits of components. On the other hand, the system balance between power production and consumption needs to be maintained by readily available generators, which regulate their output following deviations from scheduled operations. Therefore, a flexible utilization of grid capacity is achieved not only by increasing maximum power flows, but also ensuring that enough reserve capacity is optimally placed in the system. This section presents the contributions in [Pub. E], where the focus is on the ability to deliver operating reserves to the system by ensuring that network limitations are taken into account during their provision process.

3.3.1 Literature review

The connection between higher shares of wind power in electricity markets and increased levels of operating reserves is widely acknowledged in power systems analysis [20]. Several studies, however, recently discussed the implications of this trend concluding that the procurement of more reserve capacity from flexible generators does not necessarily guarantee that imbalances would be covered in real-time, due to network limitations and congested transmission lines [63,64]. Although the location of generators plays a key role in the ability to activate and deliver power to the grid, this aspect is usually not considered in the reserve market clearing process, as discussed in Section 3.1.

Two-stage stochastic programming has been proposed as an effective way to preposition reserves in the system in such a way that total expected system costs are minimized [65,66]. In fact, this approach is considered an ideal one, since the violation of revenue adequacy and cost recovery renders it incompatible with current market structures. To this end, authors of [67] developed a framework based on two-stage stochastic bilevel programming for optimally dispatching wind power in day-ahead markets. The bilevel structure allows grid operators to leverage their degree of freedom in order to steer the dispatch of the system towards the cost optimal one given by the purely stochastic model, with limited control over the clearing of electricity markets. Similarly, [68] and [69] adopted the same methodology while incorporating cross-border transmission capacity allocation and reserve procurement, respectively. Nevertheless, the fact that these studies rely on a single reserve market means that the procurement of capacity follows the least-cost merit-order curve, regardless of the physical position of generators. While they show that it is possible to regulate the total amount of reserves considering expected corrective actions, the location of reserve capacity in the system is still not accounted for.

The contribution in [Pub. E] aims at improving this latter aspect, by proposing a *zonal pre-emptive* framework which allows grid operators to define a number of zones, where reserve markets can be cleared independently of one another, while respecting the least-cost merit-order on a zonal basis. A zonal representation of the system is beneficial for procuring reserves considering major network limitations, however, the effectiveness of a zonal setup is conditional to a detailed description of the uncertainty in the system. That is why the proposed methodology indicates the best way to split the reserve capacity market, given the latest probabilistic description of stochastic power production.

Other studies proposed a dynamic partition of the system for the provision of operating reserve, however, the way the zones are defined is still open to interpretation. The method proposed in [Pub. E] relies on grid partitioning algorithms that are exclusively driven by the total expected system costs, thus without the need for additional metrics which may entail a level of arbitrariness. Grid partitioning constraints have already been used in power system research for intentional islanding of transmission systems in a two-stage stochastic problem [70,71]. However, to the best of our knowledge, [Pub. E] is the first that relies on them for defining zonal reserve markets, and the first that incorporates them in a bilevel framework.

3.3.2 Zonal pre-emptive methodology

The goal of the proposed methodology is to split the system in a number of contiguous reserve zones and set zonal reserve requirements in order to minimize total operating costs. Having both the boundaries of each zone and the corresponding reserve requirements as decision variables grants maximum flexibility to optimally position reserve capacity. The proposed methodology is able to identify potential bottlenecks in the system and dynamically redefine zonal markets so that the access to flexible reserve capacity during real-time operation is guaranteed with the minimal cost. Furthermore, the option to set aside part of the cross-zonal transmission capacity is included in order to facilitate the exchange of reserves between zones during re-dispatch actions. Figure 3.6 shows a conceptual overview of the stochastic bilevel optimization problem.

The optimal solution of the whole problem is guided by the upper-level part, where the main objective function is defined. This is comprised of three terms: reserve costs $\mathcal{C}_R$, day-ahead costs $\mathcal{C}_D$ and expected balancing costs $\mathcal{C}_B$, given a scenario set with S realizations of wind power production and their corresponding probabilities π_s. Upper-level decision variables model the degree of freedom during the sequential market clearing process described in Section 3.1. In particular, grid operators are assumed to set zone boundaries with a partitioning binary variable x, set zonal

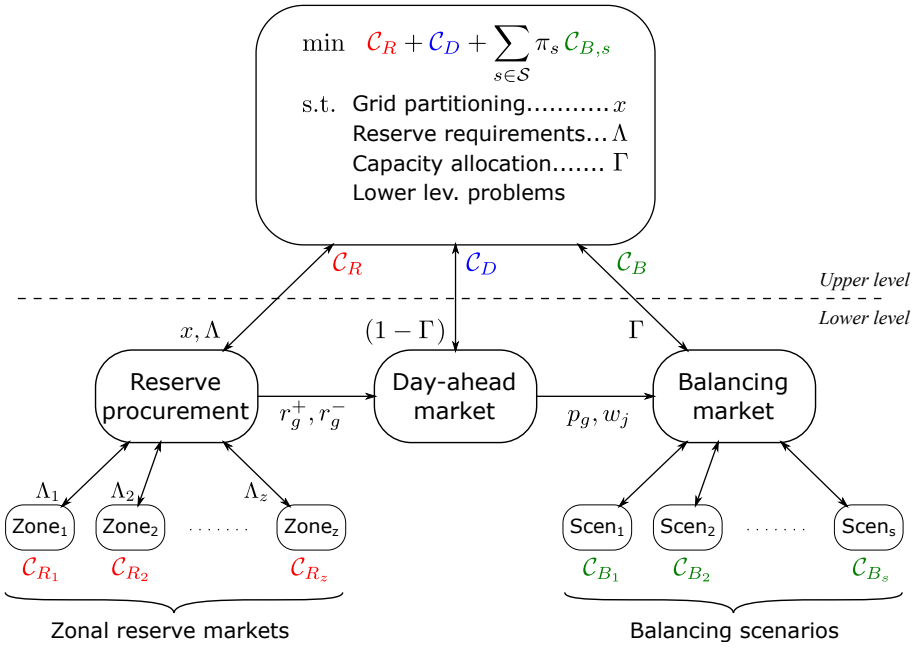

Figure 3.6: Schematic representation of the zonal pre-emptive methodology

reserve requirements Λ and cross-zonal transmission capacity Γ, expressed as a percentage of line ratings. Additionally, the solution of the upper-level problem is delimited by the optimal solution of the lower-level problems, which model each stage in the sequential market clearing. Therefore, even though the grid operator has neither control over the dispatch of single generators nor the ability to procure reserve out-of-merit, the economic efficiency of the system can be heavily influenced by optimizing those quantities that the operator is responsible for. The following sections take a closer look at the interactions in Fig. 3.6, whereas an in-depth analytical description and a solution methodology is provided in [Pub. E].

Grid partitioning

The partition of the system into a predefined number of zones follows three defining properties: zones do not overlap, they cover all nodes in the system and the corresponding sub-graphs generated by the partition are *connected*, meaning that whichever two nodes are considered inside a zone, there is always an internal path connecting them together. The connectivity requirement, in particular, is necessary to ensure that zonal reserve markets truly reflect the limited exchange possibilities in a congested transmission system. Considering the RTS-96 system [72] in Fig. 3.7, the adaptive partition enables the identification of those areas where reserves may be required the most, as opposed to a single reserve market whose clearing does not consider the location of flexible capacity. Neglecting the locational aspect is likely to entail higher operating costs, since part of the reserves may not be accessible during real-time operation, thus forcing expensive out-of-market corrective actions. Grid partitioning constraints are included in the upper-level problem and govern the solution of the lower-level ones. Such a hierarchical structure implies that the optimal configuration of the system takes into account all stages of the sequential market clearing and their associated costs.

Reserve procurement

Each zone of the partition has different reserve requirements $\Lambda_1, \ldots, \Lambda_z$, which are procured abiding by a least-cost merit-order on a zonal basis. Figure 3.7 shows a partition of the IEEE RTS-96 system into three zones together with the corresponding reserve capacity offers of generators and the final procured amount. Even though cheaper reserves are available in zone 3, the optimal solution suggests to procure them where the cost per MW is higher, i.e., zone 1 and zone 2, since generators in these zones are located closer to nodes with large share of wind power generation. This approach resembles the ability of the purely stochastic model to pre-position reserves close to the sources of potential imbalances, however, it does so without the assumption of a generator-specific resolution by defining zones, where generators can present their offers. As the number of zones increases, the total operating cost of the the system approaches the one of the purely stochastic model. Nevertheless, simulation results show that significant savings can be obtained with just two zones, thus limiting the scale of the problem and the associated computational time.

Capacity allocation

Another leverage of the zonal pre-emptive methodology is the allocation of cross-zonal transmission capacity between energy trading and balancing services. Upper-level decision variable Γ indicates the share of line rating that is set aside from the day-ahead market in order to leave a headroom on transmission lines for re-dispatch actions during real-time operations. Therefore, whenever Γ% of

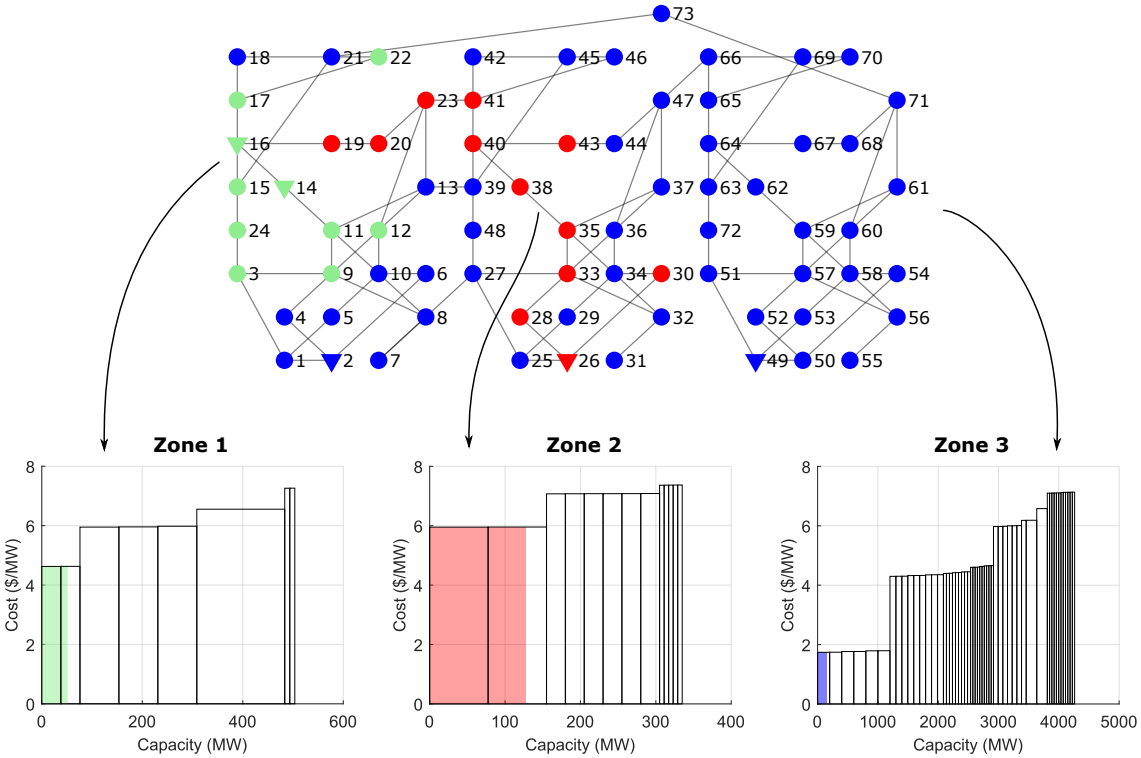

Figure 3.7: Partition into 3 zones of the IEEE RTS-96 system with corresponding reserve capacity offers from generators in each zone. Highlighted part is the procured amount. Triangles indicate nodes with wind power injection.

line capacity is reserved for the balancing market, only $(1 - \Gamma)\%$ is allocated for energy trading at the day-ahead stage on those lines that connect adjacent zones in the partition. The addition of this extra decision variable further reduces total operating costs, since more reserves can be procured from cheaper areas of the system, while ensuring that they are deliverable in case of imbalances. Total costs, however, are reduced at the expenses of higher generation cost during day-ahead stage, given the reduced network capacity for energy trading. Furthermore, simulation results show that this measure is effective only when the portion of line capacity set aside for balancing is greater than 60%. This point resembles the line switching method [73], according to which the dispatch of a system can be improved by rerouting power flows in the system with coordinated switching of transmission lines.

3.4 Remarks

In conclusion of this chapter, key points of the presented publications are listed in Table 3.1. These contributions aim at providing novel decision-making support-tools for the integration of wind power generation by offering a new perspective on the definition of flexibility in operational planning.

To answer the question in Section 3.1 about the assimilation of DTR into capacity calculations, the methodology proposed in [Pub. D] based on chance-constraints offers a risk-averse approach to do so. By setting aside a margin of transmission capacity on each line, grid operators can safeguard the system against unexpected variations in stochastic power production. The quantification of this margin is the goal of the proposed methodology, which in case of lines with DTR considers

not only wind power, but also weather-based uncertainty on the thermal state of conductors. For this reason, it is stressed the importance to adopt detailed probabilistic forecast, while considering the underlying interdependence structure. Overall, this approach allows grid operators to take advantage of the potential of DTR in wind-dominated power systems and it paves the way for the application of more advanced forecasting tools applied to DTR. To this end, the similarities between wind power and line rating forecasting could be further investigated in order to transfer the consolidated experience from the first to the second.

Although simulation results show a valid business case for DTR with significant savings for daily system operations, assessing the value of this technology should also consider other limiting factors and other measures of flexibility that grid operators can resort to. A more adaptive reserve allocation policy, for example, could be used in combination with DTR in order to coordinate the available flexibility in the system. To this end, the zonal pre-emptive methodology in [Pub. E] could prove to be a valid solution owing to its ability to identify potential bottlenecks in the system and procure reserve accordingly.

The zonal pre-emptive methodology shows that it is possible to approximate the efficiency of the stochastic market clearing with solutions that are more appealing to current electricity market structures. Rather than procuring reserve capacity from single generators in contrast with the least-cost merit-order, the dynamic definition of zones let grid operators identify critical areas in the system where reserve markets can be cleared independently of one another following consolidated practices in power system operation. The ability to redefine zonal reserve markets in such a way that total operating costs are minimized brings a significant contribution to the current debate on a coordinated European reserve capacity market [5], envisioning a zonal setup that transcends national borders.

Table 3.1: List of major assumptions and conclusions for each contribution presented in Chapter 3.

	Assumptions	**Conclusions**
[Pub. D]	• Non-parametric probabilistic forecast for hourly line ratings and wind power. Use of quantile regression with fixed lead time.	• Assuming normally distributed DTR overestimates the lower tail of the distribution. More constraint violation should be expected with this assumption.
	• Spatial correlation from historical data in Danish power system. Results simulated with moderate wind speed ($\leq$ 13 m/s).	• 90% of the available extra margin for higher power flows can be utilized assuming the same 5% risk-aversion for other lines.
	• Lossless power flows, small voltage angles and negligible voltage drops (DC-OPF assumptions). No temporally coupled constraints. 3 lines equipped with DTR.	• Wind power curtailment halved and -17.6% total cost reduction compared to STR during a 24h dispatch period
	• Reserve allocation policy in a single reserve market with a linear decision rule.	
[Pub. E]	• Parametric probabilistic forecasts of wind power forecast errors at different sites. Spatial correlation from historical data in Danish system.	• Zonal pre-emptive methodology produces a grid partitioning that considers network topology, probabilistic description of uncertainty, location, availability and reserve cost of flexible generators.
	• Error variance of Beta distributions expressed as a quadratic function of *p.u.* point forecast.	• Total costs approach the efficiency of the purely stochastic model as the number of zones increases.
	• Share of wind power generation is equal to approximately 45% and 18% in the RTS-24 and RTS-96 system, respectively.	• Adaptive partition in 2 zones sufficient to match efficiency of stochastic model in RTS-96 system.
	• Lossless power flows, small voltage angles and negligible voltage drops (DC-OPF assumptions). Single-period formulation.	• Transmission capacity allocation further reduces the costs in the RTS-24 system.

CHAPTER 4

Conclusion and future work

This last chapter recollects the content of the thesis while providing final comments on the proposed contributions in Section 4.1. Future research directions stemming from the results achieved in this thesis are outlined in Section 4.2.

4.1 Concluding remarks

The evolution of power systems is driven by impelling decarbonization targets and it proceeds at a pace which requires increased levels of flexibility, in all the categories it consists of: the infrastructure, the operation and the role of stakeholders. This thesis focuses on the first two, while taking the stance of grid operators facing growing shares of renewable energy sources in view of limited room for traditional grid expansion projects.

Under these circumstances, achieving higher utilization of existing transmission systems seems to be a necessary measure to address these challenges. The use of dynamic thermal rating (DTR) has the potential to support this goal, although several aspects limit its wide application at the time being. The large amount of data required for a reliable implementation of this technology is a first step that needs to be tackled and contributions in [Pub. A] propose potential solutions in this regard. Simplified approaches with reduced inputs offer viable options that, despite marginally increasing maximum power flows, limit the additional uncertainty introduced in the system. The uncertainty associated with weather dependent ratings is probably the biggest source of concerns for grid operators, whose responsibility is to guarantee high levels of security of supply. To this end, the modifications proposed in [Pub. A] to widely known thermal models limit the risk of overheating conductors under high current and high wind conditions, where internal temperature differences may become relevant.

The extension of DTR to larger parts of the system inevitably entails the need to adequately upgrade other components, such as power transformers. A day-ahead dispatch including thermal dynamics of both overhead lines and transformers is formulated for the first time in [Pub. B], offering the possibility to study mutual dependencies between these components. Furthermore, this approach can be used to take advantage of cyclic loading of large components at higher operating temperatures, while still respecting maximum recommended values. The inclusion of aging dynamics in [Pub. C] completes the methodology and shows that lifetime utilization of transformers can be managed depending on the needs of the stakeholders.

The integration of large shares of stochastic power productions, such as wind power generation, requires not only proper upgrade of the system, but also reviewed measures to address the underlying uncertainty. In view of the potential that DTR has to favour wind power integration and given their uncertain and correlated stochastic nature, [Pub. D] proposes a risk-averse methodology to set line ratings with DTR, based on available probabilistic forecasts. This approach let grid operators harvest the potential of DTR, while assuming the same risk aversion level that

is commonly accepted on any other line. Testing this methodology in highly congested systems with large shares of wind power generation reveals that significant savings can be attained with respect to a reference scenario, where overhead lines are operated with static thermal ratings. This approach increases flexibility in the transmission system, as large fluctuations of power due to forecast errors can be managed without violating the line thermal ratings.

Rather than allowing higher power flows on specific corridors, an alternative approach that still aims at optimizing operating costs while considering network limitations and large shares of wind power, is the methodology proposed in [Pub. E]. The need for higher flows can be anticipated by pre-positioning flexible generation capacity at strategic locations in the systems, in a way that current reserve sizing practices do not consider. As a result, the system is better prepared to handle large variation of power from stochastic producers, thus limiting the impact of uncertainty during power system operations. While leading to operating costs that closely match the ideal lower bound, the zonal pre-emptive methodology in [Pub. E] does not violate fundamental properties of electricity markets that hinder the application of more efficient methods.

To conclude, results achieved in this thesis suggest that large-scale integration of renewable energy sources can benefit from a flexible utilization of transmission grid capacity, both in terms of new infrastructural functionalities and novel operational methods. The influence of natural phenomena on power systems is already visible in the generation as well as in the demand of electricity and it is bound to grow further, embracing the transmission too. The evolution of power systems will require gaining the necessary awareness and the ability to adapt accordingly.

4.2 Future work

Potential sources of flexibility in the existing infrastructure lay also on other components that lend themselves to the application of the core physical aspect of DTR. Underground power cables, in particular, can be modelled with electro-thermal models that closely resemble those of power transformers. The similarities between the two include high values of thermal capacitance that temporally couple thermal ratings and the ability to cyclically load these components without violating critical temperature limits. However, as opposed to transformers, power cables have various heat sources that mutually affect each other: core, screen and armour losses. Modelling these components in an optimization framework poses new challenging aspects that are under consideration in [Pub. G], where dynamic network rating on overhead lines, transformers and cables is studied in a long-term grid reinforcement problem for wind power integration.

The contributions included in this thesis analysed the potential benefits of DTR applied to a pre-selected subset of overhead lines. However, the choice of those interconnections in the system that maximise the benefits of DTR has not been discussed, although this aspect would be of primal importance in highly loaded power systems. While the consolidated experience and in-depth knowledge of grid operators can certainly provide an heuristic solution to this problem, data-driven analytical tools have the potential to assist and optimize this decision. The identification of those lines where additional transmission capacity would benefit the system the most could be studied by combining bilevel optimization framework with upper-level binary decision variables, drawing from the methodological contributions in [Pub. E].

Assuming that the construction of new lines would be increasingly difficult in the future, new research opportunities arise for studying the impact of DTR on long-term planning. To this end,

the interactions of DTR with other components is of primal interest. For example, the coordinated use of DTR with energy storage systems may provide a novel case study where favourable weather conditions, such as high wind speed, are not correlated with high load demand periods. In this scenario, the higher network capacity could still be utilized to charge storage systems and maximise the usage of the grid under low-load periods. Furthermore, enhanced power flow control capabilities offered by advances in power electronics could be combined with DTR in an effort to take full advantage of the available grid capacity. The rapid diffusion of High Voltage Direct Current (HVDC) interconnections could offer further possibilities in this regard. While HVDC systems allow for controllable power flows over long distances and different market areas, DTR increases AC network capacity of relatively short lines that are thermally limited. This complementarity might be used for increasing network capacity and flexibility under high share of renewable energy sources.

The zonal pre-emptive methodology proposes a new perspective on the definition of zonal reserve capacity markets, although formulated with assumptions that may limit its applicability. A multi-period formulation could be investigated and tested providing a dynamic partition of transmission systems that optimizes operating costs over a prolonged period of time, considering the evolution of stochastic processes and ramping limitations of components. The application of the tool to large-scale case studies would require new contributions from the computational point of view, but has the potential to offer an original perspective on cross-border cooperation and integration of national power systems.

Whenever the share of renewable energy sources will have reached a predominant part in the total electricity demand, seasonal trends in solar and wind power generation will be so evident that the transmission asset will need to adapt accordingly. Under these circumstances, it is hard to imagine how power systems could be operated without increased awareness of the thermal states of all critical components. The optimal trade-off between high-resolution numerical weather prediction models and measuring equipment technologies should be further investigated to support future decision-making in power systems.

Bibliography

[1] International Energy Agency, "World Energy Outlook 2019," IEA, Paris, Tech. Rep., 2019. [Online]. Available: https://www.iea.org/reports/world-energy-outlook-2019

[2] ——, "Offshore Wind Outlook 2019," IEA, Paris, Tech. Rep., 2019. [Online]. Available: https://www.iea.org/reports/offshore-wind-outlook-2019

[3] ENTSO-E, "ENTSO-E 2025, 2030, 2040 Network Development Plan 2018 - Connecting Europe: Electricity," Brussel, Belgium, Tech. Rep., 2018. [Online]. Available: https://tyndp.entsoe.eu/tyndp2018/

[4] "Approval procedures and consensus for building transmission lines: Obstacles and solutions," *2011 8th International Conference on the European Energy Market, EEM 11*, no. May, pp. 826–831, 2011.

[5] Elia group, "Future-proofing the eu energy system towards 2030," Tech. Rep., 2019. [Online]. Available: https://www.eliagroup.eu/en/publications

[6] International Energy Agency, "Status of Power System Transformation - Power system flexibility," IEA, Tech. Rep., 2019. [Online]. Available: https://www.iea.org/reports/status-of-power-system-transformation-2019

[7] ——, "Status of Power System Transformation - Advanced Power Plant Flexibility," IEA, Tech. Rep., 2018. [Online]. Available: https://www.iea.org/reports/status-of-power-system-transformation-2018

[8] P. Kundur, *Power System Stability and Control*. McGraw-Hill, 1994, section 6.1, page 229.

[9] Cigré Working Group B2.43, *Rating Calculations TB 601*, December 2014.

[10] D. Douglass, W. Chisholm, G. Davidson, I. Grant, K. Lindsey, M. Lancaster, D. Lawry, T. McCarthy, C. Nascimento, M. Pasha, J. Reding, T. Seppa, J. Toth, and P. Waltz, "Real-Time Overhead Transmission-Line Monitoring for Dynamic Rating," *IEEE Transactions on Power Delivery*, vol. 31, no. 3, pp. 921–927, 2016.

[11] M. W. Davis, "A new thermal rating approach: The real time thermal rating system for strategic overhead conductor transmission lines – part i: General description and justification of the real time thermal rating system," *IEEE Transactions on Power Apparatus and Systems*, vol. 96, no. 3, pp. 803–809, May 1977.

[12] ENTSO-E, "Technologies for Transmission System," Brussel, Belgium, Tech. Rep., 2019. [Online]. Available: http://www.e-highway2050.eu/results/

[13] T. project, "Demonstration project 6 - Improving the flexibility of the grid (FLEXGRID)," Tech. Rep., 2013. [Online]. Available: https://windeurope.org/about-wind/reports/twenties-project/

[14] A. González, M. Mañana, , "Operational aspects of dynamic line rating. Application to a real case of grid integration of wind farms," *2016 CIGRE International Colloquium*, pp. 1–6, 2016.

[15] T. Yip, C. An, G. Lloyd, M. Aten, B. Ferri, "Dynamic line rating protection for wind farm connections," *Proceedings of CIGRE/IEEE PES joint symposium integration of wide-scale renewable resources into the power delivery system*, pp. 1–5, 2009.

[16] G. A. Orfanos, P. S. Georgilakis, and N. D. Hatziargyriou, "Transmission expansion planning of systems with increasing wind power integration," *IEEE Transactions on Power Systems*, vol. 28, no. 2, pp. 1355–1362, 2013.

[17] C. J. Wallnerstrom, Y. Huang, and L. Soder, "Impact from dynamic line rating on wind power integration," *IEEE Transactions on Smart Grid*, vol. 6, no. 1, pp. 343–350, 2015.

[18] J. Cao, W. Du, and H. F. Wang, "Weather-based optimal power flow with wind farms integration," *IEEE Transactions on Power Systems*, vol. 31, no. 4, pp. 3073–3081, 2016.

[19] S. Karimi, P. Musilek, and A. M. Knight, "Dynamic thermal rating of transmission lines: A review," *Renewable and Sustainable Energy Reviews*, vol. 91, no. August 2016, pp. 600–612, 2018. [Online]. Available: https://doi.org/10.1016/j.rser.2018.04.001

[20] J.M. Morales, A.J. Conejo and J. Pérez-Ruiz, "Economic Valuation of Reserves in Power Systems With High Penetration of Wind Power," *IEEE Trans. on Power Syst.*, vol. 24, no. 2, pp. 900–910, 2009.

[21] North American Electrical Reliability Corporation (NERC), "Glossary of Terms Used in NERC Reliability Standards," 2019. [Online]. Available: https://www.nerc.com/files/glossary_of_terms.pdf

[22] IEEE Power Engineering Society, "IEEE Standard for Calculating the Current-Temperature of Bare Overhead Conductors - IEEE Std 738-2006," IEEE, Tech. Rep., 2007.

[23] J. Heckenbergerova, P. Musilek, and K. Filimonenkov, "Assessment of seasonal static thermal ratings of overhead transmission conductors," in *2011 IEEE Power and Energy Society General Meeting*, July 2011, pp. 1–8.

[24] J. Hosek, P. Musilek, E. Lozowski, and P. Pytlak, "Effect of time resolution of meteorological inputs on dynamic thermal rating calculations," *IET Generation, Transmission Distribution*, vol. 5, no. 9, pp. 941–947, Sep. 2011.

[25] B. Clairmont, D. Douglass, J. Iglesias, and Z. Peter, "Radial and Longitudinal Temperature Gradients in Bare Stranded Conductors with High Current Densities," *Cigre session B2-108*, 2012.

[26] J. Rodriguez Alvarez and C. M. Franck, "Radial Thermal Conductivity of all-Aluminum Alloy Conductors," *IEEE Transactions on Power Delivery*, vol. 30, no. 4, pp. 1983–1990, 2015.

[27] I. Albizu, E. Fernandez, A. J. Mazon, M. Bedialauneta, and K. Sagastabeitia, "Overhead conductor monitoring system for the evaluation of the low sag behavior," *2011 IEEE PES Trondheim PowerTech: The Power of Technology for a Sustainable Society, POWERTECH 2011*, 2011.

[28] M. Kang, M. Strobach, and C. M. Franck, "Radial temperature distribution of aaac overhead line in stationary and transient conditions," *18th International Symposium on High Voltage Engineering*, 2013.

[29] "IEEE guide for loading mineral-oil-immersed transformers and step-voltage regulators - redline," *IEEE Std C57.91-2011 (Revision of IEEE Std C57.91-1995) - Redline*, pp. 1–172, Mar 2011.

[30] N. Alguacil, M. H. Banakar, and F. D. Galiana, "Electrothermal coordination Part II: Case studies," *IEEE Transactions on Power Systems*, vol. 20, no. 4, pp. 1738–1745, 2005.

[31] H. Banakar, N. Alguacil, and F. D. Galiana, "Electrothermal coordination Part I: Theory and implementation schemes," *IEEE Transactions on Power Systems*, vol. 20, no. 2, pp. 798–805, 2005.

[32] M. Tschampion, M. A. Bucher, A. Ulbig, and G. Andersson, "N-1 security assessment incorporating the flexibility offered by dynamic line rating," *19th Power Systems Computation Conference, PSCC 2016*, 2016.

[33] M. Nick, O. Alizadeh-Mousavi, R. Cherkaoui, and M. Paolone, "Security Constrained Unit Commitment with Dynamic Thermal Line Rating," *IEEE Transactions on Power Systems*, vol. 31, no. 3, pp. 2014–2025, 2016.

[34] M. Khaki, P. Musilek, J. Heckenbergerova, and D. Koval, "Electric power system cost/loss optimization using Dynamic Thermal Rating and linear programming," *2010 IEEE Electrical Power & Energy Conference*, pp. 1–6, 2010.

[35] D. Roberts, P. Taylor, and A. Michiorri, "DTR for increasing network capacity and delaying network reinforcements," *CIRED Seminar 2008: SmartGrids for Distribution*, no. 3, pp. 23–24, 2008.

[36] J. Black, S. Connor, and J. Colandairaj, "Planning network reinforcements with Dynamic Line Ratings for overhead transmission lines," *Universities Power Engineering Conference UPEC 2010 45th International*, pp. 1–6, 2010.

[37] J. Kwon and K. W. Hedman, "Transmission expansion planning model considering conductor thermal dynamics and high temperature low sag conductors," *IET Generation, Transmission & Distribution*, vol. 9, no. 15, pp. 2311–2318, 2015.

[38] A. Michiorri, P. C. Taylor, S. C. E. Jupe, and C. J. Berry, "Investigation into the influence of environmental conditions on power system ratings," *Proceedings of the Institution of Mechanical Engineers, Part A: Journal of Power and Energy*, vol. 223, no. 7, pp. 743–757, 2009.

[39] T. Bajracharya, G. Koltunowicz *et al*, "Optimization of transformer loading based on hot-spot temperature using a predictive health model," in *Int. Conf. on Condition Monitoring and Diagnosis*, Sept 2010, pp. 914–917.

[40] M. Humayun, M. Degefa, A. Safdarian, and M. Lehtonen, "Utilization improvement of transformers using demand response," *IEEE transactions on power delivery*, vol. 30, no. 1, pp. 202–210, Feb 2015.

[41] J. Yang, X. Bai, D. Strickland, L. Jenkins, and A. M. Cross, "Dynamic Network Rating for Low Carbon Distribution Network Operation—A U.K. Application," *Smart Grid, IEEE Transactions on*, vol. 6, no. 2, pp. 988–998, 2015.

[42] R. D. Christie, B. F. Wollenberg, and I. Wangensteen, "Transmission management in the deregulated environment," *Proc. of the IEEE*, vol. 88, no. 02, pp. 170 – 195, Feb. 2000.

[43] C. Ordoudis, P. Pinson, and M. Zugno, "An updated version of the IEEE rts 24-bus system for electricity market and power system operation studies," *Technical University of Denmark (DTU)*, pp. pp. 1–5, 2016.

[44] R. A. Jabr, "Modeling network losses using quadratic cones," *IEEE Transactions on Power Systems*, vol. 20, no. 1, pp. 505–506, Feb 2005.

[45] O. W. Akinbode and K. W. Hedman, "Fictitious losses in the dcopf with a piecewise linear approximation of losses," in *IEEE PES GM*, July 2013, pp. 1–5.

[46] A. Tosatto, T. Weckesser, and S. Chatzivasileiadis, "Market integration of hvdc lines: Internalizing hvdc losses in market clearing," *IEEE Transactions on Power Systems*, vol. 35, no. 1, pp. 451–461, Jan 2020.

[47] H. M. P. P. M. Z. Juan M. Morales, Antonio J. Conejo, *Integrating renewables in electricity markets*, ser. International series in operations research and management science. Springer, 2014, vol. 205.

[48] P. Pinson, "Wind Energy : Forecasting Challenges for Its Operational Management," vol. 28, no. 4, pp. 564–585, 2013.

[49] H. Madsen, *Time series analysis*. Chapman & Hall, 2008.

[50] H. Bludszuweit, J. A. Domínguez-Navarro, and A. Llombart, "Statistical analysis of wind power forecast error," *IEEE Trans. on Power Syst.*, vol. 23, no. 3, pp. 983–991, 2008.

[51] P. M. H. Tastu, Julija ; Pinson, "Space-time trajectories of wind power generation: Parameterized precision matrices under a Gaussian copula approach," *Modeling and Stochastic Learning for Forecasting in High Dimensions*, 2015.

[52] J. Zhan, C. Chung, and E. Demeter, "Time Series Modelling for Dynamic Thermal Rating of Overhead Lines," *IEEE Transactions on Power Systems*, vol. 8950, no. c, pp. 1–1, 2016.

[53] G. B. R. Koenker, *Regression Quantiles*. Econometrica, 1978.

[54] A. Michiorri, H. M. Nguyen, S. Alessandrini, J. B. Bremnes, S. Dierer, E. Ferrero, B. E. Nygaard, P. Pinson, N. Thomaidis, and S. Uski, "Forecasting for dynamic line rating," *Renewable and Sustainable Energy Reviews*, vol. 52, pp. 1713–1730, 2015.

[55] P. Pinson, H. A. Nielsen, J. K. Møller, and H. Madsen, "Non-parametric Probabilistic Forecasts of Wind Power : Required Properties and Evaluation," no. May, pp. 497–516, 2007.

[56] G. Papaefthymiou and D. Kurowicka, "Using copulas for modeling stochastic dependence in power system uncertainty analysis," *IEEE Transactions on Power Systems*, vol. 24, no. 1, pp. 40–49, 2009.

[57] F. Teng, R. Dupin, A. Michiorri, G. Kariniotakis, Y. Chen, and G. Strbac, "Understanding the Benefits of Dynamic Line Rating under Multiple Sources of Uncertainty," *IEEE Transactions on Power Systems*, vol. 8950, no. c, 2017.

[58] Y. Li, B. Hu, K. Xie, L. Wang, Y. Xiang, R. Xiao, and D. Kong, "Day-Ahead Scheduling of Power System Incorporating Network Topology Optimization and Dynamic Thermal Rating," *IEEE Access*, vol. 7, pp. 35 287–35 301, 2019.

[59] M. A. Bucher, M. Vrakopoulou, and G. Andersson, "Probabilistic N-1 security assessment incorporating dynamic line ratings," *IEEE Power and Energy Society General Meeting*, 2013.

[60] M. A. Bucher and G. Andersson, "Robust Corrective Control Measures in Power Systems with Dynamic Line Rating," *IEEE Transactions on Power Systems*, vol. 31, no. 3, pp. 2034–2043, 2016.

[61] C. Wang, R. Gao, F. Qiu, J. Wang, and L. Xin, "Risk-Based Distributionally Robust Optimal Power Flow With Dynamic Line Rating," pp. 1–14, 2017. [Online]. Available: http://arxiv.org/abs/1712.08015

[62] J. L. Aznarte and N. Siebert, "Dynamic Line Rating Using Numerical Weather Predictions and Machine Learning: A Case Study," *IEEE Transactions on Power Delivery*, vol. 32, no. 1, pp. 335–343, 2017.

[63] F. D. Galiana, F. Bouffard, J. M. Arroyo, and J. F. Restrepo, "Scheduling and pricing of coupled energy and primary, secondary, and tertiary reserves," *Proc. of the IEEE*, vol. 93, no. 11, pp. 1970–1983, Nov 2005.

[64] F. Wang and K. W. Hedman, "Dynamic reserve zones for day-ahead unit commitment with renewable resources," *IEEE Trans. on Power Syst.*, vol. 30, no. 2, pp. 612–620, 2015.

[65] A. Papavasiliou, S. S. Oren, and R. P. O'Neill, "Reserve Requirements for Wind Power Integration : A Scenario-Based Stochastic Programming Framework," *IEEE Trans. on Power Syst.*, vol. 26, no. 4, pp. 2197–2206, 2011.

[66] A. Papavasiliou and S. S. Oren, "Multiarea stochastic unit commitment for high wind penetration in a transmission constrained network." *Operations Research*, vol. 61, no. 3, pp. 578 – 592, 2013.

[67] J. M. Morales, M. Zugno, S. Pineda, and P. Pinson, "Electricity market clearing with improved scheduling of stochastic production," *European Journal of Operational Research*, vol. 235, no. 3, pp. 765–774, 2014.

[68] S. Delikaraoglou, P. Pinson, "Optimal allocation of HVDC interconnections for exchange of energy and reserve capacity services," *Energy Systems*, vol. 10, no. 3, pp. 635–675, 2019.

[69] V. Dvorkin, S. Delikaraoglou, J.M. Morales, "Setting reserve requirements to approximate the efficiency of the stochastic dispatch," *IEEE Trans. on Power Syst.*, vol. 34, no. 2, pp. 1524–1536, 2019.

[70] M. Golari, N. Fan, and J. Wang, "Two-stage stochastic optimal islanding operations under severe multiple contingencies in power grids," *Electric Power Systems Research*, vol. 114, pp. 68–77, 2014.

[71] N. Fan, D. Izraelevitz, F. Pan, P. M. Pardalos, and J. Wang, "A mixed integer programming approach for optimal power grid intentional islanding," *Energy Systems*, vol. 3, no. 1, pp. 77–93, 2012.

[72] H. Pandzic, Y. Dvorkin, T. Qiu, Y. Wang, and D. Kirschen, "Unit Commitment under Uncertainty - GAMS Models," *Library of the Renewable Energy Analysis Lab (REAL)*. [Online]. Available: http://www.ee.washington.edu/research/real/gams_code.html

[73] K. W. Hedman, S. Member, M. C. Ferris, R. P. O. Neill, E. B. Fisher, S. Member, and S. S. Oren, "Co-Optimization of Generation Unit Commitment and Transmission Switching With N-1 Reliability," vol. 25, no. 2, pp. 1052–1063, 2010.

Collection of publications

[**Pub. A**] N. Viafora, J. G. Møller, R. A. Olsen, A. S. Kristensen and J. Holbøll, "Historical Data Analysis for Extending Dynamic Line Ratings Across Power Transmission Systems," *2018 IEEE International Conference on Probabilistic Methods Applied to Power Systems (PMAPS)*, Boise, ID, 2018, pp. 1-6.

[**Pub. B**] N. Viafora, K. Morozovska, S.H.H. Kazmi, T. Laneryd, P. Hilber, J. Holbøll, "Day-ahead dispatch optimization with dynamic thermal rating of transformers and overhead lines", *(2019) Electric Power Systems Research*, 171, pp. 194-208.

[**Pub. C**] N. Viafora, J. Holbøll, S. H. H. Kazmi, T. H. Olesen and T. S. Sørensen, "Load Dispatch optimization using Dynamic Rating and Optimal Lifetime Utilization of Transformers," *2019 IEEE Milan PowerTech*, Milan, Italy, 2019, pp. 1-6.

[**Pub. D**] N. Viafora, S. Delikaraoglou, P. Pinson, J. Holbøll, "Chance-constrained optimal power flow with non-parametric probability distributions of dynamic line ratings", *(2020) International Journal of Electrical Power and Energy Systems*, 114, art. no. 105389.

[**Pub. E**] N. Viafora, S. Delikaraoglou, P. Pinson, G. Hug, J. Holbøll, "Dynamic Reserve and Capacity Allocation in Wind-Dominated Transmission Systems", submitted to *IEEE Transactions on Power Systems*

[Pub. A]

Notes

Accepted version of paper [Pub. A].
Published version available at:
https://ieeexplore.ieee.org/document/8440449

Historical Data Analysis for Extending Dynamic Line Ratings Across Power Transmission Systems

Nicola Viafora[1], Jakob G. Møller[1], Rasmus A. Olsen[2], Anders S. Kristensen[2] and Joachim Holbøll[1]
[1]Center for Electric Power and Energy, DTU Kgs. Lyngby, Denmark, nicovia@elektro.dtu.dk
[2]Energinet, Erritsø, Denmark

***Abstract*—Dynamic Line Rating (DLR) consists in an innovative way to operate power systems, which allows for higher power flows on transmission lines depending on weather conditions. Extending the application of DLR technology from one to numerous lines across a larger transmission power system presents challenges with respect to the scalability due to the large amount of data required. Firstly, a modified overhead line thermal model and the use of historical weather data are considered in this paper to preliminary assess the margin for increased rating of transmission lines. Secondly, spatial correlation of line ratings are analyzed and a comparison of various rating approaches, which rely on different combinations of weather variables, is presented. The resulting probability distributions of line ratings are compared with constant seasonal ratings highlighting the trade-off between those solutions that yield a large increase in rating at a cost of high volatility, against simpler approaches which are more conservative and require less information. The results reported are based on actual data of the western section of the Danish power transmission system.**

***Index Terms*—Dynamic line rating, historical weather data, correlation, overhead lines, thermal model**

I. Introduction

It is a common practice among Transmission System Operators (TSOs) to dimension and operate transmission lines in a very conservative way by assuming unfavourable thermal conditions, which limit the admissible line current to low values [1]. However, the analysis of historical weather data suggests that relaxing some of the existing tight thermal constrains could ease the allocation of extra capacity in the system [2]. This consideration especially applies to those lines shorter than 80 km, whose ampacity is thermally limited, as opposed to long ones where power transfer capabilities are usually dictated by voltage or stability constrains [3].

Therefore, driven by the need to increase the utilization of existing assets, Dynamic Line Rating (DLR) could provide the TSOs with a tool for enhancing grid flexibility and coping with increasing shares of intermittent renewable generation. Additionally, results from [4] show that this technology has the ability to increase transmission system reliability, especially when considering correlations between line ratings. The proven positive correlation between cooling effect on overhead line conductors and wind power generation [5], further motivates the adoption of DLR technology as a means for improving wind power integration.

Several pilot projects [6] have demonstrated the effectiveness of DLR, but it remains an open research question whether this rating approach is scalable to transmission systems as a whole that span over wide geographical areas. Extending the application of such technology to larger parts of the power system is hindered by the need of large amount of data. In order to correctly estimate the operating temperature of a conductor, state of the art thermal models from Cigré and IEEE, [7] and [8] respectively, require detailed information about local weather conditions, which are difficult assess and often affected by high uncertainty [9].

The risk associated with DLR is not exclusively due to data uncertainty. Simplified approaches in the thermal models also contribute to the possibility of overestimating the line rating. Approaching the thermal limits, the temperature gradient between the center of the conductor and its surface cannot be neglected and it can reach values as high as 20 °C [10] - [11]. Exceeding the maximum core temperature is likely to cause a violation of the clearance requirements, as above the knee-point temperature the sag mainly depends on the steel thermal dilatation [12]. Despite acknowledging the relevance of the radial temperature drop, the guide in [7] does not consider it in the rating calculations, as it assumes a uniform temperature distribution in the cross-section.

Therefore, the first contribution of this paper is to propose a modified thermal model based on [7] that accounts for the radial temperature drop in conductors. This ensures that the maximum operating temperature is not exceeded at the center, where the temperature is highest. Secondly, this paper reports the results of a preliminary assessment of thermal ratings across the western Danish transmission system. Historical weather data utilized to derive the ratings have been simulated by means of the mesoscale downscaling method presented in [13], which generates time series of wind speed and other meteorological fields for the considered geographical location.

Furthermore, a comparison of different rating approaches is discussed, studying the same thermal model applied to different combinations of weather variables. This allows to test various alternatives for implementing DLR across transmission systems, considering simple solutions that require less inputs.

The paper is organized as follows. Section II reviews the adopted guide for thermal ratings and elaborates on the modifications that have been introduced. Section III presents the historical weather data from which the DLR have been derived. Section IV presents the comparative approach to different gradations of DLR. Section V presents key statistics of thermal ratings across the considered transmission system, whereas Section VI concludes the paper.

II. Overhead Line Thermal Modelling

A. Cigré Steady State Rating

Thermal limits of overhead lines are determined by the maximum temperature at which the conductors can be operated without violating clearance requirements or compromising structural integrity of materials. Assuming the cross-section of the conductor to be isothermal, the operating temperature results from a thermal equilibrium between several heat sources and cooling mechanisms. Equation (1), known as the Heat Balance Equation (HBE), models such per-unit-length thermal balance in steady state conditions. Joule losses P_J and solar heating P_S contribute to the temperature rise over time, whereas convective cooling P_C and radiative cooling P_R act against it. Table I lists the relevant quantities that are used throughout this section.

$$P_J + P_S - P_C - P_R = 0 \tag{1}$$

The convective cooling P_C, in particular, is the term that dissipates most of the heat generated in the conductor. Equation (2) models such heat transfer mechanism where λ_f is the thermal conductivity of the air, T_s is the conductor surface temperature, T_{air} is the surrounding air temperature and Nu is the Nusselt Number which mainly depends upon wind speed, wind angle of attack and wind regime.

$$P_C = \pi \cdot \lambda_f \cdot (T_s - T_{air}) \cdot Nu \tag{2}$$

The P_i terms in (1) are highly weather dependent and for a detailed description of the various heating and cooling mechanism, the reader is referred to [7].

For steady state rating calculations under a given set of weather variables, the conductor is assumed in thermal equilibrium with the environment. The HBE is solved for the current I which solely appears in the joule losses term $P_J = I^2 \cdot R_{ac}$, where R_{ac} is the AC resistance at maximum operating temperature. The resulting value is therefore the current for which the conductor reaches asymptotically the maximum operating temperature, given a set of constant weather variables. For overhead lines operated with n bundled conductors, it has been assumed that no mutual heating occurs between bundles and that the phase current is equally distributed among the bundles so that $I_{phase} = n \cdot I_{bundle}$ holds.

B. Proposed Modifications

As the line current approaches the steady state rating, conductor current densities may be greater than 2 or 3 A/mm^2 [7]. If the steady state rating is set according to (1), the radial temperature drop can be such to require a de-rating of the line in order not to overheat the centre of the conductor. Accounting for the this aspect in the steady state estimation algorithm, can be achieved by relying on the system comprised of (3a), (3b) and (3c).

$$\begin{cases} P_J(I, T_{av}) + P_S - P_C(T_s) - P_R(T_s) = 0 & \text{(3a)} \\ T_c - T_s = \dfrac{P_H(I, T_{av})}{2\pi\lambda}\left[\dfrac{1}{2} - \left(\dfrac{D_1^2}{D^2 - D_1^2}\ln\dfrac{D}{D_1}\right)\right] & \text{(3b)} \\ T_c + T_s = 2T_{av} & \text{(3c)} \end{cases}$$

TABLE I
Nomenclature

Symbol	Unit	Name
P_J	[W/m]	Joule heating
P_S	[W/m]	Solar heating
P_C	[W/m]	Convective cooling
P_R	[W/m]	Radiative cooling
P_H	[W/m]	Total heat gain
I	[A]	Current rms
R_{ac}	[Ω/m]	AC resistance
T_c	[°C]	Conductor core temperature
T_s	[°C]	Conductor surface temperature
T_{av}	[°C]	Conductor average radial temperature
T_{air}	[°C]	Surrounding air temperature
ΔT_{cs}	[°C]	Radial temperature drop
λ_f	[W/(m·K)]	Thermal conductivity of the air
λ	[W/(m·K)]	Effective radial thermal conductivity
D	[m]	Conductor outer diameter
D_1	[m]	Inner steel core diameter.
Nu	[-]	Nusselt number

Unlike the procedure discussed in II-A where the rating is found by solely solving (3a) for the current, the system of non-linear equations in (3) is solved for I, T_{av} and T_s, which are the steady state rating, the average and the surface conductor temperature, respectively. Equation (3a) is the HBE in steady state conditions, where the dependency upon the system variables has been highlighted. Equation (3b) models the radial temperature drop and (3c) defines the average temperature in the cross-section. The maximum operating temperature is set on the center of the conductor, thus the core temperature T_c in the system has to be chosen *a priori*.

The radial temperature drop is estimated in a simplified way according to equation (3b), presented in [7]. In (3b) P_H is the total heat gain per unit length of the conductor and it is approximated with the sum of Joule losses P_J and solar heating P_S. As in [7], internal heat generation is assumed to be uniformly distributed in aluminum wires. This implies that the impact of skin effect on temperature distribution is not considered, even though the skin effect is accounted for in the AC resistance calculations. Lastly, the conductor is modelled as a uniform cylinder with λ being the effective radial thermal conductivity. This parameter accounts for interstices and air gaps between strands which worsen the heat transfer from the center to the outer surface of the conductor. λ depends on numerous factors among which is the tension of aluminum strands. Typical values range from 0.5 to 7 W/(m·K) and in this work a conservative constant value of 0.7 is assumed as suggested in [7].

Compared to (1), the solution of (3) yields the highest steady state current that results in the maximum operating temperature being reached at the center of the conductor. A lower surface temperature at the thermal equilibrium reduces the convective heat transfer and thus the ability to dissipate heat. Consequently, the ampacity obtained accounting for the radial temperature drop is reduced. Fig. 1 shows the de-rating introduced by this approach compared to the rating algorithm described in II-A. As the wind speed increases, the radial

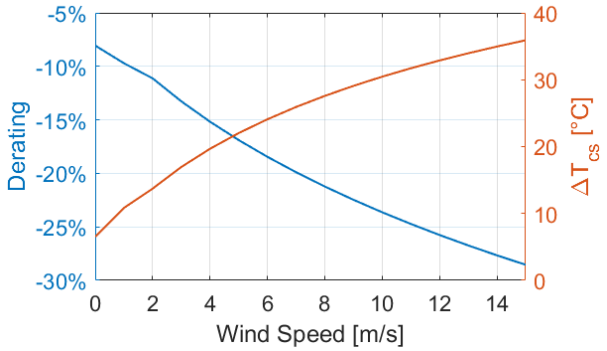

Fig. 1. Derating of line ampacity introduced in the proposed model with respect to model in [7]. Derating and corresponding radial temperature drop are derived for a Drake conductor and different values of wind speed. Other weather variables are assumed constant at the reference values in Fig. 2

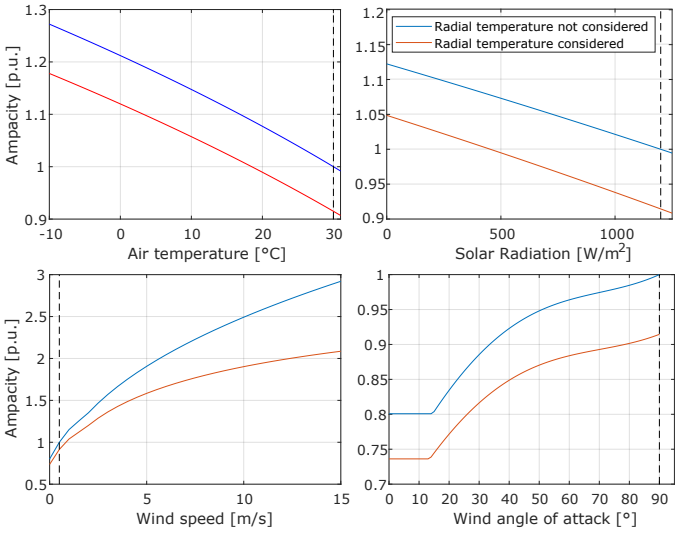

Fig. 2. Sensitivity analysis of weather variables on ampacity of a ACSR Drake conductor. Vertical dashed line shows the reference value for each variable: wind speed 0.5 m/s, wind direction 90 °, air temperature 30 °C and solar radiation 1200 W/m^2. Absorptivity = 0.8, Emissivity = 0.8

temperature drop grows larger and the rating is reduced accordingly. Attenuating the influence of the convective cooling in windy conditions also reduces the risk of overestimating the true thermal limits. Therefore, this approach offers a conservative way to account for large temperature differences within the conductor by relying on existing guides for thermal rating.

C. Sensitivity analysis

Four main weather variables are considered in the thermal rating estimation: air temperature, solar radiation, wind speed and direction. The influence of each one of these on the rating of a ACSR Drake conductor is shown in Fig. 2. From the comparison between the proposed modification and the original rating algorithm in [7], it emerges that accounting for the radial temperature drop in conductors attenuates in particular the influence of high wind speeds. Wind speed at 0.5 m/s reduces the rating by 10%, whereas at 14 m/s the attenuation reaches nearly 27%. Fig. 2 also shows that the sensitivity of other weather variables on the ampacity is not affected by the introduced modification, i.e. variations of air temperature, wind direction and solar radiation result in the same relative change in ampacity.

III. Historical Weather Data

The results presented in this study are based on simulated time series of weather data that were produced using the mesoscale numerical model "Weather, Research and Forecasting Model". The simulated weather data preserve the typical spatio-temporal correlations that real measurements would have. The specific simulation that generated the data utilized in this study is presented in [14].

Fig. 3 shows the location of the weather data points in comparison with the outline of the real transmission system. The line azimuths have been calculated in a simplified way by assuming the lines to be piece-wise straight in major sections. The weather variables considered for estimating DLR are: wind speed and direction at 15 meters above ground, air temperature and integrated solar radiation. Elevation with respect to the sea level is included and different values of terrain roughness are implemented as well depending on the estimated land use. The weather data was sampled along the direction of the transmission lines using an horizontal spacing of 5 km. Parallel lines share the same data points whereas for those lines shorter than the minimum spatial resolution a single point defines the thermal state. As discussed in [7], the poor axial temperature equalization of conductors may cause large temperature differences in a single span, due to local sheltering effects which limit the convective cooling. An accurate estimation of the local wind profile on overhead lines should also include sheltering effect due to nearby objects, but this aspect could not be accounted for in this study.

This study relied on hourly weather data that was obtained for a period of 3 years from January 2014 through January 2017. According to [15], using 60 minutes averaged values of the weather variables, the estimated DLR could be higher than the real one 1.6% of the time. This aspect consists in a second limitation of the study which is in part compensated by the adoption of the thermal model presented in Section II, as this conservatively accounts for wind speed.

IV. Methodology

For each hour of the considered time period and for all the locations considered in Fig. 3, the steady state thermal model proposed in Section II-B is solved using the weather data presented in Section III. At any given time, the value of DLR is determined as the lowest value of I in (3) reached along the line, as the location with the worst thermal condition determines the maximum loadability for the entire line.

All simulated DLRs are expressed relatively to the constant Seasonal Line Ratings (SLRs) of the considered transmission system. These line ratings are set by assuming conservative weather conditions that are listed in Table II. Conservatism in

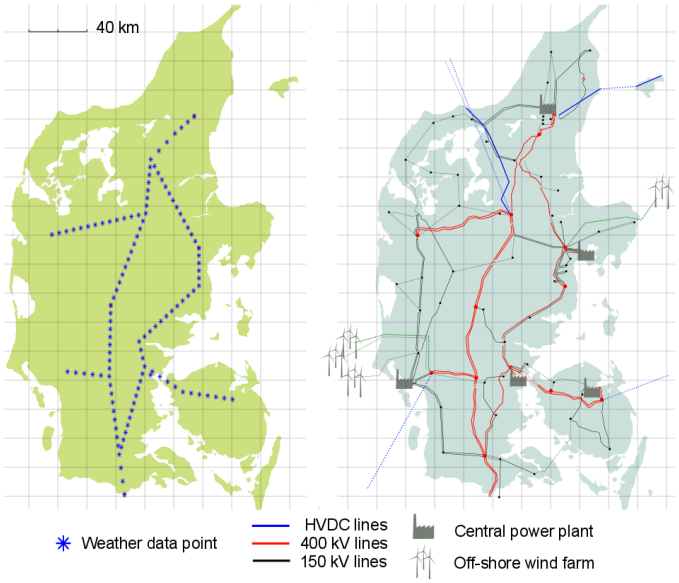

Fig. 3. Overview of the location of the weather data points (left). Overview of the western Danish transmission lines taken as a reference case (right). Weather data have been considered only for AC lines at 400 kV.

this aspect is common among TSOs, which have to limit the probability of thermal overload as much as possible during normal operation of the system. Therefore, the TSO sets a single base value of wind speed per season for the entire system: 0.6 m/s in summer and 0.7 m/s in winter. Fig. 4 shows the probability distribution of wind speed and ambient temperature respectively, considering all three years of data at disposal regardless of their location. This allows to compare the base values set by the TSO with the actual distribution of these variables. The base values of wind speed provided in Table II correspond approximately to the first 1% quantile of the distribution for both summer and winter. Air temperature values correspond to the top 15% and top 10% quantiles for summer and winter respectively. The values assumed for the incident solar radiation instead are both well beyond the top first 1% quantile and close to the highest simulated values in the three-years period, which are 900.4 W/m^2 in summer and 653.7 W/m^2 in winter.

The comparative approach adopted throughout the study serves the purpose to present different gradations of DLR, which vary in complexity, expected rating increase and overall variability. Five cases are tested by selecting specific combinations of the available weather data, i.e. air temperature, wind speed, wind direction and solar radiation. Table II lists which weather variables are considered in each case. The rationale of this approach is to gradually relax the tight assumptions of the TSO, by considering the actual time series of weather data instead of the fixed seasonal values. *Case 1* solely considers the air temperature time series keeping all the other inputs to the thermal model constant at their seasonal values. *Case 2* introduces the influence of solar radiation, thus standing for the case which is expected to yield the maximum increase in rating without accounting for the wind profile. *Case 3* and

TABLE II
WEATHER VARIABLES ASSUMED BY THE TSO AND OVERVIEW OF THE SIMULATED CASES.

		Air Temp.	Solar Radiation	Wind Speed	Wind Direction
		°C	W/m^2	m/s	°
TSO	*Summer*	20	900	0.6	90
	Winter	10	600	0.7	90
Case 1		✓	-	-	-
Case 2		✓	✓	-	-
Case 3		✓	-	✓	0
Case 4		✓	✓	✓	0
Case 5		✓	✓	✓	✓

✓ *From historical weather data*
\- *As assumed by the TSO*

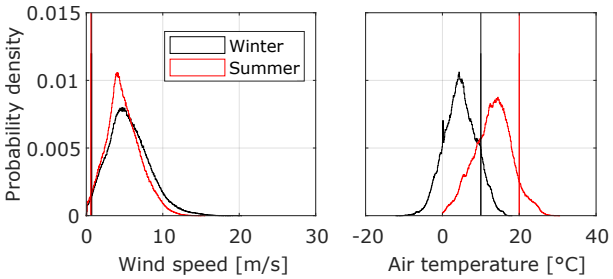

Fig. 4. Probability density distribution of weather variables across the western Danish power system. Vertical lines mark typical conservative values assumed by TSO for steady state loading calculations in winter and summer. The graphs share the same scale on the y-axis

Case 4 add the historical time series of wind speed to the first two cases. As wind speed is known to sharply increase the rating, this variable is introduced in a conservative way by assuming wind always parallel to the conductors. As the relative angle between wind direction and conductor axis is known to have an impact on the rating, these cases allow to estimate the minimum increase in rating due to wind speed. Ultimately, from the comparison of *Case 4* and *Case 5*, the impact of wind direction can be analyzed. *Case 5* considers the historical data of all the inputs and therefore stands as the best estimate of the full rating potential.

V. RESULTS

This section reports the results of the system-wide evaluation of DLR following the methodology presented in Section IV. The thermal model described in Section II-B is adopted to assess DLRs across the system. The comparison is performed in terms of probability distribution of ratings and correlation.

A. Probability distribution of ratings

Fig. 5 shows the probability density and cumulative distribution function of DLRs across the considered system. The simulated hourly ratings of each line are normalized with the corresponding SLR set by the TSO, in order to show the relative gain or reduction in line ampacity throughout the year. This also allows to aggregate the results and provide a system overview of the ratings. As SLRs differ from line to line, the reference value of "1" in Fig. 5 stands for the steady state system rating considering all 23 transmission lines at once.

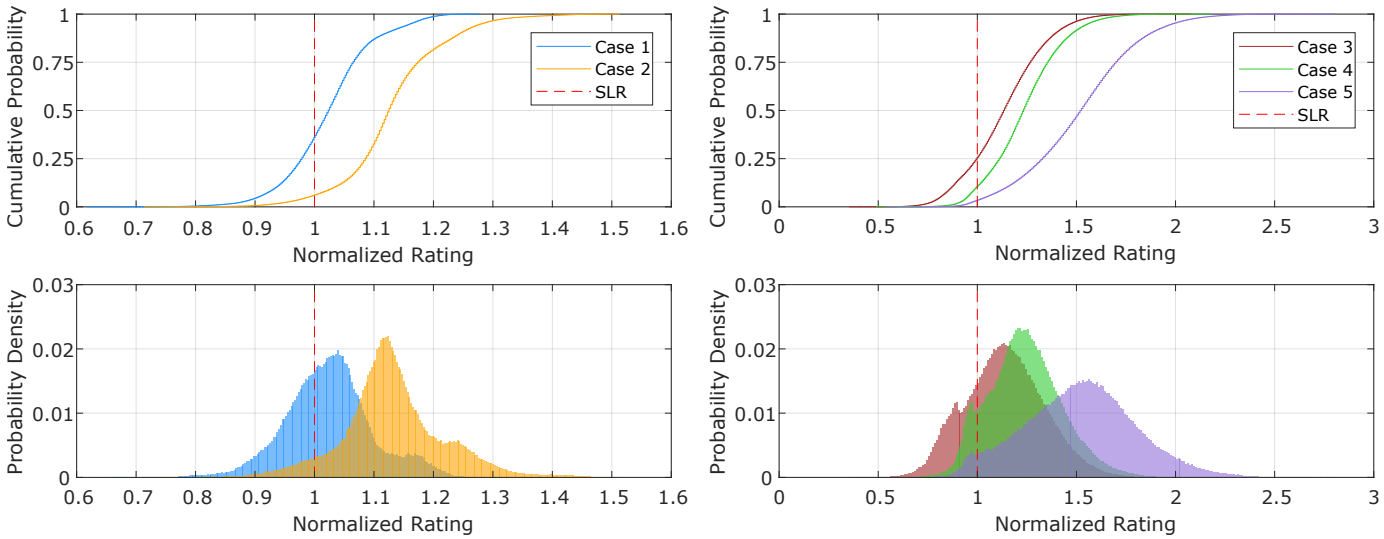

Fig. 5. Probability density and cumulative distribution function of DLRs in the system. All values are normalized with the SLR of the corresponding line. A description of the weather variables included in each case is presented in Table II in Section IV.

Table III collects key statistics of the probability distributions of DLR across the system considering the entire time period analyzed. The expected values of the distributions are derived as $E = \sum_i P(x_i) \cdot x_i$, where x_i are values of rating and $P(x_i)$ the corresponding probability.

It appears as expected that the cases which do not take the historical wind profile into account yield a lower increase in rating, as opposed to the others. Estimating the DLR solely by means of variable air temperature, as in *Case 1*, yields an increase of 2% in the expected value of the probability density distribution. Accounting for the solar radiation in *Case 2* is found to increase the rating by and additional 10%. Such weather variable plays a key role in determining the rating in low wind conditions. This behavior can be verified comparing the 0.025-quantiles in *Case 3* and *Case 4*, whose sole difference lays in the solar radiation. The lower tail region of the distribution in *Case 3* is almost 20% lower than in *Case 4*, meaning that high solar radiation in low wind conditions considerably worsen the thermal ratings.

As the number of inputs to the thermal model increases, so does the gain in rating but at the cost of introducing additional variability into the system. The sole exception from *Case 3* to *Case 4*, where σ is slightly reduced, is due to the effect of long periods with zero solar radiation in winter. Generally, those cases in which the wind speed profile is taken into account exhibit higher expected values but also higher standard deviation, as reported in Table III. *Case 5* in particular reaches the highest gain due to the combined effect of wind speed and direction yielding a 50% increase in the expected value of DLR and doubling the thermal rating with a probability of 2.5 %. Nevertheless, *Case 5* only considers the prevalent direction of each transmission line, thus overestimating the additional cooling effect. As line azimuth varies on a per-span granularity, the actual influence of wind direction is expected to be a compromise between *Case 4* and *Case 5*.

Overall, this comparative approach suggests that the TSO might have several alternatives to implement different gradations of DLR. Excluding some weather variables from the thermal model would sacrifice a part of the potential increased in rating in favour of more predictability and stability of the DLRs. Nevertheless, it has to be stressed that the conservative approaches like *Case 1* and *Case 2* still do not exclude the occurrence of low wind speed conditions.

TABLE III
KEY STATISTICS OF DLR DISTRIBUTIONS

	Quantiles		Expected value	Standard deviation
	0.025	**0.975**	**E**	σ
Case 1	0,87	1,18	1,02	0,07
Case 2	0,95	1,31	1,13	0,09
Case 3	0,77	1,53	1,14	0,20
Case 4	0,91	1,63	1,24	0,19
Case 5	0,97	2,08	1,52	0,28

B. Investigating correlation

Fig. 5 alone does not provide any information about the contemporaneity of the DLRs, as it considers the system rating as a whole. Therefore, a key aspect of DLR that has to be investigated is the correlation between line ratings, as an indicator of the ability to unlock extra transmission capacity in the system. Furthermore, as DLRs are expected to facilitate wind power integration, the correlation between line ratings and wind power generation is also a key aspect to take into consideration. Fig. 6 illustrates the values of the correlation coefficient ρ_{ij} derived by means of (4) for each of the considered approaches to DLR.

$$\rho_{ij} = \frac{\mathrm{Cov}[X_i, X_j]}{\sigma_i \sigma_i} \tag{4}$$

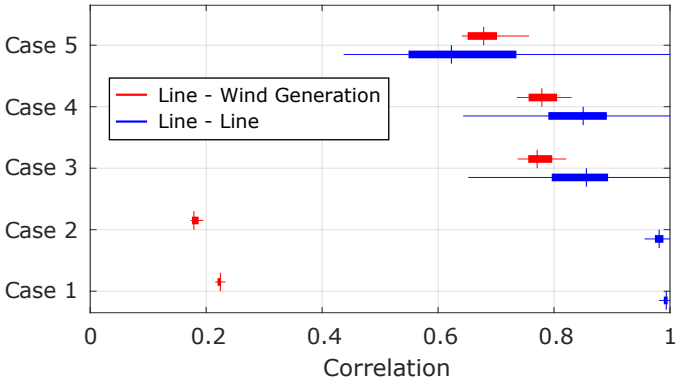

Fig. 6. Boxplot of correlation between ratings of different lines *(Line - Line)* and between line ratings and historical wind power generation in the considered power system *(Line - Wind Power Generation)*.

When estimating the correlation between lines, X_i and X_j in (4) represent the random variables describing the ratings in line i and j, respectively. From the comparison in Fig. 6 it stands out as the conservative approaches of *Case 1* and *Case 2* exhibit high correlation between the ratings of different lines. These values reflect the original correlation in the input variables, since air temperature is a slow-varying and spatially uniform variable compared to wind speed. *Case 3* and *Case 4* consider instead the historical wind speed and thus DLRs in these cases are less correlated between each other. Ultimately, accounting for the actual wind direction in the rating algorithm of *Case 5* further reduces the correlation since additional degrees of freedom are introduced in the rating estimation. When estimating the correlation of DLRs with wind power generation instead, the trend is reversed. Slow varying and stable ratings based on air temperature variations are less correlated with wind power generation compared to the other approaches which consider the wind profiles in the thermal model.

VI. Conclusions

This paper presented a system-wide analysis of dynamic line ratings based on simulated weather data across a transmission power system. This paper also introduced an overhead line thermal model that accounts for the radial temperature drop in the cross-section of the conductors. This novel approach allows for a conservative estimation of the convective cooling on overhead lines, ensuring that the maximum operating temperature is not violated at the core of the conductor. The application of the proposed thermal model to large parts of an actual transmission system revealed the margin for increased utilization of the existing asset, depending upon which weather variables are considered. Furthermore, this study considered five different combinations of the inputs to the thermal model in order to illustrate different possible gradations of DLR and test the sensitivity of the rating algorithm.

Results are offered in terms of probability distributions of hourly ratings and highlight the differences between the tested cases in terms of expected gain in the line thermal limits, variability and correlation. On the one hand, conservative approaches to DLR, which only consider part of the weather variability, require less data and information to be implemented. These ratings are also likely to be more stable and highly correlated across the system. On the other hand, accounting for the full variability of the weather would result in higher but also more volatile ratings. This study has also investigated the correlation between DLR and historical wind power generation concluding that accounting for wind speed in the thermal rating algorithm increases such value. This latter consideration in particular is recognized to be a key aspect in future studies that will investigate DLR as a means to support wind power integration, not only on a regional level, but across transmission systems.

References

[1] J. Heckenbergerova, P. Musilek and K. Filimonenkov, "*Assessment of seasonal static thermal ratings of overhead transmission conductors*", 2011 IEEE Power and Energy Society General Meeting, San Diego, CA, 2011, pp. 1-8.

[2] M. W. Davis, "*A New Thermal Rating Approach: The Real Thermal Rating System for Strategic Overhead Conductor Transmission Lines Part V Monthly and Annual Accumulative Frequency Distributions of Hourly Real-Time Thermal Rating and their Comparison with Conventional Rating-Risk Curves*" in IEEE Transactions on Power Apparatus and Systems, vol. PAS-99, no. 6, pp. 2193-2209, Nov. 1980.

[3] L. Dawson and A. Knight, "*Applicability of Dynamic Thermal Line Rating for Long Lines*", in IEEE Transactions on Power Delivery, vol. PP, no. 99, pp. 1-1.

[4] J. Teh, C. M. Lai and Y. H. Cheng, "*Impact of the Real-Time Thermal Loading on the Bulk Electric System Reliability*", in IEEE Transactions on Reliability, vol. 66, no. 4, pp. 1110-1119, Dec. 2017.

[5] G. A. Orfanos, P. S. Georgilakis and N. D. Hatziargyriou, "*Transmission Expansion Planning of Systems With Increasing Wind Power Integration*", in IEEE Transactions on Power Systems, vol. 28, no. 2, pp. 1355-1362, May 2013.

[6] TWENTIES project, "*Demonstration project 6 – Improving flexibility of the grid (FLEXGRID)*", October 2013

[7] Cigré Working Group B2.43, "*Guide for Thermal Rating Calculations of Overhead Lines*", International Council on Large Electric Systems, Technical Brochure 601, December 2014

[8] "*IEEE Standard for Calculating the Current-Temperature of Bare Overhead Conductors*", IEEE Std 738-2006, 2007

[9] A. Michiorri *et al*, "*Forecasting for dynamic line rating*, Renewable and Sustainable Energy Reviews, Volume 52, 2015, Pages 1713-1730

[10] J. Rodriguez Alvarez and C. M. Franck, "*Radial Thermal Conductivity of all-Aluminum Alloy Conductors*", in IEEE Transactions on Power Delivery, vol. 30, no. 4, pp. 1983-1990, Aug. 2015.

[11] B. Clairmont, D.A. Douglass, J. Iglesias, Z. Peter, "*Radial and Longitudinal Temperature Gradients in Bare Stranded Conductors with High Current Densities*", in Cigré Session B2-108, 2012.

[12] I. Albizu, E. Fernández, A. J. Mazón, M. Bedialauneta and K. Sagastabeitia, "*Overhead conductor monitoring system for the evaluation of the low sag behavior*", 2011 IEEE Trondheim PowerTech, Trondheim, 2011, pp. 1-6.

[13] A. Hahmann, C. Vincent, A. Peña, J. Lange and C. Hasager, "*Wind climate estimation using WRF model output: method and model sensitivities over the sea*", International Journal of Climatology, vol 35, pp. 3422-3439, 2015

[14] A. Peña Diaz, A. N. Hahmann, "*30-year mesoscale model simulations for the "Noise from wind turbines and risk of cardiovascular disease" project*, DTU Wind Energy E, Vol. 0055, 2017.

[15] J. Hosek, P. Musilek, E. Lozowski and P. Pytlak, "*Effect of time resolution of meteorological inputs on dynamic thermal rating calculations*", in IET Generation, Transmission & Distribution, vol. 5, no. 9, pp. 941-947, September 2011.

[Pub. B]

Notes

Published journal article version of [Pub. B].
Available at:
https://doi.org/10.1016/j.epsr.2019.02.026

Electric Power Systems Research 171 (2019) 194–208

Contents lists available at ScienceDirect

Electric Power Systems Research

journal homepage: www.elsevier.com/locate/epsr

Day-ahead dispatch optimization with dynamic thermal rating of transformers and overhead lines

Nicola Viafora[a,*], Kateryna Morozovska[b], Syed Hamza Hasan Kazmi[c], Tor Laneryd[d], Patrik Hilber[b], Joachim Holbøll[a]

[a] Dept. of Electrical Engineering, Technical University of Denmark, Lyngby, Denmark
[b] Dept. of Electromagnetic Engineering, School of Electrical Engineering and Computer Science, KTH Royal Institute of Technology, Stockholm, Sweden
[c] Ørsted Offshore Wind A/S, Gentofte, Denmark
[d] Corporate Research, ABB AB, Västerås, Sweden

ARTICLE INFO

Keywords:
Dynamic line rating
Dynamic transformer rating
Power system optimization
Optimal power dispatch
Wind power integration

ABSTRACT

Several studies have demonstrated how Dynamic Line Rating (DLR) could be an effective solution for increasing transmission capacity of existing overhead lines. As opposed to Static Line Ratings (SLR), DLR allows for higher power flows depending on real time thermal state of conductors, which highly depend on actual weather conditions. Similarly, recent advances in transformer thermal modelling revealed the feasibility of Dynamic Transformer Rating (DTR) based on the temporal evolution of top oil and winding hot spot temperatures. However, the joint dynamic thermal rating of both overhead lines and transformers in transmission networks has not been thoroughly addressed yet in the literature.

This paper proposes a day-ahead dispatch optimization problem based on DC-Optimal Power Flow, where transformer top oil and hot spot dynamics are directly accounted for together with dynamic line ratings of selected transmission lines. Simulated weather data from an actual power system are mapped to the IEEE RTS 24 bus system thus allowing for the estimation of DLR on several lines and the influence of ambient temperature on transformer rating. Results indicate the potential benefits that using DLR in conjunction with DTR could provide for the optimal power system dispatch. The proposed approach does not only indicate advantages compared to standard rating scenarios, but also shows a positive impact that dynamic line rating has on unlocking transformer constraints and vice versa.

1. Introduction

The electrical power system is evolving and so are the associated challenges. These challenges include aging infrastructure and integration of decentralized generation in the network. Moreover, the influx of Renewable Energy Sources (RES) at points in the grid, which were not initially planned to deal with more energy, can result in extensive bottlenecks in the system [1]. Some of these bottlenecks can be rectified or large-scale investments in the grid can at least be delayed by using dynamic rating for major components including Over Head Lines (OHL), transformers and cables.

Dynamic rating of Overhead Lines, or Dynamic Line Rating (DLR), makes use of the under-utilized potential of power lines, which are traditionally over-dimensioned by assuming conservative weather conditions. The thermal rating guidelines for OHL [2] and [3], from IEEE and Cigré respectively, report considerable upgrade in line ratings if one switches from conservative static rating to dynamic rating based on varying weather conditions.

Similarly, Dynamic Transformer Rating (DTR) allows the transformers to be used beyond their nameplate ratings by setting a limit on maximum thermal capacity for given ambient temperature and load profile. The maximum thermal capacity is determined by the section of the transformer that is under the largest thermal stress, which is usually at the top region of the winding insulation [4]. The dynamic thermal assessment of a transformer can be performed using a number of thermo-electric models of varying accuracy in [4], [5] and [6].

On the one hand, the applications of dynamic rating for OHL and transformers as individual network components have been discussed extensively in the existing literature [7]. The facilitation of wind power integration using DLR has been explored in [8], [9] and [10], whereas similar studies have been performed using DTR for cases with transformers as primary system bottlenecks [11], [12]. On the other hand,

* Corresponding author.
E-mail address: nicovia@elektro.dtu.dk (N. Viafora).

https://doi.org/10.1016/j.epsr.2019.02.026
Received 31 October 2018; Received in revised form 31 January 2019; Accepted 22 February 2019

Nomenclature

q_J	Joule losses, [W/m]
q_S	Solar heating, [W/m]
q_C	Convective cooling, [W/m]
q_R	Radiative cooling, [W/m]
$C_{\text{th,ohl}}$	Thermal capacitance of OHL conductor, [kWh/°C]
ΔT_{cs}	Radial temperature drop, [°C]
$I_{\text{ohl}}^{\max}$	*Per unit* maximum allowed loading of OHL conductor
ϑ_c	Core temperature of OHL conductor, [°C]
ϑ_s	Surface temperature of OHL conductor, [°C]
λ	Equivalent radial thermal conductivity, [WKm^{-1}]
D	Outer diameter of OHL conductor, [m]
D_1	Inner steel core diameter of OHL conductor, [m]
ϑ_{av}	Average conductor temperature for cross-sectional area, [°C]
τ_0	Thermal time constant for oil in transformers, [h]
τ_h	Thermal time constant for winding, [h]
ϑ_{u}	Ultimate top-oil temperature rise for transformer load I, [°C]
ϑ_{top}	Transformer top-oil temperature (TOT), [°C]
ϑ_{hu}	Ultimate hot-spot temperature rise for transformer load I, [°C]
ϑ_{hst}	Transformer hot-spot temperature (HST),[°C]
ϑ_{amb}	Ambient temperature, [°C]
I_{trf}	*Per unit* transformer load current with rated load current as base
ϑ_{or}	Top-oil rise over ambient temperature ϑ_{amb} at rated load, [°C]
L_{fl}	Total transformer losses at rated load, [W]
R	Ratio of load losses to no-load losses at rated load for transformer
$C_{\text{th,trf}}$	Thermal capacitance of oil in transformer, [MWh/°C]
ν	empirically derived coefficient known as oil exponent
μ	empirically derived coefficient - constant
ϑ_{hr}	Rated host-spot temperature rise for load I, [°C]
ONAN	Oil Natural Air Natural transformer cooling mode
ONAF	Oil Natural Air Forced transformer cooling mode
OFAF	Non directed Oil Forced Air Forced transformer cooling mode
ODAF	Directed Oil Forced Air Forced transformer cooling mode
DLR	Dynamic Line Rating
SLR	Static Line Rating
DTR	Dynamic Transformer Rating
STR	Static Transformer Rating
TOT	Transformer Top Oil Temperature
HST	Transformer Hot Spot Temperature
HBE	Heat Balance Equation for OHL conductor thermal rating
OHL	Overhead Line
TRF	Transformer
$\mathcal{N},\mathcal{G},\mathcal{W},\mathcal{L}$	set of buses, conventional generators, wind farms and branches in the power system
$\boldsymbol{M}$	Power Transfer Distribution Factor matrix
$\boldsymbol{B}_n$, $\boldsymbol{B}_l$	Bus admittance matrix and branch admittance matrix
F_ℓ	*Per unit* power flow through branch ℓ in the system
$\boldsymbol{P}^{\text{inj}}$	*Per unit* nodal power injection in the system
$\boldsymbol{P}^{\text{gen}}$	*Per unit* nodal power generation at each bus
$\boldsymbol{P}^{\text{wnd}}$	*Per unit* nodal wind power generation at each bus
$\boldsymbol{P}^{\text{dem}}$	*Per unit* nodal power demand at each bus
$\boldsymbol{P}^{\text{sh}}$	*Per unit* nodal load shedding
S^{base}	Apparent power base for *per unit* conversion, [MVA]
S^{trf}	Nameplate apparent power rating of transformers, [MVA]
S^{ohl}	Apparent power static line rating of overhead lines, [MVA]
I_{ohl}	*Per unit* line loading
S^{trf}	Nameplate apparent power rating of transformers, [MVA]
$\Delta P_g^{\max}$	Maximum ramping rate of conventional generator g, [pu/h]
P_g	*Per unit* scheduled output for generator g
P_w	*Per unit* dispatched wind power generation for wind farm w
P_w^{av}	*Per unit* available wind power generation for wind farm w
P_n	*Per unit* load demand at bus n
P_n^{sh}	*Per unit* load shedding at bus n
m	Linear mass of OHL conductor, [kg/m]
c	Specific heat capacity of OHL conductor, [J/(kg°C)]
$\Delta\vartheta_{\text{av}}$	Average conductor temperature change, [°C]
Δt	Time resolution equal to 1, [min]
K_1, K_2, K_3	Constants in discretized transformer top-oil model
n, g, w, ℓ	Index for buses, generators, wind farms and branches
$\Delta_{\%}(x)$	Percentage cost reduction
Cost(x)	Total dispatch cost of case x
$\text{Cost}_{\text{STR-SLR}}$	Total dispatch cost for reference case with STR-SLR

systematic application of dynamic rating of multiple components in a network has been a topical research question in recent times. The impact of weather variability on the ratings of major system components including OHL, transformers and cables has been discussed in [13]. Yang et al. discuss the utilization of dynamic network rating for distribution networks in UK (11 kV) to facilitate low carbon electricity network operation [14]. Similarly, the applicability of dynamic rating of several network components for the Swedish grid has been extensively discussed in [15].

Building upon the concept of electro-thermal coordination introduced in [16] and [17], where the power system is dispatched according to temperature of overhead lines rather than their rated values, this paper addresses a novel methodology for transmission power system dispatch. The minimization of load-dispatch cost in the day-ahead market is accomplished by using not only dynamic rating of OHL, but also transformers, which have not been considered so far in the literature. This paper presents a Dynamic DC - Optimal Power flow problem in order to dispatch a power system over a period of 24 hours, considering thermal dynamics in transformers and overhead lines. This approach maximizes the utilization of low cost RES generation and unlocks extra capacity in the entire network.

The IEEE RTS 24-bus network [18] is adjusted with additional wind power generation as well as application of dynamic rating on a transformer and a number of appropriate lines. In this paper, actual load and generation patterns of the Danish transmission system are used in supplement with the actual weather data for Denmark to demonstrate realistic system behavior. The cost-optimized day-ahead hourly load dispatch is compared for different scenarios with DLR and DTR. The concluding argument shows the benefits that combination of DLR and DTR can bring to the system as well as the influence, which dynamically rated lines have on unlocking additional transformer capacity and vice versa. In addition to one day-ahead planning, an analysis of weekly market needs and seasonal load differences are taken into account for more a broader view on the synergies between DLR and DTR.

The rest of the paper is structured as follows. Section 2 elaborates the thermal models used for key temperature estimation and for determination of real-time dynamic rating of OHLs and transformers. The DC Optimal Power Flow (DCOPF) problem devised for this paper for hourly load dispatch cost optimization in the day ahead market is also explained in this section. Section 3 provides a brief background of the test system and presents a comprehensive classification of the test cases that have been formulated for the proposed problem. The results are

then discussed in Section 4 and Section 5 concludes the paper.

2. Methodology

In this section, the thermal models used for calculating dynamic ratings of overhead lines and transformers are discussed. In order to incorporate them in the proposed optimization problem, thermal models are modified accordingly. This section also presents the formulation of the DCOPF problem for load dispatch optimization defining key constraints that set thermal limits of respective components.

2.1. Dynamic line rating

2.1.1. Review of state-of-the-art thermal models

IEEE standard 738 [2] and the *Cigré Technical Brochure 601* [3] are widely recognized as the state-of-the-art thermal models for overhead lines. Despite some differences in the terms of how the convective cooling is accounted for [19], both sources model the conductor thermal equilibrium with a Heat Balance Equation (HBE). Taking as a reference the *Cigré* formulation, the HBE is shown in (1).

$$m\,c\,\frac{d\vartheta_{\mathrm{av}}}{\mathrm{dt}} = q_J + q_S - q_C - q_R \tag{1}$$

The first order differential equation in (1) models a per-unit-length thermal balance in W/m. Joule losses q_J and solar heating q_S contribute to the temperature rise over time $\mathrm{d}\vartheta_{\mathrm{av}}/\mathrm{d}t$, whereas convective cooling q_C and radiative cooling q_R act against it. The heat power terms in the right-hand side of (1) are highly weather dependent: the convective cooling mainly depends upon wind speed, wind angle of attack and ambient air temperature; the radiative cooling depends upon the fourth power of air temperature; and solar heating is determined by the amount of solar radiation that reaches the conductor. Additional terms in the right-hand side of (1) could be introduced to model corona heating, magnetic heating and evaporative cooling as well, but they are not accounted for in this study. For a detailed description of the various heating and cooling mechanism, references [2] and [3] offer an exhaustive treatise.

The thermal capacitance $C_{\mathrm{th,ohl}}$ of the conductor is modelled in (1) as the product of m and c, which stand for the linear mass of the conductor and its specific heat capacity, respectively. These two parameters in the left-hand side of (1) take into account the thermal inertia of the conductor, whose temperature cannot vary instantaneously following a change in the heat balance. The time that the temperature takes to reach 63.2% of its asymptotic value after a step change in current is defined as the thermal time constant and it is usually around 15 min. Fig. 1 shows an example of the evolution of conductor temperature following a step change in current, assuming that weather conditions remain unaltered.

The temperature profile in Fig. 1 has been derived following the steps of the temperature tracking algorithm described in [3]. In particular, the conductor used in this example is a “Drake” 26/7 ACSR, whose outer diameter, core diameter and outer strand diameter are 28.143, 10.4 and 4.44 mm, respectively. Wind speed is fixed at 1.9 m/s and the associated angle of attack at 55°, whereas ambient temperature is kept constant at 24 °C. No solar heating has been considered in this illustrative example and the average conductor temperature is assumed to be uniform in the cross-section. Under these assumption the temperature tracking algorithm has been implemented as follows with (2) and (3), using a time resolution Δt equal to 1 minute.

$$\Delta\vartheta_{\mathrm{av},t} = (q_{J,t} + q_{S,t} - q_{C,t} - q_{R,t})\cdot\frac{\Delta t}{C_{\mathrm{th,ohl}}} \tag{2}$$

$$\vartheta_{\mathrm{av},t+1} = \vartheta_{\mathrm{av},t} + \Delta\vartheta_{\mathrm{av},t} \tag{3}$$

where the heat balance terms q are evaluated at each time step t, $\Delta\vartheta_{\mathrm{av},t}$ is the change in conductor temperature at time t and $\vartheta_{\mathrm{av},t+1}$ the updated temperature. Under these conditions, the transient in conductor's temperature is extinguished within one hour after the step change in current and the temperature has stabilized at its steady state value.

This consideration supports the assumption of using the steady state version of the HBE (1) in the hourly dispatch optimization problem presented in Section 2.4. Hourly values of DLR are derived by solving the HBE for the rms current that appears in the Joule losses term q_J. As discussed in [20], using hourly values of DLR introduces an approximation in the temperature estimation of the conductor and increases the risk of overloading the line during the thermal transient. However, since in this study the hourly ratings are assumed to be used at an early stage in the dispatch problem, this approximation is adopted nonetheless. For estimation of DLR closer to real-time operation, a finer time resolution is required.

2.1.2. Accounting for radial temperature drop

The ultimate hourly values of DLR adopted in this study have been derived by means of a modified version of the *Cigré* thermal model first presented in [21]. This modified version of the steady state rating algorithm has been introduced in order to consider the radial temperature drop in conductors in a simplified way under high current densities scenarios.

As the line current approaches the steady state rating, conductors undergo high current densities, i.e. greater than 2 or 3 A/mm^2 [3] and the heat generated within the conductor needs to flow to the outer surface, as shown in Fig. 2. Under these conditions, the temperature gradient between the center of the conductor and its surface should not be neglected, as it can reach significantly high values [22], [23]. Exceeding the maximum core temperature is likely to cause a violation of the clearance requirements, as above the knee-point temperature the

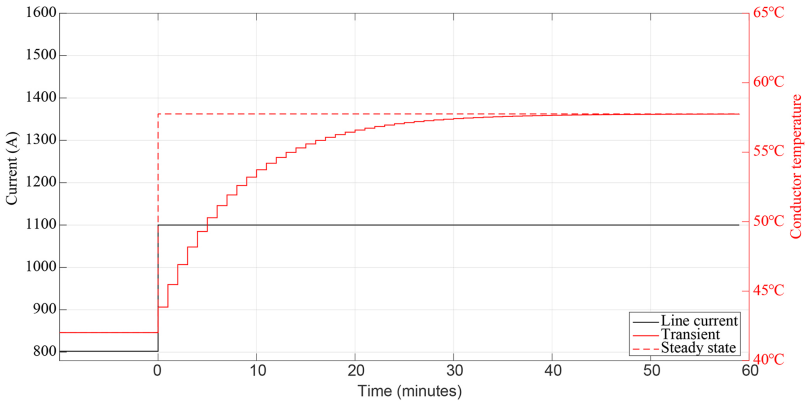

Fig. 1. Comparison of OHL conductor temperature rise for transient thermal model and its steady state approximation for a step change in line current. The conductor used in this example is a “Drake” 26/7 ACSR.

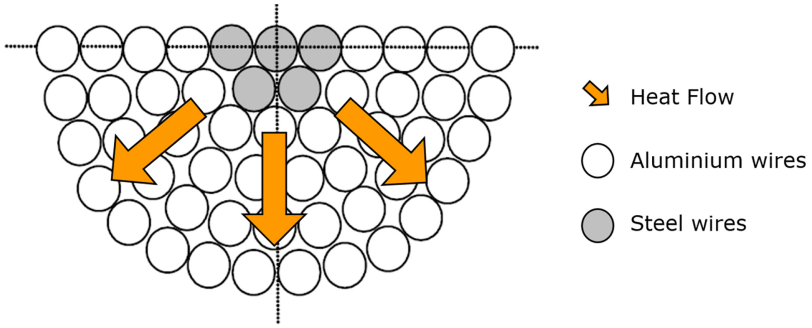

Fig. 2. Concept of radial heat flow across Aluminium Conductor Steel Reinforced (ACSR) cross-section.

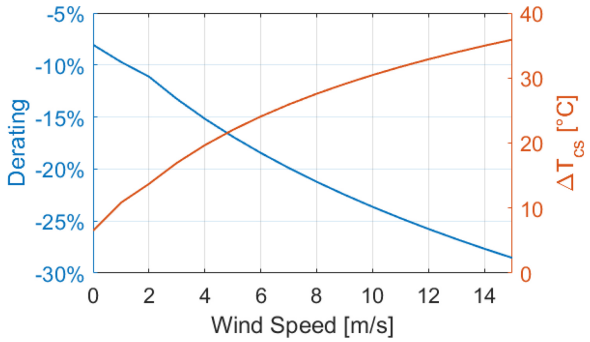

Fig. 3. Conductor thermal rating reduction (Derating - blue) with respect to *Cigré* model [3] after accounting for radial temperature difference ΔT_{cs} (red) between core and surface [21].

sag mainly depends on the steel thermal dilatation [24]. In order to include this aspect in the steady state algorithm, the system of non-linear equations (4), (5) and (6) is used instead of the standard procedure discussed in [3], where conductor temperature is assumed to be constant in the whole cross-section.

$$q_J(I_{\text{ohl}}^{\max}, \vartheta_{\text{av}}) + q_S - q_C(\vartheta_s) - q_R(\vartheta_s) = 0 \tag{4}$$

$$\vartheta_c - \vartheta_s = \frac{q_H(I_{\text{ohl}}^{\max}, \vartheta_{\text{av}})}{2\pi\lambda}\left[\frac{1}{2} - \left(\frac{D_1^2}{D^2 - D_1^2}\ln\frac{D}{D_1}\right)\right] \tag{5}$$

$$\vartheta_c - \vartheta_s = \frac{q_H(I_{\text{ohl}}^{\max}, \vartheta_{\text{av}})}{2\pi\lambda}\left[\frac{1}{2} - \left(\frac{D_1^2}{D^2 - D_1^2}\ln\frac{D}{D_1}\right)\right] \tag{6}$$

where ϑ_c is the core temperature of the conductor, ϑ_s is the surface temperature and ϑ_{av} indicates the average value in the cross section. Maximum operating temperature of the conductor is set at the core, assuming that the inner part of the cross section is the hottest on the conductor. The system of equations is solved for the maximum steady state current $I_{\text{ohl}}^{\max}$ and the corresponding surface and average temperature, ϑ_s and ϑ_{av}, respectively. The value of $I_{\text{ohl}}^{\max}$ represents the highest current rating that would result in the maximum operating temperature being reached at the center of the conductor.

The first equation (4) is the HBE in steady state conditions, where the time derivative of the conductor temperature is set to 0. The second equation (5) approximates the radial temperature drop in the cross section with a relation presented and discussed in the *Cigré Technical Brochure 601* [3]. The third and last equation in the system expresses the average temperature as a function of core and surface temperature.

The estimation of the radial temperature drop by means of (5) depends on the total heat gain q_H beside geometrical and material properties of the conductor. For ACSR conductors, internal heat generation is assumed to be uniformly distributed in aluminum wires as the steel conducts very little current, whereas for full-body mono-metallic ones, the heat generation is assumed in the entire cross-section instead. This simplified expression of the radial temperature drop in (5) depends on both geometric and material properties and thus it can be applied to different type of conductors. Nevertheless, the impact on different conductor designs in terms of thermal rating is not addressed in this paper. The equivalent radial thermal conductivity λ is expressed in WK m^{-1} and depends on various factors among which is the tension of the strands. A conservative value of 0.7 is assumed, as suggested in [3]. D and D_1 are the outer diameter of conductor and the inner steel core diameter, respectively.

Overall, this approach allows to distinguish between core and surface temperature in the calculation of the heating and cooling terms of the HBE. In particular, convective and radiative cooling are found to be dependent on surface temperature rather than average temperature. Therefore, by solving at once the system of equations (4), (5) and (6), this aspect is taken into account. Most importantly, the presence of equation (5) in the modified rating algorithm, couples the radial temperature difference with the HBE and ensures that the maximum operating temperature is not violated in the core. Accounting for radial temperature drop $\Delta T_{cs} = \vartheta_c - \vartheta_s$ reduces the rating compared to the *Cigré* model, as it can be seen in Fig. 3. Imposing the maximum operating temperature on the core and not on the average value in the cross-section, results in a lower convective cooling and thus a lower ratings for a given set of weather variables.

This condition is especially accentuated under high wind speed conditions, where the radial temperature drop increases significantly. Fig. 3 shows the de-rating introduced by the proposed algorithm with respect to the standard thermal rating approach in the Cigré guide [3]. As wind speed increases, so does the temperature difference between outer and inner strands in the conductor and therefore the rating is reduced accordingly.

Consider the following example where wind speed is 8 m/s and perpendicular to the conductor, ambient temperature is 5 °C and solar radiation is negligible. Under these conditions the thermal rating of a "Drake" conductor would be 2.835 kA according to [3] and 2.261 kA according to the proposed algorithm. Assuming common and very conservative assumptions, i.e. wind speed at 0.5 m/s and ambient temperature at 15 °C for winter, the static rating of the same conductor would be 1.169 kA meaning that the proposed approach would still yield a +93% increase in rating despite being nearly 20% less than the value derived with [3].

The optimization problem that is later presented in Section 2.4 can be implemented with different rating strategies as long as they are in the form of a time series of hourly values. This rating approach in particular can be seen as conservative way to account for convective cooling on overhead lines and benefit from the increased capacity of DLR introducing a safety margin under high wind speed scenarios.

2.1.3. Weather data for DLR

Time series of DLR hourly values have been derived with the reviewed steady state rating algorithm in conjunction with weather values simulated across the Danish power system. As described in [21], time series of wind speed, wind direction, ambient temperature and

solar radiation have been derived along the coordinates of the 400 kV transmission system with a mesoscale downscaling method [25]. This approach has allowed the estimation of hourly values of DLR which are normalized with the seasonal rating in operation at the Danish TSO, Energinet.

2.2. Dynamic transformer rating

As opposed to DLR, the dynamic loading of transformers can be performed by determining two temperatures which are critical for transformer operation: Top-Oil Temperature (TOT) and Hot-Spot Temperature (HST). These temperatures can be approximated with sufficient accuracy using a number of thermal models for given ambient temperature and load profiles [4][6][26]. The accuracy of these models varies but so does the respective practicality.

2.2.1. Estimation of top oil temperature

The ANSI/IEEE Clause 7 top-oil rise model [4] corrected for ambient temperature, given in (7), has been chosen as the basis for dynamic calculation of TOT, mainly because of its established popularity and large-scale acceptance in the industry, as well as its mathematical suitability for convex optimization problems [4].

$$\tau_0 \frac{d\vartheta_{top}}{dt} = -\vartheta_{top} + \vartheta_{amb} + \vartheta_u \tag{7}$$

where,

$$\tau_0 = C_{th,trf} \cdot \left(\frac{\vartheta_{or}}{L_{fl}}\right) \tag{8}$$

$$\vartheta_u = \vartheta_{or}\left(\frac{I_{trf}^2 R + 1}{R + 1}\right)^{\nu} \tag{9}$$

where τ_0 is thermal time constant for oil expressed in hours; ϑ_{amb} is the ambient temperature in °C; ϑ_u in °C is the ultimate top-oil rise over ambient temperature ϑ_{amb} for load I_{trf}; ϑ_{top} in °C is top-oil temperature (TOT); I_{trf} is the transformer load current in p.u. with rated load current as base; ϑ_{or} in °C is the top-oil rise over ambient temperature ϑ_{amb} at rated load; L_{fl} is total losses at rated load; R is ratio of load losses to no-load losses at rated load; $C_{th,trf}$ in MWh/°C is thermal capacity approximated using [4].

Also, ν represents the empirically derived coefficient known as oil exponent, which varies with transformer cooling mode (ONAN, OFAF etc.). The non-linear dependence of heat flow on temperature difference varies the convective cooling process and is therefore dependent on the cooling mode. The empirical values of ν for different cooling modes are given below, as suggested in [4]

$$\nu = \begin{cases} 0.8 & \text{for ONAN} \\ 0.9 & \text{for ONAF and OFAF} \\ 1.0 & \text{for ODAF} \end{cases} \tag{10}$$

The model of (7) can be converted into discrete form using backward Euler rule. The resulting equation is provided in (11), where Δt is the time resolution.

$$\vartheta_{top}(t) = \frac{\tau_0}{\tau_0 + \Delta t}\vartheta_{top}(t-1) + \frac{\Delta t}{\tau_0 + \Delta t}\left[\left(\frac{I_{trf}^2(t)R + 1}{R + 1}\right)^{\nu}\vartheta_{or} + \vartheta_{amb}(t)\right] \tag{11}$$

The discretised IEEE Clause 7 model of (11) is still not suitable for the sought optimization problem, due to the non-integer exponential ν. Therefore it is further simplified by assuming a straightforward approximation: the cooling mode of all the transformers in the simulated system is assumed to be ODAF (directed) ($\nu \approx 1$). Consequently, the chosen model is linearized to fit into the optimization problem and the final form is shown in (12).

$$\vartheta_{top}(t) = K_1 I_{trf}^2(t) + K_2\vartheta_{amb}(t) + (1 - K_2)\vartheta_{top}(t-1) + K_3 \tag{12}$$

where,

$$K_1 = \frac{\Delta t\, R\, \vartheta_{or}}{(\tau_0 + \Delta t)(R + 1)} \tag{13}$$

$$K_2 = \frac{\Delta t}{\tau_0 + \Delta t} \tag{14}$$

$$K_3 = \frac{\Delta t\, \vartheta_{or}}{(\tau_0 + \Delta t)(R + 1)} \tag{15}$$

2.2.2. Estimation of hot spot temperature

The HST model of IEEE Loading Guide C57.91 [4] is used in this paper, which is given by the differential equation of (16).

$$\tau_h \frac{d\vartheta_{hst}}{dt} + \vartheta_{hst} = \vartheta_{hu} + \vartheta_{top} \tag{16}$$

where τ_h is thermal time constant for winding expressed in hours; ϑ_{hu} in °C is the ultimate hot-spot temperature rise over TOT for load I_{trf}; ϑ_{hst} is the HST in °C; while, ϑ_{top} is top-oil temperature (TOT) calculated in (7). The ultimate HST rise over TOT for load I_{trf}, which is the per-unit load current is given by(17)

$$\vartheta_{hu} = \vartheta_{hr} I_{trf}^{2\mu} \tag{17}$$

where ϑ_{hr} in °C is the rated HST rise over TOT for p.u. load I_{trf}; Identical to the empirical factor ν, μ is also an empirically derived exponent which represents the impact of transformer cooling mode on the change in resistance and oil viscosity. The values suggested in [4] are mentioned in (18)

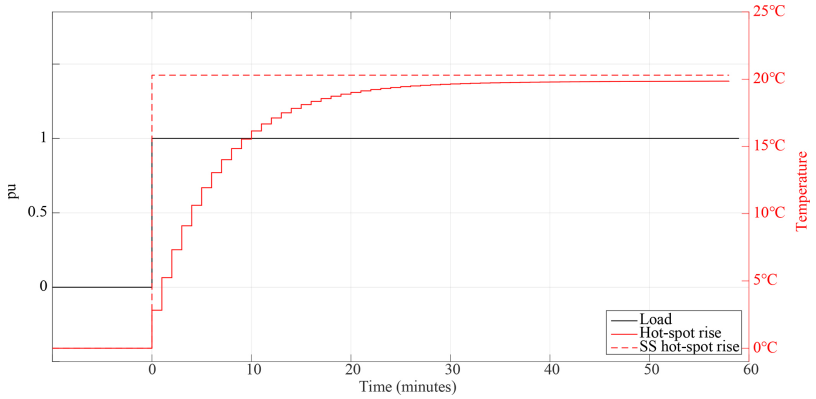

Fig. 4. Comparison of transformer hot-spot temperature rise for IEEE Clause 7 model [4] and its steady state approximation of Eq. (19) for unit step change in load.

$$\mu = \begin{cases} 0.8 & \text{for ONAN, ONAF, and OFAF} \\ 1.0 & \text{for ODAF} \end{cases} \tag{18}$$

The value of μ is set to 1 for the reasons similar to the choice of ν. A second approximation that has been introduced considers the steady state version of (16) where the rate of change of hot-spot temperature is set to 0. Since the goal of this paper is to optimize the hourly load-dispatch, while the winding τ_h thermal time constant is usually around 7-8 min [6], the ultimate HST would be reached by the end of each hour for a certain load change. Consequently, the final hot-spot temperature model is expressed in (19). The accuracy of this approximation is confirmed by comparing the HST rise for a step change in transformer load in Fig. 4. It is perceivable that the difference between the estimated hot-spot temperatures is minimal by the end of the 60-min mark, which is also verified for different load conditions.

$$\vartheta_{\text{hst}} = \vartheta_{\text{hr}} I_{\text{trf}}^2 + \vartheta_{\text{top}}(t) \tag{19}$$

2.3. Wind power simulation

In order to simulate a power system with large penetration of wind generation, historical wind power production data from the Danish system has been used. Fig. 5 shows the aggregate wind power production in the western part of the Danish system (DK1) as a function of the average wind speed simulated across the same region over the same period. Weather data have been simulated by means of a mesoscale down-scaling method according to the study presented in [25].

With the intent to simulate wind power production time series at several locations in a test power system, the following procedure has been adopted [27]. Firstly, an error function erf(x) has been fitted to the scatter plot of available wind power production normalized with the historical maximum. The red profile shown in Fig. 5 served the purpose to emulate a multi-turbine wind power curve. Secondly, available wind speed time series at various locations in the Danish system have been transformed into wind power time series by applying the fitted error function. This approach allowed to simulate wind power time series at different locations, preserving the spatio-temporal correlation structure of a real power system. Beside the correlation between wind power at different locations, the positive correlation between wind power and dynamic line ratings is also accounted for with this data-driven approach.

2.4. DCOPF problem formulation with DLR and DTR

The considered power system consists of a set of buses, $\mathcal{N}$; a set of conventional generators, $\mathcal{G}$; a set of wind farms, $\mathcal{W}$ and a set of branches, $\mathcal{L}$, that includes all transmission lines and power transformers. The number of elements in each set is identified as $|\mathcal{N}|$, $|\mathcal{G}|$, $|\mathcal{W}|$ and $|\mathcal{L}|$, respectively. The subsets of transmission lines with DLR and SLR are identified as $\mathcal{L}_{\text{DLR}}$ and $\mathcal{L}_{\text{SLR}}$, respectively. Similarly, the subsets of transformers with DTR and STR are identified as $\mathcal{L}_{\text{DTR}}$ and $\mathcal{L}_{\text{STR}}$.

This study adopts a DC approximation of the full AC power flow equations. The active power flow on each branch is modelled by means of the Power Transfer Distribution Factor matrix $\boldsymbol{M}$ [28], thus without the need to introduce bus voltage angles in the set of decision variables. The matrix $\boldsymbol{M} \in \mathbb{R}^{|\mathcal{L}|\times|\mathcal{N}|}$ expresses the constant coefficients of the linear relationship between the power injections at each bus and the power flows on the branches. It is defined as $\boldsymbol{M} = \boldsymbol{B}_l \boldsymbol{B}_n^{-1}$, where $\boldsymbol{B}_l$ is the branch admittance matrix and $\boldsymbol{B}_n$ is the bus admittance matrix in which the row and column corresponding to the slack bus are set to 0. The power flow F_ℓ on branch ℓ can then be expressed as $F_\ell = \boldsymbol{M}_\ell \boldsymbol{P}^{\text{inj}}$, where $\boldsymbol{M}_\ell$ is the ℓ-th row of matrix $\boldsymbol{M}$ and $\boldsymbol{P}^{\text{inj}}$ represents a column vector of *per unit* power injection at each bus in the system. For those branches ℓ^* referring to a transformer, the *per unit* load at time t is defined as (20). Similarly, for the other branches referring to transmission lines, the *per unit* load is defined in (21).

$$I_{\text{trf}_{\ell^*,t}} = \boldsymbol{M}_{\ell^*} \boldsymbol{P}_t^{\text{inj}} \frac{S^{\text{base}}}{S_{\ell^*}^{\text{trf}}} \tag{20}$$

$$I_{\text{ohl}_{\ell,t}} = \boldsymbol{M}_{\ell} \boldsymbol{P}_t^{\text{inj}} \frac{S^{\text{base}}}{S_{\ell}^{\text{ohl}}} \tag{21}$$

where S^{base}, $S_{\ell^*}^{\text{trf}}$ and S_{ℓ}^{ohl} are the base apparent power values in MVA for the system, the transformer on branch ℓ^* and transmission lines on branch ℓ. This allows to express the transformer load in *per unit* and relate the branch power flow to the specific nameplate rating. In a similar fashion, utilization of overhead lines is represented by $I_{\text{ohl}_{\ell,t}}$. The nodal power injection for a given time slot t can be written in its extensive form as in (22).

$$\boldsymbol{P}_t^{\text{inj}} = \boldsymbol{P}_t^{\text{gen}} + \boldsymbol{P}_t^{\text{wnd}} - (\boldsymbol{P}_t^{\text{dem}} - \boldsymbol{P}_t^{\text{sh}}) \tag{22}$$

where $\boldsymbol{P}_t^{\text{gen}} = \left(\sum_{g\in G_1} P_{g,t}, \ldots, \sum_{g\in G_n} P_{g,t}\right) \in \mathbb{R}^{|\mathcal{N}|}$ collects total thermal generation at each bus, thus representing a generic power system where a group of generators G_i with different cost functions might be connected to the same *i-th* bus. Similarly, $\boldsymbol{P}_t^{\text{wnd}}$, $\boldsymbol{P}_t^{\text{dem}}$, $\boldsymbol{P}_t^{\text{sh}}$ represent dispatched wind power, load demand and load shedding at each bus in the system for a given time t, respectively.

The optimization problem in (23) is the Dynamic DC - Optimal Power Flow (DDCOPF), where transformer top-oil and hot-spot thermal dynamics have been accounted for together with dynamic line ratings. The objective is to find the optimal 24-hours day-ahead energy dispatch, which minimizes total generation cost over the period $\mathcal{T}$. For a more accurate representation of the actual dynamics in the power system, the DDCOPF may be extended to a Unit Commitment study where generators' start-up and shut-down actions are included as well by means of binary decision variables. N-1 security constraints could also be integrated starting from the base formulation of the DDCOPF that is presented in this paper. The DDCOPF is formulated in a compact form as follows

$$\min_{\Xi} \sum_{t\in\mathcal{T}} \left(\sum_{g\in\mathcal{G}} c_g P_{g,t} + \sum_{n\in\mathcal{N}} c^{\text{sh}} P_{n,t}^{\text{sh}} \right) \tag{23a}$$

$$\text{s. t.} \sum_{g\in\mathcal{G}} P_{g,t} + \sum_{w\in\mathcal{W}} P_{w,t} - \sum_{n\in\mathcal{N}} (P_{n,t} - P_{n,t}^{\text{sh}}) = 0 \quad \forall\, t \in \mathcal{T} \tag{23b}$$

$$P_g^{\min} \le P_{g,t} \le P_g^{\max} \quad \forall\, g \in \mathcal{G}, \quad \forall\, t \in \mathcal{T} \tag{23c}$$

$$-\Delta P_g^{\max} \le P_{g,t} - P_{g,t-1} \le \Delta P_g^{\max} \quad \forall\, g \in \mathcal{G}, \quad \forall\, t \in \mathcal{T} \tag{23d}$$

$$-1 \le I_{\text{ohl}_{\ell,t}} \le 1 \quad \forall\, \ell \in \mathcal{L}_{\mathcal{SLR}}, \quad \forall\, t \in \mathcal{T} \tag{23e}$$

$$-I_{\text{ohl}_{\ell,t}}^{\max} \le I_{\text{ohl}_{\ell,t}} \le I_{\text{ohl}_{\ell,t}}^{\max} \quad \forall\, \ell \in \mathcal{L}_{\mathcal{DLR}}, \quad \forall\, t \in \mathcal{T} \tag{23f}$$

$$-1 \le I_{\text{trf}_{\ell,t}} \le 1 \quad \forall\, \ell \in \mathcal{L}_{\mathcal{STR}}, \quad \forall\, t \in \mathcal{T} \tag{23g}$$

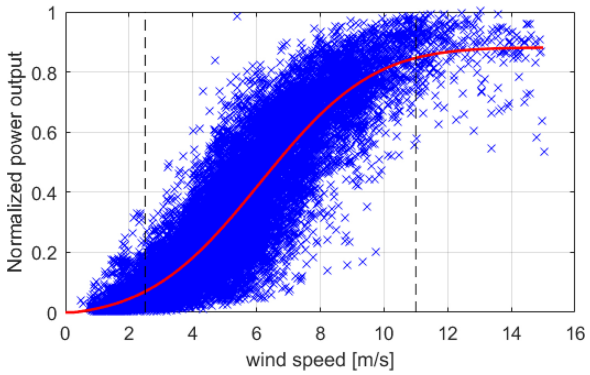

Fig. 5. Aggregate wind power production in the western Danish power system (DK1) over a 3-years period. Scatter plot as a function of average wind speed simulated in DK1 over the same period (blue). Fitted error function (red) [27].

$$\vartheta_{\text{top}_{\ell,t}} \leq \vartheta_{\text{top}}^{\max} \quad \forall\, \ell \in \mathcal{L}_{\text{DTR}}, \quad \forall\, t \in \mathcal{T} \tag{23h}$$

$$\vartheta_{\text{hst}_{\ell,t}} \leq \vartheta_{\text{hst}}^{\max} \quad \forall\, \ell \in \mathcal{L}_{\text{DTR}}, \quad \forall\, t \in \mathcal{T} \tag{23i}$$

$$0 \leq P_{n,t}^{\text{sh}} \leq P_{n,t} \quad \forall\, n \in \mathcal{N}, \quad \forall\, t \in \mathcal{T} \tag{23j}$$

$$0 \leq P_{w,t} \leq P_{w,t}^{\text{av}} \quad \forall\, w \in \mathcal{W}, \quad \forall\, t \in \mathcal{T} \tag{23k}$$

$$\vartheta_{\text{top}_{\ell,t}} = K_1 I_{\text{trf}_{\ell,t}}^2 + K_2 \vartheta_{\text{amb}_t} + (1 - K_2)\vartheta_{\text{top}_{\ell,t-1}} + K_3 \tag{24}$$

$$\vartheta_{\text{hst}_{\ell,t}} = \vartheta_{\text{top}_{\ell,t}} + \vartheta_{\text{hr}} I_{\text{trf}_{\ell,t}}^2 \tag{25}$$

where $\Xi = [P_{g,t}, P_{n,t}^{\text{sh}}, P_{w,t}]$ is the set of decision variables that for each time step t represent scheduled generator's output $P_{g,t}$, shed load $P_{n,t}^{\text{sh}}$ and dispatched wind power $P_{w,t}$ for every generator, bus and wind farm, respectively.

The objective function in (23a) consists in the cost of dispatching the system over period $\mathcal{T}$ considering linear generation cost functions and the additional cost of remedial corrective actions such as load shedding. This latter term models extreme conditions with a low probability of occurrence, but it serves the purpose to guarantee feasibility for each scenario of load demand and available wind power $P_{w,t}^{\text{av}}$. Constraint (23b) enforces system day-ahead power balance for each hour in the considered time period. Constraints (23c) and (23d) impose operational limits on conventional generators in terms of their power outputs and ramping capabilities. On the one hand, power flow limits on transmission lines equipped with DLR are enforced with constraints (23f), where $I_{\text{ohl}}^{\max}$ represents hourly dynamic ratings that have been calculated as described in Section 2.1. On the other hand, lines that are statically rated are constrained by means of (23e).

Alternatively to the method presented in this paper, DLR could be integrated in an optimization framework by directly constraining conductor temperature, as presented in [29], [30] and [16]. In order to preserve convexity in the optimization problem, this latter approach would require a convex approximation of the heat balance equation, which is highly non-linear and non-convex as a function of conductor temperature. As discussed in [30], Joule heating, convective cooling and radiative cooling may be integrated in a convex optimization problem adopting conservative relaxations and linearized versions of the original equations.

The load on those transformers that are statically rated according to their *per unit* value is modelled with constraint (23g), whereas those that are dynamically rated are constrained by means of (23h) and (23i). Top-oil and hot-spot temperature variations of dynamically rated transformers are bounded by predefined values that ensure they are used within their thermal capabilities without jeopardizing their reliability. The extensive form of the constraints associated with the transformer utilization is shown in (24) and (25), where linearized IEEE models are shown again. Top-oil temperature of transformer, ϑ_{top}, is expressed as a function of its squared *per unit* load I_{trf}^2, ambient temperature ϑ_{amb} and value of top-oil temperature reached in the previous time step. Coefficients K_1, K_2 and K_3 are constants that solely depend on transformer construction, as discussed in Section 2.2. Unlike ϑ_{top}, the constraint on hot-spot temperature ϑ_{hst} is imposed in terms of its steady state value, since short term thermal transients are assumed to be extinguished within one hour as shown in Fig. 4 in Section 2.2.

It is important to notice how the constraints related to transformers with DTR are strongly coupled in time throughout the entire dispatch period, due to the high thermal capacitance of top-oil dynamics. This aspect reflects the importance of considering recent loading history for DTR as opposed to DLR, where temperature transients are much faster. Lastly, constraints (23j) and (23k) impose physical limitation on the amount of load that can be shed and the availability of wind power generation, respectively.

From a convex optimization point of view, constraining top-oil and hot-spot temperature is achieved by means of quadratic inequality constraints (23h) and (23i). Recalling that the composition of a convex function with an affine expression is convex [31], it can be verified that inequalities (23h) and (23i) are convex in terms of the set of decision variables Ξ.

$$\begin{aligned} x &\in \mathbb{R}^n && \text{: decision variable} \\ A \in \mathbb{R}^{m\times n},\ b &\in \mathbb{R}^m && \text{: constants} \\ Ax + b & && \text{: affine combination} \\ f(\cdot)\colon \mathbb{R}^m &\to \mathbb{R} && \text{: convex function} \\ f(Ax + b) & && \text{: convex} \end{aligned}$$

In the DC power flow approximation, the *per unit* transformer load I_{trf} is an affine combination of decision variables, i.e. the power injection terms at each bus scaled with the $\boldsymbol{M}$ matrix as shown in (20). Thus, the

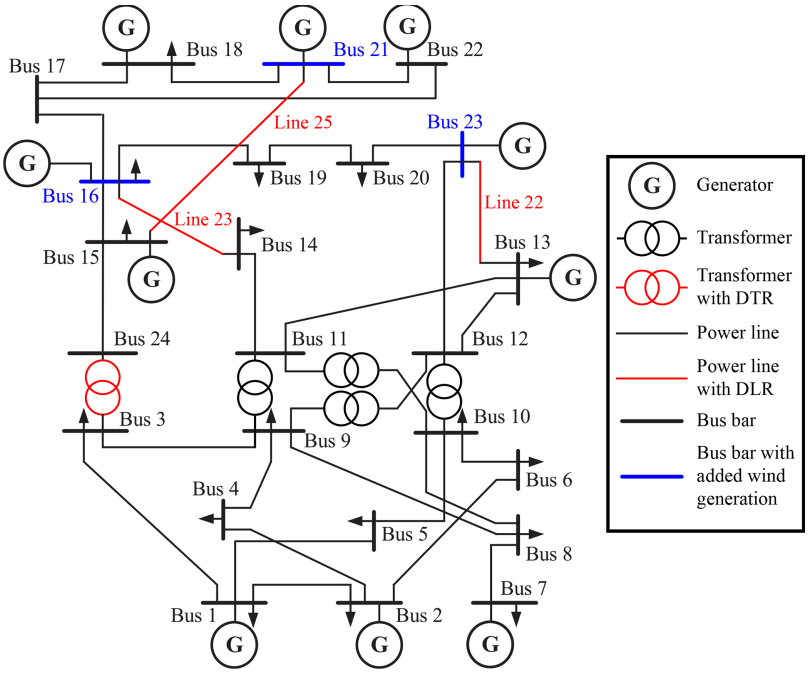

Fig. 6. Modified IEEE RTS 24-bus system [18].

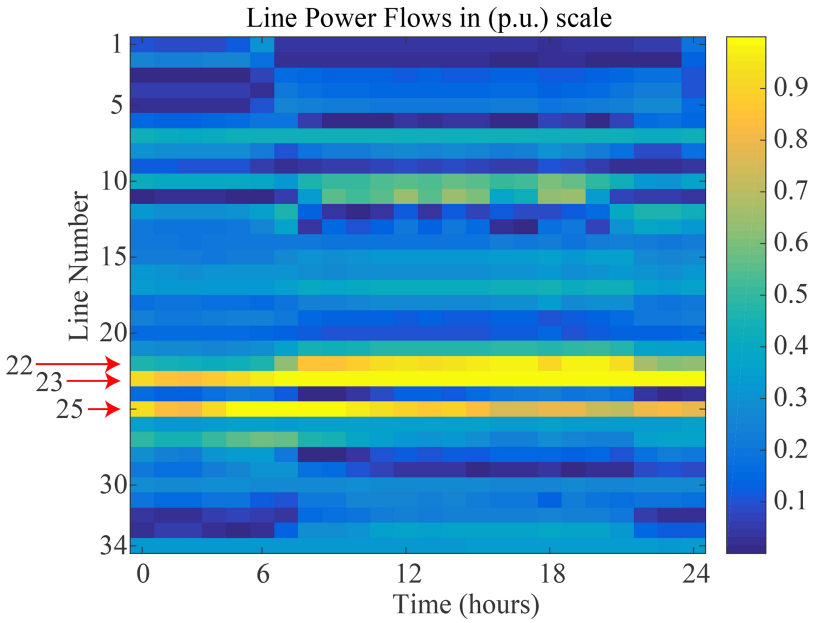

Fig. 7. 24-hour loading of individual lines resulting from a DDCOPF simulation of the IEEE RTS 24-bus system with integrated wind generation. Data from 01 Feb 2016.

Table 1
Input data for transformer thermal model

Quantity	Value	Unit
Base power	175	MVA
DC losses	411.8	kW
Eddy losses	29.5	kW
Stray losses	43.4	kW
ϑ_{or}	38.3	°C
ϑ_{hr}	20.3	°C
$C_{th,trf}$	59.6	kWh/K
τ_h	7	min

Table 2
Test cases classification

	Lines		Transformers	
Title	**Rating**	**Constraint**	**Rating**	**Constraint**
SLR STR	Static	$I_{ohl} \leq 1$	Static	$I_{trf} \leq 1$
DLR STR	Dynamic	$I_{ohl} \leq I_{ohl}^{max}$	Static	$I_{trf} \leq 1$
SLR DTR	Static	$I_{ohl} \leq 1$	Dynamic	$\vartheta_{hst} \leq \vartheta_{hst}^{max}$
DLR DTR	Dynamic	$I_{ohl} \leq I_{ohl}^{max}$	Dynamic	$\vartheta_{hst} \leq \vartheta_{hst}^{max}$

squared value I_{trf}^2 retains convexity since it results from a composition between an affine expression and a convex function $f(\cdot) = \alpha(\cdot)^2$, where α is a positive coefficient.

In order to preserve convexity for each time step t, a second important observation has to be made. Consider in (26) the extensive form of constraint (24), where also the $\vartheta_{top_{\ell,t-1}}$ is expanded up to one previous time step. To ease the notation in this context, the index ℓ referring to the branch is dropped as well as the subscript "trf" for transformer load.

$$\begin{aligned}\vartheta_{top_t} = \; & K_1 I_t^2 + K_2 \vartheta_{amb_t} \cdots \\ & + (1-K_2)[K_1 I_{t-1}^2 + K_2 \vartheta_{amb_{t-1}} + (1-K_2)\vartheta_{top_{t-2}} + K_3] + K_3\end{aligned} \tag{26}$$

It can be noticed that ϑ_{top_t} is convex in Ξ only if all the coefficients that multiply the quadratic terms are positive. This can be visualized with an inductive reasoning, by considering constraint (23h) at the last time step for $t = T$ in the optimization problem. The following list shows which coefficient is associated to which quadratic term in the extensive formulation of (26) for $t = T$.

Quadraticterm		Coefficient
I_T^2	$\rightarrow$	K_1
I_{T-1}^2	$\rightarrow$	$(1-K_2)K_1$
I_{T-2}^2	$\rightarrow$	$(1-K_2)^2 K_1$
$\vdots$	$\rightarrow$	$\vdots$
I_1^2	$\rightarrow$	$(1-K_2)^{T-1} K_1$

Coefficient K_1 is positive by construction since it is a ratio of positive quantities, as shown in Section 2.2. Coefficient K_2 is positive as well and it is smaller than 1 by construction, thus guaranteeing that $(1 - K_2) > 0$. As a result, every quadratic term in (24) is multiplied by a positive coefficient ensuring the convexity of the inequality constraints for each time step t. A similar conclusion can be drawn for inequality constraint (23i) since ϑ_{hr} is strictly greater than 0.

To conclude this section, the resulting problem has a scalar affine objective function, affine equality constraints for the system power balance, conic quadratic inequality constraints for top-oil and hot-spot temperature and affine inequalities for the remainder of the constraints. The convexity of the problem guarantees that a global optimal solution exists and can be attained in a computationally-efficient way by relying on readily available solvers. In this study, the resulting optimization problem has been solved with the Matlab-based optimization toolbox CVX [32], which allows for a direct implementation of convex problems.

3. Case study

This section briefly explains the test system used in this paper. The modifications made to this system and the rationale behind these changes are presented. Different test cases are comprehensively discussed in this section.

3.1. IEEE 24-bus test system with wind generation

The test system adopted in this study is based on the modified IEEE

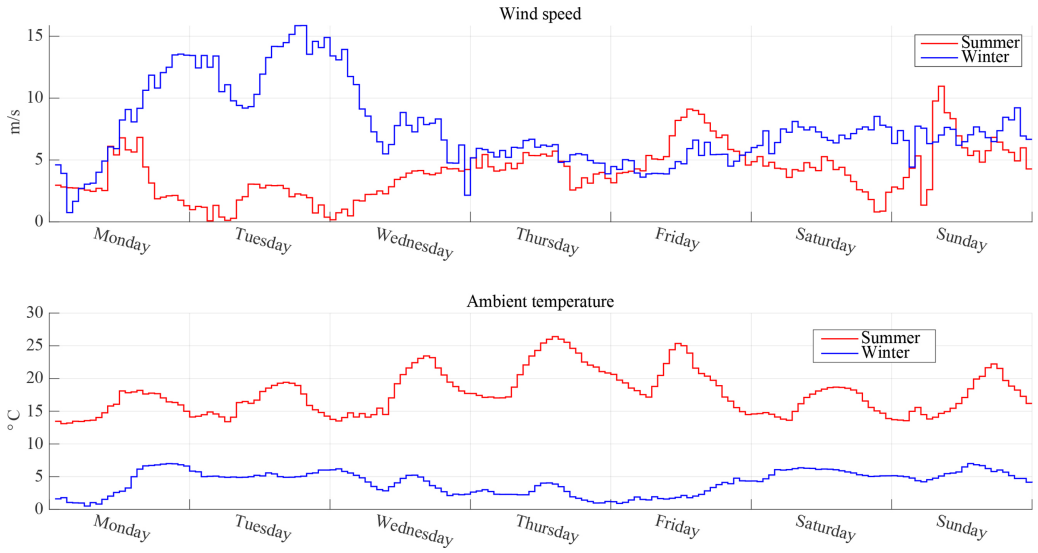

Fig. 8. Hourly wind speeds and ambient temperatures for winter 2016 (week 05 - Blue) and summer 2016 (week 34 - Red).

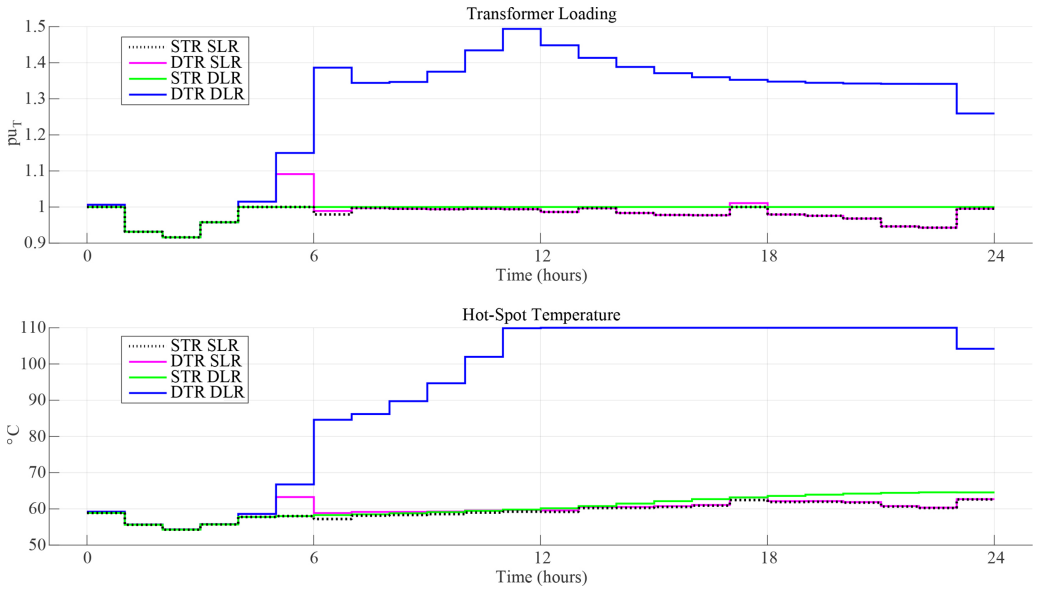

Fig. 9. Transformer results for cost-optimized hourly load dispatch for a weekday in winter 2016 (01 Feb). Top: Transformer load in pu. Bottom: Transformer hot spot temperature in (°C).

RTS 24-bus system [18], where selected components have been derated in order to highlight the impact of DLR and DTR. The test system is shown in Fig. 6. Historical daily load profile from the Danish system has been scaled with the peak load demand provided in [18] and increased by 10%.

In contrast to [18], wind power production is only located at Buses 16, 21 and 23. However, the installed wind power capacity at each of these buses has been doubled from 200 to 400 MV with respect to the original test case. Wind power generation located far from the main load center is expected to further stress the transmission system and highlight the value of dynamic rating on various components.

Transmission lines marked with red have been derated to introduce additional bottlenecks in the grid, as suggested in [18]. MVA ratings of transmission lines between node pairs (13;23), (14;16) and (15;21) have been reduced from 500, 500 and 1000 to 250, 250 and 400, respectively. A preliminary simulation of a 24h dispatch with static ratings has shown that such lines are the best candidates for DLR. Fig. 7 shows the utilization of each line in the system over the 24h dispatch period with static ratings. It can be clearly seen that derated lines constitute a congestion in the system and limit the power flow across the network. Without any loss of generality, this case study does not account for the N-1 security limit, thus components are loaded up to their thermal rating.

The transformer chosen for dynamic rating application is between Bus 3 and Bus 24. The data necessary for dynamic thermal estimation of the chosen transformer is provided in Table 1. The preliminary power flow simulations suggest that this transformer is strategically important as it favours the integration of wind power from Bus 16. Furthermore, unlike other transformers in the system, the absence of alternative feeders on the respective buses makes this transformer critical for operation.

The selection of components for dynamic rating application in a real power system would be based on well-established industrial practices, which dictate future grid expansion in case of system congestion. Possible criteria that could be adopted in order to identify the need for dynamic rating on certain lines and transformer are mentioned below, but their thorough treatise is outside the scope of this work.

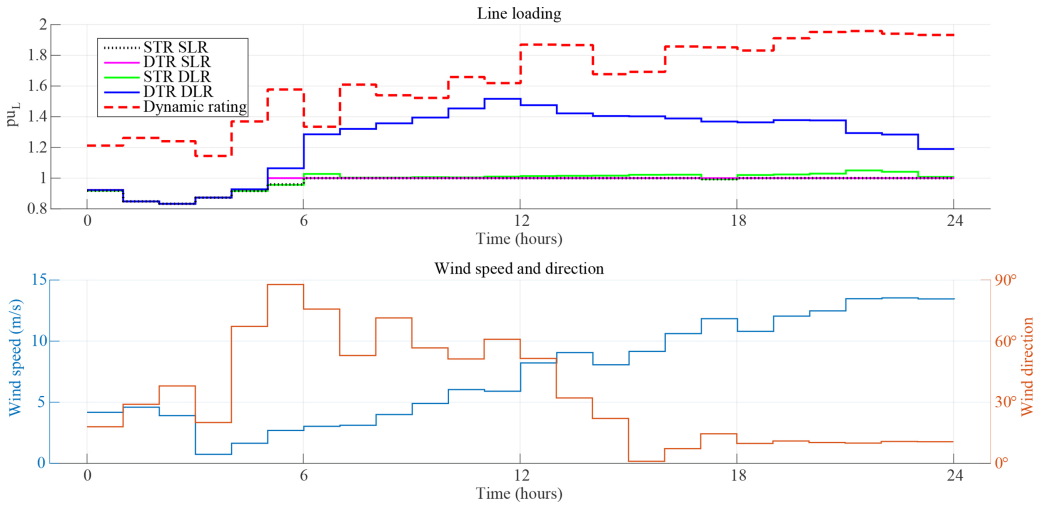

Fig. 10. Results for cost-optimized hourly load dispatch for a weekday in winter 2016 (01 Feb) for Line 23 of Fig. 6. Top: Line loading and dynamic rating in pu. Bottom: Wind speed (m/s) and wind direction (°) with respect to Line 23.

Table 3
Comparison of load-dispatch cost reduction for 4 cases of Table 2 for 01-Feb-2016 (winter)

	Cost Reduction $\Delta_{\%}$	
	STR	**DTR**
SLR	0	−0.1 %
DLR	−0.5 %	−11.4 %

1 Failure rate of the surrounding components
2 Estimated repair time in case of faults
3 Cost of possible load interruption
4 Integration of newly built generating units from renewable sources.

3.2. Test case classification

In order to correctly identify the necessity of using DLR and DTR together, different test cases have been prepared. The tested cases can be classified into four categories. Each of these cases represent a unique combination of dynamic loading for OHLs and transformer. The individual test cases and the respective constraints are provided in Table 2.

Table 2 classifies all the cases that have been tested with the proposed methodology. The form of the constraints for the considered components is shown as well. It is recalled that I_{ohl} is the line load normalized by the static line rating, $I_{\mathrm{ohl}}^{\max}$ is the dynamic line rating computed with the rating algorithm presented in Section 2.1, I_{trf} is the transformer per unit loading and finally ϑ_{hst} and $\vartheta_{\mathrm{hst}}^{\max}$ are hot spot temperature and its maximum allowed value (110 °C).

3.3. Weather Data for the Analysis

Dynamic line and transformer ratings are highly dependent on the weather variability. Since the actual load and generation patterns of the Danish grid are being used in this paper, it is tangible to use the actual Danish weather data for rest of the analysis. A brief scrutiny of the weather data from Denmark reveals significant difference for wind speeds and ambient temperatures during summer and winter periods. This hourly-pattern is presented in Figure 8, where week 34 of year 2016 (22 to 28 August) represents summer, while week 5 of the same year (01 to 07 February) has been used for winter depiction. Henceforth, all the test cases specified in Section 3.2 are analyzed for both the

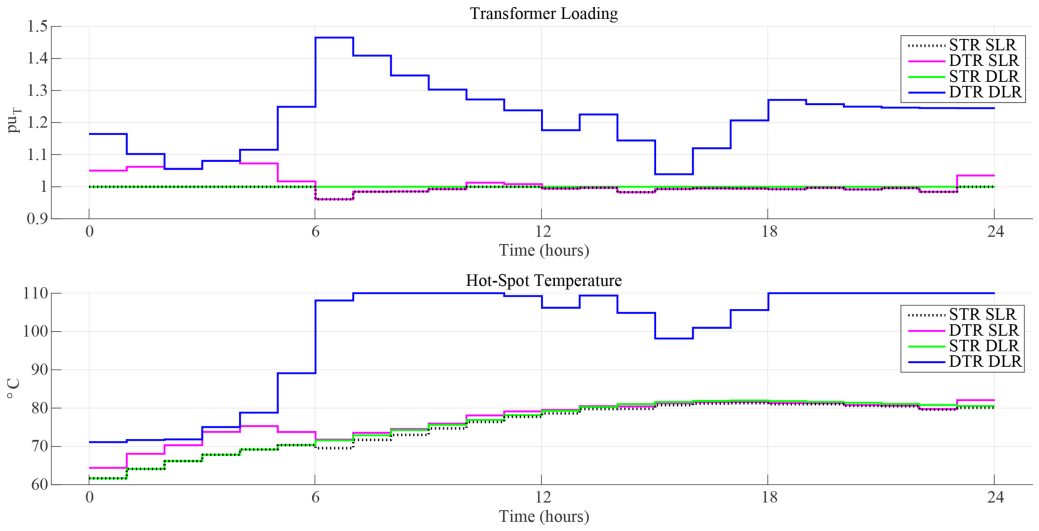

Fig. 11. Transformer results for cost-optimized hourly load dispatch for a weekday in summer 2016 (25 Aug). Top: Transformer load in pu. Bottom: Transformer hot spot temperature in (°C).

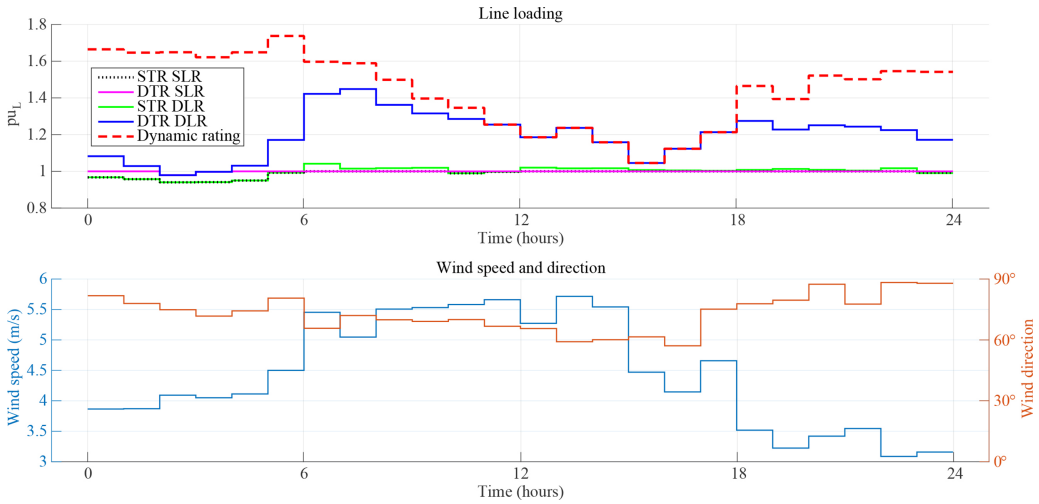

Fig. 12. Results for cost-optimized hourly load dispatch for a weekday in summer 2016 (25 Aug) for Line 23 of Fig. 6. Top: Line loading and dynamic rating in pu. Bottom: Wind speed (m/s) and wind direction (°) with respect to Line 23.

Table 4
Comparison of load-dispatch cost reduction for 4 cases of Table 2 for 25-Aug-2016 (summer)

	Cost Reduction $\Delta_{\%}$	
	STR	**DTR**
SLR	0	−0.3 %
DLR	−0.3 %	−7.4 %

summer and winter seasons.

4. Results and discussion

This section begins with the comparison of transformer and overhead line hourly load profiles for a 24-hour period during winter and summer. The respective 24-hour periods were chosen to represent two critical weather conditions: low ambient temperature and high wind speed against high ambient temperature and low wind speed. All the four case studies from Table 2 are compared by analyzing the cost of power dispatch for one day for each case. The results are presented in terms of percentage reduction taking as a reference the case with STR and SLR. Cost reduction are then calculated as in (27), where Cost(x) indicates the total dispatch cost for the x-th case as opposed to $\text{Cost}_{\text{STR-SLR}}$ which indicates the total cost of the reference case.

$$\Delta_{\%}(x) = \left(1 - \frac{\text{Cost}(x)}{\text{Cost}_{\text{STR-SLR}}}\right)\cdot 100 \tag{27}$$

The hourly dispatch cost and dynamic loading of the components is also considered for a week in both winter and summer thus highlighting daily load and temperature cycles in different seasons.

4.1. Analysis of day ahead hourly dispatch during winter

The day-ahead hourly dispatch optimization for winter has been performed with data from the 01 Feb 2016. This day has been chosen because of sharp rise and fall in loading pattern of a weekday. The temporal evolution of transformer and line loading along with the respective limiting factors for actual load, generation and weather patterns from Denmark are provided in Fig. 9 and Fig. 10. The results for different test cases of Table 2 are superimposed over each other in these

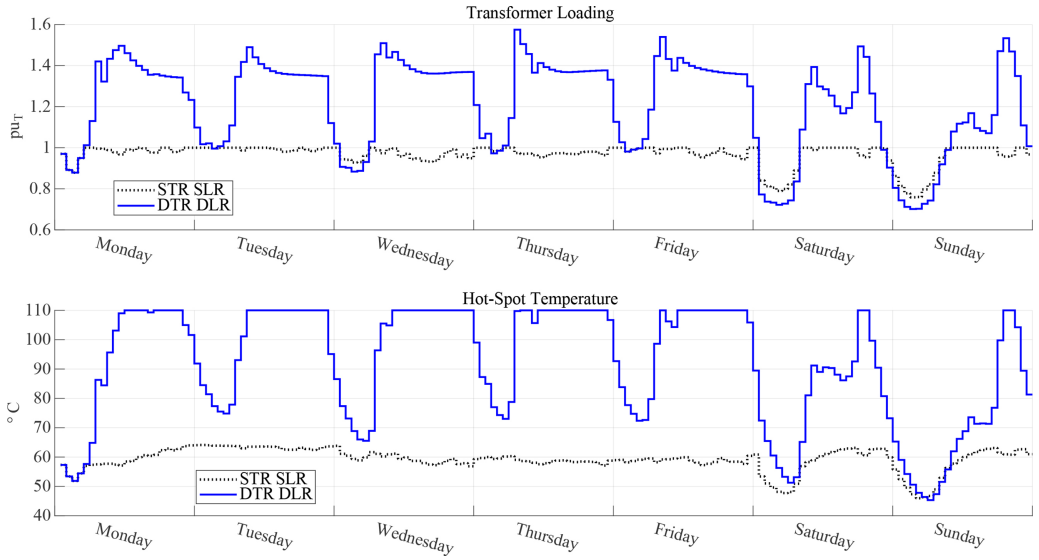

Fig. 13. Transformer results for cost-optimized hourly load dispatch for week 05 in 2016 (winter). Top: Transformer load in pu. Bottom: Transformer hot spot temperature in (°C).

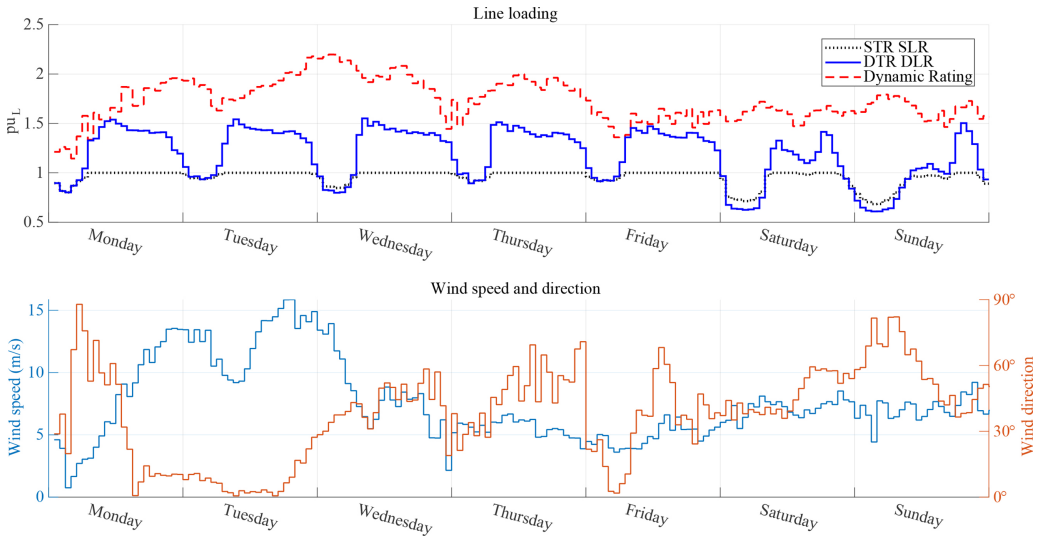

Fig. 14. Results for cost-optimized hourly load dispatch for week 05 in 2016 (winter) for Line 23 of Fig. 6. Top: Line loading and dynamic rating in pu. Bottom: Wind speed (m/s) and wind direction (°) with respect to Line 23.

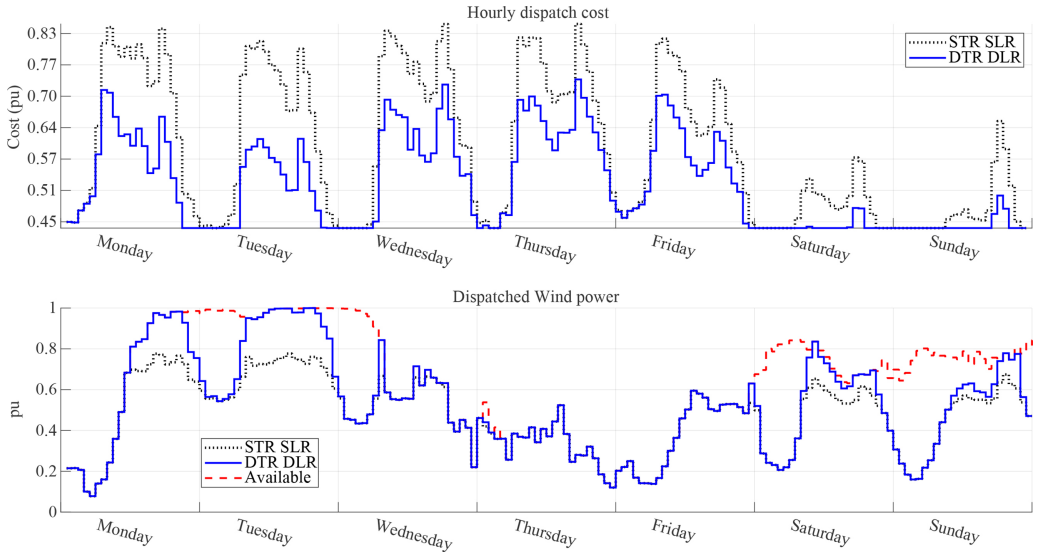

Fig. 15. Results for cost-optimized hourly load dispatch for week 05 in 2016 (winter). Top: Hourly dispatch cost in pu. Bottom: Available and dispatched wind generation in pu.

figures. Referring to Fig. 6, dynamic loading of the following components are elaborated only: Line 23 and transformer between bus 24 and bus 3. This is done because these components are loaded extremely close to their rated capacity (1 p.u.) for the entire 24-hour period, which is evident by the STR + SLR profiles in Figures 9 and 10 .

Fig. 9 reveals that the application of DTR with and without dynamic rating of lines would improve transformer utilization during certain periods. However, for the given system, the transformer is optimally utilized for the DTR + DLR case only. This proves the fact that the system bottlenecks exist in the red-marked transformer as well as OHLs in the modified IEEE RTS 24-bus system of Fig. 6. It is evident that the transformer can be loaded as high as 1.5 p.u. on a cold winter day. However the rating is decreased over time once the maximum HST is reached and the rating stabilizes around 1.35 p.u. for the given load and ambient conditions.

Since the rating of a overhead line is highly dependent on the ambient temperature, wind speed and its direction with respect to the OHL, Fig. 10 has been provided for verification of this phenomena for line 23. The red-dashed line determining the real-time dynamic rating of OHL for given ambient conditions and the wind speed graph in the bottom show rising trends as the day proceeds. The line rating is also found to be high for low speed wind flowing perpendicularly to the OHL between hours 4 and 9. Comparable to the transformer loading, DLR for line 23 appears to be more relevant for DTR + DLR case as compared to rest of the cases, because of the system bottlenecks. The trend of line loading for DTR + DLR case between hours 8 and 22 is evidently similar to the transformer loading, which proves that the line 23 has not been loaded to its available dynamic rating (i.e. red-dashed and blue lines do not converge) because the corresponding transformer's maximum HST is reached.

The hourly load dispatch cost for the 24-hour period in winter is compared for different test cases in Table 3. The STR + SLR case has been used as the base case for comparison. It is evident that for the given system with congestion lying both in the transformer and OHLs, STR + DLR and DTR + SLR cases do not result in significant cost reduction. The DTR + DLR case is found to be optimal for this system on a cold winter day.

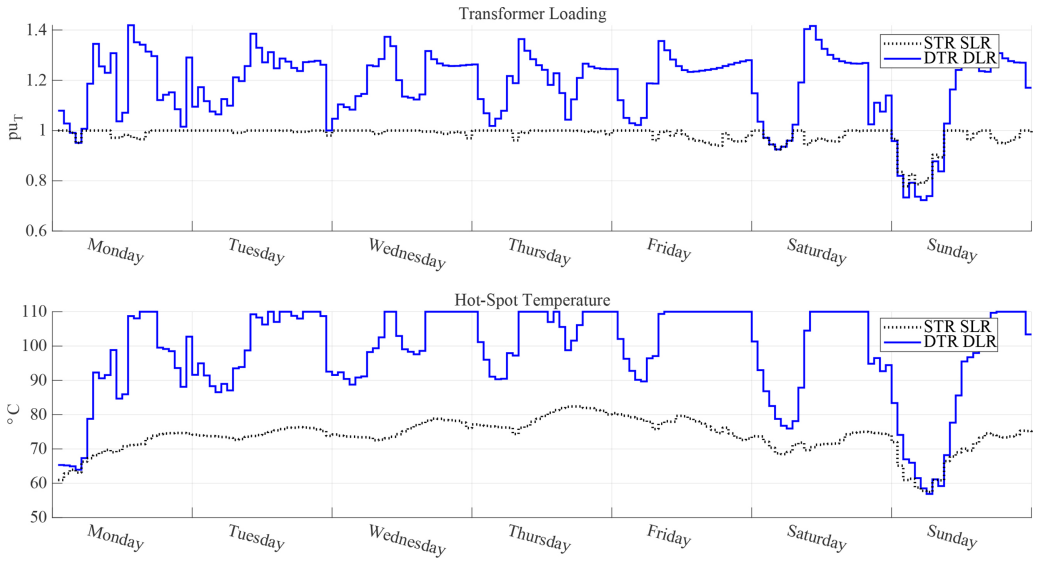

Fig. 16. Transformer results for cost-optimized hourly load dispatch for week 34 in 2016 (summer). Top: Transformer load in pu. Bottom: Transformer hot spot temperature in (°C).

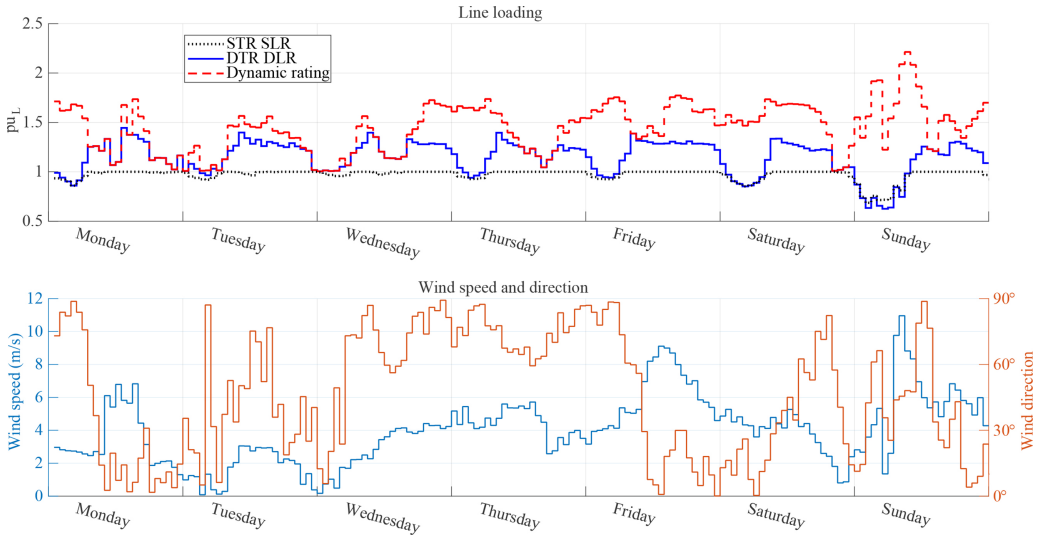

Fig. 17. Results for cost-optimized hourly load dispatch for week 34 in 2016 (summer) for Line 23 of Fig. 6. Top: Line loading and dynamic rating in pu. Bottom: Wind speed (m/s) and wind direction (°) with respect to Line 23.

4.2. Analysis of day ahead hourly dispatch during summer

Figs. 11 and 12 show the loading profile of the transformer and line for Thursday 25 August, during summer of 2016. The overall behavior of transformer and line loading is comparable to winter. DTR + DLR case appears to utilize the components optimally, but in contrast with winter, the blue line representing DTR + DLR appears to be much closer to the remaining cases during low wind speeds and high ambient temperature periods.

As a result of high ambient temperature around midday on 25 August (Thursday), the real-time dynamic rating of line reduces in Fig. 12. Unlike winter, transformer HST is not always the limiting factor in this case and the bottleneck shifts to the OHL rating during high ambient temperature periods. It is interesting to note that the dynamic rating of OHL would have decreased below the 1 p.u. mark, if convective cooling due to wind was not taken into account.

Table 4

4.3. Analysis for winter Week with Increased Wind Generation Capacity

In Fig. 13 and Fig. 14, the loading for power transformer and line 23 are compared for cases without dynamic rating (SLR + STR) and with dynamic rating (DLR + DTR) for week 05 during winter 2016. It is observed that the utilization of transformer and OHL has improved significantly for the combined dynamic rating case. Both the transformer and OHL are often loaded beyond the respective rated capacities, especially during high load demand periods. The dynamic rating capacity of the OHL is not fully utilized because the maximum HST limit is reached for the transformer during high load periods.

The impact of combined dynamic rating on hourly dispatch cost is presented in Fig. 15. The per unit cost of the hourly load dispatch shows significant reduction during high wind periods. The wind energy which needs to be curtailed for SLR + STR case is fully utilized for the combined dynamic loading case. The curtailment of wind energy in DTR + DLR case is only performed during low-load periods (night, weekends etc.). This utilization can further be improved by accounting for storage and energy trade to the neighboring systems through interlinks.

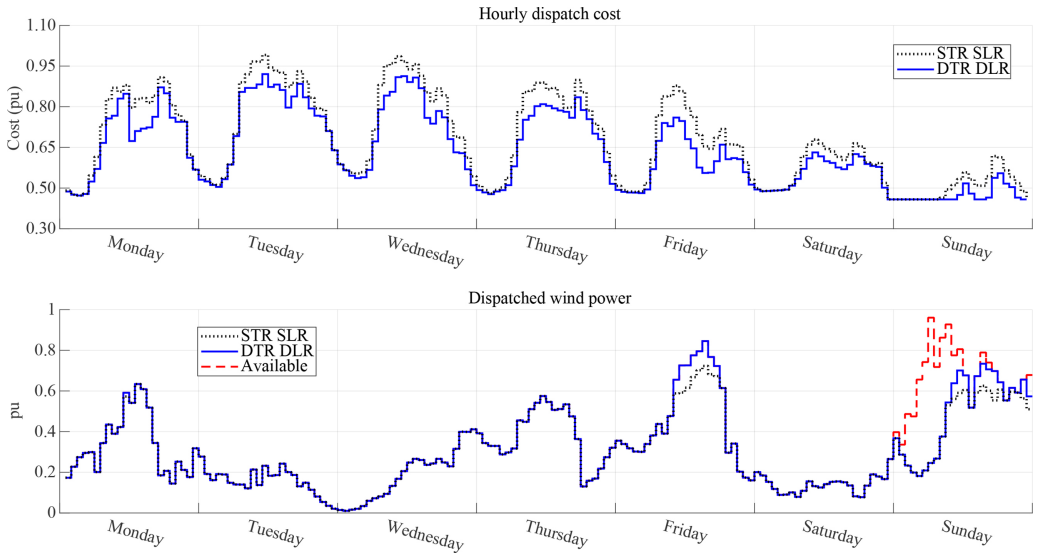

Fig. 18. Results for cost-optimized hourly load dispatch for week 34 in 2016 (summer). Top: Hourly dispatch cost in pu. Bottom: Available and dispatched wind generation in pu.

4.4. Analysis for summer week with increased wind generation capacity

The optimal day-ahead power dispatch is performed for week 34 in summer 2016. The transformer and line loading results in Fig. 16 and 17 present a similar but contrasting picture as compared to winter. The dynamic rating of line is often utilized completely for the DTR + DLR case and the maximum HST for transformer is not reached as frequently. This is because the real-time line ratings are reduced during low wind speed and high ambient temperature periods, which are more common during summer. Nevertheless, the utilization of transformer and OHL is improved significantly by employing DTR + DTR.

The hourly dispatch cost analysis and wind energy utilization is presented in Fig. 18. For the warmest week in 2016, the reduction in dispatch cost is not as significant as for winter. However, this is primarily because the wind generation in this period is extremely low, which results in almost no wind energy curtailment for the STR + SLR case.

4.5. Future improvements

This paper discusses the novel application of DLR and DTR together in a grid for load dispatch and cost optimization. More accurate thermal models for OHLs and transformers could be chosen and adapted to convex optimization problems for power system dispatch. The IEEE model [4] used for thermal estimation of transformer does not account for the oil viscosity variation with respect to temperature. This variation can be significant for low ambient temperatures, which is often the case in Scandinavia or other parts of the world during winter. The utilization of more advanced models including Susa [6] can help resolve this issue. Moreover the different transformer cooling modes affecting the values of ν and μ are to be employed as well.

Nevertheless, the employment of these modifications would make the problem highly nonlinear and issues due to local minima will have to be resolved for the resulting non-convex optimization problem. Therefore, the trade-off between accuracy and computational complexity should be further investigated. The proposed methodology opted for a compromise that favoured the ease of implementation and that could always guarantee an optimal solution, hence the use of convex optimization. Also, the incorporation of existing thermal models that are widely adopted in the industry has been done with only minor modifications in order to preserve their appeal.

Another aspect that is not treated in this study is the uncertainty associated with dynamic ratings as they depend on aleatory weather variables. Unexpected changes in temperature and wind power forecast errors may require additional corrective actions in order to keep the system balanced. These aspects may be more relevant close to real-time operation of the power system rather than in the day-ahead planning phase. However, should the uncertainty be considered, the proposed methodology could be extended accordingly by means of various approaches in the literature such as stochastic programming or chance-constrained programming [27].

The focus of this work is rather to show positive synergies between dynamic rating of various components across a power system and how a coordinate approach to dynamic rating could increase network capacity.

5. Conclusion

This paper proposes a novel methodological approach where both dynamic line rating (DLR) and dynamic transformer rating (DTR) are adopted for optimizing the day-ahead energy dispatch. The optimization problem based on DC optimal power flow is devised and the thermal models for OHLs and transformers are modified to fit a convex optimization problem. Conic inequality constraints are adopted to incorporate IEEE transformer thermal models into the base DC Optimal Power Flow, thus preserving the convexity of the original linear problem. The proposed methodology is then tested on the modified IEEE RTS 24-bus system with additional wind generation for daily and weekly load dispatch using weather, load and generation patterns of an actual transmission power system. Results demonstrate the synergy of combining DLR and DTR for maximising the integration of low-cost, decentralized and wind-based energy resources. Most importantly, it is highlighted how only the combination of the DLR and DTR yields a substantial increase in network capacity that translates into reduced dispatch cost. Dynamic rating of individual components would still result in a more flexible and efficient power system, but assessing their impact would require to consider the system as a whole. Results also indicate that although cost optimization is more prominent in winter due to low ambient temperatures and higher wind speeds, the applicability of the proposed methodology remains relevant during summer season as well.

Acknowledgement

Authors would like to thank Energinet, Ørsted Offshore Wind A/S, Innovation Fund Denmark, SweGRIDS, Swedish Energy Agency and Energiforsk AB Wind Research Program for project sponsorship. Authors would like to thank Rasmus A. Olsen and Anders S. Kristensen from Energinet for their valuable supervision. The continued guidance of Troels Stybe Sørensen and Thomas Herskind Olesen from Ørsted Offshore Wind A/S throughout the project is also appreciated by the authors. Authors would also like to thank Claes Ahlrot from E.ON. AB, Sweden for providing feedback and guidance for the project.

The OPTIMUM framework project collaboration between DTU, Energinet and Ørsted oversees this work. This project was also conducted under STandUP for Wind framework.

References

[1] R. Brown, H. Willis, The economics of aging infrastructure, IEEE Power Energy Mag. 04 (03) (2006) 36–43.
[2] IEEE standard for calculating the current-temperature relationship of bare overhead conductors, IEEE std 738-2012 (Revision of IEEE std 738-2006 - incorporates IEEE std 738-2012 cor 1-2013) (2013) 1-72. doi:10.1109/IEEESTD.2013.6692858.
[3] J. Iglesias, G. Watt, D. Douglass, V. Morgan, R. Stephen, M. Bertinat, D. Muftic, R. Puffer, D. Guery, S. Ueda, K. Bakic, S. Hoffmann, Guide for thermal rating calculation of overhead lines, CIGRE working group B2.43 (2014) 93.
[4] IEEE guide for loading mineral-oil-immersed transformers and step-voltage regulators. IEEE std c57. 91-2011 (March 2012). doi:10.1109/IEEESTD.2012.6166928.
[5] IEC, IEC 60076-7:2005 Power transformers - Part 7: Loading guide for oil-immersed power transformers 60076 (7).
[6] D. Susa, M. Lehtonen, H. Nordman, Dynamic thermal modelling of power transformers, IEEE Trans. Power Del. 20 (1) (2005) 197–204.
[7] K. Morozovska, Dynamic rating of power lines and transformers for wind energy integration, no. 2018:37 in TRITA-EECS-AVL, KTH, Electromagnetic Engineering, Stockholm, Sweden, QC 20180423, 2018.
[8] S. Talpur, C. Wallnerstrom, C. Flood, P. Hilber, Implementation of dynamic line rating in a sub-transmission system for wind power integration, Smart Grid Renew. Energy 6 (8) (2015) 233–249 QC, 20150824.
[9] C. Wallnerstrom, H. Yalin, L. Soder, Impact from dynamic line rating on wind power integration, IEEE Trans. Smart Grid 6 (1) (2015) 343–350, https://doi.org/10.1109/TSG.2014.2341353.
[10] J. Fu, D. Morrow, S. Abdelkader, Integration of wind power into existing transmission network by dynamic overhead line rating, in: 11th International workshop on large-scale integration of wind power into power systems as well as on transmission networks for offshore wind power plants (2012) 5.
[11] T. Jalal, N. Rashid, B. van Vliet, Implementation of dynamic transformer rating in a distribution network, in: 2012 IEEE International conference on power system technology (POWERCON), doi:10.1109/PowerCon.2012.6401328, 2012, pp. 1–5.
[12] G. Bajracharya, T. Koltunowicz, R.R. Negenborn, D. Djairam, B.D. Schutter, J.J. Smit, Optimization of transformer loading based on hot-spot temperature using a predictive health model, Proceedings of the 2010 International Conference on Condition Monitoring and Diagnosis (CMD 2010) 19 (2010) 914–917.
[13] A. Michiorri, P.C. Taylor, S.C.E. Jupe, C.J. Berry, Investigation into the influence of environmental conditions on power system ratings, Proceedings of the Institution of Mechanical Engineers, Part A: Journal of Power and Energy 223 (7) (2009) 743–757 doi:10.1243/09576509JPE718.
[14] J. Yang, X. Bai, L. Jenkins, A.M. Cross, Dynamic network rating for low carbon distribution network operation — a u.k. application, IEEE Trans. Smart Grid 06 (2) (2015) 988–998.
[15] C. Wallnerstrom, P. Hilber, P. Soderstrom, R. Saers, O. Hansson, Potential of dynamic rating in Sweden, in: 2014 International conference on probabilistic methods applied to power systems (PMAPS), doi:10.1109/PMAPS.2014.6960605, 2014, pp. 1–6.
[16] H. Banakar, N. Alguacil, F.D. Galiana, Electrothermal coordination Part I: Theory and implementation schemes, IEEE Trans. Power Syst. 20 (2) (2005) 798–805, https://doi.org/10.1109/TPWRS.2005.846196.
[17] N. Alguacil, M.H. Banakar, F.D. Galiana, Electrothermal coordination Part II: Case studies, IEEE Trans. Power Syst. 20 (4) (2005) 1738–1745, https://doi.org/10.1109/TPWRS.2005.857836.
[18] C. Ordoudis, P. Pinson, M. Zugno, An updated version of the IEEE rts 24-bus system for electricity market and power system operation studies, Technical University of Denmark (DTU) (2016) 1–5.
[19] A. Michiorri, H.M. Nguyen, S. Alessandrini, J.B. Bremnes, S. Dierer, E. Ferrero, B.E. Nygaard, P. Pinson, N. Thomaidis, S. Uski, Forecasting for dynamic line rating, Renew. Sustain. Energy Rev. 52 (2015) 1713–1730, https://doi.org/10.1016/j.rser.2015.07.134.
[20] J. Hosek, P. Musilek, E. Lozowski, P. Pytlak, Effect of time resolution of meteorological inputs on dynamic thermal rating calculations, IET Generation, Transmission & Distribution 5 (9) (2011) 941 doi:10.1049/iet-gtd.2011.0039. URL http://digital-library.theiet.org/content/journals/10.1049/iet-gtd.2011.0039.
[21] N. Viafora, J.G. Møller, R.A. Olsen, A.S. Kristensen, J. Holbøll, Historical data analysis for extending dynamic line ratings across power transmission systems, in: 2018 IEEE International Conference on Probabilistic Methods Applied to Power Systems (PMAPS), doi:10.1109/PMAPS.2018.8440449, 2018, pp. 1–6.
[22] B. Clairmont, D. Douglass, J. Iglesias, Z. Peter, Radial and Longitudinal Temperature Gradients in Bare Stranded Conductors with High Current Densities, Cigre session B2-108. doi:B2-108.
[23] J. Rodriguez Alvarez, C.M. Franck, Radial Thermal Conductivity of all-Aluminum Alloy Conductors, IEEE Trans. Power Del. 30 (4) (2015) 1983–1990, https://doi.org/10.1109/TPWRD.2015.2431374.
[24] I. Albizu, E. Fernandez, A.J. Mazon, M. Bedialauneta, K. Sagastabeitia, Overhead conductor monitoring system for the evaluation of the low sag behavior, 2011 IEEE PES Trondheim PowerTech: The Power of Technology for a Sustainable Society, POWERTECH 2011. doi:10.1109/PTC.2011.6019149, 2011.
[25] A. Hahmann, C. Vincent, A. Pe na, J. Lange, C. Hasager, Wind climate estimation using WRF model output: method and model sensitivities over the sea, Int. J. Climatol. 35 (2015) 3422–3439.
[26] G. Swift, T.S. Molinski, W. Lehn, A fundamental approach to transformer thermal modeling. I. theory and equivalent circuit, IEEE Trans. Power Del. 16 (2) (2001) 171–175.
[27] N. Viafora, S. Delikaraoglou, P. Pinson, J. Holbøll, Chance-constrained optimal power flow with non-parametric probability distributions of dynamic line ratings, International Journal of Electrical Power and Energy Systems.
[28] R.D. Christie, B.F. Wollenberg, I. Wangensteen, Transmission management in the deregulated environment, Proc. of the IEEE 88 (02) (2000) 170–195.
[29] M. Tschampion, M.A. Bucher, A. Ulbig, G. Andersson, N-1 security assessment incorporating the flexibility offered by dynamic line rating, 19th Power Systems Computation Conference, PSCC 2016. doi:10.1109/PSCC.2016.7540880, 2016.
[30] M. Nick, O. Alizadeh-Mousavi, R. Cherkaoui, M. Paolone, Security Constrained Unit Commitment with Dynamic Thermal Line Rating, IEEE Trans. Power Syst. 31 (3) (2016) 2014–2025, https://doi.org/10.1109/TPWRS.2015.2445826.
[31] B. Boyd, V. Vandenberghe, F. Faybusovich, Convex optimization, Vol. 51, 2006. arXiv:1111.6189v1, doi:10.1109/TAC.2006.884922. URL http://ieeexplore.ieee.org/lpdocs/epic03/wrapper.htm?arnumber=4012317.
[32] M. Grant, S. Boyd, CVX: Matlab software for disciplined convex programming, version 2.1, http://cvxr.com/cvx (Mar. 2014).

[Pub. C]

Notes

Accepted version of paper [Pub. C].
Published version available at:
https://ieeexplore.ieee.org/document/8811002

Load Dispatch Optimization using Dynamic Rating and Optimal Lifetime Utilization of Transformers

Nicola Viafora* and Joachim Holbøll
Dept. of Electrical Engineering
Technical University of Denmark, DTU
Kgs. Lyngby, Denmark
*nicovia@elektro.dtu.dk

Syed Hamza H. Kazmi †, Thomas H. Olesen and Troels S. Sørensen
Ørsted Offshore Wind A/S,
Gentofte, Denmark
†syeka@orsted.dk

***Abstract*—Power transformers are critical power system components that are generally loaded conservatively, resulting in marginal utilization of their designed lifetime. Dynamic Transformer Rating (DTR) increases the utilization of this asset by limiting its Hot Spot Temperature (HST) rather than the *per unit* load, thereby increasing available network capacity. However, residual lifetime would still be unutilized according to current dimensioning criteria and state-of-the-art lifetime aging models. This paper proposes a novel methodology for DTR, where both thermal and aging dynamics are accounted for in a multi-period DCOPF formulation. Power losses are accounted for by means of an iterative approach that preserves convexity of the optimization problem. The proposed methodology leads to an optimal lifetime utilization of transformers and favours the integration of wind power generation. This novel DTR approach can be beneficial for applications with limited asset lifetime like offshore windfarms or for postponing grid reinforcements for short period of time.**

***Index Terms*—DCOPF, dynamic transformer rating, lifetime model, losses, wind power integration**

I. Introduction

The integration of renewable-based energy sources, with particular regard to wind power generation, can be hindered by limitations in the thermal overload capability of the existing network. Power transformers in transmission and distribution systems are critical components that may constitute a bottleneck as they are conservatively operated. Dynamic Transformer Rating (DTR) can help resolve these bottlenecks by allowing the transformers to be loaded beyond their nameplate rating according to the actual thermal state [1].

Loading guides [2] and [3] allow large power transformers to be dynamically rated up to the Hot Spot Temperature (HST) of 160 °C. However, the traditional operation philosophy and protection design prevent transformers from being operated beyond HST of 110 °C, which is rarely reached because of favorable ambient conditions. Consequently, transformers are distinctly underutilized and the remaining lifetime by the end of designed period (usually 35-40 years) is significant. This can heavily influence the business case for applications like offshore windfarms, which are traditionally designed to operate for 25 years only. Moreover, optimal transformer utilization can help increase the economic turnover and decrease the Cost of Energy (CoE) for such applications.

Unlike offshore windfarms, transmission and distribution utilities may keep old transformers in operation with increased care and condition-based maintenance. In this case, the increased network capacity provided by DTR can help to defer investments for transmission system operators, which are facing a large and rapid growth of renewable energy sources.

This paper builds upon a recent work in [4], where transformer loadability is directly accounted for in a multi-period DC - Optimal Power Flow (DCOPF) algorithm. The novelty of the proposed DTR approach consists in assessing the remaining transformer lifetime using [2] and [3], based on historical load and ambient conditions. Based on this assessment, the solution of the DCOPF considers not only transformer thermal dynamics, but aging rate and cumulative lifetime utilization as well. This loading approach results in a controlled accelerated aging but without breaching the designed lifetime limit. As a result, the transformer is used more effectively compared to common loadability practices as well as other DTR approaches suggested in [5] and [6].

The IEEE RTS 24-bus network with additional wind generation [7] is used as a test system based on actual weather, load and generation data from the Danish system. The presented case study demonstrates the relevance of the method as a means to improve the utilization of low-cost wind energy while accounting for power losses in the transmission system. The proposed methodology could also be incorporated in more detailed cost-benefit analysis and grid expansion planning studies due to its ability to account for transformers' degradation under variable conditions.

The remainder of the paper is organized as follows. The DTR models from [2] are discussed in Section II. Section III elaborates the thermal aging phenomena in transformer and presents the novel DTR approach. The optimization problem for day-ahead dispatch is formulated in Section IV. The case study is presented in Section V, while the results are discussed in Section VI. Section VII concludes the paper.

II. Dynamic Transformer Rating Model

Dynamic loading of transformers can be performed by determining two critical temperatures: Top-Oil Temperature (TOT) and Hot-Spot Temperature (HST). This estimation is performed by using the ANSI/IEEE Clause 7 model [2],

because of the well-established popularity in the industry and mathematical suitability as compared to other models [3] [8].

These temperatures are calculated using the non-linear differential equations (1) - (2) which require further simplification to prevent non-convexity of the optimization problem [2].

$$\tau_0 \frac{d\vartheta_{\text{top}}}{dt} + \vartheta_{\text{top}} = \vartheta_{\text{amb}} + \vartheta_{\text{or}} \left(\frac{I_{\text{trf}}^2 R + 1}{R + 1} \right)^{\nu} \tag{1}$$

$$\tau_h \frac{d\vartheta_{\text{hst}}}{dt} + \vartheta_{\text{hst}} = \vartheta_{\text{top}} + \vartheta_{\text{hr}} I_{\text{trf}}^{2\mu} \tag{2}$$

where τ_0 and τ_h are the thermal time constants for oil and winding respectively which are expressed in hours; ϑ_{amb} is the ambient temperature in °C; ϑ_{top} and ϑ_{hst} represent top-oil and hot-spot temperatures respectively in °C; I_{trf} is the transformer load current in p.u. with rated load current as base; R is ratio of load losses to no-load losses at rated load; ϑ_{or} in °C is the top-oil rise over ambient temperature ϑ_{amb} at rated load, while ϑ_{hr} in °C is the rated HST rise over TOT for rated load. The empirically derived exponents ν and μ represent the impact of transformer cooling mode (ONAN, OFAF etc.) on the change in thermal resistance and oil viscosity. The constants have different values for different cooling modes, which are provided in [2].

In order to keep the optimization problem convex, some simplifications are made to the TOT and HST models of (1) and (2). Firstly, the selected transformer is assumed to operate continuously at *Oil-Directed-Air-Forced (ODAF)* mode, allowing both the constants ν and μ to be set to 1, as in the linearized model in [9]. Secondly, hot-spot temperature is modelled in terms of its steady state value, since hourly values are used in the optimization problem. Therefore it is assumed that short term thermal transients would be extinguished within one hour due to the small thermal time constant, as verified by authors of [4]. As opposed to oil time constant τ_0, which is in the range of 60 to 90 minutes, winding time constant τ_h is approximately 7-8 minutes. Resulting top-oil and hot-spot temperature dynamics are modelled by means of linearized IEEE thermal models shown in (3) and (4), respectively.

$$\vartheta_{\text{top}_t} = K_1 I_{\text{trf}_t}^2 + K_2 \vartheta_{\text{amb}_t} + K_3 \vartheta_{\text{top}_{t-1}} + K_4 \tag{3}$$

$$\vartheta_{\text{hst}_t} = \vartheta_{\text{top}_t} + \vartheta_{\text{hr}} I_{\text{trf}_t}^2 \tag{4}$$

Top-oil temperature depends on the squared *per unit* load I_{trf}^2, ambient temperature ϑ_{amb} and value of top-oil temperature reached in the previous time step. This latter term is responsible of coupling top-oil temperature values in time thus reflecting the importance of considering recent loading history for transformers. Lastly, Coefficients K are constants that solely depend on transformer construction.

III. Optimal Lifetime Evaluation of Transformers

A. Thermal Aging of Transformers

The limit for thermal capacity of a transformer is based on the maximum allowable stress on relevant materials. These limits are effectively explored and defined in [2] and [3]. The thermal limits for power transformers greater than 100 MVA rating are provided in Table I for different types of dynamic loading beyond nameplate rating. However, the continuous HST limit for designed transformer lifetime is 110 °C for thermally upgraded paper. This temperature ceiling is scarcely ever reached because of over-dimensioning, protection philosophies and favorable ambient conditions. The thermal stress is known to be maximum at HST location. The heat transfer from HST serves as catalyst for chemical reactions, which accelerates the aging of insulation paper [1]. The Arrhenius reaction rate theory has been adapted in [2] to calculate the transformer loss of life. The relative aging rate for a transformer, also called aging acceleration factor Λ, with thermally upgraded insulation paper is given by (5), while the transformer loss of life is given by (6)

TABLE I
Temperature limits for transformers [2] [3]

	Normal Cyclic Load	**Emergency Load** (long-term)	**Emergency Load** (<30 min)
Hot Spot Temp.	120 °C	140 °C	160 / 180 °C
Top Oil Temp.	105 °C	115 °C	115 / 110 °C

$$\Lambda(t) = e^{\left(\frac{15000}{110+273} - \frac{15000}{\vartheta_{\text{hst}}(t)+273} \right)} \tag{5}$$

$$\lambda(t) = \int_{t_0}^{t} \Lambda(\tau)\, d\tau \tag{6}$$

where Λ is unit-less and represents the aging acceleration factor for reference HST of 110 °C for thermally upgraded insulation paper; $\vartheta_{\text{hst}}(t)$ is the actual hot spot temperature in °C at time *t*; $\lambda(t)$ represents the cumulative loss-of-life for time period from t_0 up to t and in this paper it is expressed in years. Hence the lifetime utilization of transformer is directly dependent on HST. It must be mentioned that the factor Λ represents the thermal aging of paper insulation only and the impacts of residual moisture content in paper and oil along with other aging phenomena on transformer lifetime are not assessed in this paper.

B. Dynamic Rating and Improved Lifetime Utilization

Static Transformer Rating (STR) limits continuous load current to 1 pu for power transformers and cyclic load current to 1.3 pu [2]- [3]. In contrast to this approach, DTR allows the transformer to be loaded based on HST instead of the rated capacity and thereby prevents this temperature from violating the limits of Table I [5] - [6]. The methodology for DTR used in this paper additionally evaluates the consumed lifetime λ of a transformer and it sets the loadability accordingly.

Referring to Fig. 1, it is assumed that until time t_0 the transformer has continuously operated at HST of 98 °C. The relative aging rate Λ is 0.282, which is represented by the slope of black line in the figure. Consequently, the transformer loss-of-life at this point would be $\lambda_A = 0.282\ t_0$. The difference

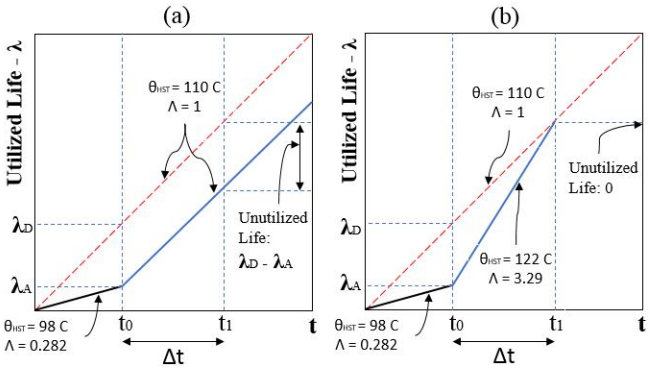

Fig. 1. Methodology for optimal transformer utilization. (a) Fixed HST limit of 110 C. (b) Utilized lifetime (λ) dependent HST limit ($\vartheta_{\text{hst,max}}$ = 140 C)

between designed loss-of-life λ_D for HST of 110 °C and actual λ would continue to increase, if the transformer would keep this loading strategy. DTR can prevent this difference from increasing further by loading the transformer in a way that keeps the HST closer to the design limit of 110 °C, as shown in Fig. 1a. But even with this approach, the residual transformer lifetime by the end of design life would be significant.Therefore, the transformer loading strategy proposed in this paper is meant to maximize component's utilization by considering not only temperature dynamics, but aging rate as well. Fig. 1b illustrates the underlying concept of Enhanced Dynamic Transformer Rating (DTR$^+$).For the period between t_0 and t_1, the limiting factor consists in the designed loss-of-life λ_D, i.e. the red dashed line, rather than the maximum slope associated with HST of 110. As a result, the upper temperature limit is increased to 122°C and the transformer could be loaded even more, thus decresing the unitilized lifetime.

IV. Problem Formulation

In this section the multi-period DCOPF is formulated, where transformer thermal and aging dynamics are directly accounted for along with transmission system losses. The proposed contribution is based on piece-wise linearized transformer aging functions that are incorporated into a DCOPF problem. The same approach could be embedded equally in a ACOPF framework for a more detailed approach.

A. Base DCOPF with quadratic losses

In the considered system the sets of buses, branches, conventional generators and windfarms are indicated with $\mathcal{N}$, $\mathcal{L}$, $\mathcal{G}$ and $\mathcal{W}$, respectively. While the transformers subsets with STR, DTR and DTR$^+$ are identified with $\mathcal{L}_{\text{STR}}$, $\mathcal{L}_{\text{DTR}}$ and $\mathcal{L}_{\text{DTR}^+}$.

This study adopts a DC approximation of the full AC power flow equations. The active power flow on each branch is modelled by means of the Power Transfer Distribution Factor matrix $\boldsymbol{M}$. The matrix $\boldsymbol{M} \in \mathbb{R}^{|\mathcal{L}|\times|\mathcal{N}|}$ expresses the sensitivities of the power flow on each line with respect to the nodal power injections, where the $|\cdot|$ operator indicates the cardinality of the set. The power flow f_ℓ on branch ℓ can then be expressed as $f_\ell = \boldsymbol{M}_\ell \boldsymbol{P}^{\text{inj}}$, where $\boldsymbol{M}_\ell$ is the ℓ-th row of matrix $\boldsymbol{M}$ and $\boldsymbol{P}^{\text{inj}}$ represents a column vector of *per unit* power injection at each bus in the system.

Branch power losses $\boldsymbol{L}$ that are dissipated on transmission lines and transformers are expressed in terms of additional load demand $\boldsymbol{L}^{\text{bus}}$ at each bus. Losses that occur on branch ℓ are equally divided between sending and receiving bus by means of a loss allocation matrix $\boldsymbol{Y} \in \mathbb{R}^{|\mathcal{N}|\times|\mathcal{L}|}$ whose (n,ℓ) component is defined in (7).

$$Y(n,\ell) = \begin{cases} 0.5 & \text{if line } \ell \text{ is connected to bus } n \\ 0 & \text{otherwise} \end{cases} \tag{7}$$

The nodal power injection at bus n can then be written as

$$P_n^{\text{inj}} = P_g + P_w - \left(P_n - P_n^{\text{sh}} + L_n^{\text{bus}}\right) \tag{8}$$

where P_g and P_w represent thermal and wind power generation; P_n and P_n^{sh} represent net load demand and load shedding; L_n^{bus} expresses nodal power losses where $L_n^{\text{bus}} = \boldsymbol{Y}_n \boldsymbol{L}$ and $\boldsymbol{Y}_n$ is the *n*-th row of the loss allocation matrix.

In order to consider quadratic power losses in the DCOPF while preserving its convexity, an iterative approach has been implemented. This method is inspired by existing algorithms in the literature that account for power losses by means of quadratic inequality constraints [10]. However, as discussed in [11], these approaches may introduce additional fictitious losses in the presence of negative locational marginal prices due to congestions in the transmission system. Therefore, the iterative approach adopted in this study introduces an upper bound for power losses which is lowered accordingly at each iteration, should the losses be overestimated. The main steps are:

1) Set the upper bound for power losses to the value corresponding at the maximum power flow and set a tolerance δ for the convergence.
$$L_{(1)}^{\max} = R\, f^{\max^2} \tag{9}$$
2) Solve DCOPF (12) and obtain resulting power flows $f_{(k)}$ and power losses $L_{(k)}$ for the *k*-th iteration.
3) Compute the difference between estimated losses and actual losses for the resulting power flows.
$$\Delta L_{(k)} = L_{(k)} - R f_{(k)}^2 \tag{10}$$
If $\Delta L_{(k)} \leq \delta$ a solution is found, otherwise proceed to next step.
4) Update the upper bound for power losses with the losses corresponding to the power flows at step *k*, plus a small margin ε. Then return to step 2.
$$L_{(k+1)}^{\max} = R f_{(k)}^2 + \varepsilon \tag{11}$$

This iterative approach allows to solve the DCOPF with a quadratic representation of power losses while still preserving the original convexity, which guarantees uniqueness of the solution. This is achieved by gradually reducing the size of the feasible region for branch losses.

The optimization problem in (12) is the base multi-period DCOPF for a generic iteration (k), where losses are accounted

for. The objective is to find the optimal 24-hours day-ahead energy dispatch, which minimizes total generation cost over the period $\mathcal{T}$, where all constraints have to hold $\forall t \in \mathcal{T}$. The base lossy-DCOPF is formulated in a compact form in (12) and it is solved in the matlab-based modeling system CVX [12] using a Mosek academic license.

$$\min_{\Xi} \quad \sum_{t\in\mathcal{T}} \left(\sum_{g\in\mathcal{G}} c_g P_{g,t} + \sum_{w\in\mathcal{W}} c_w P_{w,t} + \sum_{n\in\mathcal{N}} c^{\text{sh}} P^{\text{sh}}_{n,t} \right) \tag{12a}$$

s.t.

$$\sum_{g\in\mathcal{G}} P_{g,t} + \sum_{w\in\mathcal{W}} P_{w,t} - \sum_{n\in\mathcal{N}} (P_{n,t} - P^{\text{sh}}_{n,t} + L^{\text{bus}}_{n,t}) = 0, \tag{12b}$$

$$P^{\min}_g \le P_{g,t} \le P^{\max}_g \qquad \forall g \in \mathcal{G}, \tag{12c}$$

$$-\Delta P^{\max}_g \le P_{g,t} - P_{g,t-1} \le \Delta P^{\max}_g \qquad \forall g \in \mathcal{G}, \tag{12d}$$

$$-f^{\max} \le f_{\ell,t} \le f^{\max} \qquad \forall \ell \in \mathcal{L}, \tag{12e}$$

$$R f^2_{\ell,t} \le L_{\ell,t} \le L^{\max}_{(k)} \qquad \forall \ell \in \mathcal{L}, \tag{12f}$$

$$0 \le P_{w,t} \le P^{\text{av}}_w \qquad \forall w \in \mathcal{W}, \tag{12g}$$

$$0 \le P^{\text{sh}}_{n,t} \le P_n \qquad \forall n \in \mathcal{N} \tag{12h}$$

where $\Xi = [P_{g,t}, P^{\text{sh}}_{n,t}, P_{w,t}, L_{\ell,t}]$ is the set of decision variables that for each time step *t* represent scheduled generator's output $P_{g,t}$, shed load $P^{\text{sh}}_{n,t}$ and dispatched wind power $P_{w,t}$ for every generator, bus and wind farm, respectively. Branch power losses $L_{\ell,t}$ are modelled by means of an auxiliary decision variable in conjunction with quadratic and linear inequality constraints.

The objective function in (12a) consists of three terms: the cost of dispatching conventional generators in the system over period $\mathcal{T}$ considering linear generation cost functions; a small, negligible cost for dispatching wind power in order to improve convergence of the algorithm; the additional cost of preemptive corrective actions such as load shedding. Constraint (12b) enforces system day-ahead power balance for each hour in the considered time period. Constraints (12c) and (12d) impose operational limits on conventional generators in terms of their power outputs and ramping capabilities, whereas branch power flow are limited by constraints (12e). Branch power losses are bounded by constraints (12f). The lower bound consists in their correct quadratic representation, whereas the upper one is necessary to avoid the introduction of fictitious losses. This term is the sole to be iteratively reduced whenever power losses do not lie close enough to the lower boundary in terms of the chosen tolerance δ. Lastly, constraints (12g) and (12h) impose physical limitations on the availability of wind power generation at each bus and the amount of load that can be shed, respectively. Available nodal wind power injections P^{av}_w is modelled as in [4], where time series of wind speed at several locations in the Danish power system are converted to wind power generation time series by means of a multi-turbine wind power curve fitted on historical data. Decision variable P_w in the optimization problem selects the available amount to be dispatched depending on the load demand or the presence of congestions in the grid.

B. Additional constraints for STR

In order to express the loading of the transformer on branch ℓ, the power flow f_ℓ is scaled accordingly with the ratio of base system *per unit* power S^{base} to the nameplate rating of the transformer S^{trf}_ℓ. This scaling factor allows to show the loading I_{trf_ℓ} defined in (13) relatively to the size of the transformer.

$$I_{\text{trf}_{\ell,t}} = f_{\ell,t} \frac{S^{\text{base}}}{S^{\text{trf}}_\ell} \tag{13}$$

The subset $\mathcal{L}_{\text{STR}}$ of transformers that are statically rated can then be represented in the base DCOPF (12) by introducing additional constraints (14) that limit the power flow on the corresponding branch ℓ for all considered time periods.

$$-1 \le I_{\text{trf}_{\ell,t}} \le 1, \qquad \forall \ell \in \mathcal{L}_{\text{STR}}, \quad \forall t \in \mathcal{T} \tag{14}$$

C. Additional constraints for DTR

The loading of transformers that are dynamically rated is limited by operating hot-spot and top-oil temperatures rather than *per unit* load. Top-oil and hot-spot temperature variations are bounded by predefined values that ensure transformers are used within their thermal capabilities, according to state-of-the-art loading guidelines. As discussed in [4], ϑ_{top} and ϑ_{hst} are modelled by means of quadratic inequality constraints which keep the resulting optimization problem a convex one. The extensive form of such values is provided in expressions (3) and (4) in Section II.

$$\vartheta_{\text{top}_{\ell,t}} \le \vartheta^{\max}_{\text{top}} \qquad \forall \ell \in \mathcal{L}_{\text{DTR}}, \quad \forall t \in \mathcal{T} \tag{15}$$

$$\vartheta_{\text{hst}_{\ell,t}} \le \vartheta^{\max}_{\text{hst}} \qquad \forall \ell \in \mathcal{L}_{\text{DTR}}, \quad \forall t \in \mathcal{T} \tag{16}$$

Adding (15) and (16) to the base DCOPF formulation in (12) will consider the effect of having transformers dynamically rated during the 24-hours dispatch period.

D. Additional constraints for DTR⁺

The third loading strategy proposed in this paper takes into account not only temperature dynamics, but also transformer aging rate. This aspect is likely to play a role only in the long term, but it provides indication of how the transformers loading could be affected by cumulative lifetime consumption during continued high temperature operation. In order to do so, the exponential aging acceleration factor Λ defined in Section III is included in the base DCOPF (12) by means of a set of linear inequality constraints that form a convex piece-wise linear approximation. Coefficients m_i and q_i in (17) are the slope and intercept values of the *i*-th tangent line that forms the approximation of Λ.

$$\Delta\lambda_t = \max_i \{m_i \vartheta_{\text{hst}_t} + q_i\} \approx \Lambda_t \tag{17}$$

The expression in (17) relates the transformer hot-spot operating temperature ϑ_{hst_t} to the corresponding incremental lifetime utilization $\Delta\lambda_t$. The cumulative lifetime utilization λ_t is then evaluated in a discrete form in (18)

$$\lambda_t = \lambda_{t-1} + \Delta\lambda_t \tag{18}$$

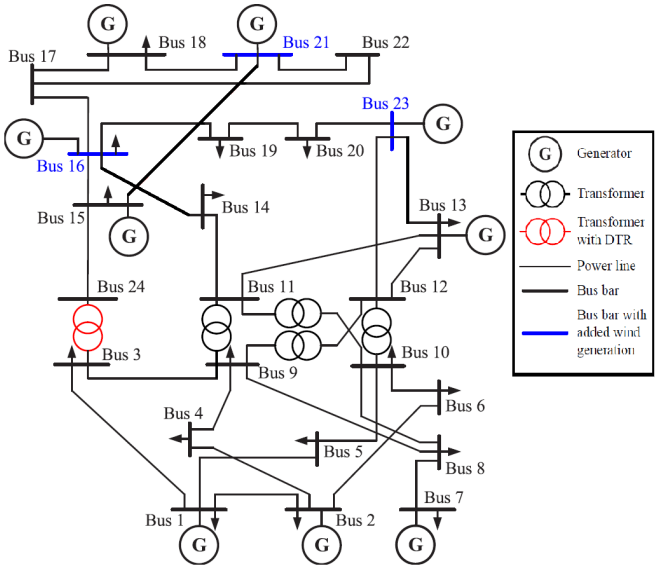

Fig. 2. Modified IEEE RTS 24-bus system [7]

As the transformer is dynamically rated considering lifetime consumption as well, constraints (15) and (16) are added to the base DCOPF (12) together with (19), where λ_0 represents the initial lifetime of the component, α the desired maximum aging rate which in this study has been assumed 1 and t is the time counter during the simulation.

$$\lambda_{\ell,t} \leq \lambda_0 + \alpha t \qquad \forall \ell \in \mathcal{L}_{\text{DTR}^+}, \quad \forall t \in \mathcal{T} \qquad (19)$$

Ultimately, this approach allows to set a higher temperature limit on transformer operation as long as the designed lifetime consumption limit is not reached. Once the upper boundary of lifetime utilization is met, the binding constraint will switch from hot-spot temperature to used cumulative lifetime, thus limiting the operation of the component accordingly.

V. Case Study

The IEEE RTS 24-bus network with additional wind generation from [7] has been adopted in this study with some modifications. Referring to Fig. 2, wind generation is concentrated at Bus 16, 21 and 23, whereas different nameplate ratings are considered for the transformer located between bus 3 and 24, namely 150, 175 and 200 MVA. The data used to model transformer thermal dynamics is provided in [8].

The multi-period DCOPF problem of Section IV is solved in a moving window of 24 hours for the 3-year period between 2014 and 2016. Different test cases compare the system and transformer performance for STR, DTR with $\vartheta_{\text{hst}}^{\max}$ at 110 °C and DTR$^+$ with $\vartheta_{\text{hst}}^{\max}$ at 140 °C combined with optimal lifetime utilization. The assumptions for the DTR$^+$ test case are quite conservative. The transformer is assumed to be in operation for 3 years with DTR resulting in cumulative loss-of-life of 1.5 years, which is cautiously chosen based on operational experience of large transformers.

Historical daily load profiles from the Danish power system have been scaled accordingly with respect to the peak demand in [7]. Total load demand is then increased by 25 percent during the central hours of each day in order to account for future network changes and to enhance the need for DTR in the given system. Lastly, historical time series of ambient temperature from the same system have been used in the thermal rating algorithm for transformers. This allows to take the weather correlation between wind speed and ambient temperature into account. Such a correlation will be reflected between the available wind power generation and the loadability of transformers.

VI. Results and Discussion

The analysis starts from considering the overall impact of the tested loading strategies on the cumulative lifetime utilization of a 175 MVA transformer, shown in the left part of Fig. 3. It stands out as the STR approach practically does not cause any significant aging over the entire 3-years period, in agreement with conservative common loading practices. As opposed to STR, DTR$^+$ pushes the utilization of the component to the designed limit in less than 1 year. Once the maximum aging rate is met, the component will keep using the available designed lifetime at disposal, according to the proposed loading strategy presented in this paper.

The resulting aging profiles can be motivated by considering a three-day period in Fig. 4, where transformer loading and corresponding hot-spot temperatures are shown. As long as the transformer load is limited in terms of its *per unit* nameplate rating, the associated hot-spot temperature remains well below the allowed operational limits due to favourable weather conditions and dimensioning criteria. The resulting low HST profile coupled with the exponential aging acceleration factor shown in the right part of Fig. 3 will yield a close-to-zero aging rate for STR. However, in this condition the transformer branch constitutes a bottleneck in the grid, thus causing increased dispatch costs for the system.

Moving the transformer limiting factor from the *per unit* load to the hot-spot temperature by means of DTR allows to significantly increase the power flow. This would help releasing grid congestions and dispatching more wind power generation from the buses where it is located, at a cost of

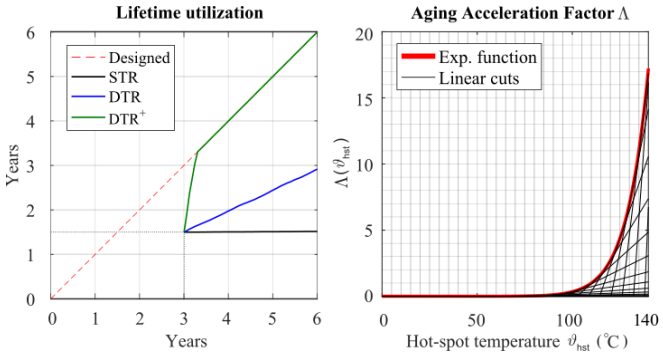

Fig. 3. Cumulative lifetime utilization over the 3-years period for different loading strategies (left). Exponential aging acceleration factor and fitted linear approximations (right).

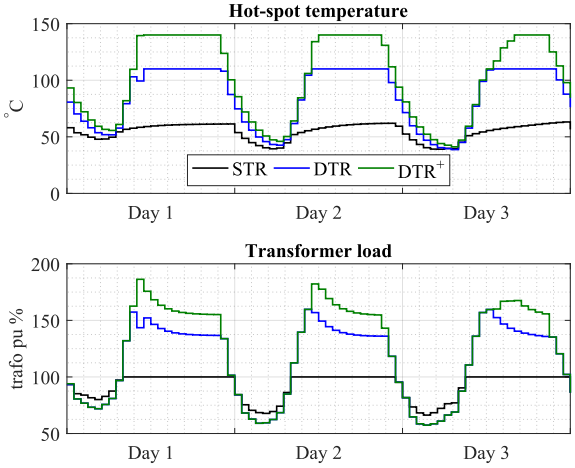

Fig. 4. Transformer hot-spot temperature (above) and transformer load (below). Focus on three days for STR, DTR and DTR+

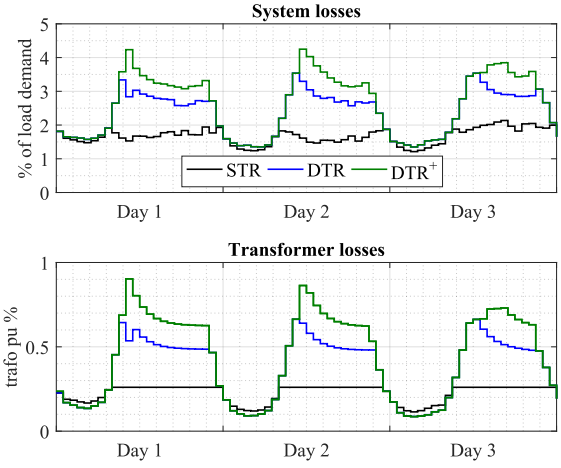

Fig. 5. Total system losses (above) and transformer losses (below). Focus on three days for STR, DTR and DTR+

increasing the lifetime utilization of the component. This mechanism is further enhanced by considering DTR+, which allows the transformer hot spot temperature to be set even higher, as long as the aging rate does not reach the predefined limit, as shown in Fig. 3. Once the maximum aging rate is reached, the constraint on lifetime utilization will prevent the hot-spot temperature to reach the maximum value, thus resulting in a lowered loading capability.

The operation beyond nameplate rating causes additional power losses, not only in the component that is being dynamically rated, but in the remainder of the system as well. This aspect can be seen in Fig. 5, where transformer and system losses are shown for the same 3-days period. Relieving grid congestions by means of DTR or DTR+ will result in increased power flows across the grid, which will in turn cause additional system losses. Despite increasing system losses, the solution of the multi-period DCOPF suggests that there would still be economic benefits from the increased power flow in the grid, as summarized in Table II, where losses are taken into account.

TABLE II
COST REDUCTION AND LIFETIME USE AFTER 1 YEAR COMPARED TO STR

Transformer Size (MVA)	**Cost Reduction (%)**		**Used Lifetime (%)**	
	DTR	DTR+	DTR	DTR+
150	-10.1	-11.5	+41.5	+166
175	-8.1	-8.8	+31.1	+166
200	-6.4	-7.1	+24.2	+166

VII. CONCLUSION

This paper proposes a novel approach for optimal transformer lifetime utilization. This approach incorporates both thermal and aging dynamics into a convex optimization problem based on a multi-period DCOPF, while accounting for quadratic power losses in the system. The proposed algorithm maximizes the transformer utilization ensuring that neither thermal nor aging rate limits are violated during operation. The results suggest that the proposed DTR algorithm reduces the cost of load dispatch and yields a substantial increase in network capacity. It is also observed that accounting for the temperature-dependent aging rate can allow a better utilization of the transformer designed lifetime. This aspect is likely to improve the business case for applications with limited asset lifetime like offshore windfarms. It could also be beneficial for TSO which have to face rapid growth of renewable-based generation and postpone the required grid reinforcements.

REFERENCES

[1] J. Rossenlind, "Lifetime modeling and management of transformers," Ph.D. dissertation, KTH, Electromagnetic Eng., Stockholm, 2013.
[2] "IEEE guide for loading mineral-oil-immersed transformers and step-voltage regulators - redline," *IEEE Std C57.91-2011 (Revision of IEEE Std C57.91-1995) - Redline*, pp. 1–172, Mar 2011.
[3] IEC, "IEC 60076-7:2005 power transformers - part 7: Loading guide for oil-immersed power transformers," vol. 60076, no. 7, 2005.
[4] N. Viafora, K. Morozovska *et al*, "Day-ahead dispatch optimization with dynamic thermal rating of transformers and overhead lines," *Electric Power Systems Research*, vol. 171, pp. 194–208, 2019.
[5] M. Humayun, M. Degefa, A. Safdarian, and M. Lehtonen, "Utilization improvement of transformers using demand response," *IEEE transactions on power delivery*, vol. 30, no. 1, pp. 202–210, Feb 2015.
[6] T. Bajracharya, G. Koltunowicz *et al*, "Optimization of transformer loading based on hot-spot temperature using a predictive health model," in *Int. Conf. on Condition Monitoring and Diagnosis*, Sept 2010, pp. 914–917.
[7] C. Ordoudis, P. Pinson, J. Morales González, and M. Zugno, *An Updated Version of the IEEE RTS 24-Bus System for Electricity Market and Power System Operation Studies.* Technical University of Denmark, 2016.
[8] D. Susa, M. Lehtonen, and H. Nordman, "Dynamic thermal modelling of power transformers," *IEEE Trans. on Power Del.*, vol. 20, no. 1, pp. 197–204, 2005.
[9] L. Jauregui-Rivera and D. J. Tylavsky, "Acceptability of four transformer top-oil thermal models—part i: Defining metrics," *IEEE Transactions on Power Delivery*, vol. 23, no. 2, pp. 860–865, April 2008.
[10] R. A. Jabr, "Modeling network losses using quadratic cones," *IEEE Transactions on Power Systems*, vol. 20, no. 1, pp. 505–506, Feb 2005.
[11] O. W. Akinbode and K. W. Hedman, "Fictitious losses in the dcopf with a piecewise linear approximation of losses," in *IEEE PES GM*, July 2013, pp. 1–5.
[12] M. Grant and S. Boyd, "CVX: Matlab software for disciplined convex programming, version 2.1," http://cvxr.com/cvx, Mar. 2014.

[Pub. D]

Notes

Published journal article version of [Pub. D].
Available at:
https://doi.org/10.1016/j.ijepes.2019.105389

Electrical Power and Energy Systems 114 (2020) 105389

Contents lists available at ScienceDirect

Electrical Power and Energy Systems

journal homepage: www.elsevier.com/locate/ijepes

Chance-constrained optimal power flow with non-parametric probability distributions of dynamic line ratings

Nicola Viafora[a,*], Stefanos Delikaraoglou[b], Pierre Pinson[a], Joachim Holbøll[a]

[a] Dept. of Electrical Engineering, Technical University of Denmark, Lyngby, Denmark
[b] EEH - Power Systems Laboratory of ETH Zurich, Zurich, Switzerland

ARTICLE INFO

Keywords:
Dynamic line rating
Chance constraints
Non-parametric distribution
Wind power
Uncertainty

ABSTRACT

Compared to Seasonal Line Rating (SLR), Dynamic Line Rating (DLR) allows for higher power flows on overhead transmission lines, depending on the actual weather conditions. Nevertheless, the potential of DLR has to be traded off against the additional uncertainty associated with varying ratings. This paper proposes a DC-Optimal Power Flow (DCOPF) algorithm that accounts for DLR uncertainty by means of Chance-Constraints (CC). The goal is to determine the optimal day-ahead dispatch taking the cost of reserve procurement into account. The key contribution of this paper consists in considering both non-parametric predictive distributions of DLR and the combined wind power uncertainty in the optimization problem. Our results highlight the benefits of DLR in wind-dominated power systems, assuming typical risk aversion levels in the line rating estimation.

1. Introduction

Overhead transmission lines are traditionally dimensioned in a conservative way by assuming constant and unfavourable thermal conditions which restrict the power flow. Guidelines for thermal rating of conductors [1] suggest that DLR could yield a substantial upgrade, especially under windy conditions. Nevertheless, the potential of DLR has to be traded off against the additional uncertainty associated with varying ratings, which may compromise security. In this regard, several studies have investigated how the uncertainty associated with DLR can be accounted for in the power system operation.

Various methodological approaches have been explored in the literature with a strong focus on considering both energy and reserve dispatch under different sources of uncertainty. Authors in [2] propose a two-stage stochastic optimization problem coupled with a probabilistic forecasting model. This approach optimizes the day-ahead scheduling with a risk-neutral approach towards the realization of uncertain variables, i.e., line ratings, wind power and line outages. The study in [3] instead considers uncertainty in load demand and wind power generation by combining affine arithmetic and probabilistic methods such as Monte Carlo. Authors of [4] have addressed the influence of DLR on the security constrained unit commitment, whereas in [5] this problem is considered in a stochastic programming framework together with network topology changes.

One of the major aspects that is investigated in the literature is how to set the dynamic line ratings while keeping the required level of conservatism during power system operation. To this extent, a robust optimization framework is proposed by authors of [6], where corrective actions for dealing with uncertain ratings are discussed. A similar approach is followed in [7] where a distributionally robust optimization algorithm is implemented to co-optimize energy and reserves in large scale power systems, whereas authors in [8] compared various methodologies for the optimal line rating selection for different market structures and grid operators' objectives. Lastly in [9], DLRs are incorporated into a N-1 security assessment using CC and a copula approach to model the correlation structure between ratings. The CC formulation approach in particular allows to evaluate the margin for higher utilization of the grid, assuming the same risk level that the TSOs accept with SLR and thus it is preferred in this paper over other methodologies.

As discussed in [10], when the uncertainty in the chance constraints is modelled with elliptical distributions, the constraint is convex, given that the safety level is high enough. The Normal distribution is part of this class of distributions and it is commonly used to reformulate chance constraints analytically, thus preserving the convexity of the optimization problem.

However, this assumption introduces an approximation error whenever the uncertainty does not follow a distribution from this class. Authors of [11] show that weather-dependent line ratings follow non-parametric probability distributions, thus leading to potential

* Corresponding author at: Elektrovej, Building 325, DK-2800 Kgs. Lyngby, Denmark.
E-mail address: nicovia@elektro.dtu.dk (N. Viafora).

https://doi.org/10.1016/j.ijepes.2019.105389
Received 14 March 2019; Received in revised form 22 May 2019; Accepted 26 June 2019

Nomenclature

Subscripts

ℓ	line index
g	conventional generator index
m	Gaussian component
n	bus index
t	time index
w	wind farm index

Superscripts

cut	wind power curtailment
dw	downward reserve
inj	nodal injection
max	upper bound of variable
min	lower bound of variable
sh	load shedding
tot	total value of variable over the corresponding set
up	upward reserve

Sets

$\mathscr{G}/G$	Set/Number of conventional generators
$\mathscr{L}/L$	Set/Number of lines in the system
$\mathscr{L}_{\text{dlr}}/L_{\text{dlr}}$	Set/Number of lines with DLR
$\mathscr{L}_{\text{slr}}/L_{\text{slr}}$	Set/Number of lines with SLR
$\mathscr{N}/N$	Set/Number of nodes
$\mathscr{W}/W$	Set/Number of wind farms

Parameters

α_g, α_n	participation factors per generator $g \in \mathscr{G}$ and per bus $n \in \mathscr{N}$.
$\boldsymbol{\alpha}$	column vector of nodal participation factors $\boldsymbol{\alpha} = (\alpha_1, ..., \alpha_N)^\top$
$\boldsymbol{\beta}$, $\boldsymbol{\beta}_0$	coefficients of linear quantile regression
$\hat{\boldsymbol{f}}$	probabilistic forecast
$\boldsymbol{a}_\ell$	coefficients for linear summation of random variables in power flow constraint, $\forall\ \ell \in \mathscr{L}$
$\boldsymbol{B}_{\text{bus}}$, $\boldsymbol{B}_{\text{line}}$	bus and line admittance matrix
$\boldsymbol{S}$	Power Transfer Distribution Factor matrix
$\boldsymbol{x}_t$	point forecast time series of weather variables
ΔF_ℓ	power flow uncertainty, $\forall\ \ell \in \mathscr{L}$
ΔP^{tot}	total power imbalance in the system
ΔT_{rd}	conductor radial temperature drop
δ_ℓ^+, δ_ℓ^-	uncertainty margins for power flow, $\forall\ \ell \in \mathscr{L}_{\text{slr}}$
Γ	adjustable parameter set for GMM
$\hat{F}_\ell$	expected line power flow, $\forall\ \ell \in \mathscr{L}$
$\hat{P}_w$	wind power point forecast for day-ahead, $\forall\ w \in \mathscr{W}$
μ, Σ, ω	mean value, covariance matrix and weight of Gaussian component
ν	number of regression variables in probabilistic forecast
ρ	Spearman's rank correlation matrix
τ	number of quantiles in probabilistic forecast
ε	risk aversion level
c	linear costs terms in objective function
d	dimension of Gaussian component
F_ℓ	line power flow, $\forall\ \ell \in \mathscr{L}$
f_ℓ^+, f_ℓ^-	chosen upper and lower bound for power flow constraints, $\forall\ \ell \in \mathscr{L}_{\text{dlr}}$
h	lead time of probabilistic forecast
I	maximum conductor current
M	number of Gaussian components
q_c	convective cooling
q_j	joule heating
q_r	radiative cooling
q_s	solar heating
r_g^{up}, r_g^{dw}	bounds for probabilistic reserve procurement constraints, $\forall\ g \in \mathscr{G}$
T_{av}	average conductor temperature in cross-section
T_c	conductor core temperature
T_s	conductor surface temperature

Decision variables

P_g, $\boldsymbol{P_g}$	scheduled power output per generator $g \in \mathscr{G}$ and per bus vector notation
P_n^{sh}, $\boldsymbol{P_n^{\text{sh}}}$	load shedding $\forall\ n \in \mathscr{N}$; scalar and vector notation
P_w^{cut}, $\boldsymbol{P_w^{\text{cut}}}$	curtailed wind power per wind farm $w \in \mathscr{W}$ and per bus vector notation.
R_g^{dw}	downward reserve procurement $\forall\ g \in \mathscr{G}$
R_g^{up}	upward reserve procurement $\forall\ g \in \mathscr{G}$

Random variables

$\boldsymbol{X}_\ell$, $\boldsymbol{x}$	multivariate random variable for line rating and nodal wind power generation, $\forall\ \ell \in \mathscr{L}_{\text{dlr}}$
ΔP_w, $\boldsymbol{\Delta P_w}$	wind power forecast error for wind farm $w \in \mathscr{W}$ and per bus vector notation
$F_\ell^{\max}$	dynamic line rating $\forall\ \ell \in \mathscr{L}_{\text{dlr}}$, static line rating $\forall\ \ell \in \mathscr{L}_{\text{slr}}$
P_w, $\boldsymbol{P_w}$	available wind power generation per wind farm $w \in \mathscr{W}$ and per bus vector notation
Y_ℓ^+, Y_ℓ^-, y	univariate random variables for stochastic part of bidirectional power flow constraint, $\forall\ \ell \in \mathscr{L}$

Abbreviations

CC	Chance-Constraints
CDF	Cumulative Distribution Function
DLR	Dynamic Line Rating
GMM	Gaussian Mixture Model
HBE	Heat Balance Equation
OPF	Optimal Power Flow
PDF	Probability Density Function
RMS	Root Medium Square
SLR	Static Line Rating
TSO	Transmission System Operator

inaccuracies. Furthermore, existing studies which adopt a CC approach do not account for other sources of uncertainty, e.g., wind power forecast errors. This limitation is likely to yield a higher re-dispatch cost since potential synergies and correlations between power flows and DLRs are not taken into account.

The key contribution of this paper is to propose a methodological approach based on CC-Optimal Power Flow (CC-OPF), considering non-parametric predictive distributions of DLR and the combined wind power uncertainty. We account for the positive correlation structure of line ratings and nodal wind power injections across the system by means of their joint predictive distribution. This approach allows the grid operator to handle probabilistic forecast of line ratings dropping any assumption on the shape of their distribution, while considering their correlation with wind power. Using non-parametric predictive distributions of DLR, as opposed to the prevailing assumption of normality, sets the framework for relying upon more detailed DLR

forecasting algorithms, such as the one presented in [12].

The objective of the proposed model is to seek the optimal day-ahead system dispatch for typical risk aversion levels of the TSO, considering the procurement cost of reserve necessary for real-time re-dispatch actions. This methodology can serve as a decision-support tool for the TSO who has to set the line ratings in its network before the day-ahead market clearing, accounting thought for possible deviations during real-time operation. A quantile regression algorithm is used to provide non-parametric probabilistic forecasts of DLRs, which are then incorporated in the CC-OPF formulation. This latter step is performed by adapting the methodology presented in [13], where Gaussian Mixture Models are used to represent correlated non-Gaussian random variables in an optimal power flow algorithm.

The paper is structured as follows. Section 2 introduces the principles of DLR modelling whereas Section 3 describes how probabilistic forecasts have been obtained. The Chance-Constrained problem formulation is presented and a solution methodology is described in Sections 4 and 5, respectively. The proposed methodology is tested in a case study presented in Section 6 whereas numerical results are given in Section 7. Lastly, Section 8 concludes the paper.

2. Modelling of dynamic line ratings

Overhead line ratings are simulated by means of a modified model based on the Cigré guide for thermal rating calculations [1]. In the Cigré guide, line ratings are determined by solving the heat balance equation (HBE)

$$q_j(I) + q_s - q_c - q_r = 0 \tag{1}$$

which describes the thermal equilibrium between several heating and cooling mechanisms of the conductors, such as Joule losses q_j, solar heating q_s, convective and radiative cooling denoted as q_c and q_r, respectively. In steady state conditions the HBE can be solved directly for the RMS current I, which solely appears in the Joule losses term. For a detailed description of the estimation of the q terms in (1) the reader is referred to [1]. The modified rating algorithm adopted in this study has been proposed by the authors in [14] and accounts for the radial temperature drop in the conductors. As the line current approaches the thermal limit, the assumption of constant temperature distribution within the conductors may lead to excessive heating in the core. Violating the maximum operating temperature would cause the line to elongate and sag beyond the limits set by the TSO [15]. In order to account for this aspect, the following system of non-linear equations

$$q_j(I,\, T_{\text{av}}) + q_s - q_c(T_s) - q_r(T_s) = 0 \tag{2}$$

$$T_c - T_s = \Delta T_{cs}(I,\, T_{\text{av}}) \tag{3}$$

$$T_c + T_s = 2T_{\text{av}} \tag{4}$$

is solved for the current I, the average temperature T_{av} and the surface temperature T_s of the conductor. Core temperature T_c is set beforehand to the maximum operating temperature of the line. Eq. (2) is the HBE where the dependency upon the current, the surface temperature and the average temperature of the conductors is stressed. Eq. (3) expresses the difference between the core and the surface temperature with a simplified relation ΔT_{cs} presented in [1]. This quantity depends upon several properties of the conductor as well as the current and the average temperature. The explicit form is omitted in this paper being outside the scope of the study. Lastly, (4) couples the variables T_s and T_{av} assuming that the radial temperature is linear in the cross-section. Ultimately, as opposed to (1) the solution of (2)–(4) yields a more conservative rating especially under high windy conditions, when the radial temperature drop is not negligible. All terms that appear in the HBE are highly weather dependent. The weather variables that have been considered for the estimation of the thermal ratings are wind speed, wind direction, air temperature and solar radiation. This study relies on hourly weather data over a three-year period time that have been simulated across the Danish power system. Time series of weather variables have been simulated with the mesoscale downscaling method presented in [16].

3. Probabilistic forecasts

In this study, both DLRs and wind power generation are modelled as random variables described by certain predictive probability density distributions.

3.1. DLR forecasts

Probabilistic forecasts of DLR are derived with a multivariate linear quantile regression algorithm [17] trained on two years of simulated data. The remaining data from the third year is considered as a point-forecasts time series $\boldsymbol{x_t}$ available to the TSO. Wind speed, wind direction, air temperature and solar radiation were considered as the regressors for the line ratings estimated as described in Section 2. Matrix $\boldsymbol{\beta} \in \mathbb{R}^{\tau \times v}$ contains the coefficients of the linear regression per quantile, where τ indicates the number of quantiles and v the number of variables, whereas $\boldsymbol{\beta_0} \in \mathbb{R}^{\tau \times h}$ collects all the intercept terms. The probabilistic forecast for lead time h issued at time t is determined by collecting all the predictions per quantile in $\hat{\boldsymbol{f}}_{t+h}$ using the following expression

$$\hat{\boldsymbol{f}}_{t+h} = \boldsymbol{\beta}^{\top}\boldsymbol{x}_{t+h} + \boldsymbol{\beta}_0. \tag{5}$$

The same lead time $h = 1$ is considered for all the forecasts, thus not accounting for the increasing uncertainty in the prediction, as the lead time increases. The probabilistic forecast is then found by linearly interpolating the values of $\hat{\boldsymbol{f}}_t$ between quantiles with a chosen granularity.

Fig. 1(a) shows an example of probabilistic forecast for a certain time t given the point forecasts of wind speed (7.64 m/s), wind direction (56.4°), air temperature (3.26 °C) and solar radiation (100 W/m^2). The probabilistic forecast increases the awareness regarding the

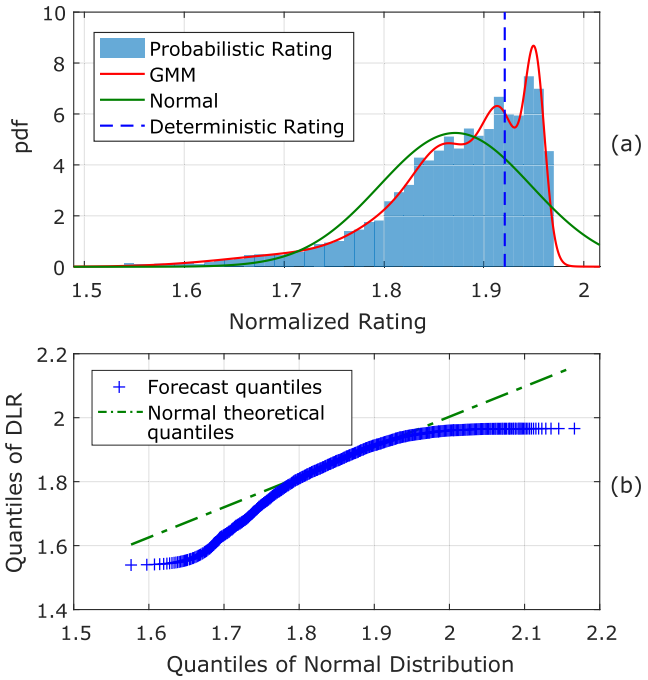

Fig. 1. (a) Example of predictive probability density function of DLR and fitted distributions. Point forecasts of weather variables are: wind speed = 7.64 m/s, wind direction = 56.4 °, air temperature = 3.26 °C and solar radiation = 100 W/m^2. (b) QQ-Plot for testing normality of the distribution.

uncertainty on DLR, as opposed to the deterministic rating which is found by applying the thermal model to the point forecasts values. This can help the TSO in setting the rating in advance with a chosen confidence level, thus keeping an appropriate distance from the true thermal limit of the lines.

The assumption of normality in the predictive distribution of DLR is tested with an Anderson-Darling hypothesis test that rejects the null hypothesis at a 5 % significance level. This result can also be visualized with the quantile-quantile (QQ) plot in Fig. 1(b), from which it is clear that the predictive distribution does not follow a Gaussian distribution. The assumption of normality in particular is found to overestimate the lower tail region of the probabilistic forecast. This is of special interest in chance-constrained optimization, since the TSO seeks high confidence in the minimum capacity of the transmission system.

The need to replicate closely the true distribution of line ratings motivated the adoption of a non-parametric probability distribution such as the Gaussian Mixture Model (GMM). Using the notation of [13], the PDF of a random variable $\boldsymbol{X}$ can be approximated as a convex combination of M Gaussian distributions

$$\mathrm{PDF}_{\boldsymbol{X}}(\boldsymbol{x}) = \sum_{m=1}^{M} \omega_m \left[N_m(\boldsymbol{x};\mu_m, \Sigma_m)\right] \tag{6}$$

$$\sum_{m=1}^{M} \omega_m = 1, \quad \omega_m > 0 \quad \forall\, m \tag{7}$$

where $m = 1, ...,M$ indicates the components in the GMM. An adjustable set of parameters $\Gamma = \{\omega_1, ...,\omega_M, \mu_1, ...,\mu_M, \Sigma_1, ...,\Sigma_M\}$ is estimated in order to approximate any shape of the original distribution, where ω_m is a weight coefficient, $\mu_m \in \mathbb{R}^d$ is the vector of mean values and $\Sigma_m \in \mathbb{R}^{d\times d}$ is the variance-covariance matrix for the m-th Gaussian component with d dimensions. The scalar weights $\{\omega_m\}_{m=1}^{M}$ are part of the unit simplex.

The flexibility of a non-parametric probability distribution is particularly useful for modelling the uncertainty in DLR forecasts, since the shape of the predictive distributions is found to vary greatly within short time frames. The GMM fit has been performed using dedicated MATLAB functions. The number of components in the mixture has to be fixed before estimating the adjustable set of parameters Γ. There are several methods discussed in the literature on how to fix the number of components in the mixture. Authors of [19] optimize it by minimizing the Euclidean distance between the fitted and the actual PDF in a two-stage optimization model. This paper adopts a simplified approach, similarly to [20], where the number of components is fixed to 10 based on preliminary tests. The Bayesian Information Criterion (BIC) is used to find the best trade-off between computational performance and goodness of fit.

3.2. Wind power forecasts

A similar approach is adopted to generate probabilistic forecasts of wind power production in various sites. The average wind speed at each time step is used as the sole regressor for the aggregate wind power production from the Danish power system. Then, a piecewise polynomial quantile regression is used to fit the data shown in Fig. 2. A linear model is adopted below 1.5 m/s and above 13 m/s, whereas for the intermediate wind speed range a polynomial of degree 7 is found to best fit the available data. The solid red line shows the fitted error function $erf(x)$ which is used as a multi-turbine wind power curve model in order to transform wind speed time series into wind power production.

In this study, GMMs are used to model both univariate predictive distributions of DLR and wind power generation, as well as their joint density distributions. The methodology adopted to derive the joint distribution is described in Section 5. Fig. 3 shows the marginal predictive distribution of wind power for a given site and time that has been obtained using of the non-linear quantile regression algorithm. In order to account for the double-bounded nature of wind power generation, the GMM distributions are truncated accordingly as in [18], in order to respect the capacity limitation of each wind farm.

4. Chance-Constrained OPF

In the considered transmission system, $\mathcal{N}$ indicates the set of nodes, $\mathcal{G}$ the set of conventional generators, $\mathcal{W}$ the set of wind farms and $\mathcal{L}$ the set of transmission lines. The subsets of $\mathcal{L}$ indicated with $\mathcal{L}_{\mathrm{dlr}}$ and $\mathcal{L}_{\mathrm{slr}}$ differentiate the lines equipped with DLR between those that are not. The size of each set is given by N, G, W, L, L_{dlr} and L_{slr}, respectively.

4.1. Power flow model

This study uses a DC approximation of the full AC power flow equations. The active power flow on each line is modelled as a function of the nodal power injections P^{inj} and the Power Transfer Distribution Factor matrix S[21]. The matrix $S \in \mathbb{R}^{L\times N}$ expresses the constant coefficients of the linear relationship between the power injections and the power flows on the lines. It is defined as $S = B_{\mathrm{line}}B_{\mathrm{bus}}^{-1}$ and it is a function of the line admittance matrix B_{line} and the bus admittance matrix B_{bus}, in which the row and column corresponding to the slack bus are deleted. The power flow F_ℓ on line ℓ can then be expressed as $F_\ell = S_{(\ell,\cdot)}P^{\mathrm{inj}}$, where $S_{(\ell,\cdot)}$ is the ℓ-th row of the matrix S.

4.2. Reserve activation policy

The policy for reserve activation across the power system is set according to a linear decision rule. All conventional generators are assumed to respond proportionally to the fluctuations in the system in case of a deviation from the expected wind power generation. Total wind power forecast errors are expressed as $\Delta P^{\mathrm{tot}} = \sum_w P_w - \hat{P}_w$, with P_w and $\hat{P}_w$ being the actual and the expected wind power generation of wind farm w, respectively. This mechanism enables a decentralized real-time operation of the power system, since upward and downward reserve deployment from each unit g compensate a portion α_g of the total power imbalance. The values of α_g are predefined constant inputs that are set prior to the optimization in order to preserve the convexity of the problem. In particular, their values are defined as

$$\alpha_g = \frac{P_g^{\max} - P_g^{\min}}{\sum_g \left(P_g^{\max} - P_g^{\min}\right)} \tag{8}$$

where $P_g^{\max}$ and $P_g^{\min}$ are the maximum and minimum capacity of generating unit g. This predefined policy corresponds to the case described in [22], where the TSO does not consider the location of the reserve during the procurement phase.

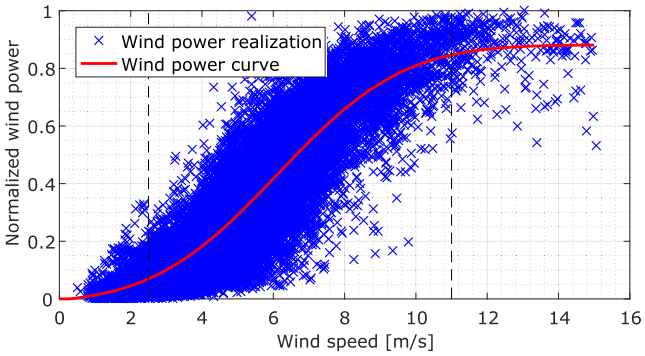

Fig. 2. Scatter plot of aggregated wind power production as a function of mean wind speed in the Danish power system and fitted error function.

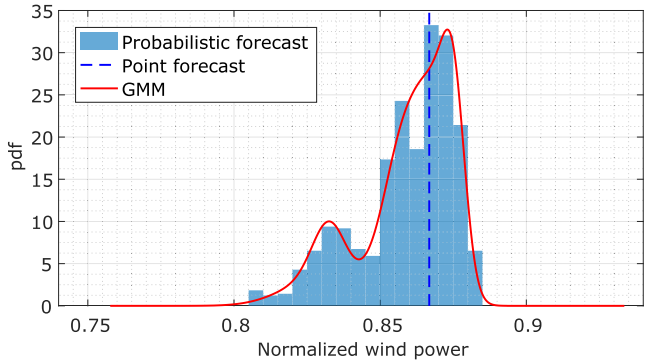

Fig. 3. Probabilistic forecast of wind power from one site at a given time with fitted GMM distribution.

4.3. Problem formulation

To find the optimal day-ahead dispatch and reserved capacity for each generator, we employ a Chance-Constrained DC-Optimal Power Flow (CC-DCOPF) model formulation, where forecast errors in wind power generation and transmission line ratings are treated as random variables. The associated probability density distributions are assumed to be known in advance by means of the probabilistic forecasting algorithm described in Section 3. The CC-DCOPF optimization problem is formulated as follows

$$\underset{\Xi}{\text{minimize}} \sum_{g\in\mathscr{G}} \left(c_g P_g + c_g^{\text{up}} R_g^{\text{up}} + c_g^{\text{dw}} R_g^{\text{dw}} \right) + \sum_{w\in\mathscr{W}} c^{\text{cut}} P_w^{\text{cut}} + \sum_{n\in\mathscr{N}} c^{\text{sh}} P_n^{\text{sh}} \tag{9a}$$

subject to

$$\sum_{g\in\mathscr{G}} P_g + \sum_{w\in\mathscr{W}} \left(\widehat{P}_w - P_w^{\text{cut}} \right) - \sum_{n\in\mathscr{N}} \left(P_n - P_n^{\text{sh}} \right) = 0, \tag{9b}$$

$$P_g + R_g^{\text{up}} \leqslant P_g^{\max} \;\forall\, g \in \mathscr{G}, \tag{9c}$$

$$P_g - R_g^{\text{dw}} \geqslant P_g^{\min} \;\forall\, g \in \mathscr{G}, \tag{9d}$$

$$\mathbb{P}\{S_{(\ell,\cdot)} P^{\text{inj}} \leqslant F_\ell^{\max}\} \geqslant 1 - \varepsilon_\ell \;\forall\, \ell \in \mathscr{L}, \tag{9e}$$

$$\mathbb{P}\{S_{(\ell,\cdot)} P^{\text{inj}} \geqslant -F_\ell^{\max}\} \geqslant 1 - \varepsilon_\ell \;\forall\, \ell \in \mathscr{L}, \tag{9f}$$

$$\mathbb{P}\{-\alpha_g \Delta P^{\text{tot}} \leqslant R_g^{\text{up}}\} \geqslant 1 - \varepsilon_g \;\forall\, g \in \mathscr{G}, \tag{9g}$$

$$\mathbb{P}\{-\alpha_g \Delta P^{\text{tot}} \geqslant -R_g^{\text{dw}}\} \geqslant 1 - \varepsilon_g \;\forall\, g \in \mathscr{G}, \tag{9h}$$

$$0 \leqslant P_w^{\text{cut}} \leqslant \widehat{P}_w \;\forall\, w \in \mathscr{W}, \tag{9i}$$

$$0 \leqslant P_n^{\text{sh}} \leqslant P_n \;\forall\, n \in \mathscr{N} \tag{9j}$$

$$P_g,\, R_g^{\text{up}},\, R_g^{\text{dw}} \geqslant 0 \;\forall\, g \in \mathscr{G} \tag{9k}$$

where $\Xi = \{P_g, R_g^{\text{up}}, R_g^{\text{dw}}, \forall\, g \in \mathscr{G}; P_w^{\text{cut}}, P_w^{\text{sh}}, \forall\, w \in \mathscr{W}\}$ is the set of optimization variables. Variable P_g denotes the scheduled power output for conventional generator g, whereas R_g^{up} and R_g^{dw} represent upward and downward reserve capacities, respectively, to be procured by the TSO. Additionally, wind curtailment P_w^{cut} and load shedding P_w^{sh} have been considered in order to guarantee feasibility at the day-ahead stage. These last variables should be considered as last-resort corrective actions that could be implemented in real-time operation.

The first term in the objective function (9a) represents the linear dispatch cost for generator g at the day-ahead market stage. The second and third terms account for the upward and downward reserve procurement cost, respectively. The equality constraint (9b) models the system day-ahead power balance based on expected value of wind power generation. Inequality constraints (9c) and (9d) impose the upper and lower bounds for active power generation considering both the scheduled generation and the activation of the reserves. Probabilistic constraints in (9e) and (9f) ensure that the power flow on line ℓ does not exceed the rating $F_\ell^{\max}$ with a probability greater than $1 - \varepsilon_\ell$. Among these constraints, those referring to lines that are dynamically rated have to be distinguished from those that are operated with conventional SLR. In the former case, the rating itself is considered as a random variable, whereas in the latter it is assumed to be fixed. This will lead to different reformulations, as detailed in the next section.

The vector notation is used to express the various power injections terms P^{inj} on a per-bus basis, whereas the scalar terms P_w^{tot} and $\widehat{P}_w^{\text{tot}}$ represent the total wind power production available in the system and its predicted value, respectively. The power injections P^{inj} at each bus are modelled as

$$P^{\text{inj}} = P_g - \boldsymbol{\alpha}\Delta P^{\text{tot}} + (P_w - P_w^{\text{cut}}) - (P_n - P_n^{\text{sh}}) \tag{10}$$

where it can be seen the dependence upon the total power imbalance $\Delta P^{\text{tot}} = P_w^{\text{tot}} - \widehat{P}_w^{\text{tot}}$. The linear decision rule coefficient per bus is defined as $\alpha_n = \sum_{g\in G_n} \alpha_g$ and indicates the share of imbalance that is compensated by the set of generators G_n at bus n, whereas the column vector $\boldsymbol{\alpha} = (\alpha_1, \ldots, \alpha_N)^\top$ collects together all α_n Other probabilistic constraints (9g) and (9h) guarantee that the upward or downward reserve procured by generator g is sufficient to cover the imbalance with a probability not lower than $1 - \varepsilon_g$. Hence, reserve requirements do not need to be specified ex-ante since they are endogenously optimized by the model. Constraints (9i) and (9j) limit the auxiliary variables so that wind curtailment and load shedding are bounded by wind availability and load level. Finally, constraints (9k) declare the remaining design variables to be non-negative.

5. Solution methodology

Chance constraints in optimization problem (9) are re-formulated into linear deterministic inequalities by adopting the method presented in [13], that is extended in order to treat overhead line ratings as additional random variables.

5.1. Power flow constraints

The proposed methodology is shown for the probabilistic power flow constraints on the ℓ-th line equipped with DLR (9e), assuming a positive power flow $F_\ell \geqslant 0$. The corresponding extensive form can be rearranged in (11)

$$\mathbb{P}\{F_\ell^{\max} + S_{(\ell,\cdot)}\boldsymbol{\alpha}\Delta P_w^{\text{tot}} - S_{(\ell,\cdot)}\Delta P_w \leqslant S_{(\ell,\cdot)}(P_g + \widehat{P}_w - P_w^{\text{cut}} - P_n + P_n^{\text{sh}})\} \leqslant \varepsilon_\ell \tag{11}$$

$$Y_\ell^+ = F_\ell^{\max} + S_{(\ell,\cdot)}\boldsymbol{\alpha}\Delta P_w^{\text{tot}} - S_{(\ell,\cdot)}\Delta P_w \tag{12}$$

$$\widehat{F}_\ell = S_{(\ell,\cdot)}(P_g + \widehat{P}_w - P_w^{\text{cut}} - P_n + P_n^{\text{sh}}) \tag{13}$$

Let the left hand side of the inner inequality of (11) be denoted Y_ℓ^+ and the right hand side $\widehat{F}_\ell$, as in (12) and (13), respectively. Notice that $\widehat{F}_\ell$ collects either decision variables of the original problem or quantities that are assumed to be known in advance, such as the wind power point forecasts. Also notice that $\widehat{F}_\ell$ represents the expected power flow on line ℓ, i.e., the value corresponding to the scenario in which no reserve is activated and wind power realizations assume the point forecast values. Variable Y_ℓ^+ instead consists of a linear summation of variables that have been considered random, i.e., line rating $F_\ell^{\max}$ and wind power forecast errors ΔP_w at various locations in the system. Constraints in the form of (11) can be reformulated to linear inequalities using the following relationships

$$\mathbb{P}\{Y_\ell^+ \leqslant \widehat{F}_\ell\} \leqslant \varepsilon_\ell \rightarrow \text{CDF}_{Y_\ell^+}(\widehat{F}_\ell) \leqslant \varepsilon_\ell \rightarrow \widehat{F}_\ell \leqslant \text{CDF}_{Y_\ell^+}^{-1}(\varepsilon_\ell). \tag{14}$$

The quantity $f_\ell^+ = \text{CDF}_{Y_\ell^+}^{-1}(\varepsilon_\ell)$ represents the upper bound for power

flow on line ℓ, which guarantees that any realization of wind power and DLR will not lead to a violation probability higher than ε_ℓ. Therefore, the challenge is to model the univariate random variable Y_ℓ^+ in order to calculate its inverse cumulative distribution function (CDF) at the desired confidence levels ε_ℓ. To achieve this goal, a new multivariate random variable X_ℓ is defined so that the target variable Y_ℓ^+ can be expressed as a linear combination of the elements of X_ℓ, as shown in (15)–(17), where $\Delta P_w = (\Delta P_{w,1}, ..., \Delta P_{w,N})^\top$ represents the wind power forecast errors per bus

$$Y_\ell^+ = a_\ell^\top X_\ell \tag{15}$$

$$X_\ell = (F_\ell^{\max}, \Delta P_{w,1}, ..., \Delta P_{w,N})^\top \tag{16}$$

$$a_\ell^\top = (1, -S_{(\ell,1)} + S_{(\ell,\cdot)}\boldsymbol{\alpha}, ..., -S_{(\ell,N)} + S_{(\ell,\cdot)}\boldsymbol{\alpha}). \tag{17}$$

Therefore, X_ℓ collects all the random variables that affect the stochastic line flow on the ℓ-th line and a_ℓ comprises a combination of fixed values that depend on the system topology and the chosen reserve policy. Similar coefficients a_ℓ and the corresponding value of f_ℓ^- can be derived for constraint (9f). For those lines that are not dynamically rated, the term $F_\ell^{\max}$ can be included in the right hand side of (11), thus not appearing in X_ℓ.

In order to capture the observed historical correlation between DLR and wind power production at various sites, their joint probability distribution is estimated with a Normal copula [23]. As discussed in [23], rank correlation is preferred over the common linear correlation matrix, which measures the degree of linear relationship between random variables. Rank correlation instead is found to be more appropriate to model stochastic dependence as it measures the similarities in the respective rankings. Spearman's correlation matrix is therefore adopted to model the correlation structure.

This step is preliminary to fitting a multivariate GMM to the joint probability density distribution. Fig. 4 shows an example of such multivariate GMM for a bivariate case with one line being dynamically rated and a single bus with wind power production. It can be noticed the high correlation between the two quantities, which in this way is accounted for in the solution of the CC-DCOPF. As discussed in [13], the use of GMM is preferred to copulas because of the linear invariance property of the former, which allows a straightforward manipulation of the PDF of X_ℓ, shown in (18), into the PDF of Y_ℓ^+ as shown in (19)

$$\mathrm{PDF}_{X_\ell}(x) = \sum_{m=1}^{M} \omega_m \left[N_m(x; \boldsymbol{\mu}_m, \boldsymbol{\Sigma}_m)\right] \tag{18}$$

$$\mathrm{PDF}_{Y_\ell^+}(y) = \sum_{m=1}^{M} \omega_m \left[N_m(y; a_\ell^\top \boldsymbol{\mu}_m, a_\ell^\top \boldsymbol{\Sigma}_m a_\ell)\right]. \tag{19}$$

Having the PDF of Y_ℓ^+, its inverse CDF is obtained numerically with a look-up-table, as opposed to the analytical way based on polynomial approximations described in [13].

The following methodology is adopted for reformulating all chance constraints in the original problem. This leads to various univariate random variables that model the stochastic part of each constraint. The term denoted $\Delta F_\ell = -S_{(\ell,\cdot)}\boldsymbol{\alpha}\Delta P_w^{\mathrm{tot}} + S_{(\ell,\cdot)}\Delta P_w$ expresses the power flow uncertainty on line ℓ due to nodal wind power injections and the generators' reserve activation in real time. This term can be used to express Y_ℓ^+ and Y_ℓ^- in (20) and (21), which are necessary to distinguish the two cases of bidirectional power flow, i.e., original constraints (9e) and (9f)

$$Y_\ell^+ = \begin{cases} F_\ell^{\max} - \Delta F_\ell & \forall\ \ell \in \mathscr{L}_{\mathrm{dlr}} \\ -\Delta F_\ell & \forall\ \ell \in \mathscr{L}_{\mathrm{slr}} \end{cases} \tag{20}$$

$$Y_\ell^- = \begin{cases} F_\ell^{\max} + \Delta F_\ell & \forall\ \ell \in \mathscr{L}_{\mathrm{dlr}} \\ \Delta F_\ell & \forall\ \ell \in \mathscr{L}_{\mathrm{slr}}. \end{cases} \tag{21}$$

For lines that are not equipped with DLR, the proposed methodology coincides with the one presented in [13], where the uncertain variables consist in non-Gaussian correlated wind power forecast errors ΔP_w. The quantities δ_ℓ^+ and δ_ℓ^- defined in (22) and (23), respectively, represent uncertainty margins to be introduced in the static line ratings in order to respect the risk aversion level requirements set by the TSO

$$\delta_\ell^+ = \mathrm{CDF}^{-1}_{Y_\ell^+}(\varepsilon_\ell) \quad \forall\ \ell \in \mathscr{L}_{\mathrm{slr}} \tag{22}$$

$$\delta_\ell^- = -\mathrm{CDF}^{-1}_{Y_\ell^-}(\varepsilon_\ell) \quad \forall\ \ell \in \mathscr{L}_{\mathrm{slr}}. \tag{23}$$

5.2. Reserve procurement constraints

A similar procedure is adopted to reformulate the probabilistic reserve procurement constraints (9g) and (9h), where the uncertain variable is the total power imbalance ΔP^{tot} due to forecasts errors. The associated univariate PDF is modelled with a GMM, whose mean $\mu_{w_m}^{\mathrm{tot}}$ and standard deviation $\sigma_{w_m}^{\mathrm{tot}}$ are derived for each component m as

$$\mu_{w_m}^{\mathrm{tot}} = \mathbb{1}^\top \boldsymbol{\mu}_{w_m} \quad m = 1, ..., M \tag{24}$$

$$\sigma_{w_m}^{\mathrm{tot}} = \sqrt{\mathbb{1}^\top \boldsymbol{\Sigma}_{w_m} \mathbb{1}} \quad m = 1, ..., M \tag{25}$$

where $\mathbb{1} \in \mathbb{R}^W$ is a vector of ones, $\boldsymbol{\mu}_{w_m}$ and $\boldsymbol{\Sigma}_{w_m}$ are the vector of mean values and the covariance matrix for the m-th component in the GMM, respectively. The inverse CDF of the total wind power forecast error is then used to reformulate the chance constraints. Upper and lower bounds for the probabilistic reserve procurement constraints are derived in (26) and (27), respectively

$$r_g^{\mathrm{up}} = \mathrm{CDF}^{-1}_{\Delta P_w^{\mathrm{tot}}}(\varepsilon_g) \quad \forall\ g \in \mathscr{G} \tag{26}$$

$$r_g^{\mathrm{dw}} = \mathrm{CDF}^{-1}_{\Delta P_w^{\mathrm{tot}}}\left(1 - \varepsilon_g\right) \quad \forall\ g \in \mathscr{G}. \tag{27}$$

5.3. Deterministic equivalent problem

The final optimization problem with re-formulated chance constraints is presented in (28)

$$\underset{\Xi}{\text{minimize}} \sum_{g\in\mathscr{G}} \left(c_g P_g + c_g^{\mathrm{up}} R_g^{\mathrm{up}} + c_g^{\mathrm{dw}} R_g^{\mathrm{dw}}\right) + \sum_{w\in\mathscr{W}} c^{\mathrm{cut}} P_w^{\mathrm{cut}} + \sum_{n\in\mathscr{N}} c^{\mathrm{sh}} P_n^{\mathrm{sh}} \tag{28a}$$

subject to

$$\sum_{g\in\mathscr{G}} P_g + \sum_{w\in\mathscr{W}} \left(\widehat{P}_w - P_w^{\mathrm{cut}}\right) - \sum_{n\in\mathscr{N}} \left(P_n - P_n^{\mathrm{sh}}\right) = 0, \tag{28b}$$

$$P_g + R_g^{\mathrm{up}} \leqslant P_g^{\max} \ \forall\ g \in \mathscr{G}, \tag{28c}$$

$$P_g - R_g^{\mathrm{dw}} \geqslant P_g^{\min} \ \forall\ g \in \mathscr{G}, \tag{28d}$$

$$-f_\ell^- \leqslant \widehat{F}_\ell \leqslant f_\ell^+ \ \forall\ \ell \in \mathscr{L}_{\mathrm{dlr}}, \tag{28e}$$

$$-F_\ell^{\max} + \delta_\ell^- \leqslant \widehat{F}_\ell \leqslant F_\ell^{\max} - \delta_\ell^+ \ \forall\ \ell \in \mathscr{L}_{\mathrm{slr}}, \tag{28f}$$

$$-R_g^{\mathrm{up}} \alpha_g^{-1} \leqslant r_g^{\mathrm{up}} \ \forall\ g \in \mathscr{G}, \tag{28g}$$

$$R_g^{\mathrm{dw}} \alpha_g^{-1} \geqslant r_g^{\mathrm{dw}} \ \forall\ g \in \mathscr{G}, \tag{28h}$$

$$0 \leqslant P_w^{\mathrm{cut}} \leqslant \widehat{P}_w \ \forall\ w \in \mathscr{W}, \tag{28i}$$

$$0 \leqslant P_n^{\mathrm{sh}} \leqslant P_n \ \forall\ n \in \mathscr{N}, \tag{28j}$$

$$P_g, R_g^{\mathrm{up}}, R_g^{\mathrm{dw}} \geqslant 0 \ \forall\ g \in \mathscr{G}, \tag{28k}$$

where the objective function and the decision variables remain the

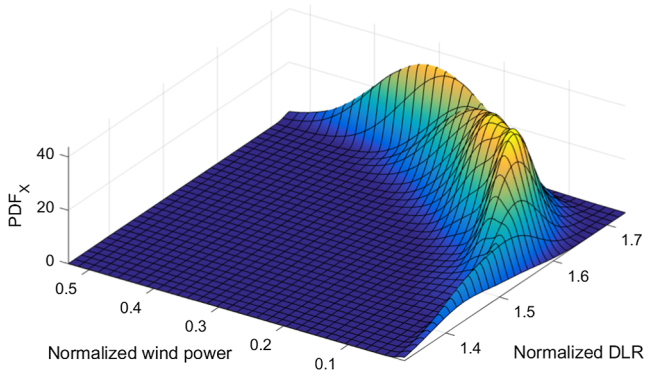

Fig. 4. Example of multivariate joint predictive probability density distribution of one line with DLR and one wind farm.

same of the original problem as well as constraints (28b)–(28d) and (28i)–(28k). Constraints in (28e) account for power flow limits on lines equipped with DLR considering positive and negative direction of the flow. The upper and lower bounds f_ℓ^+ and f_ℓ^- inherently account for the correlated uncertainty in wind power injections and line ratings. Similarly, (28f) limit the bidirectional power flow on lines with SLR, where the rating $F_\ell^{\max}$ is a parameter of the problem and not a random variable. Lastly, (28h) and (28i) are the reformulated chance constraints for the adequacy of the reserve procurement R_g^{up} and R_g^{dw}.

The values of the inverse CDFs are calculated with a look-up-table approach and they are passed on to the optimization problem as parameters. Therefore, the resulting optimization problem has linear objective function and linear constraints and can thus readily solved with existing solvers in a computationally efficient way. The optimization problem has been solved with the Matlab-based programming language CVX [24].

6. Case study

The proposed methodology is tested on a modified IEEE RTS 24-bus system [25], shown in Fig. 5, where selected transmission lines are dynamically rated on an hourly basis. The original rating of lines marked in red is reduced in order to stress the grid and introduce bottlenecks, as suggested in [25]. These lines are considered the candidates for DLR in order to verify the benefits of increased power flows in congested networks with a high share of renewable energy production from wind power. This paper focuses on a case where wind farms are located far from the main load centers. This condition is modelled by localizing wind power generation in the upper part of the system at buses 16, 21 and 23, while doubling the installed capacity. Additionally, the reference peak load demand in [25] has been increased by 10%. Overall, these assumptions are expected to further stress the grid as most of the load demand is located in the lower part of the system.

A 24-h dispatch period is considered using simulated weather data corresponding to the 30-01-2016. This time frame simulates a period with moderate to high wind speed (4 m/s to 13 m/s) and low ambient temperature (3 °C), thus offering the opportunity to study the effect of positive correlation between wind power production and DLR on a system level. The advantage of the proposed formulation is that it allows to compare the use of DLR with the traditional practice to set SLR, but keeping the same accepted risk of overload on the transmission system, i.e., typically 5%.

A total of 5 cases is considered in order to test the impact of correlation and the use of GMM on the final results:

1. *Deterministic*: this case serves only as a benchmark and it assumes that random variables take the corresponding point forecast values. This implies that no reserve is procured and that DLR is computed with expected values of weather variables.
2. *Normal without correlation*: Normal distributions are fitted to both wind power forecast errors and DLR marginals. No correlation is assumed neither between wind power from different sites nor between wind power and DLR. The correlation matrix ρ is therefore set to the identity matrix.
3. *Normal with correlation*: Wind power and DLR are modelled with normal distributions. Spatial correlations are taken into account in the joint probabilistic forecasts descried in Section 5.
4. *GMM without correlation*: Wind power and DLR are modelled with non-parametric distributions, as described in Section 3. Correlation matrix is set to the identity matrix.
5. *GMM with correlation*: Wind power and DLR marginal distributions are modelled with non-parametric distributions as well as the corresponding joint predictive distribution. Spatial correlation is included.

This set of cases highlights the impact of GMM vs Normal distributions with or without spatial correlation. Spearman's rank correlation matrix used in the simulations is

$$\rho = \begin{array}{c} \\ \ell 25 \\ \ell 22 \\ \ell 23 \\ \text{w21} \\ \text{w23} \\ \text{w16} \end{array} \begin{array}{c} \begin{array}{cccccc} \ell 25 & \ell 22 & \ell 23 & \text{w21} & \text{w23} & \text{w16} \end{array} \\ \left(\begin{array}{cccccc} 1 & 0.80 & 0.81 & 0.76 & 0.67 & 0.61 \\ 0.80 & 1 & 0.71 & 0.64 & 0.74 & 0.58 \\ 0.81 & 0.71 & 1 & 0.66 & 0.62 & 0.70 \\ 0.76 & 0.64 & 0.66 & 1 & 0.84 & 0.79 \\ 0.67 & 0.74 & 0.62 & 0.84 & 1 & 0.77 \\ 0.61 & 0.58 & 0.70 & 0.79 & 0.77 & 1 \end{array}\right) \end{array} \quad (29)$$

where the upper-left block contains the correlation between DLR of different lines, namely lines 25, 22 and 23, whereas the lower-right corresponds to the correlation matrix of wind power at buses 21, 23 and 16. The off-diagonal block matrices express the correlation between DLR and wind power at various sites. Matrix (29) is based on simulated historical weather data from the Danish power system, which are derived in [16].

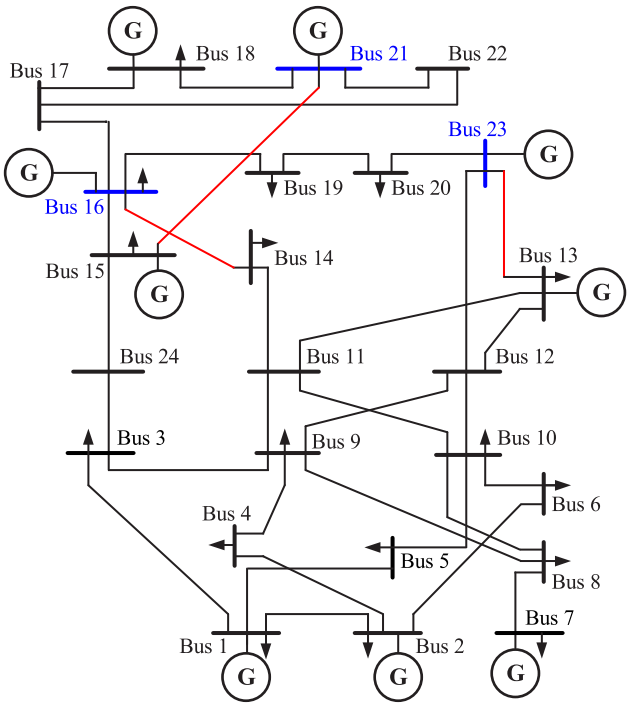

Fig. 5. IEEE RTS 24-bus test system where lines equipped with DLR are marked in red and the bus with wind power generation in blue. (For interpretation of the references to colour in this figure legend, the reader is referred to the web version of this article.)

The robustness of each solution is tested by counting the number of violations of each chance constraint in (9), following a realization of the uncertainty. A high number of samples, $N_s = 10^4$, is generated from the joint predictive distribution formed with the marginals of all the uncertain variables, i.e., wind farms and DLR. Wind power and line rating realizations are then substituted in the corresponding constraints together with the solutions of (28) for each tested case. While different cases assume different distributions of the uncertainty, the realizations are always generated from the same multivariate distribution that is modelled with GMM and it considers spatial correlation. This procedure allows to capture the realization of correlated random variables and their impact on constraint violations.

7. Numerical results

This section presents the resulting violation probabilities of each group of chance constraints. The influence of DLR on the energy dispatch and reserve procurement problem is tested in 5 different cases and it is expressed in terms of total cost reductions over the considered period.

7.1. Reserve procurement

Probabilistic constraints on reserve procurement in the CC-DCOPF problem (9) depend on the total wind power realization. Table 1 and Table 2 present the violation probabilities from time step 15 to 19 of constraints (9g) and (9h), respectively.

The violation probability depends on the modelling assumption on wind power uncertainty. As expected, the deterministic model always violates either one of the two constraints as it does not account for any stochastic behavior. Constraints (9g) and (9h) are mutually exclusive, thus the sum of their violation probabilities indicates the total probability of violating reserve requirement.

Unlike other cases, modelling wind power uncertainty with GMM ensures that the actual violation probability is close to the sought risk level in either directions, i.e., 2%. The results obtained in this test are motivated with Fig. 6 that shows the histogram of wind power realizations for a given time step. The corresponding distributions that are assumed in the solution of the chance constraints are shown as well. Neglecting correlation in wind power generation causes the variance of the overall distribution to be underestimated. Therefore those cases that do not account for it largely violate the 2% limit.

Table 1
Upward reserve violation probabilities.

	Time step				
	t = 15	*t = 16*	*t = 17*	*t = 18*	*t = 19*
Determ.	43,8%	43,0%	44,1%	44,1%	43,3%
Norm. w/o corr.	11,4%	11,8%	10,7%	10,6%	11,2%
Norm. w/corr.	4,2%	4,0%	4,0%	4,5%	2,9%
GMM w/o corr.	9,6%	8,9%	9,3%	9,7%	10,5%
GMM w/corr.	2,1%	2,2%	1,9%	2,0%	1,9%

Table 2
Downward reserve violation probabilities.

	Time step				
	t = 15	*t = 16*	*t = 17*	*t = 18*	*t = 19*
Determ.	56,2%	57,1%	55,9%	55,9%	56,7%
Norm. w/o corr.	8,8%	9,5%	8,9%	9,5%	9,7%
Norm. w/corr.	0,2%	0,1%	0,2%	0,0%	1,1%
GMM w/o corr.	11,2%	11,5%	11,2%	11,1%	10,7%
GMM w/corr.	1,8%	2,1%	2,0%	1,8%	2,1%

As far as the use of the Normal distribution is concerned, it can be seen that due to the skewness of wind power realizations, upward and downward reserve requirements are over- and underestimated, respectively. Furthermore, the fitted normal distribution does not respect the limits on installed capacity as the tail crosses the line indicating the maximum.

7.2. Power flows

Table 3 and Table 4 report the violation probabilities for line 23 with SLR and DLR, respectively, as this line in particular is the mostly loaded in the CC-DCOPF solution. It stands out that the deterministic approach consistently violates the line ratings, whereas the use of GMM better approximates the chosen risk level of 5% when the power flow constraint is binding.

7.2.1. Lines with SLR

Fig. 7 shows the expected power flow on line 23, i.e., the value corresponding to wind power point forecasts at the day-ahead stage, as well as 20 power flow realizations in real time. For a given time step, the chosen rating for line ℓ is found by keeping a margin δ_ℓ from the SLR. The variability of the power flow on a line with SLR reflects the uncertainty in wind power generation across the system that is mapped to the line through the power transfer distribution matrix S. Therefore, violation probabilities in Table 3 are strongly related to how wind power uncertainty is modelled. Those cases that do not account for correlation clearly result in more violations. Underestimating the variance of the power flow leads to a smaller uncertainty margin δ, thus the expected power flow is closer to the rating of the line and violations in real time are more likely to occur.

The Normal distribution is found to either under- or overestimate the power flow depending on the skewness of the associated distribution. Negative skewness in the actual power flow distribution lead to an overestimated margin from the actual rating and viceversa. As far as line 23 is concerned, violation probability is close to 5% meaning that for this line the use of the normal distribution is a conservative approach. Any deviation from the 5% level has been attributed to approximations in the fitting of GMM.

7.2.2. Lines with DLR

For lines equipped with DLR, the uncertainty associated to the power flow constraints depends not only on wind power realizations, but on line rating realizations too. This aspect is taken into account by the chosen rating f_ℓ. The correlation between wind power and DLR plays an important role, as it allows to respect the desired violation probability, despite significant overlapping between the marginal distributions. Fig. 8 shows power flow and rating realizations on line 23 with DLR, whereas Fig. 9 shows the corresponding probability

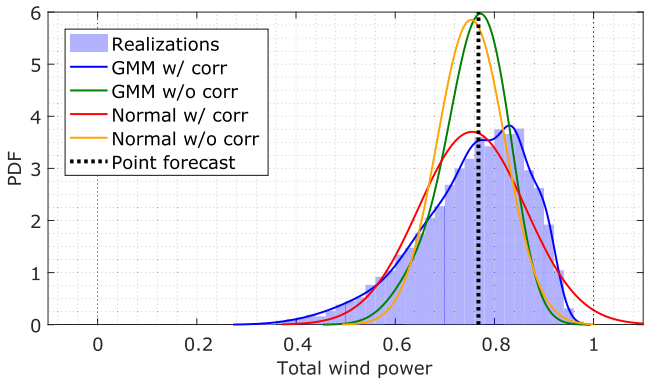

Fig. 6. Histogram of total wind power realizations for time step $t = 7$ with distributions used to reformulate chance constraints.

Table 3
Power flow limit violation probability for line 23 with SLR.

	Time step				
	t = 15	*t = 16*	*t = 17*	*t = 18*	*t = 19*
Determ.	55,7%	57,4%	55,8%	56,3%	56,4%
Norm. w/o corr.	8,1%	9,1%	8,6%	8,7%	9,7%
Norm. w/corr.	2,3%	2,4%	2,4%	1,4%	4,9%
GMM w/o corr.	9,8%	11,1%	10,6%	10,4%	10,7%
GMM w/corr.	4,6%	5,0%	5,3%	4,5%	5,0%

Table 4
Power flow limit violation probability for line 23 with DLR. Value in brackets when not binding.

	Time step				
	t = 15	*t = 16*	*t = 17*	*t = 18*	*t = 19*
Determ.	36,7%	62,6%	59,1%	58,8%	51,2%
Norm. w/o corr.	1,2%	1,0%	1,4%	1,3%	1,7%
Norm. w/corr.	(0,2)%	(0,8)%	7,0%	8,0%	(2,1)%
GMM w/o corr.	0,6%	0,6%	0,8%	0,7%	0,8%
GMM w/corr.	(0,6)%	(2,4)%	5,3%	4,8%	(2,2)%

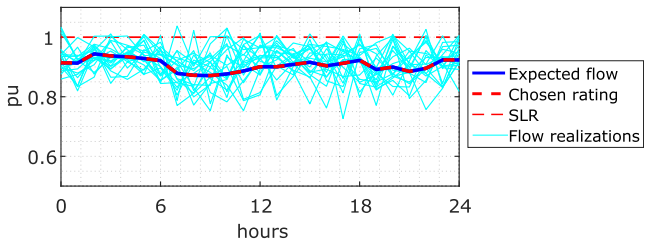

Fig. 7. Power flow on line 23 with SLR. Random variables are modelled by means of GMM w/correlation.

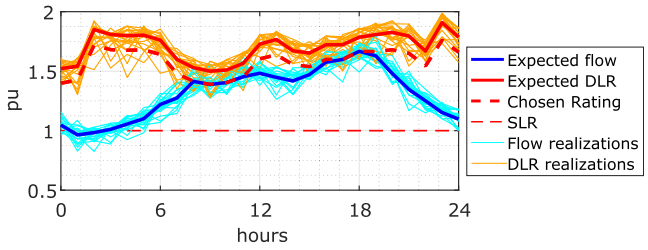

Fig. 8. Power flow on line 23 with DLR. Random variables are modelled by means of GMM w/correlation.

distributions. If correlation is not taken into account, marginal distributions of power flow and line rating do not overlap as much. This condition is necessary to fulfill the chosen risk level when realizations are assumed to be independent. Consequently, when correlated samples of wind power and DLR are generated, the violation probabilities are well below 5%, as reported in Table 4.

As described in Section 3, the Normal distribution overestimates the minimum rating of lines with DLR. This aspect is reflected in the violation probabilities at time $t = 17$ and $t = 18$, when the power flow constraint is binding. The violation probability reaches a value of 8% which exceeds the 5% level set in the optimization problem.

Overall, the proposed methodology based on GMM allows to exploit the correlation between line rating and wind power for a desired risk

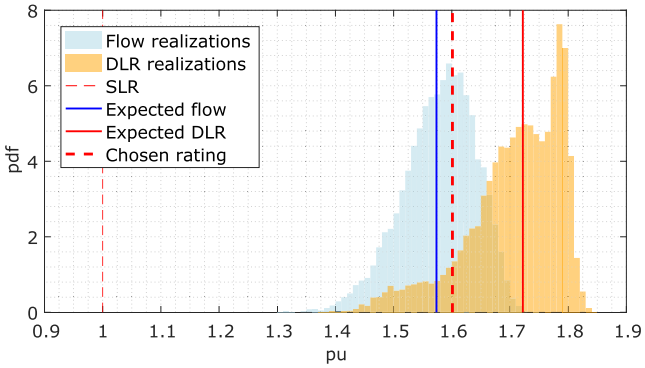

Fig. 9. Power flow and rating distribution on line 23 with DLR at t = 16. Random variables are modelled by means of GMM with correlation.

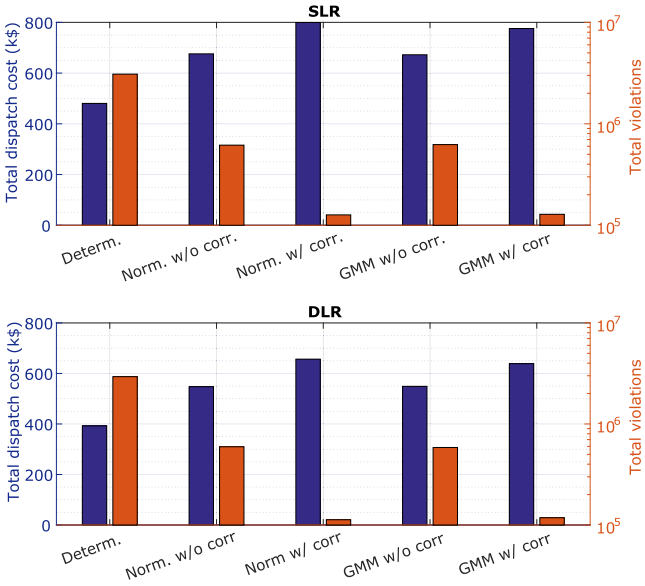

Fig. 10. Total dispatch cost and total number of constraint violations with SLR and DLR.

aversion level. Depending on weather conditions, power flows with DLR can be significantly higher as opposed to SLR, thus unlocking extra transmission capacity. Line 23 reaches the maximum expected loading $\widehat{F}_{23}$ of 1.66 times the static line thermal rating.

7.3. Costs

Fig. 10 highlights the trade-off between total costs and overall number of constraint violations. The solution to the deterministic problem provides the cheapest solution, as it does not account for reserve, but constraints would be violated following the realizations of wind power and line ratings. It is also found that regardless of the assumption on the shape of the distribution, modelling total wind power uncertainty without accounting for correlation leads to underestimate the variance of the corresponding distribution and thus the reserve requirements. This also motivates the high number of total violations in those cases that do not account for correlation, despite the lower violation probabilities of power flow constraints. The most conservative solution would be to consider correlation between wind power, but not between wind power and DLR. As far as the use of GMM is concerned, Fig. 10 suggests that the difference in terms of cost and total number of violations is negligible. However, it has been shown that assuming normally distributed DLR leads to underestimate the actual line rating, thus leading to higher violation probabilities when power flow

Table 5
Comparison of total costs with SLR or DLR modelled by means of GMM with correlation.

	SLR	DLR	
	(k$)	(k$)	Δ
Day-ahead dispatch	512,6	425,6	−17,0%
Upward reserve	114,1	110,6	−3,1%
Downward reserve	62,6	63,8	+1,9%
Wind curtailment	86,4	38,8	−55,1%
Load shedding	0	0	0%
Total	775,7	638,8	−17,6%

constraints are binding.

Table 5 compares the costs obtained by solving the CC-DCOPF with or without DLR on selected transmission lines. The relative change in percentage is indicated with Δ. These results refer to the case where the uncertainty is modelled by means of GMM while accounting for correlation. DLR considerably reduces the amount of curtailed wind power, which in turn lowers the day-ahead dispatch cost. The reduction of wind power curtailments is of special interest for TSOs that needs to integrate large amount of renewable energy sources into existing power systems. Reserves requirements are only marginally affected by DLR due to the *a priori* reserve policy scheme with fixed participation factors α_g. Overall, the use of DLR on 3 lines yields a total cost reduction of 17,6%.

8. Conclusion

This paper presented a novel methodological approach based on CC-DCOPF, which allows to integrate non-parametric probabilistic forecasts of DLR and wind power generation into an energy dispatch and reserve procurement problem. Both marginal and joint predictive distributions of DLR and wind power have been modelled with GMMs, by means of which it possible to account for their correlated and non-parametric nature. Individual chance constraints with separable structure are then reformulated into linear inequalities so that the original optimization problem can be readily solved with existing solvers. The proposed methodology has been tested on a modified IEEE RTS 24-bus system, highlighting the effectiveness of considering the positive correlation between DLR and wind power in terms of increased power flows. Furthermore, the use of GMMs has been compared to the assumption of normally distributed uncertainty. Due to the negative skewness in the line rating probabilistic forecast, the assumption of normality leads to increased violation probability of the power flow constraints with DLR, whenever these are binding. Overall, the extra transmission capacity unlocked by DLR reduces the total dispatch costs for the day-ahead market, whereas reserve costs have been only marginally affected due to the fixed balancing scheme. The results presented indicate that the use of DLR in a wind-dominated and highly congested network has the potential to reduce wind power curtailment considerably.

Although DLR proved to increase the power flow significantly, a more accurate representation of power system dynamics is required in order to precisely quantify the benefits for TSOs. These include the use of full AC power flow equations, ramping capabilities of generators and other components in the power system.

Future work will address these issues, as well as the synergy of DLR with different reserve allocation policies.

Declaration of Competing Interest

The authors declare that they have no known competing financial interests or personal relationships that could have appeared to influence the work reported in this paper.

Acknowledgement

Authors would like to thank Rasmus A. Olsen and Anders S. Kristensen from the Danish TSO, Energinet, for supervision and sharing of data on the transmission system.

References

[1] Cigré Working Group B2.43. Guide for thermal rating calculations of overhead lines. International Council on Large Electric Systems, T.B. 601; Dec. 2014.
[2] Teng F, Dupin R, Michiorri A, Kariniotakis G, Chen Y, Strbac G. Understanding the benefits of dynamic line rating under multiple sources of uncertainty. IEEE Trans Power Syst 2018;33(3):3306–14.
[3] Fang Duo, Zou Mingzhe, Coletta Guido, Vaccaro Alfredo, Djokic Sasa Z. Handling uncertainties with affine arithmetic and probabilistic OPF for increased utilisation of overhead transmission lines. Electric Power Syst Res 2019;170:364–77.
[4] Nick M, Alizadeh-Mousavi O, Cherkaoui R, Paolone M. Security constrained unit commitment with dynamic thermal line rating. IEEE Trans Power Syst 2016;31(3):2014–25.
[5] Shi J, Oren SS. Flexible line ratings in stochastic unit commitment for power systems with large-scale renewable generation. In: Energy systems, https://doi.org/10.1007/s12667-018-0306-8.
[6] Bucher MA, Andersson G. Robust corrective control measures in power systems with dynamic line rating. IEEE Trans Power Syst 2016;31(3):2034–43.
[7] Wang C, Gao R, Qiu F, Wang J, Xin L. Risk-based distributionally robust optimal power flow with dynamic line rating. IEEE Trans Power Syst 2018;33(6):6074–86.
[8] Dupin R, Michiorri A, Kariniotakis G. Optimal dynamic line rating forecasts selection based on ampacity probabilistic forecasting and network operators' risk aversion. In: IEEE transactions on power systems. https://doi.org/10.1109/TPWRS.2018.2889973.
[9] Bucher MA, Vrakopoulou M, Andersson G. Probabilistic N-1 security assessment incorporating dynamic line ratings. 2013 IEEE PES general meeting, Vancouver, BC. 2013. p. 1–5.
[10] van Ackooij W, Malick J. Eventual convexity of probability constraints with elliptical distributions. MathProgram 2019;175:1–2.
[11] Zhan J, Chung CY, Demeter E. Time series modeling for dynamic thermal rating of overhead lines. IEEE Trans Power Syst 2017;32(3):2172–82.
[12] Aznarte JL, Siebert N. Dynamic line rating using numerical weather predictions and machine learning: a case study. IEEE Trans Power Deliv 2017;32(1):335–43.
[13] Wang Z, Shen C, Liu F, Wu X, Liu C, Gao F. Chance-constrained economic dispatch with non-gaussian correlated wind power uncertainty. IEEE Trans Power Syst 2017;32(6):4880–93.
[14] Viafora N, Møller JG, Olsen RA, Kristensen AS, Holbøll J. Historical data analysis for extending dynamic line ratings across power transmission systems. In: 2018 International conference on probabilistic methods applied to power system (PMAPS), Boise; 2018.
[15] Rodriguez Alvarez J, Franck CM. Radial thermal conductivity of all-aluminum alloy conductors. IEEE Trans Power Deliv 2015;30(4):1983–90.
[16] Hahmann A, Vincent C, Peña A, Lange J, Hasager C. Wind climate estimation using WRF model output: method and model sensitivities over the sea. Int J Climatol 2015;35:3422–39.
[17] Koenker R, Bassett G. Regression quantiles. Econometrica 1978.
[18] Cui M, Wang Z, Feng C, Zhang J. A truncated Gaussian mixture model for distributions of wind power ramping features. 2017 IEEE power & energy society general meeting, Chicago, IL. 2017. p. 1–5.
[19] Cui M, Feng C, Wang Z, Zhang J. Statistical representation of wind power ramps using a generalized gaussian mixture model. IEEE Trans Sustain Energy 2018;9(1):261–72.
[20] Singh R, Pal BC, Jabr RA. Statistical representation of distribution system loads using gaussian mixture model. IEEE Trans Power Syst 2010;25(1):29–37.
[21] Christie RD, Wollenberg BF, Wangensteen I. Transmission management in the deregulated environment. Proc IEEE 2000;88(2):170–95.
[22] Roald L, Krause T, Andersson G. Integrated balancing and congestion management under forecast uncertainty. 2016 IEEE international energy conference (ENERGYCON), Leuven. 2016. p. 1–6.
[23] Papaefthymiou G, Kurowicka D. Using copulas for modeling stochastic dependence in power system uncertainty analysis. IEEE Trans Power Syst 2009;24(1):40–9.
[24] Michael Grant and Stephen Boyd. CVX: Matlab software for disciplined convex programming, version 2.0 beta. http://cvxr.com/cvx, Sept. 2013.
[25] Ordoudis C, Pinson P, Morales González JM, Zugno M. An updated version of the IEEE RTS 24-Bus system for electricity market and power system operation studies. Technical University of Denmark; 2016.

[Pub. E]

Notes

Submitted for publication at IEEE Transaction on Power Systems on 20th March 2020.

Dynamic Reserve and Transmission Capacity Allocation in Wind-Dominated Power Systems

Nicola Viafora, *Student Member, IEEE,* Stefanos Delikaraoglou, *Member, IEEE,* Pierre Pinson, *Fellow, IEEE,* Gabriela Hug, *Senior Member, IEEE,* Joachim Holbøll, *Senior Member, IEEE*

***Abstract*—The large shares of wind power generation in electricity markets motivate higher levels of operating reserves. However, current reserve sizing practices fail to account for important topological aspects that might hinder their deployment, thus resulting in high operating costs. Zonal reserve procurement mitigates such inefficiencies, however, the way the zones are defined is still open to interpretation. This paper challenges the efficiency of predetermined zonal setups that neglect the location of stochastic power production in the system, as well as the availability, cost and accessibility of flexible generating units. To this end, we propose a novel reserve procurement approach, formulated as a two-stage stochastic bilevel model, in which the upper level identifies a number of contiguous reserve zones using dynamic grid partitioning and sets zonal requirements based on the total expected operating costs. Using two standard IEEE reliability test cases, we show how the efficient partitioning of reserve zones can reduce expected system cost and promote the integration of stochastic renewables.**

***Index Terms*—Zonal reserve requirements, bilevel optimization, stochastic programming, grid partitioning, transmission capacity allocation.**

NOMENCLATURE

A. Sets and Indices

$n \in \mathcal{N}$	Set of nodes.
$\ell \in \mathcal{L}$	Set of transmission lines.
$g \in \mathcal{G}$	Set of conventional generators.
$j \in \mathcal{J}$	Set of wind power generators.
$z \in \mathcal{Z}$	Set of partitions.
$s \in \mathcal{S}$	Set of scenarios.

B. Parameters

$\overline{P}_g, \underline{P}_g$	Max/min generator's output.
F_ℓ	Line rating.
R_g^+, R_g^-	Up/down reserve capacity offer.
Λ^+, Λ^-	Up/down deterministic reserve requirement.
$C_g, C_g^{+/-}$	Generation and up/down reserve cost.
$C^{\text{sh}}, C^{\text{ct}}$	Load shedding and wind curtailment cost.
$\boldsymbol{H}$	Incidence matrices.
$\boldsymbol{M}$	Power transfer distribution factor matrix.
$D_n, \boldsymbol{D}$	Nodal load demand.
π_s	Probability of scenario.
$\widehat{W}_j, W_{j,s}$	Wind power point forecast and realization.

C. Decision variables

$x_{n,z}$	Binary variable for grid partitioning.
y_z	Number of nodes per zone.
$\varphi_{\ell,z}$	Flowing units on line ℓ in zone z for expressing zone connectivity.
$c_{n,z}$	Root node selection.
$r_{g,z}^+, r_{g,z}^-$	Up/down procured reserve.
λ_z^+, λ_z^-	Up/down zonal reserve requirement.
$\widehat{f}_\ell, f_{\ell,s}$	Expected power flow and realization in scen. s.
$p_g, \boldsymbol{p}$	Day-ahead dispatch of conventional generators.
$p_{g,s}^+, p_{g,s}^-$	Up/down reserve deployment per scenario.
$w_j, w_{j,s}^{\text{ct}}$	Scheduled and curtailed wind power.
$d_{n,s}^{\text{sh}}$	Nodal load shedding per scenario.
$w_{j,s}^{\text{ct}}$	Wind power curtailment per scenario.
Γ_ℓ	Capacity allocation margin at day-ahead market.

I. INTRODUCTION

Several studies indicate that high shares of wind power generation require significantly more operating reserves to accommodate the uncertainty and the variability arising from forecast errors and inherent fluctuations in the wind regime [1]. However, simply increasing the reserve capacity requirements does not guarantee that the system will have access to sufficient flexible resources during real-time operation, since the existing reserve capacity market is myopic about the grid topology limitations. As a result, in cases when operating reserves cannot be delivered due to network congestions, system operators have to resort to more expensive corrective actions, such as wind curtailment and load shedding.

An implicit way to account for network limitations during the reserve procurement process is to consider a zonal representation of the system. This approximation allows system operators to differentiate zonal reserve requirements based on expected congestion patterns and the location of stochastic power production. Nevertheless, the effectiveness of this approach is limited by the ability to define and update zone boundaries based on the operating conditions. Despite being an approximation of the true network topology, this zonal splitting approach is readily compatible with the current market structure and allows to convey to the reserve market more complete information about the balancing needs of the system at specific locations. This is a fundamental property of the more advanced energy and reserves co-optimization models based on two-stage stochastic programming [2], which however comes at the expense of violating the cost recovery and revenue adequacy properties for some uncertainty realizations [3].

This latter consideration has motivated several studies to use a stochastic bilevel programming approach that preserves the existing market structure and its desirable economic properties not only in expectation, but for every uncertainty outcome. Authors in [3] adopt this framework for optimally dispatching wind power in an energy-only market, whereas authors in [4] employ an analogous approach to define the optimal reserve

requirements in view of wind power uncertainty. In a similar vein, [5] extends this model to account for the allocation of cross-border transmission capacity between energy and reserves. Although these models have shown to improve the total expected cost in a sequential market-clearing architecture, they still lack the ability to optimally position reserves in the system, as the ideal stochastic model does. This stems from the merit-order principle enforced by the existing market design, which restricts the procurement of reserves from the cheapest generators, regardless of their location in the system.

The aforementioned studies considered either a single zone or a predefined zonal setup for the reserve procurement. This paper proposes a novel Zonal Preemptive methodology, where not only zonal reserve requirements are defined, but the zone boundaries themselves are considered as decision variables. The goal is to improve the positioning of reserves in the system, while remaining compatible with the current market structure. In this work, we build upon [4] and [5] and we embed grid partitioning algorithms in the stochastic bilevel problem in order to identify a number of zonal reserve markets to be cleared independently. Grid partitioning algorithms have been used already in power system research for intentional islanding studies in [6]-[7]. However, to the best of our knowledge, this is the first attempt to rely on them for setting zonal reserve requirements. The proposed approach can be used as a decision-support tool for the grid operators for the redefinition of reserve zones based on the location of stochastic power production, cost and expected accessibility of flexible generators' reserve capacity.

While zonal reserve allocation is not a novel concept, the way the zones are defined is still open to interpretation. Existing studies base the partitioning of the system on heuristic methods that consider: active and reactive power flow sensitivities [8]; data-driven clustering techniques [9]; weighted power transfer distribution factors (PTDFs) [10]; reserve market clearing prices [11] or simply use pre-defined partitions [12] that can be based on geographical boundaries or ownership. The proposed approach relies instead on a partitioning scheme that is solely driven by the total expected costs, thus without the need of any additional metric.

We extend our formulation to include the ability to exchange reserve between neighbouring zones as in [5]. Setting aside part of the transmission capacity for reserve accessibility has shown to lower the total operating costs [13]. However, as the zones are defined dynamically, so are the cross-zonal lines eligible for reserve sharing. The proposed methodology addresses this issue by adapting the grid partitioning constraints accordingly. Simulation results are showcased based on both IEEE RTS-24 and IEEE RTS-96 systems, where we benchmark our methodology against a sequential approach, the stochastic energy and reserve co-optimization and the stochastic bilevel with a single or predefined zones.

The remainder of the paper is organized as follows. Various reserve procurement and dispatch models are reviewed in Section II, the proposed model is explained in details in Section III whereas a solution methodology is presented in Section IV. Lastly, Section V elaborates on selected simulation results and Section VI draws final conclusions.

II. Reserve Procurement and Dispatch Models

We first provide the mathematical formulation of the existing European market design, based on the sequential clearing of the reserve capacity, day-ahead energy and balancing markets. We then provide a compact formulation of the stochastic energy and reserve co-optimization model, emphasizing its main differences compared to the sequential approach.

A. Sequential Approach

Let Λ^+ and Λ^- indicate the upward and downward reserve requirements. These are provided as exogenous parameters to the reserve market clearing algorithm that is formulated as

$$\min_{\Xi_{\mathrm{R}}} \quad \mathcal{C}_{\mathrm{R}} = \sum_{g\in\mathcal{G}} \left(C_g^+ r_g^+ + C_g^- r_g^-\right) \tag{1a}$$

$$\text{s.t.} \quad \sum_{g\in\mathcal{G}} r_g^+ \geq \Lambda^+, \quad \sum_{g\in\mathcal{G}} r_g^- \geq \Lambda^-, \tag{1b}$$

$$0 \leq r_g^+ \leq R_g^+, \quad 0 \leq r_g^- \leq R_g^-, \qquad \forall g \in \mathcal{G}, \tag{1c}$$

where $\Xi_{\mathrm{R}} = \{r_g^+, r_g^-, \forall g\}$ is the set of free variables, i.e., up- and downward reserve capacity procured from each generator. Constraints (1b) guarantee that the pre-determined reserve requirements Λ are met, whereas (1c) limit the amount of reserve that can be procured to generators' capacity offers.

Having reserve capacity procurement $r_g^{+,*}$ and $r_g^{-,*}$ from model (1) as fixed parameters, the optimal day-ahead energy schedule for conventional p_g and stochastic w_j generators is obtained solving the following problem

$$\min_{\Xi_{\mathrm{D}}} \quad \mathcal{C}_{\mathrm{D}} = \sum_{g\in\mathcal{G}} C_g p_g \tag{2a}$$

$$\text{s.t.} \quad \sum_{g\in\mathcal{G}} p_g + \sum_{j\in\mathcal{J}} w_j = \sum_{n\in\mathcal{N}} D_n, \tag{2b}$$

$$\underline{P}_g + r_g^{-,*} \leq p_g \leq \overline{P}_g - r_g^{+,*}, \qquad \forall g \in \mathcal{G}, \tag{2c}$$

$$0 \leq w_j \leq \widehat{W}_j, \qquad \forall j \in \mathcal{J}, \tag{2d}$$

$$\widehat{f}_\ell = \boldsymbol{M}_{(\ell,\cdot)} \left(\boldsymbol{H}_{\mathrm{G}}^\top \boldsymbol{p} + \boldsymbol{H}_{\mathrm{J}}^\top \boldsymbol{w} - \boldsymbol{D}\right), \qquad \forall \ell \in \mathcal{L}, \tag{2e}$$

$$-F_\ell \leq \widehat{f}_\ell \leq F_\ell, \qquad \forall \ell \in \mathcal{L} \tag{2f}$$

where $\Xi_{\mathrm{D}} = \{p_g, \forall g;\ w_j, \forall j\}$ collects the decision variables. The day-ahead power balance is enforced by constraint (2b), whereas the production of conventional units is bounded by the minimum and maximum generation limits and procured reserves in constraint (2c). Stochastic producers are assumed to be wind power generators only, whose dispatch is limited to the available point forecast $\widehat{W}_j$ in constraint (2d). Employing a DC network approximation, power flows are modelled by (2e) using the PTDF matrix $\boldsymbol{M}$ and are in turn restricted by the corresponding transmission capacity limits in (2f). Appropriate incidence matrices $\boldsymbol{H}_{\mathrm{G}}$ and $\boldsymbol{H}_{\mathrm{J}}$ map conventional and stochastic generators to the respective buses in the system.

Approaching the hour of the delivery when wind power realization $W_{j,s'}$ is known, the balancing market is cleared using the following model to ensure that any deviation from the day-ahead schedule p_g^*, w_j^* is balanced by appropriate re-dispatch actions for the uncertainty realization $s = s'$.

$$\min_{\Xi_{\mathrm{B},s'}} \quad \mathcal{C}_{\mathrm{B},s'} = \sum_{g\in\mathcal{G}} C_g \left(p^{+}_{g,s'} - p^{-}_{g,s'}\right) + \sum_{j\in\mathcal{J}} C^{\mathrm{ct}} w^{\mathrm{ct}}_{j,s'} + \sum_{n\in\mathcal{N}} C^{\mathrm{sh}} d^{\mathrm{sh}}_{n,s'} \tag{3a}$$

s.t.

$$\sum_{g\in\mathcal{G}} \left(p^{+}_{g,s'} - p^{-}_{g,s'}\right) + \sum_{j\in\mathcal{J}} \left(\Delta W_{j,s'} - w^{\mathrm{ct}}_{j,s'}\right) + \sum_{n\in\mathcal{N}} d^{\mathrm{sh}}_{n,s'} = 0 \tag{3b}$$

$$0 \le p^{+}_{g,s'} \le r^{+,*}_{g}, \qquad \forall g \in \mathcal{G}, \tag{3c}$$

$$0 \le p^{-}_{g,s'} \le r^{-,*}_{g}, \qquad \forall g \in \mathcal{G}, \tag{3d}$$

$$0 \le d^{\mathrm{sh}}_{n,s'} \le D_n, \qquad \forall n \in \mathcal{N}, \tag{3e}$$

$$0 \le w^{\mathrm{ct}}_{j,s'} \le W_{j,s'}, \qquad \forall j \in \mathcal{J}, \tag{3f}$$

$$-F_\ell \le f_{\ell,s'} \le F_\ell, \qquad \forall \ell \in \mathcal{L}, \tag{3g}$$

$$f_{\ell,s'} = \boldsymbol{M}_{(\ell,\cdot)}\left[\boldsymbol{H}^{\top}_{\mathrm{G}}\left(\boldsymbol{p}^{*} + \boldsymbol{p}^{+}_{s'} - \boldsymbol{p}^{-}_{s'}\right) + \boldsymbol{H}^{\top}_{\mathrm{J}}\left(\boldsymbol{W}_{s'} - \boldsymbol{w}^{\mathrm{ct}}\right) - \left(\boldsymbol{D} - \boldsymbol{d}^{\mathrm{sh}}_{s'}\right)\right], \qquad \forall \ell \in \mathcal{L} \tag{3h}$$

where $\Xi_{\mathrm{B},s'} = \{p^{+}_{g,s'}, p^{-}_{g,s'}, \forall g;\ w^{\mathrm{ct}}_{j,s'}, \forall j;\ d^{\mathrm{sh}}_{n,s'}, \forall n\}$ is the set of decision variables and $\Delta W_{j,s'} = W_{j,s'} - w^{*}_{j}$ represents the system imbalance. The objective function (3a) includes a cost C_g for the activation of reserves from those generators that were cleared to provide reserves and have already received a capacity payment. Additionally, we assume that the grid operator has to face a cost C^{ct} and C^{sh} for wind power curtailment and load not supplied, respectively. Constraint (3b) is the real-time power balance, whereas constraints (3c)-(3d) limit the activation of reserve to the procured values in (1). The use of corrective actions is limited by constraints (3e)-(3f), which model load shedding and wind curtailment, respectively. Finally, (3g) enforce power flow limits, where real-time power flows in each scenario are modelled in (3h).

B. Stochastic Energy and Reserve Co-Optimization

An improved method based on two-stage stochastic programming allows the grid operator to jointly co-optimize reserve and energy. In this framework, the first stage models reserve as well as day-ahead energy scheduling, whereas the second stage corresponds to the balancing market under each considered realization of the uncertain variables. The two-stage stochastic problem is formulated as

$$\min_{\Xi_{\mathrm{S}}} \quad \mathcal{C}_{\mathrm{S}} = \mathcal{C}_{\mathrm{R}} + \mathcal{C}_{\mathrm{D}} + \sum_{s\in\mathcal{S}} \pi_s \mathcal{C}_{\mathrm{B},s} \tag{4a}$$

$$\text{s.t.} \quad \text{(1c)}, \quad \text{Reserve market}$$

$$\text{(2b)} - \text{(2e)}, \quad \text{Day-ahead market}$$

$$\text{(3b)} - \text{(3h)}, \quad \text{Balancing market}, \qquad \forall s \in \mathcal{S}$$

where $\Xi_{\mathrm{S}} = \{\Xi_{\mathrm{R}} \cup \Xi_{\mathrm{D}} \cup \Xi_{\mathrm{B},s}, \forall s\}$ is the set of decision variables. The stochastic co-optimization of energy and reserves attains perfect temporal coordination, as opposed to the sequential model that separates the day-ahead and balancing decisions. Each generator is pre-positioned even out of merit order in a way that allows optimal delivery to the system in case of deviations from the day-ahead schedule. For this reason, we use the stochastic co-optimization approach as a benchmark to our proposed methodology, since it provides a lower bound to the total operational costs.

III. Reserve and Capacity Allocation Models

This section introduces the concepts and the mathematical formulations that underpin the contributions of this work. The bilevel models in [4] and [5] are enhanced with a set of upper-level grid partitioning constraints described in III-A. These enable the operator to identify a pre-specified number of zones in the system, where zonal reserve markets can be cleared following the problem formulation in III-B.The model is complemented with a set of upper-level decision variables that account for the optimal allocation of transmission capacity between energy trading and re-dispatch actions in III-C. Lastly, the full problem formulation of the proposed Zonal Preemptive methodology is presented in III-D.

A. Grid Partitioning

Let $\Theta = (\mathcal{N}, \mathcal{L})$ be a directed graph with $\mathcal{N}$ nodes and $\mathcal{L}$ edges describing the single-phase equivalent topology of a power system. The partition of such a graph into $\mathcal{Z}$ connected sub-graphs or zones can be achieved by assigning as many binary variables $x_{n,z} \in \{0,1\}$ as the number of zones to each node. If node n belongs to zone z, then $x_{n,z} = 1$; otherwise $x_{n,z} = 0$. Three important properties need to be satisfied in order to get the desired partition: (1) the zones are mutually exclusive; (2) each node belongs to a zone; (3) the sub-graphs determined by the partition are connected, i.e., whichever two points are selected inside a zone, there always exists a path connecting them within the same zone. The first two properties are satisfied with

$$\sum_{z\in\mathcal{Z}} x_{n,z} = 1, \quad \forall n \in \mathcal{N}, \tag{5}$$

whereas, to achieve the third property, this paper adopts the single-commodity flow method presented in [6].This method relies on *flowing units*, which bear no physical meaning, but allow to express the connectivity as the ability to reach all nodes in a zone, while staying within its boundaries. This method works by injecting y_z units, i.e., as many as the number of nodes in the z-th zone, into a single arbitrary node of each sub-graph and enforcing

$$y_z = \sum_{n\in\mathcal{N}} x_{n,z}, \quad \underline{y}_z \le y_z \le \overline{y}_z, \qquad \forall z \in \mathcal{Z}, \tag{6}$$

where the quantity y_z can be bounded by $\underline{y}_z$ and $\overline{y}_z$ in order to require a minimum or a maximum size of each zone in the system, respectively. A sub-graph is then connected if all the injected units can flow to the nodes in that sub-graph, without violating nodal flow balance and branch flow limit constraints. Nodal flow balance is expressed in a matrix notation as

$$\boldsymbol{H}^{\top}_{(\cdot,n)}\boldsymbol{\varphi}_{(\cdot,z)} + c_{n,z}y_z = x_{n,z}, \quad \forall n \in \mathcal{N}, \quad \forall z \in \mathcal{Z}, \tag{7}$$

where $\boldsymbol{H}_{(\cdot,n)}$ indicates the n-th column of the branch incidence matrix, whose ℓ-th value is 1 if line ℓ enters node n, -1 if it leaves it, or 0 otherwise and $\boldsymbol{\varphi}_{(\cdot,z)}$ collects the flow of units injected in zone z over all branches in the system. Therefore, the scalar product $\boldsymbol{H}^{\top}_{(\cdot,n)}\boldsymbol{\varphi}_{(\cdot,z)}$ describes the net in- or out-coming flow of units to or from node n in zone z. The bilinear term $c_{n,z}y_z$ represents instead the injection of

y_z flow units into the root nodes defined by $c_{n,z}$, whereas the right-hand-side acts as a sink, i.e., if node n is included in zone z, it retains one unit.

Note that unlike [6], this novel version of the single-commodity flow method does not require the root nodes $c_{n,z}$ to be pre-specified. This requirement limits the degrees of freedom of the partitioning algorithm, as it relies on the choice of the initial nodes, from which the sub-graphs are generated. This last step is not necessary here, since $c_{n,z}$ is treated as a binary variable, which selects a node where the units are injected. The following constraints are added to ensure that the selected root nodes are mutually exclusive and that only one node per zone is selected as the root, i.e,

$$\sum_{z\in\mathcal{Z}} c_{n,z} \leq 1, \qquad \forall n \in \mathcal{N}, \tag{8}$$

$$\sum_{n\in\mathcal{N}} c_{n,z} = 1, \qquad \forall z \in \mathcal{Z}. \tag{9}$$

Finally, the branch flow limits are specifically defined to restrict the flow of units $\varphi_{\ell,z}$ to those lines that have both ends included in the same sub-graph. This aspect is modelled using the following constraints

$$-\Phi_{\mathrm{F}_{\ell,z}} \leq \varphi_{\ell,z} \leq \Phi_{\mathrm{F}_{\ell,z}}, \qquad \forall \ell \in \mathcal{L}, \quad \forall z \in \mathcal{Z}, \tag{10}$$

$$-\Phi_{\mathrm{T}_{\ell,z}} \leq \varphi_{\ell,z} \leq \Phi_{\mathrm{T}_{\ell,z}}, \qquad \forall \ell \in \mathcal{L}, \quad \forall z \in \mathcal{Z}, \tag{11}$$

$$\Phi_{\mathrm{F}_{\ell,z}} = y_z \left(\boldsymbol{H}_{\mathrm{F}_{(\ell,\cdot)}} \boldsymbol{x}_{(\cdot,z)}\right), \qquad \forall \ell \in \mathcal{L}, \quad \forall z \in \mathcal{Z}, \tag{12}$$

$$\Phi_{\mathrm{T}_{\ell,z}} = y_z \left(\boldsymbol{H}_{\mathrm{T}_{(\ell,\cdot)}} \boldsymbol{x}_{(\cdot,z)}\right), \qquad \forall \ell \in \mathcal{L}, \quad \forall z \in \mathcal{Z}. \tag{13}$$

where $\boldsymbol{H}_{\mathrm{F}}$ and $\boldsymbol{H}_{\mathrm{T}}$ indicate "from" and "to" incidence matrices, respectively. For any given sub-graph, the maximum flow of units on each branch is bounded both by $\Phi_{\mathrm{T}_{\ell,z}}$ and $\Phi_{\mathrm{F}_{\ell,z}}$, which are equal to the injected quantity y_z, if the line is fully within the sub-graph, or 0, otherwise. This condition is modelled with the scalar products $\boldsymbol{H}_{\mathrm{F}_{(\ell,\cdot)}}\boldsymbol{x}_{(\cdot,z)}$ and $\boldsymbol{H}_{\mathrm{T}_{(\ell,\cdot)}}\boldsymbol{x}_{(\cdot,z)}$, whose values are either 1, if the "from" or "to" node of line ℓ is included in zone z, or 0, if not. Therefore, the flow of units is prevented, unless both scalar products in (12)-(13) are equal to 1. In this case, $\varphi_{\ell,z}$ is limited by y_z, which always represents an upper bound to the highest possible flow of units.

To summarize, the grid partitioning requires the set of decision variables $\Xi_{\mathrm{G}} = \{x_{n,z}, c_{n,z}, \forall n, \forall z;\ y_z, \forall z;\ \varphi_{\ell,z}, \forall \ell, \forall z\}$ constrained by (5) - (13) in the upper-level problem of the proposed bilevel methodology. Section IV of the paper describes in detail the linearization of the bilinear terms that appear in constraints (7), (12) and (13) using the big-M approach [14].

B. Dynamic Reserve Procurement

The proposed methodology allows the grid operator to identify and clear $\mathcal{Z}$ independent reserve markets, each of them corresponding to a zone of the partition. Although the objective remains to minimize the total procurement cost of reserves, zonal requirements can be differentiated while respecting the merit order of generators that participate in each reserve market. The dynamic reserve procurement model constitutes one of the two lower-level problems in the bilevel structure of the proposed methodology and it is formulated as

$$\min_{\Xi_{\mathrm{R}_z}} \quad \mathcal{C}_{\mathrm{R},z} = \sum_{g\in\mathcal{G}} \left(C_g^+ r_g^+ + C_g^- r_g^-\right) \tag{14a}$$

s.t.

$$\sum_{g\in\mathcal{G}} r_{g,z}^+ \geq \lambda_z^+, \qquad \forall z \in \mathcal{Z}, \tag{14b}$$

$$\sum_{g\in\mathcal{G}} r_{g,z}^- \geq \lambda_z^-, \qquad \forall z \in \mathcal{Z}, \tag{14c}$$

$$0 \leq r_{g,z}^+ \leq R_g^+ \left(\boldsymbol{H}_{\mathrm{G}_{(g,\cdot)}} \boldsymbol{x}_{(\cdot,z)}\right), \qquad \forall z \in \mathcal{Z}, \quad \forall g \in \mathcal{G}, \tag{14d}$$

$$0 \leq r_{g,z}^- \leq R_g^- \left(\boldsymbol{H}_{\mathrm{G}_{(g,\cdot)}} \boldsymbol{x}_{(\cdot,z)}\right), \qquad \forall z \in \mathcal{Z}, \quad \forall g \in \mathcal{G}, \tag{14e}$$

$$r_g^+ = \sum_{z\in\mathcal{Z}} r_{g,z}^+, \qquad \forall g \in \mathcal{G}, \tag{14f}$$

$$r_g^- = \sum_{z\in\mathcal{Z}} r_{g,z}^-, \qquad \forall g \in \mathcal{G} \tag{14g}$$

where $\Xi_{\mathrm{R}_z} = \{r_{g,z}^+, r_{g,z}^-, \forall g, \forall z\}$ is the set of decision variables: $r_{g,z}^+$ and $r_{g,z}^-$ represent up- and downward reserve from generator g in zone z, respectively. Note that since $x_{n,z}$ is an upper-level variable, it enters (14) as a parameter, thus rendering the sub-problem a linear one. This structure allows to use the associated Karush-Kuhn-Tucker (KKT) conditions to reformulate the bilevel structure into a mathematical problem with equilibrium constraints (MPEC). The upward and downward zonal requirements λ_z^+ and λ_z^- imposed through (14b)-(14c) also enter this formulation as parameters, since they are upper-level decision variables. Zonal reserve requirements λ_z are fulfilled by generators that belong to the corresponding zones. The scalar product in (14d)-(14e) between $\boldsymbol{H}_{\mathrm{G}_{(g,\cdot)}}$ and $\boldsymbol{x}_{(\cdot,z)}$ indicates whether generator g is eligible for providing reserve to zone z. Finally, (14f)-(14g) define the overall reserve to be acquired from each generator.

C. Transmission Capacity Allocation

In cases when flexible resources are concentrated in a certain zone of the system, the grid operator could set aside part of the cross-zonal transmission capacity in order to facilitate the exchange of reserves. This aspect is modelled in the proposed formulation by means of an additional set of upper-level decision variables $\Xi_{\mathrm{C}} = \{h_{\ell,z}, \Gamma_{\ell,z}, \Gamma_{\ell}\}$, which defines the available capacity for energy trading on each cross-zonal line. Consider, for example, Fig. 1 where a 4-bus system is partitioned in two possible configurations. Note that as the

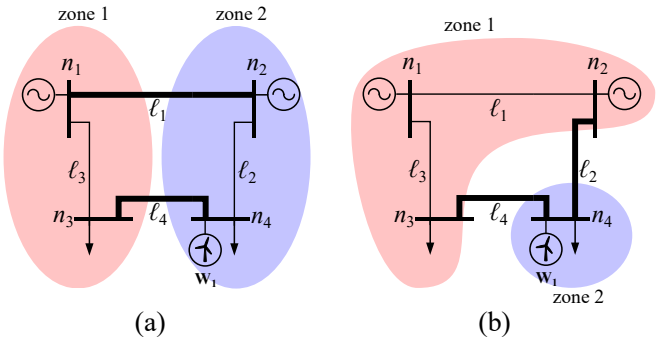

Fig. 1. Illustrative case of two possible configurations of grid partitioning on a 4-bus system. Thicker lines indicates cross-zonal interconnections.

zones are defined dynamically, so are the cross-zonal lines eligible for reserve exchange, i.e., lines ℓ_1 and ℓ_4 in Fig. 1(a) as opposed to lines ℓ_2 and ℓ_4 in Fig. 1(b). Therefore, the partitioning identifies endogenously the lines, whose capacity can be set aside for reserve exchange, through an auxiliary integer variable $h_{\ell,z}$, defined as the number of nodes that a line ℓ has in zone z according to the following expression

$$h_{\ell,z} = \boldsymbol{H}_{\mathrm{F}_{(\ell,\cdot)}} \boldsymbol{x}_{(\cdot,z)} + \boldsymbol{H}_{\mathrm{T}_{(\ell,\cdot)}} \boldsymbol{x}_{(\cdot,z)}, \quad \forall \ell \in \mathcal{L}, \forall z \in \mathcal{Z}. \tag{15}$$

The values that $h_{\ell,z}$ can take are: 0, 1 or 2 and they reflect all possible configurations between lines and zones. In the first case $h_{\ell,z} = 0$, the line is totally outside the considered zone, e.g., line ℓ_2 with respect to zone 1 in Fig. 1(a); in the second case $h_{\ell,z} = 1$, the line is cross-zonal because only one of the two nodes is included in a zone, e.g., line ℓ_1 in Fig. 1(a); in the third case, $h_{\ell,z} = 2$ indicates a line that is fully included in the considered zone, e.g., ℓ_1 in Fig. 1(b). Only when $h_{\ell,z} = 1$ a portion of the capacity of line ℓ is set aside, while the other cases identify domestic lines whose capacity is entirely allocated for energy trading in the day-ahead market. The following set of constraints limits the capacity allocation for reserve exchange $\Gamma_{\ell,z}$ to or from zone z on line ℓ,

$$\Gamma_{\ell,z} \leq \chi F_\ell \, h_{\ell,z}, \qquad \forall \ell \in \mathcal{L}, \quad \forall z \in \mathcal{Z}, \tag{16}$$

$$\Gamma_{\ell,z} \leq \chi F_\ell \, (2 - h_{\ell,z}), \qquad \forall \ell \in \mathcal{L}, \quad \forall z \in \mathcal{Z}, \tag{17}$$

where a predefined parameter χ is included in order to limit the maximum capacity that can be withdrawn from day-ahead market and F_ℓ indicates the line rating. When $h_{\ell,z}$ is either 0 or 2, one of the above constraints binds $\Gamma_{\ell,z}$ to be zero, thus preventing any capacity of that line to be set aside. In the remaining case, $h_{\ell,z} = 1$, both (16) and (17) state that the share of capacity can be up to the $\chi\%$ of the line rating. The remaining constraints include

$$0 \leq \Gamma_{\ell,z} \leq \Gamma_\ell, \qquad \forall \ell \in \mathcal{L}, \quad \forall z \in \mathcal{Z}, \tag{18}$$

$$\Gamma_\ell = \frac{1}{2} \sum_z \Gamma_{\ell,z}, \qquad \forall \ell \in \mathcal{L}, \tag{19}$$

that serve a twofold purpose. The first is to enforce non-negativity of $\Gamma_{\ell,z}$, the second is to define Γ_ℓ, which is used to define uniquely the value of capacity to be set aside on each line ℓ, regardless of the zone considered. Note how the use of $\frac{1}{2}$ prevents counting the line capacity twice in (19).

Therefore, with transmission capacity allocation day-ahead power flows are bounded by $F_\ell - \Gamma_\ell$, rather than F_ℓ. This limits the expected power flows at the day-ahead stage, in order to ensure that enough transmission capacity is available during real-time operation.

D. Zonal Preemptive Problem Formulation

The proposed methodology builds upon recent work that adopted a stochastic bilevel framework for setting reserve requirements [4]-[5]. While previous studies considered either a single zone or a predefined zonal setup, we improve the positioning and accessibility of reserves by defining zone boundaries together with their reserve requirements. The complete problem formulation, where both reserve and transmission capacity are dynamically allocated, is formulated as

$$\min_{\Xi_{\mathrm{M}_z}} \quad \mathcal{C}_{\mathrm{M}_z} = \mathcal{C}_{\mathrm{R}} + \mathcal{C}_{\mathrm{D}} + \sum_{s \in \mathcal{S}} \pi_s \, \mathcal{C}_{\mathrm{B},s} \tag{20a}$$

$$\text{s.t.} \quad (r_g^+, r_g^-) \in \arg \left\{ \begin{array}{l} \text{minimize} \quad \mathcal{C}_{R_z} \\ \Xi'_{\mathrm{R}_z} \\ \text{subject to} \\ \text{constraints (14b)} - \text{(14g)} \end{array} \right\}, \tag{20b}$$

$$(p_g, w_j) \in \arg \left\{ \begin{array}{l} \text{minimize} \quad \mathcal{C}_{\mathrm{D}} \\ \Xi'_D \\ \text{subject to} \\ \text{constraints (2b)} - \text{(2f)} \end{array} \right\}, \tag{20c}$$

$$\lambda_z^+ \geq 0, \quad \lambda_z^- \geq 0, \qquad \forall z \in \mathcal{Z}, \tag{20d}$$

$$\text{(3b)} - \text{(3h)}, \quad \text{Balancing market}, \qquad \forall s \in \mathcal{S},$$

$$\text{(5)} - \text{(13)}, \quad \text{Grid partitioning},$$

$$\text{(15)} - \text{(19)}, \quad \text{Capacity allocation},$$

where $\Xi_{\mathrm{M}_z} = \{\lambda_z^+, \lambda_z^-, \forall z \cup \Xi_{\mathrm{R}} \cup \Xi_{\mathrm{D}} \cup \Xi_{\mathrm{B,s}}, \forall s \cup \Xi_{\mathrm{G}} \cup \Xi_{\mathrm{C}}\}$ is the set of upper-level decision variables. This comprises: zonal reserve requirements λ_z; reserve, day-ahead and balancing market decision variables, which are constrained by the corresponding lower level problems; grid partitioning and transmission capacity allocation variables Ξ_{G} and Ξ_{C}, respectively. Lower-level problem (20b) accounts for the dynamic reserve allocation strategy described in III-B, whereas (20c) is the same day-ahead market clearing model as in model (2) where line ratings F_ℓ are substituted with $(F_\ell - \Gamma_\ell)$.

The solution of (20) provides the grid operator with a suggestion of how to split the system into a pre-defined number of zones, where reserve markets could be cleared independently of one another, thus remaining fully compatible with the least-cost merit-order principle in each zonal reserve market. Therefore, unlike the preemptive model in [4], it additionally allows to identify those portions of the grid where reserve is required the most and it sets different reserve requirements λ_z, accordingly. This latter property resembles the ability of the purely stochastic model to preposition reserves anywhere in the system down to a generator-specific resolution. However, since such a degree of freedom cannot be attained in practice, the proposed formulation circumvents this aspect by enforcing a minimal zonal size.

IV. Solution Approach

All bilinear terms that appear in the grid partitioning constraints can be expressed as a product between a binary and an integer variable, i.e., $y_z \left(\boldsymbol{H}_{\mathrm{F}_{(\ell,\cdot)}} \boldsymbol{x}_{(\cdot,z)}\right)$, $y_z \left(\boldsymbol{H}_{\mathrm{T}_{(\ell,\cdot)}} \boldsymbol{x}_{(\cdot,z)}\right)$ and $c_{n,z} y_z$. The linearization of these terms is illustrated for the latter case, by introducing an auxiliary variable $u_{n,z}$ that replaces the product $c_{n,z} y_z$ in (7) according to the Big-M approach [14]. The following constraints are added

$$y_z - M\,(1 - c_{n,z}) \leq u_{n,z} \leq y_z - m\,(1 - c_{n,z}) \tag{21}$$

$$m \cdot c_{n,z} \leq u_{n,z} \leq M \cdot c_{n,z} \tag{22}$$

where $m = 1$ and $M = \mathcal{N}$, i.e., the number of nodes in the system. Note that the specific values of m and M are used for all the bilinear terms that appear in the grid partitioning constraints. These values are straightforward to derive: each

bilinear term is either 0 or equal to the sub-graph cardinality y_z, thus 1 and N always represent valid bounds.

For any feasible partition of the system defined by the upper level variables, each lower level problem is linear and convex. Thus, the bilevel problem is reformulated as an MPEC, where each lower-level problem is replaced by the corresponding KKT conditions. This step introduces additional auxiliary binary variables in order to linearize the complementarity slackness constraints in the KKT conditions. The MPEC problem is then recast as a single-level mixed-integer linear problem (MILP) by using the Big-M method. This solution approach is typically used in power systems research, although authors of [15] recently pointed out some critical limitations. Finally, considering the special structure of the problem, whose second-stage constraints are independent per scenario, a multi-cut Bender's decomposition scheme is implemented [16]. The complete set of KKT conditions of the lower-level problems, along with the formulations of the Bender's master problem and sub-problems, are provided in the electronic companion of the paper.

V. Results

A. Wind Power Scenarios

In this paper, probabilistic forecast errors of wind power generation are assumed to follow a Beta distribution, whose parameters are calculated according to [17] and the error variance follows a quadratic function of the *per unit* point forecast. The spatial correlation structure in wind power generation at different locations is modelled by means of a Gaussian copula function with a rank correlation matrix based on actual wind power realizations from the Danish system [18]. A large number of scenarios is then generated by sampling the resulting multivariate joint probabilistic forecast for a single time-period. In order to keep computational tractability in the stochastic programs, scenario sets Ω_i are reduced accordingly to 100 realizations using the fast-forward scenario reduction technique [19].

B. Stability Analysis (IEEE RTS-24 System)

The proposed methodology is showcased on a modified version of the IEEE RTS-24 system, whose detailed parameters are available in [20]. In particular, three lines are de-rated and six wind farms with 200 MV installed capacity are included in the system at selected locations. Simulation results are benchmarked against the stochastic co-optimization of energy and reserve (4) and the conventional approach of sequentially cleared markets, i.e., (1), (2) and (3). Reserve requirements Λ in model (1) are calculated as

$$\Lambda^{+} = \widehat{W}_{\text{tot}} - \widehat{\boldsymbol{F}}_{W}^{-1}(q) \tag{23}$$

$$\Lambda^{-} = \widehat{\boldsymbol{F}}_{W}^{-1}(1-q) - \widehat{W}_{\text{tot}}; \tag{24}$$

where $\widehat{W}_{\text{tot}}$ and $\widehat{\boldsymbol{F}}_{W}$ represent the expected value and the predictive CDF of the total wind power probabilistic forecast, respectively, while the pre-determined quantile q of the distribution is chosen in line with grid operator's risk aversion. The proposed methodology is tested either with or without transmission capacity allocation, where three values of the parameter χ are considered in the former case and a minimal zonal size of 4 nodes is always required.

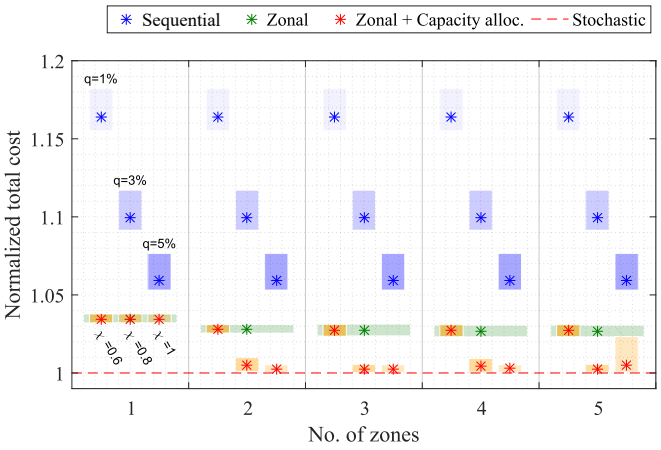

Fig. 2. Stability analysis in the RTS 24 bus system. Asterisks represent the mean values, upper and lower edges of rectangles represent max and min values, respectively.

In order to test the stability of the considered models against small deviations in the uncertain wind power generation, up- and downward reserve levels obtained with scenario set Ω_1 are plugged into (2) and (3), where the uncertainty is described by 10 different scenario sets Ω_i ($i = 2, \ldots, 11$), based on the same multivariate probabilistic forecast. Figure 2 shows the corresponding total cost, which are normalized with the solution of the stochastic model obtained with each set Ω_i. It stands out that the zonal approach outperforms the sequential one both in terms of stability and cost effectiveness, regardless of the chosen quantile q for setting reserve levels. The zonal model shows an improvement with just 2 zones, whereas it coincides with model [4] when a single zone is considered.

The effect of allowing transmission capacity allocation on cross-zonal lines is to lower the costs further, provided that more than 60% of eligible line capacities is withdrawn from the day-ahead market. This result resembles the line-switching approach, where the cost effectiveness of a dispatch can be improved if power flows are re-routed by switching off selected lines. In this case, reducing the capacity allocated to the day-ahead market ensures that enough headroom is available for balancing the system, thus avoiding bottlenecks that would result in expensive corrective actions.

C. Cost Breakdown

Table I shows the cost breakdown of selected models solved with the same scenario set Ω_1. The conventional model in this case relies on the top and bottom 3% of the total wind power distribution for setting reserve requirements. This approach results in higher cost for reserves, as it cannot account neither for their location in the system nor for the network constraints that might limit their accessibility. Instead, the preemptive model with a single zone is able to regulate reserve requirements based on expected re-dispatch actions. Although improving the results considerably, this approach still relies on a single reserve market and thus it follows the merit order

TABLE I
COST BREAKDOWN OF SELECTED MODELS

		Reserve cost [k$]	Day-ahead cost [k$]	Balancing cost [k$]	Total cost [k$]
Sequential		6.015	24.41	0.322	30.75
Stochastic		3.135	25.53	-0.960	27.70
		No capacity allocation χ = 0%			
Zonal	**Z = 1**	3.810	24.34	0.432	28.59
	Z = 2	3.861	24.09	0.455	28.40
	Z = 3	3.903	24.02	0.440	28.36
	Z = 4	3.901	24.01	0.434	28.35
		Capacity allocation χ = 100%			
Zonal	**Z = 1**	3.810	24.34	0.432	28.59
	Z = 2	3.160	25.54	-0.997	27.70
	Z = 3	3.216	25.48	-0.990	27.70
	Z = 4	3.169	25.54	-1.003	27.70

of generators' reserve capacity offers. The implication is that while total reserve levels can be fine-tuned, their location and position in the system cannot.

This aspect motivates the introduction of a zonal setup that provides the grid operator with additional flexibility to approximate the ideal solution. As the number of zones increases, so does the ability to lower the costs towards the stochastic model and to optimally allocate reserves. Note that the partitioning in the proposed methodology is solely driven by the total expected costs and it does not require any root node to be pre-specified, which could introduce a degree of arbitrariness in the partition. Therefore, it inherently considers the availability of reserves in the system, their procurement and their activation costs given the network limitations. Table II summarizes the zonal reserve costs referring to the case of 3 zones in Fig. 3. The zonal setup allows to procure nearly 60% of total requirements from zone 2, where the cost per MW is lower. Zone 3 instead procures less reserve, but from more expensive generators ensuring that enough balancing power is located close to wind farms at nodes 3 and 5.

Two effects are evident as we include transmission capacity allocation on cross-zonal lines: the first is that reserve costs decrease, since more power can be reserved from cheaper generators, while ensuring that they can deliver it to the grid; the second is that day-ahead costs increase, as we reduce the network capacity available for energy trading. A consequence of this latter aspect is that less wind power will be dispatched at this stage. To compensate for that and to avoid expensive wind curtailment penalties, more downward reserve needs to be procured and activated, as can be seen from Table II.

D. RTS-96 Case Study

The proposed methodology is also tested in the 3-area RTS-96 system, for which relevant data is taken from [4]. The system is considered during the peak hour with a total demand of 7.5 GW, 18% of which is covered by wind power located in 5 locations. Original line ratings are used, whereas the minimum power output of controllable units is set to 0.

TABLE II
ZONAL RESERVE COST OF GRID PARTITIONS IN FIG. 3

	(a) No capacity allocation χ = 0%				**(b) Capacity allocation χ = 100%**			
	Reserve volume [MW]			Avg. cost [$/MW]	Reserve volume [MW]			Avg. cost [$/MW]
	Up	*Dw*	*Total*		*Up*	*Dw*	*Total*	
Zone 1	60.0	35.7	95.7	15	0	67.9	67.9	8.54
Zone 2	75.9	112.1	188.0	12	27.5	143.9	171.4	9.72
Zone 3	40.0	0	40.0	14.3	30.0	30.0	60.0	13.33
Total	175.9	147.8	323.7	12.7	57.5	241.8	299.3	10.23

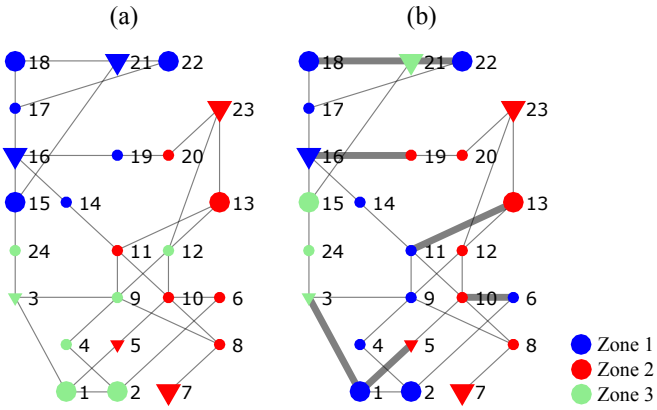

Fig. 3. Partition of the RTS-24 system into 3 zones without (a) and with (b) transmission capacity allocation on selected lines. Triangles indicate wind power, large markers indicate the presence of generators.

In order to exclude the generator-specific resolution of the stochastic approach, a minimal zonal size of 10 nodes has been enforced in this system.

Figure 4 shows the resulting total expected costs, where we compare the proposed methodology to the sequential approach with varying reserve requirements (i.e. corresponding to different quantiles q in (24) and (23)) and a zonal model with a predetermined partitioning variable $x_{n,z}$, according to the standard partitioning of this system into three zones. In this way, we isolate the contribution of the flexible zone boundaries definition provided by the proposed Zonal Preemptive approach. The partition into 3 zones is shown in Fig. (5) together with the common subdivision of the RTS-96 system into 3 areas. The total expected costs indicate that tuning reserve requirements while considering a single reserve market, i.e., $Z = 1$, does not result in significant savings, as opposed to the sequential approach. The Zonal Preemptive approach with a fixed partition that adheres to the 3 areas in Fig. 5 performs better than the single zone. However, as the zones are dynamically determined by the partitioning variables $x_{n,z}$, the total costs fall near the lower bound represented by the stochastic co-optimization of energy and reserve. It suffices to split the system into 2 zones to stay within the 0.1% increase from the lower bound, even without allocating transmission capacity on cross-zonal lines.

The resulting large-scale MILP problem is solved with Gurobi setting a 0.1% optimality gap on a quad-core laptop

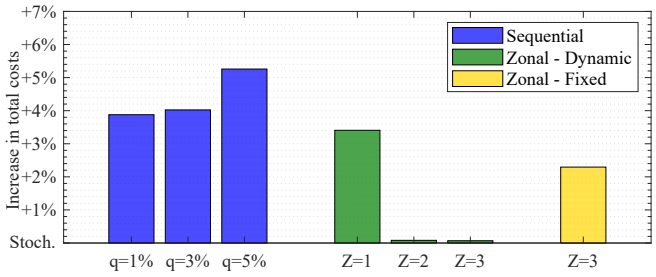

Fig. 4. Increase in total expected costs for the load demand peak hour in the RTS-96 system. Costs normalized with the stochastic solution.

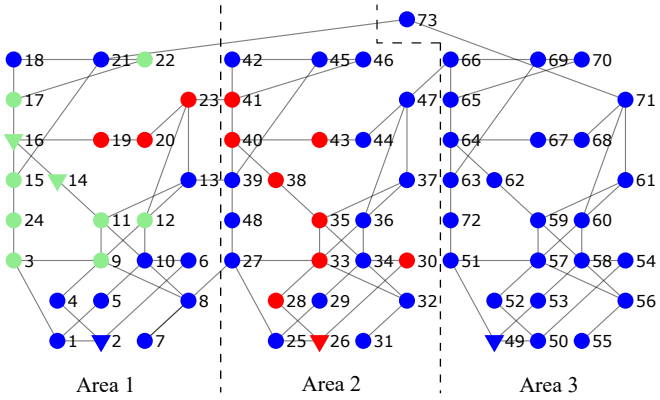

Fig. 5. Partition of the 3-area IEEE RTS-96 system according to the Zonal Preemptive model with $\chi = 0$. Triangles indicate wind farms.

with 8 GB of RAM and 2.4 GHz of CPU. Bender's decomposition converged in $3.50 \cdot 10^2$ s with 1 zone, $2.15 \cdot 10^3$ s with 2 zones and $4.04 \cdot 10^4$ s with 3 zones.

VI. Conclusion

This paper described a novel methodology for reserve procurement that further approximates the efficiency of the stochastic co-optimization of energy and reserves in terms of total operating costs, while still respecting the existing market rules. Building upon recent work on stochastic bilevel optimization, we embed grid partitioning constraints in the upper-level problem and use them to determine not only the zonal reserve requirements but the zonal boundaries as well.

Unlike other partitioning schemes, our methodology is solely driven by the total expected system costs and the most recent uncertainty forecasts, instead of relying on historical data that may not reflect the actual system state. The proposed model allows grid operators to perform a dynamic zoning of the system for reserve procurement, depending upon generation uncertainty and network limitations. In addition, this zonal preemptive model can contribute to the ongoing policy discussion towards a common European reserve capacity market, where reserve zones are dynamically defined upon system conditions instead of geographical borders. Simulation results show that the stochastic lower bound can be adequately approximated with only two zones, even if a minimal zonal size is required. This result suggests that the computational burden of the proposed approach can be reduced by limiting the number of reserve zones, without a major efficiency loss in terms of expected system cost. Moreover, the combination of dynamic reserve procurement with cross-zonal transmission capacity allocation has shown to be beneficial in highly congested system. Setting aside part of the available transmission capacity grants the grid operator additional flexibility to approach the efficiency of the stochastic dispatch.

Future work will address the current limitations of the proposed methodology considering inter-temporal constraints, which may affect the partitioning of the system and the deployment of reserves.

References

[1] J.M. Morales, A.J. Conejo and J. Pérez-Ruiz, "Economic Valuation of Reserves in Power Systems With High Penetration of Wind Power," *IEEE Trans. on Power Syst.*, vol. 24, no. 2, pp. 900–910, 2009.

[2] A. Papavasiliou and S. S. Oren, "Multiarea stochastic unit commitment for high wind penetration in a transmission constrained network." *Operations Research*, vol. 61, no. 3, pp. 578 – 592, 2013.

[3] J. M. Morales, M. Zugno, S. Pineda, and P. Pinson, "Electricity market clearing with improved scheduling of stochastic production," *European Journal of Operational Research*, vol. 235, no. 3, pp. 765–774, 2014.

[4] V. Dvorkin, S. Delikaraoglou, J.M. Morales, "Setting reserve requirements to approximate the efficiency of the stochastic dispatch," *IEEE Trans. on Power Syst.*, vol. 34, no. 2, pp. 1524–1536, 2019.

[5] S. Delikaraoglou, P. Pinson, "Optimal allocation of HVDC interconnections for exchange of energy and reserve capacity services," *Energy Systems*, vol. 10, no. 3, pp. 635–675, 2019.

[6] N. Fan, D. Izraelevitz, F. Pan, P. M. Pardalos, and J. Wang, "A mixed integer programming approach for optimal power grid intentional islanding," *Energy Systems*, vol. 3, no. 1, pp. 77–93, 2012.

[7] M. Golari, N. Fan, and J. Wang, "Two-stage stochastic optimal islanding operations under severe multiple contingencies in power grids," *Electric Power Systems Research*, vol. 114, pp. 68–77, 2014.

[8] A. Kumar, S. C. Srivastava, and S. N. Singh, "A zonal congestion management approach using real and reactive power rescheduling," *IEEE Trans. on Power Syst.*, vol. 19, no. 1, pp. 554–562, Feb 2004.

[9] F. Wang and K. W. Hedman, "Reserve zone determination based on statistical clustering methods," in *2012 North American Power Symposium (NAPS)*, Sep. 2012, pp. 1–6.

[10] F. Wang and K. W. Hedman, "Dynamic reserve zones for day-ahead unit commitment with renewable resources," *IEEE Trans. on Power Syst.*, vol. 30, no. 2, pp. 612–620, 2015.

[11] Y. Chen, P. Gribik, and J. Gardner, "Incorporating Post Zonal Reserve Deployment Transmission Constraints Into Energy and Ancillary Service Co-Optimization," *IEEE Trans. on Power Syst.*, vol. 29, no. 2, pp. 537–549, 2014.

[12] A. Ahmadi-Khatir, M. Bozorg, and R. Cherkaoui, "Probabilistic spinning reserve provision model in multi-control zone power system," *IEEE Trans. on Power Syst.*, vol. 28, no. 3, pp. 2819–2829, Aug 2013.

[13] Y. T. Gebrekiros, G. L. Doorman, H. Farahmand, and S. Jaehnert, "Benefits of cross-border reserve procurement based on pre-allocation of transmission capacity," *IEEE Grenoble Conf. PowerTech*, pp. 1–6, 2013.

[14] F. Trespalacios and I. Grossmann, "Review of mixed-integer nonlinear and generalized disjunctive programming methods," *Chemie-Ingenieur-Technik*, vol. 86, no. 7, pp. 991–1012, 2014, cited By 72.

[15] S. Pineda and J. M. Morales, "Solving linear bilevel problems using big-ms: Not all that glitters is gold," *IEEE Transactions on Power Systems*, vol. 34, no. 3, pp. 2469–2471, 2019.

[16] A. J. Conejo, E. Castillo, R. Mínguez, and R. García-Bertrand, *Decomposition techniques in mathematical programming: Engineering and science applications*. Springer, 2006.

[17] H. Bludszuweit, J. A. Domínguez-Navarro, and A. Llombart, "Statistical analysis of wind power forecast error," *IEEE Trans. on Power Syst.*, vol. 23, no. 3, pp. 983–991, 2008.

[18] G. Papaefthymiou and D. Kurowicka, "Using copulas for modeling stochastic dependence in power system uncertainty analysis," *IEEE Trans. on Power Syst.*, vol. 24, no. 1, pp. 40–49, 2009.

[19] J. Dupačová, G. Consigli, and S. W. Wallace, "Scenarios for Multistage Stochastic Programs," *Annals of Operations Research*, vol. 100, no. 1-4, pp. 25–53, 2000.

[20] C. Ordoudis, P. Pinson, and M. Zugno, "An updated version of the IEEE rts 24-bus system for electricity market and power system operation studies," *Technical University of Denmark (DTU)*, pp. pp. 1–5, 2016.

COMPANION PAPER

This document serves as the electronic companion of paper "Dynamic Reserve and Transmission Capacity Allocation in Wind-Dominated Power Systems". Appendix A presents the Karush-Kuhn-Tucker (KKT) conditions of the dynamic reserve procurement problem in Section III-B and the day-ahead market clearing in Section II. Appendix B presents the multi-cut Bender's decomposition scheme that is used to solve the proposed methodology on large-scale systems.

APPENDIX A

The dual variables in the KKT conditions are indicated as γ^* for constraint $(*)$, where equation numbers are referred to the main paper. The corresponding optimization problems are repeated in a standard notation to ease the identification of dual variables. Symbol $\perp$ indicates the complementarity conditions between the constraints and the rest of the symbols is in accordance with the nomenclature in the main paper.

A. Zonal reserve market

1) Problem formulation:

$$\min_{\Xi_{\mathrm{R}_z}} \quad \mathcal{C}_{\mathrm{R},z} = \sum_{g\in\mathcal{G}} \left(C_g^+ r_g^+ + C_g^- r_g^-\right) \tag{25a}$$

s.t.

$$\lambda_z^+ - \sum_{g\in\mathcal{G}} r_{g,z}^+ \le 0, \qquad \forall z\in\mathcal{Z}, \tag{25b}$$

$$\lambda_z^- - \sum_{g\in\mathcal{G}} r_{g,z}^- \le 0, \qquad \forall z\in\mathcal{Z}, \tag{25c}$$

$$r_{g,z}^+ - R_g^+ \left(\boldsymbol{H}_{\mathrm{G}_{(g,\cdot)}} \boldsymbol{x}_{(\cdot,z)}\right) \le 0, \quad \forall z\in\mathcal{Z}, \quad \forall g\in\mathcal{G}, \tag{25d}$$

$$r_{g,z}^- - R_g^- \left(\boldsymbol{H}_{\mathrm{G}_{(g,\cdot)}} \boldsymbol{x}_{(\cdot,z)}\right) \le 0, \quad \forall z\in\mathcal{Z}, \quad \forall g\in\mathcal{G}, \tag{25e}$$

$$-r_{g,z}^+ \le 0 \qquad \forall z\in\mathcal{Z}, \quad \forall g\in\mathcal{G}, \tag{25f}$$

$$-r_{g,z}^- \le 0 \qquad \forall z\in\mathcal{Z}, \quad \forall g\in\mathcal{G}, \tag{25g}$$

$$r_g^+ - \sum_{z\in\mathcal{Z}} r_{g,z}^+ = 0, \qquad \forall g\in\mathcal{G}, \tag{25h}$$

$$r_g^- - \sum_{z\in\mathcal{Z}} r_{g,z}^- = 0, \qquad \forall g\in\mathcal{G} \tag{25i}$$

2) KKT conditions:

$$C_g^+ - \gamma_z^{(25\mathrm{b})} + \gamma_{g,z}^{(25\mathrm{d})} - \gamma_{g,z}^{(25\mathrm{f})} + \gamma_g^{(25\mathrm{h})} = 0, \qquad \forall g, \forall z, \tag{26}$$

$$C_g^- - \gamma_z^{(25\mathrm{c})} + \gamma_{g,z}^{(25\mathrm{e})} - \gamma_{g,z}^{(25\mathrm{g})} + \gamma_g^{(25\mathrm{i})} = 0, \qquad \forall g, \forall z, \tag{27}$$

$$0 \ge \lambda_z^+ - \sum_{g\in\mathcal{G}} r_{g,z}^+ \quad \perp \quad \gamma_z^{(25\mathrm{b})} \ge 0, \qquad \forall z \tag{28}$$

$$0 \ge \lambda_z^- - \sum_{g\in\mathcal{G}} r_{g,z}^- \quad \perp \quad \gamma_z^{(25\mathrm{c})} \ge 0, \qquad \forall z \tag{29}$$

$$0 \ge r_{g,z}^+ - R_g^+ \left(\boldsymbol{H}_{\mathrm{G}_{(g,\cdot)}} \boldsymbol{x}_{(\cdot,z)}\right) \perp \gamma_{g,z}^{(25\mathrm{d})} \ge 0, \qquad \forall g, \forall z \tag{30}$$

$$0 \ge r_{g,z}^- - R_g^- \left(\boldsymbol{H}_{\mathrm{G}_{(g,\cdot)}} \boldsymbol{x}_{(\cdot,z)}\right) \perp \gamma_{g,z}^{(25\mathrm{e})} \ge 0, \qquad \forall g, \forall z \tag{31}$$

$$0 \ge -r_{g,z}^+ \quad \perp \quad \gamma_{g,z}^{(25\mathrm{f})} \ge 0, \qquad \forall g, \forall z \tag{32}$$

$$0 \ge -r_{g,z}^- \quad \perp \quad \gamma_{g,z}^{(25\mathrm{g})} \ge 0, \qquad \forall g, \forall z \tag{33}$$

$$r_g^+ - \sum_{z\in\mathcal{Z}} r_{g,z}^+ = 0, \qquad \forall g, \tag{34}$$

$$r_g^- - \sum_{z\in\mathcal{Z}} r_{g,z}^- = 0, \qquad \forall g. \tag{35}$$

B. Day-ahead market

1) Problem formulation:

$$\min_{\Xi_{\mathrm{D}}} \quad \mathcal{C}_{\mathrm{D}} = \sum_{g\in\mathcal{G}} C_g p_g \tag{36a}$$

s.t.

$$\sum_{g\in\mathcal{G}} p_g + \sum_{j\in\mathcal{J}} w_j - \sum_{n\in\mathcal{N}} D_n = 0, \tag{36b}$$

$$\underline{P}_g + r_g^{-,*} - p_g \le 0 \qquad \forall g\in\mathcal{G}, \tag{36c}$$

$$p_g - \overline{P}_g + r_g^{+,*} \le 0, \qquad \forall g\in\mathcal{G}, \tag{36d}$$

$$-w_j \le 0, \qquad \forall j\in\mathcal{J}, \tag{36e}$$

$$w_j - \widehat{W}_j \le 0, \qquad \forall j\in\mathcal{J}, \tag{36f}$$

$$\boldsymbol{M}_{(\ell,\cdot)} \left(\boldsymbol{H}_{\mathrm{G}}^\top \boldsymbol{p} + \boldsymbol{H}_{\mathrm{J}}^\top \boldsymbol{w} - \boldsymbol{D}\right) - F_\ell \le 0, \qquad \forall \ell\in\mathcal{L}, \tag{36g}$$

$$-F_\ell - \boldsymbol{M}_{(\ell,\cdot)} \left(\boldsymbol{H}_{\mathrm{G}}^\top \boldsymbol{p} + \boldsymbol{H}_{\mathrm{J}}^\top \boldsymbol{w} - \boldsymbol{D}\right) \le 0, \qquad \forall \ell\in\mathcal{L}, \tag{36h}$$

2) KKT conditions:

$$C_g + \gamma^{(36\mathrm{b})} - \gamma_g^{(36\mathrm{c})} + \gamma_g^{(36\mathrm{d})} \cdots + \sum_{\ell\in\mathcal{L}} (\gamma_\ell^{(36\mathrm{g})} - \gamma_\ell^{(36\mathrm{h})}) \boldsymbol{M}_{(\ell,\cdot)} \boldsymbol{H}_{\mathrm{G}}^\top \mathbb{1}_g = 0, \qquad \forall g\in\mathcal{G}, \tag{37}$$

$$\gamma^{(36\mathrm{b})} - \gamma^{(36\mathrm{e})} + \gamma^{(36\mathrm{f})} \cdots + \sum_{\ell\in\mathcal{L}} (\gamma_\ell^{(36\mathrm{g})} - \gamma_\ell^{(36\mathrm{h})}) \boldsymbol{M}_{(\ell,\cdot)} \boldsymbol{H}_{\mathrm{J}}^\top \mathbb{1}_j = 0, \qquad \forall j\in\mathcal{J}, \tag{38}$$

$$\sum_{g\in\mathcal{G}} p_g + \sum_{j\in\mathcal{J}} w_j - \sum_{n\in\mathcal{N}} D_n = 0 \tag{39}$$

$$0 \ge \underline{P}_g + r_g^{-,*} - p_g \quad \perp \quad \gamma_g^{(36\mathrm{c})} \ge 0, \qquad \forall g\in\mathcal{G}, \tag{40}$$

$$0 \ge p_g - \overline{P}_g + r_g^{+,*} \quad \perp \quad \gamma_g^{(36\mathrm{d})} \ge 0, \qquad \forall g\in\mathcal{G}, \tag{41}$$

$$0 \ge -w_j \quad \perp \quad \gamma_j^{(36\mathrm{e})} \ge 0, \qquad \forall j\in\mathcal{J}, \tag{42}$$

$$0 \ge w_j - \widehat{W}_j \quad \perp \quad \gamma_j^{(36\mathrm{f})} \ge 0, \qquad \forall j\in\mathcal{J}, \tag{43}$$

$$0 \ge \boldsymbol{M}_{(\ell,\cdot)} \left(\boldsymbol{H}_{\mathrm{G}}^\top \boldsymbol{p} + \boldsymbol{H}_{\mathrm{J}}^\top \boldsymbol{w} - \boldsymbol{D}\right) - F_\ell \quad \perp \quad \gamma_\ell^{(36\mathrm{g})} \ge 0, \qquad \forall \ell\in\mathcal{L}, \tag{44}$$

$$0 \ge -F_\ell - \boldsymbol{M}_{(\ell,\cdot)} \left(\boldsymbol{H}_{\mathrm{G}}^\top \boldsymbol{p} + \boldsymbol{H}_{\mathrm{J}}^\top \boldsymbol{w} - \boldsymbol{D}\right) \quad \perp \quad \gamma_\ell^{(36\mathrm{h})} \ge 0, \qquad \forall \ell\in\mathcal{L}. \tag{45}$$

APPENDIX B

A multi-cut Bender's decomposition scheme is implemented [16]. The master problem at iteration η is formulated as

$$\min_{\Xi_{\mathrm{MP}}} \quad \mathcal{C}_{\mathrm{R}} + \mathcal{C}_{\mathrm{D}} + \sum_{s\in\mathcal{S}} \pi_s \vartheta_s \tag{46a}$$

s.t. (26) - (35), KKT of zonal reserve market

(37) - (45), KKT of day-ahead market

(20d), Zonal reserve requirements,

(5) – (9), Grid partitioning,

(15) – (19), Capacity allocation,

$$\vartheta_s \ge \vartheta_0 \qquad \forall s\in\mathcal{S} \tag{46b}$$

$$\vartheta_s \ge \mathcal{C}_{\mathrm{B},s}^{(k)} + \sum_g \gamma_{g,s}^{(47\mathrm{b})^{(k)}} \left(r_g^+ - r_g^{+;(k)}\right) \cdots \tag{46c}$$

$$+ \sum_g \gamma_{g,s}^{(47\mathrm{c})^{(k)}} \left(r_g^- - r_g^{-;(k)}\right) + \sum_g \gamma_{g,s}^{(47\mathrm{d})^{(k)}} \left(p_g - p_g^{(k)}\right) \cdots$$

$$+ \sum_j \gamma_{j,s}^{(47\mathrm{e})^{(k)}} \left(w_j - w_j^{(k)}\right), \forall s\in\mathcal{S}, \forall k = 1,\ldots,\eta-1$$

where $\gamma^{(*)^{(k)}}$ are the dual variables of constraints $(*)$ in the sub-problem, whose formulation for scenario $s = s'$ and iteration η is the following

$$\min_{\Xi_{\text{SP}}} \quad \mathcal{C}_{\text{B},s'} = \sum_{g\in\mathcal{G}} C_g \left(p^{+}_{g,s'} - p^{-}_{g,s'}\right) + \sum_{j\in\mathcal{J}} C^{\text{ct}} w^{\text{ct}}_{j,s'} + \sum_{n\in\mathcal{N}} C^{\text{sh}} d^{\text{sh}}_{n,s'} \tag{47a}$$

$$\text{s.t.} \quad r^{+}_{g} = r^{+;(\eta)}_{g} \quad : \gamma^{(47\text{b})^{(\eta)}}_{g,s'} \tag{47b}$$

$$r^{-}_{g} = r^{-;(\eta)}_{g} \quad : \gamma^{(47\text{c})^{(\eta)}}_{g,s'} \tag{47c}$$

$$p_g = p^{(\eta)}_{g} \quad : \gamma^{(47\text{d})^{(\eta)}}_{g,s'} \tag{47d}$$

$$w^{+}_{j} = w^{(\eta)}_{j} \quad : \gamma^{(47\text{e})^{(\eta)}}_{j,s'} \tag{47e}$$

$$\text{(3b)} - \text{(3h)}, \quad \text{Balancing market}, \quad s = s',$$

where first-stage decision variables r^{+}_{g}, r^{-}_{g}, p_g and w_j are fixed to the solution of the master problem at the current iteration. As the problem has complete recourse, no need for feasibility cuts is required and $\mathcal{S}$ new optimality cuts are added to the master problem at each iteration. The algorithm converges to a solution when the condition $|\sum_s \pi_s \vartheta_s - \sum_s \pi_s \mathcal{C}^{(\eta)}_{\text{B},s}| \leq \varepsilon$ is satisfied for a predefined tolerance ε.

Department of Electrical Engineering
Center for Electric Power and Energy (CEE)
Technical University of Denmark
Elektrovej, Building 325
DK-2800 Kgs. Lyngby
Denmark

www.elektro.dtu.dk/cee
Tel: (+45) 45 25 35 00
Fax: (+45) 45 88 61 11
E-mail: cee@elektro.dtu.dk